Durham E-Theses

Study of Triplet Exciton Dynamics in Small Organic Molecule Films Using Time Resolved Optical Spectroscopy

JANKUS, VYGINTAS

How to cite:

JANKUS, VYGINTAS (2010) *Study of Triplet Exciton Dynamics in Small Organic Molecule Films Using Time Resolved Optical Spectroscopy*, Durham theses, Durham University. Available at Durham E-Theses Online: http://etheses.dur.ac.uk/495/

Use policy

Study of Triplet Exciton Dynamics in Small Organic Molecule Films Using Time Resolved Optical Spectroscopy

Vygintas Jankus

A thesis submitted to the Faculty of Science at the University of Durham for the Degree of Doctor of Philosophy

Abstract

In recent years it has become clear that knowledge of triplet transport in single layer and multilayer films can be crucial in improving the efficiency of organic light emitting devices and solar cells. This thesis reports an investigation of triplet exciton dynamics in small organic molecule single and multilayer layer films using optical time resolved nanosecond spectroscopy. A diligent step by step approach, leading towards the investigation of complex donor/spacer/acceptor multilayer structures is used. First of all, single layer films to be a constituents of multilayer structures were studied by measuring fluorescence, delayed fluorescence and phosphorescence. 4,4'-N,N'-dicarbazolyl-1,1'-biphenyl (CBP) widely used in organic light emitting diodes is characterized. Evidence is provided that in some of these spectra emission comes from trap states rather than the CBP molecule itself. Also N,N'-diphenyl-N,N'-bis(1-naphthyl)-1,1'-biphenyl-4,4''-diamine (NPB) has been investigated. Results indicate that bimolecular triplet recombination is dominant and that triplet transport has dispersive features even at room temperature in NPB films. Then films of heavy metal iridium complexes *fac*-tris(2-phenylpyridine) iridium (Ir(ppy)$_3$) and iridium(III)tris(1-phenylisoquinoline) (Ir(piq)$_3$) are put into the spotlight. New states previously not reported are identified and decay with the slope -1 characteristic of more than one iridium complex and previously not published in literature is observed. Triplet interface sites in bilayer Ir(piq)$_3$/NPB films obstructing triplet migration are determined and triplet movement across interface is experimentally captured for the first time. The origin of these interface trap states is suggested. Then this system is upgraded into Ir(ppy)$_3$/NPB/Ir(piq)$_3$ and triplet transfer from Ir(ppy)$_3$ to Ir(piq)$_3$ via NPB is investigated. A model of triplet exciton dynamics in Ir(piq)$_3$/NPB films using classical diffusion equations is presented with interface sites included. Computer simulations were performed and the results are in very good agreement with the experimental ones. Finally problems encountered are identified and main guidelines on how to do research in complicated multilayer structures are set.

Study of Triplet Exciton Dynamics in Small Organic Molecule Films Using Time Resolved Optical Spectroscopy

by

Vygintas Jankus

Department of Physics

Durham University

A thesis submitted to the Faculty of Science at the University of Durham for the Degree of Doctor of Philosophy

September 2010

Declaration

All material contained in this thesis is original and is the result of my own work except where explicit reference is made to the work of others.

This thesis has not been submitted in whole or part for the award of a degree at this or any other university.

Acknowledgments

Table of Contents

List of figures and tables

and $D_{PIQ} = 1.7 \times 10^{-5} cm^2 \; s^{-1}$. The NPB/Ir(piq)$_3$ interface characteristics were: f=0.002, k_a= 9.10^{-1} cm s^{-1}, $E_a = 0.39 eV$…..176

List of abbreviations

Alq$_3$ – tris(8-hydroxyquinoline) aluminum

CBP – 4,4-N, N'-dicarbazolyl-1,1'-biphenyl

EQE – external quantum efficiency

DF – delayed fluorescence, DIP - di-indenoperylene, DOS- density of states

Fc – ferrocene, FIrpic - Bis(4,6-difluorophenylpyridinato-N,C2)picolinatoiridium

HOMO – highest occupied molecular orbital

iCCD – intensified charged coupled device, ITO – indium tin oxide, ISC – intersystem crossing

Ir(piq)$_3$ - iridium (III) tris(1-phenylisoquinoline), Ir(ppy)$_3$ - *fac*-tris(2-phenylpyridine) Iridium (III)

LE – low energy, LUMO – lowest unoccupied molecular orbital

MLCT – metal to ligand charge transfer, *mer*-Ir(ppy)$_3$ - *mer*-tris(2-phenylpyridine) Iridium (III), MTHF - methyl tetrahydrofuran

Nd:YAG – neodymium doped yttrium aluminum garnet, NPB - N,N'-diphenyl-N,N'-bis(1-naphthyl)-1,1'-biphenyl-4,4''-diamine

(W)(PH)OLED – (white)(phosphorescent)organic light emitting diode

PF – prompt fluorescence, PH – phosphorescence, PL – photoluminescence, PLQY – photoluminescence quantum yield, PMMA - poly(methyl methacrylate), PTCDA - perylene-3,4,9,10-tetracarboxylic-3,4,9,10-dianhydride), PtOEP - Pt(II) Octaethylporphine

Ru - tris(2,2'-bipyridine)ruthenium(II)

SLR – spin lattice relaxation, SubPC - boron subphthalyocyanine

TAPC - 1,1-bis((di-4-tolylamino)phenyl)cyclohexane, TPD - N,N'-bis(3-methylphenyl)-(1,1'-biphenyl)-4,4'-diamine, TTA – triplet-triplet annihilation

1 Introduction

Artificial lighting is one of the most important aspects of our lives. One could hardly imagine cities without streetlights or houses without illumination during dark periods of day or night. It increases the number of hours people can work as well as makes us feel more comfortable and safer. Unfortunately, it consumes a huge part of our energy resources thus this is not only a huge benefit but also a huge cost to society. For example, in the United States only, lighting consumes ~ 765 TW hours of electricity which accounts for 8.2 % of all energy consumed in the USA and ~ 22% of electricity produced [1]. The cost of this for a US consumer is ~60 billion dollars per year[1]. There are few calculations of the world consumption of electricity for lighting but one can easily imagine how the cost would rocket if Europe and Asia were added. Thus, people need viable alternatives of lighting in order to reduce the energy consumed by lighting. The US Department of Energy hopes that solid-state lighting (SSL), inorganic light emitting diodes (LEDs) and organic light emitting diodes (OLEDs), could be that alternative. Provided OLEDs and LEDs achieve projected performance, they anticipate that SSL could reduce US energy consumption by 29 % by the year 2025, which can effectively be converted into ~125 billion US dollars[1]. Thus, OLEDs and LEDs are indeed very attractive lighting architectures. Furthermore, OLEDs unlike LEDs can be manufactured on flexible substrates, which could open completely new areas of business and combine the arts with lighting. Some companies have already presented flexible OLED prototypes [2]. In 2009 Samsung demonstrated an S shaped OLED display, as well Universal Display Corporation announced that they were able to manufacture active matrix OLED on polyethylene naphthalate substrate (from DuPont) which is the first step towards manufacturable flexible displays[2]. Other companies, such as General Electric, Holst Center, Philips have released flexible OLED prototype videos too [2].

However, lots of work needs to be done not only in making OLEDs flexible but also in increasing power and external quantum efficiencies. Assuming that only singlet states are utilized in the production of light, spin statistics indicates that during charge recombination there is a fundamental 25% limit of device efficiency due to the triplet (non-radiative species) to singlet (radiative) exciton creation ration of 3:1 in OLEDs[3-5]. The external quantum efficiency of devices (EQE) depends on four factors:

$$EQE = \eta_{out} \cdot \eta_{fl} \cdot \gamma \cdot \eta_{fr} \qquad (1.1)$$

where, η_{out} - light out coupling efficiency considered to be 20% [4-6]. η_{fl} - fluorescence efficiency (also called internal efficiency), let us assume it to be 1, as it is possible to synthesize

organic materials having nearly unity efficiency[7-9]. γ - charge balance factor which can be assumed to be 1 if highest occupied molecular orbital (HOMO) level, lowest unoccupied molecular orbital (LUMO) level of organic layers and workfunctions of electrodes are adjusted in appropriate manner. η_{fr} - singlet formation ratio is assumed to be 25 %. The total external quantum efficiency (EQE) is 5% (EQE~0.2·1·1·0.25=0.05)[5-6]. It is clear from the numbers that one could increase the quantum efficiency of OLEDs fourfold by utilization of triplet excitons. There are ways to do this.

First, one could use heavy metal complexes as emissive dopants where phosphorescence efficiency is increased due to spin orbit coupling[10-13]. In this way, one could harvest 75% of triplets by transferring them to heavy metal dopants to produce light. There were some very successful attempts to use this method and almost 100% internal QE (20% external) was reported using blue, green and red phosphorescent heavy metal complexes to produce white light in OLEDs[14]. However, it was observed that blue emitting heavy metal complexes are not very stable. For example it was found that Bis(4,6-difluorophenylpyridinato-N,C2)picolinatoiridium (FIrpic) degrades during the vacuum deposition[15]. This is not very acceptable for the long term device performance, therefore hybrid schemes have been proposed whereby phosphorescent and fluorescent dopants are combined in OLED where the 25% of singlet excitons generated are used by blue fluorescent emitters and simultaneously the other 75% triplet excitons are harvested to produce green and red light by phosphorescent emitters[16-18]. The mechanism allowing this to happen is the difference between singlet and triplet exciton diffusion lengths. For example, one scheme places[17-18] the fluorescent blue material at the recombination zone with the phosphorescent green and red complexes doped in subsequent layers separated by interlayers within the diffusion length of triplet excitons, but which are much further than the diffusion length of singlet excitons. In both cases, phosphorescent or hybrid white organic light emitting devices, triplet diffusion can be used to harvest excitons and this has been demonstrated by Leo *et al* where the power efficiency of their devices has surpassed that of fluorescent tubes[19]. Another possibility to increase device efficiency without using high quantum yield heavy metal complexes is to use triplet-triplet annihilation (TTA) and subsequent delayed fluorescence from singlet state[5-6]. Assuming that eight annihilating triplets would generate one singlet and regenerate three triplets (if quintuplet states are not accessible energetically) one comes to the conclusion that five triplets generate one singlet state. In this way theoretical maximum quantum efficiency could reach 8%[6]. Indeed Kondakov showed that it is possible to enhance efficiency in employing TTA to produce light[6].

Thus good understanding of triplet state dynamics in films and in multilayer films, diffusion properties, and triplet-triplet annihilation (and subsequent delayed fluorescence) is of crucial importance for improving OLEDs further. Although it is possible to study triplet migration and

TTA 'in situ' - in OLEDs[5], diligent time-resolved studies of long lived excited states are very difficult to perform owing to a high RC time constant and other processes such as charge carrier transport, exciton-polaron annihilation which might prevent the exposure of genuine properties of triplet transport[20-22]. Furthermore it is of interest from fundamental research point of view as there are lots of aspects of triplet transport which still needs to be unveiled. A few studies analyzing triplet exciton dynamics in single layer amorphous organic films have been published already[23-25]. Unfortunately, there are no published studies on triplet migration across interfaces between thin amorphous layers. Although there have been a few studies where multilayer structures have been used to determine triplet properties (diffusion constants, triplet-triplet annihilation constants) [20, 26-28], however, the dynamics of triplets excitons across an interface has not been captured experimentally. Clearly in the big picture of triplet exciton migration in films this piece of information is missing. This has been overlooked despite the fact that transfer of excitons across the interface might be a major controlling factor in efficient triplet harvesting within OLEDs. For these reasons, time-resolved photoluminescence studies were chosen to gain insight into properties of triplet dynamics in single layer and multilayer films; both delayed fluorescence and phosphorescence are used to probe triplet movement in the material. Mainly small molecule sublimed organic single, bi or multilayer films have been fabricated. A gated time resolved spectroscopy system having nanosecond resolution has been used to investigate phosphorescence and delayed fluorescence of those films, the main elements of which are picosecond laser excitation source, spectrograph and gated intensified CCD camera.

In this thesis a step-by-step systematic approach is chosen to determine rules of triplet behavior in multilayer films and in the interfaces between the layers. First of all, relevant background theory, experiments, and Monte Carlo simulations will be reviewed in chapters 2 and 3. Experimental equipment used in the thesis will be discussed shortly in chapter 4. An effort will be made to choose suitable donor material, spacer material and acceptor material in order to simulate triplet harvesting processes (donor to acceptor via spacer layer). However before creating multilayer structures, triplet dynamics in single layer films needs to be unveiled. Thus two chapters about triplet exciton dynamics in thin single layer films will follow where, an effort will be put into demonstrating the importance of such a systematic approach to creating multilayer structures. For example, it will be shown that it is relevant to understand simple photophysics of the spacer material as some of them can undergo emission from trap states e.g. 4,4-N, N′-dicarbazolyl-1,1′-biphenyl (CBP) (chapter 5). The existence of the latter can decrease the rate of triplet transfer through spacer layer – as triplets are trapped in the spacer trap sites. As well additional parameters (transfer rate to trap states) have to be considered when modeling or simulating physical processes in the system. If the traps are of chemical origins, very different radiative lifetimes can be expected in comparison with lifetimes of genuine CBP molecule. Furthermore, it might be difficult to analyze data spectroscopically as emission from

trap states might cover spectral areas where emission from other layers should appear – for example from donor or acceptor. Thus another spacer, namely N,N'-diphenyl-N,N'-bis(1-naphthyl)-1,1'-biphenyl-4,4''-diamine (NPB) (chapter 6) rather than CBP, has been chosen for use as a spacer in the final structure of multilayer films. Even though this material is without obvious emission from traps a few other problems had to be overcome. First of all, before modeling triplet transfer in multilayer films it is relevant to choose the theoretical framework for modeling. Normally in the literature, triplet diffusion is modeled using classical diffusion equations[27]. However there are some reports claiming that triplet transport is dispersive i.e. the diffusion coefficient used in rate equations is not a constant but varies in time[23, 25, 29]. Furthermore, it is not possible to cast this into any analytical expression which makes use of classical rate equations almost impossible[30-32]. In most of the reports about triplet diffusion researchers tend to ignore the dispersive migration without any experimental justification and confine themselves with a few ambiguous sentences[20, 27-28]. With the hope to avoid this type of ignorance, in chapter 6, the dispersive migration regime analysis in NPB films will be presented, the transition between dispersive and non-dispersive regime will be determined and dispersive migration importance to modeling will be discussed. In the same chapter the influence of film thickness on triplet migration will overviewed as well.

In chapter 7 reasons are presented for choosing iridium metal ligand complexes as a donor and acceptor materials. Properties of the chosen donor material *fac* - tris(2-phenylpyridine) iridium (Ir(ppy)$_3$) are overviewed. As Ir(ppy)$_3$ is a very widely used material[8, 33-36], lots of research has been published already which is concisely presented. Unfortunately most of them are conflicting with one another, thus reasons are suggested for these inconsistencies and a clearer picture of triplet exciton dynamics in Ir(ppy)$_3$ films is presented. In addition to this, new findings uncovered during the work done for this thesis is discussed – new emitting species uncovered, triplet exciton migration downhill in the density of states is proved, and a new type of decay never observed before in iridium metal complexes is presented. Properties of iridium(III)tris(1-phenylisoquinoline) Ir(piq)$_3$, an acceptor material in multilayer films, are also summarized.

Before evaporating multilayer structures and modeling triplet dynamics in them diligent literature review has been performed which can be found in chapter 8. In this chapter methods of determining triplet dynamical properties are summarized. Weak and strong points of each method are identified. With the knowledge of this and previous chapters on hand, multilayer structure analysis can easier be performed.

It is generally accepted that simple exothermic triplet transfer between bulk states of two amorphous films occurs (assuming one of them is of much higher triplet energy than the other). In chapter 9 section 1, it is proposed that this is not always the case especially at the interface

between NPB and Ir(piq)$_3$ layers and that the intermediate interface states might be involved. By using time-resolved optical spectroscopy triplet dynamics at the interface of two neat amorphous layers will be exposed. This is not only interesting for OLED device engineers but also for spectroscopists as peculiar form of decay from these types of films are uncovered and discussed. Furthermore a new chapter in the understanding of this physical phenomenon is opened and hopefully will trigger more experimental, computational and theoretical research on triplet movement in interfaces between two amorphous organic layers.

Time resolved luminescence studies on trilayer structures comprising an interlayer NPB, between layers of Ir(piq)$_3$ and Ir(ppy)$_3$ are reported in chapter 9. Structures of the form sapphire/Ir(ppy)$_3$ 5 nm/NPB x nm/Ir(piq)$_3$ 5 nm/ TAPC 100nm/ aluminum 200nm have been sublimed where x is the thickness of NPB inter layer which have been changed from 0 nm to 20 nm. Abbreviation TAPC stands for (1,1-bis((di-4-tolylamino)phenyl)cyclohexane. Ir(ppy)$_3$ is used as a triplet donor, Ir(piq)$_3$ as an acceptor and TAPC and Aluminum are used as neutral capping layers. Here donor Ir(ppy)$_3$ and acceptor Ir(piq)$_3$ are excited with 450 nm nanosecond laser pulse (NPB absorption is negligible at 450 nm) and then emission from acceptor Ir(piq)$_3$ is observed with an iCCD camera. Change of acceptor Ir(piq)$_3$ emission is observed with the change of NPB spacer thickness. In this chapter it is explained how knowledge of triplet dynamics in single layer films are used to get information from complicated time resolved spectra. The importance of the sequence of layer evaporation is shown and relation between such a simple technical aspect and the physics of triplet exciton dynamics between layers is discussed which turned out to be crucial to triplet movement in the interfaces of the analyzed system.

In chapter 9 section 3 new mathematical modeling of triplet migration in bilayer sapphire/Ir(piq)$_3$/NPB films with interface sites is presented. Computer simulated curves fit the experiments very well and confirms the correctness of the model.

In the last chapter the main problems encountered during the course of the thesis are discussed. Guidelines are formulated on how to build structures for further experiments and how to choose materials for the analysis of these types of physical problems. Main hindrances in simulations are named and possible solutions suggested. Finally, conclusions are drawn.

References

1.   B. W. D'Andrade and S. R. Forrest, Adv. Mater. 16 (18), 1585-1595 (2004).

2.   OLED-Info.com, edited by R. Mertins, accessed on 10/09/2010.

3.   P. W. Atkins, *Molecular Quantum Mechanics*, Second Edition ed. (Oxford University Press, 1983).

4.   Z. Kafafi, *Organic Electroluminescence* (Tailor & Francis Group, LLC, 2005).

5.   D. Y. Kondakov, J. Appl. Phys. 102, 114504 (11) (2007).

6.   D. Y. Kondakov, J. Soc. Inf. Disp. 17 (2), 137-144 (2009).

7.   C. Adachi, M. A. Baldo, M. E. Thompson and S. R. Forrest, J. Appl. Phys. 90 (10), 5048-5051 (2001).

8.   Y. Kawamura, K. Goushi, J. Brooks, J. J. Brown, H. Sasabe and C. Adachi, Appl. Phys. Lett. 86 (7), 071104 (2005).

9.   T. Aimono, Y. Kawamura, K. Goushi, H. Yamamoto, H. Sasabe and C. Adachi, Appl. Phys. Lett. 86 (7), 071110 (2005).

10.   M. A. Baldo, D. F. O'Brien, Y. You, A. Shoustikov, S. Sibley, M. E. Thompson and S. R. Forrest, Nature 395 (6698), 151-154 (1998).

11.   S. Lamansky, P. Djurovich, D. Murphy, F. Abdel-Razzaq, H. E. Lee, C. Adachi, P. E. Burrows, S. R. Forrest and M. E. Thompson, J. Am. Chem. Soc. 123 (18), 4304-4312 (2001).

12.   B. W. D'Andrade, M. E. Thompson and S. R. Forrest, Adv. Mater. 14 (2), 147-151 (2002).

13.   Y. Sun and S. R. Forrest, Appl. Phys. Lett. 91 (26), 263503 (2007).

14.   Y. R. Sun and S. R. Forrest, Org. Electron. 9 (6), 994-1001 (2008).

15.   V. Sivasubramaniam, F. Brodkorb, S. Hanning, H. P. Loebl, V. van Elsbergen, H. Boerner, U. Scherf and M. Kreyenschmidt, J. Fluor. Chem. 130 (7), 640-649 (2009).

16.   M. A. Baldo, M. E. Thompson and S. R. Forrest, Nature 403 (6771), 750-753 (2000).

17.   G. Schwartz, S. Reineke, T. C. Rosenow, K. Walzer and K. Leo, Adv. Funct. Mater. 19 (9), 1319-1333 (2009).

18.   M. E. Kondakova, J. C. Deaton, T. D. Pawlik, D. J. Giesen, D. Y. Kondakov, R. H. Young, T. L. Royster, D. L. Comfort and J. D. Shore, J. Appl. Phys. 107 (1), 014515 (2010).

19.   S. Reineke, F. Lindner, G. Schwartz, N. Seidler, K. Walzer, B. Lussem and K. Leo, Nature 459 (7244), 234-238 (2009).

20.   S. Reineke, K. Walzer and K. Leo, Phys. Rev. B 75 (12), 125328 (2007).

21.   F. X. Zang, T. C. Sum, A. C. H. Huan, T. L. Li, W. L. Li and F. R. Zhu, Appl. Phys. Lett. 93 (2), 023309 (2008).

22.   D. Hertel and K. Meerholz, J. Phys. Chem. B 111 (42), 12075-12080 (2007).

23.   C. Rothe and A. P. Monkman, Phys. Rev. B 68 (7), 075208 (2003).

24.   R. Richert and H. Bassler, Chem. Phys. Lett. 118 (3), 235-239 (1985).

25.   V. Jankus, C. Winscom and A. P. Monkman, J. Phys.-Condens. Matter 22 (18), 185802 (2010).

26.   M. A. Baldo and S. R. Forrest, Phys. Rev. B 62 (16), 10958-10966 (2000).

27.   N. C. Giebink, Y. Sun and S. R. Forrest, Org. Electron. 7 (5), 375-386 (2006).

28.   M. A. Baldo, C. Adachi and S. R. Forrest, Phys. Rev. B 62 (16), 10967-10977 (2000).

29.   D. Hertel, H. Bassler, R. Guentner and U. Scherf, J. Chem. Phys. 115 (21), 10007-10013 (2001).

30.   M. Grunewald, B. Pohlmann, B. Movaghar and D. Wurtz, Philos. Mag. B-Phys. Condens. Matter Stat. Mech. Electron. Opt. Magn. Prop. 49 (4), 341-356 (1984).

31.   B. Movaghar, M. Grunewald, B. Ries, H. Bassler and D. Wurtz, Phys. Rev. B 33 (8), 5545-5554 (1986).

32.   B. Movaghar, B. Ries and M. Grunewald, Phys. Rev. B 34 (8), 5574-5582 (1986).

33.   H. J. Peng, X. L. Zhu, J. X. Sun, X. M. Yu, M. Wong and H. S. Kwok, Appl. Phys. Lett. 88 (3), 033509 (2006).

34.   D. Tanaka, H. Sasabe, Y. J. Li, S. J. Su, T. Takeda and J. Kido, Jpn. J. Appl. Phys. Part 2 - Lett. Express Lett. 46 (1-3), L10-L12 (2007).

35.   J. H. Lee, H. H. Tsai, M. K. Leung, C. C. Yang and C. C. Chao, Appl. Phys. Lett. 90 (24), 243501 (2007).

36.   H. I. Baek and C. H. Lee, J. Phys. D-Appl. Phys. 41 (10), 105101 (2008).

2 Theory: excited states in conjugated molecules

In this thesis, we will be dealing mainly with organic materials. Majority of materials based on carbon atoms are called organic. However, only conjugated aromatic hydrocarbons are used in OLEDs (figure 2.1). The molecules of organic materials in a solid state are connected with Wan der Walls type bonds whereas for example inorganic materials are connected via much stronger covalent (or ionic) bonding. Thus, organic films tend to form more disordered structures than for example inorganic semiconductors. In addition, even in a solid state individual molecule properties are extremely important in organic films due to reasons outlined below. That is why before exploring luminescence properties in the solid state organic materials researchers tend to investigate materials in dilute solutions as it might give some insight into the behavior of excitons in films. Indeed, in Chapter 5 of this thesis it will be shown how studies of organic materials dissolved in solution can help to elucidate behavior of phosphorescence and fluorescence in thin films.
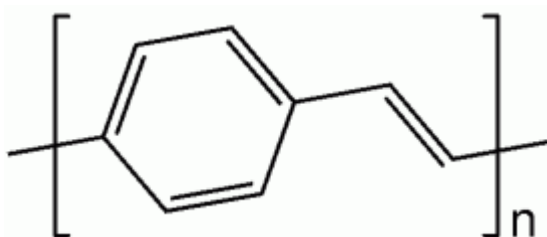
Figure 2.1 Chemical structure of conjugated molecule poly(p-phenylene vinylene) PPV.

2.1 Conjugation in organic molecules

A carbon atom, the main constituent of organic molecules, has six electrons, two of them being in the inner s type orbital and four of them in the outer orbital. Two electrons out of these four in the outer orbital are in an s type orbital whereas two are in a p type orbital. In non-conjugated organic molecule such as methane, the outer orbital electrons can form four equivalent hybridized sp^3 bonds that accounts for the four bonds that the carbon atom can form with other atoms (e.g. hydrogen). In conjugated molecules and polymers the carbon atom hybridise to three sp^2 orbitals and one p_z orbital (for example in ethene). The three sp^2 orbitals lie in one plane, separated 120°, and form strongly localised σ bonds. The remaining p_z orbital forms a π bond where electrons are not as localised as electrons in the σ bonds. If in conjugated polymer the extended carbon chain (backbone) is built up by sp^2 bonded carbon atoms and their number is large, the electrons in the π orbitals can be delocalized over several carbon atoms and are perpendicular to the plane of σ bonds[1]. In molecules π orbitals may be delocalized over all or

part of the molecule. Depending on the overlap of the π orbitals the range of the delocalisation can differ and the extension of the delocalisation defines the conjugation length of the polymer. Consequently, the conductivity characteristics of the polymer or molecule depend on the conjugation length of polymer or molecule[2]. Further, not only conductivity characteristics depend on the π orbitals, but also the photophysical properties[3]. After irradiation with electromagnetic waves normally the electrons from the π orbitals participate in absorption and fluorescence and upon absorption of a photon having the resonating energy with the possible transition, bonding π electrons are excited to the antibonding π* states. In molecules containing heteroatoms (other than C and H) for example nitrogen, non-bonding n orbitals may form. The electrons of these orbitals as well participate in transitions upon the absorption of photons causing n electron to be excited to σ* or π* states. Pauli exclusion principle implies that orbitals have to be filled in pairs with electrons having opposite spins or one electron has to be spin up and one has to be spin down[4]. More in detail this is explained in the next section.

2.2 Forbidden and allowed photophysical transitions

After irradiation with electromagnetic energy organic materials can absorb photons if their energy resonates with optically allowed transitions. After the transition the electron cloud of the molecule is redistributed to a different electronic configuration – from ground state to the excited state. The transition is called allowed if it fulfils certain quantum mechanical rules. The transition is called forbidden if it does not fulfill this set of rules. The possibility of the transition (and consequently oscillator strength) depends on characteristics of electronic states - multiplicity, symmetry, parity and energy[1, 3-4].

First, the probability of transition depends on multiplicity, which is the characteristic that describes electronic state degeneracy. The multiplicity concept comes from electron spin angular momentum which is described by quantum number $s=\pm\frac{1}{2}$. Most important are the states having the multiplicity 3 and 1. According to Pauli's exclusion principle electrons in the same orbit must have opposite spins, so spin number equals zero and multiplicity equals to 1 (singlet state). However in some cases an excited electron and a ground state electron have the same spin direction, the spin number of the state equals to 1 and multiplicity equals to 3 (triplet state). In other words, m (multiplicity) equals to 2s+1. Experimentally this can be detected if one applies a magnetic field to triplet and singlet state. The former splits into three levels whereas the latter state does not. Further, optical transitions from singlet states to triplet states are forbidden (conservation of spin) and optical transition can take place only between the states of the same multiplicity i.e. singlet to singlet and triplet to triplet. Nevertheless, transitions from triplet to singlet multiplicity can still have a finite value and normally is of the order of

10^8 smaller than same multiplicity transitions[3]. This happens due to spin orbit coupling which couples wavefunctions of singlet and triplet states. Heavy metals such as iridium in organic complexes can induce much stronger spin orbit coupling and forbidden triplet to singlet transitions become more allowed and can be very efficient in certain cases[5-6].

Electron dipole transitions between the same symmetry states are forbidden. In other words, the orbitals of the initial and final states have to occupy the same region of space (have large spatial amplitude overlap). It is because of this reason π- π^* transitions are allowed as it is in the same plane and have large spatial overlap. This could not be said about σ orbitals.

Further, the wavefunction of the electronic state having a sign change after reflection through a centre of symmetry is called even (*garade*) and the one, which does not possess the sign change – odd (*ungarade*). Another rule, parity rule, says that transition from the wavefunction of the ground state having even (*garade*) parity to the excited state with odd (*ungarade*) parity is allowed, and transitions from even to even parity and odd to odd are forbidden.

2.3 Main optical transitions in organic molecules

In very general form, photophysical processes in organic molecules are defined as resulting from electronic excitation upon irradiation normally with non-ionizing electromagnetic radiation. Those processes are classified as unimolecular, biphotonic and bimolecular processes[3]. In this section, unimolecular processes that are relevant to the work done in this thesis will be mentioned. To make the discussion easier the following notation was introduced (see Jablonski[7] diagram in figure 2.2) – S_0 - ground singlet state, S_1- first excited singlet state, S_n- higher excited single states, T_1 - first excited triplet state, T_n - higher excited triplet state. Most of processes start with absorption when electron from the singlet ground state is excited to lowest state S_1^v or any other higher singlet state S_n^v. Here v superscript denotes the vibrational energy level. Spin orientation of electrons in each state is indicated in the diagram. Excitations can undergo internal conversion from higher vibronic states to the lowest 0th vibronic state of excited electronic state. Further the excited electron may undergo intersystem crossing to a triplet state and internal conversion (IC-curved lines) from triplet state higher vibronics to the lowest vibronics state of the triplet. Then few events can follow - either triplet-triplet absorption if more photons are available or non-radiative decay from triplet state (not shown) or radiative decay normally termed phosphorescence (PH) which is a formally forbidden process but takes place due to spin orbit coupling. The rate of PH in organic isolated molecules is normally of the order of seconds. From first singlet excited state either a non-radiative decay (IC) or radiative decay termed fluorescence can take place. The fluorescence lifetime is typically in the order of

hundreds of picoseconds to nanoseconds. One has to mention Kasha's rule, which states that all transitions to the ground state, take place via the lowest singlet or triplet excited states. There are some exceptions but this in most cases holds true[3]. Finally radiative transition normally competes with non-radiative. The former lifetime decrease with an increase of the size of molecule [2]. The latter (k_{nr}) depends exponentially on the energy gap ΔE i.e. $k_{nr} \sim \exp(-\Delta E)$ [2].
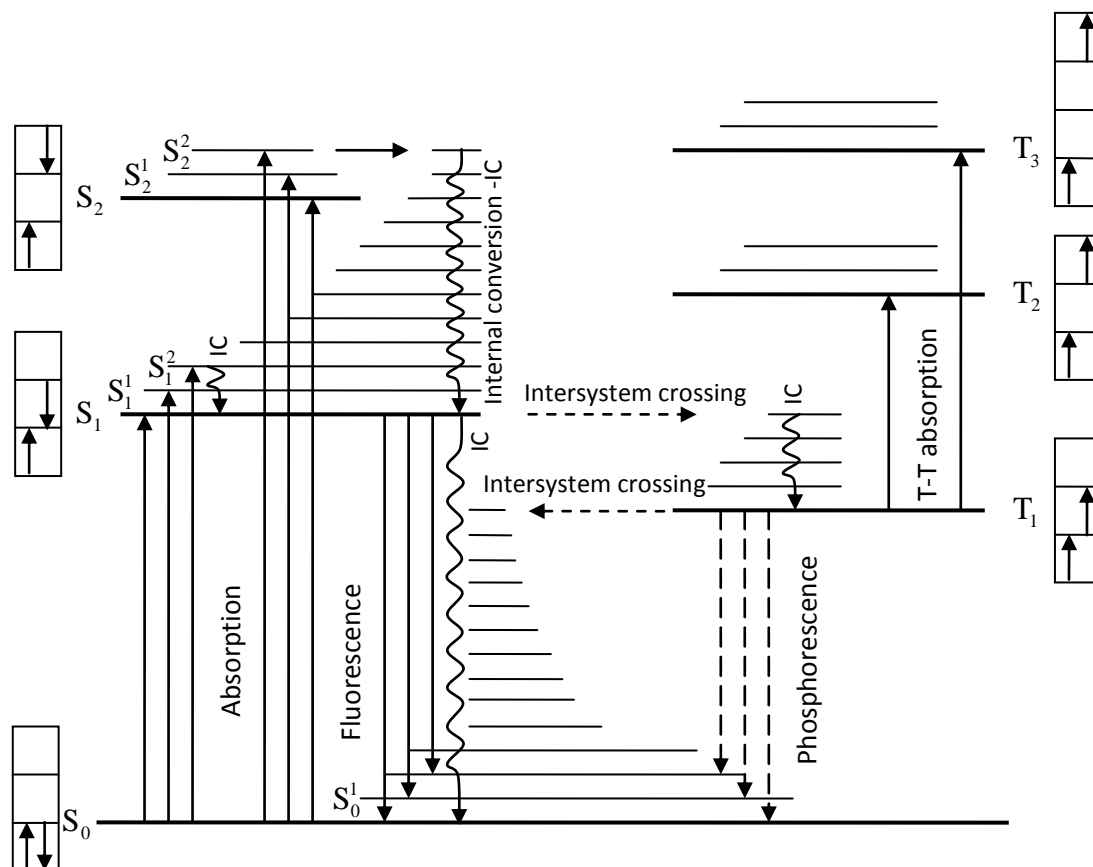
Figure 2.2 Jablonski diagram of some photophysical transitions. Adopted from refs [7-8]. IC is internal conversion (vibrational relaxation). More details in text.

2.4 Rotational and vibrational levels and their relevance to electronic transitions

The total energy of a molecule in the ground state is:

$$E_{TOT} = E_e + E_v + E_r, \qquad (2.1)$$

where E_{TOT} - denotes total energy of the ground state, E_e - electronic energy, E_v - vibrational energy, E_r - rotational energy. Normally rotational modes are important only in gases and are not relevant at room temperature in liquid and solid organic materials. Thus having in mind that only electronic and vibrational energies are important, one could depict absorption in the Jablonski diagram as shown in figure 2.2. For a given electronic state the vibrational levels are labelled 1,2,3 in superscript, no subscript indicating no excess vibrational energy. The transition from 1 vibrational level of the ground singlet state to the S_1 level is called a hot band transition (not shown in the diagram). The physical interpretation of the vibronic transitions (*vibr*ational-electr*onic*) could be seen as the change of equilibrium distance between carbon atoms. For example, consider a $\pi\pi^*$ transition where orbitals become antibonding in the excited state instead of bonding in the ground states. This can be expressed as energy interplay as potential curves in a configurational coordinate space (figure 2.3). However, the rate at which an electronic transition takes place is much shorter (in the range of 10^{15} s^{-1}) than the time needed for the carbon atoms to rearrange themselves after excitation. This is the basis for the Franck-Condon principle which says that intermolecular separation is constant during the absorption of photons (electronic transition) and all the transitions are represented by a vertical line in the diagram configurational coordinate diagram i.e. Franck – Condon diagram (figure 2.3). [1-2]
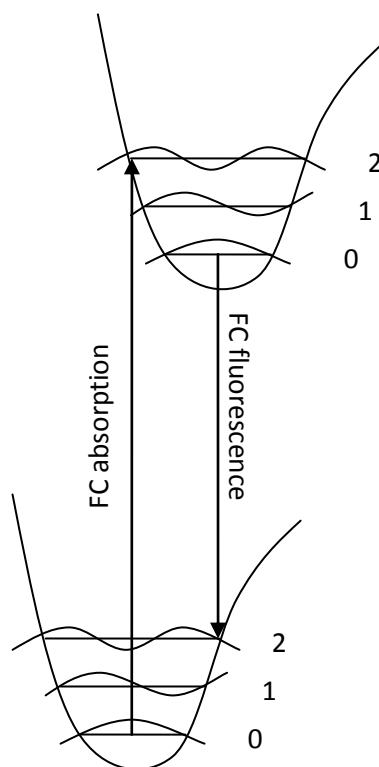
Figure 2.3 Schematic potential energy diagram of wavefunctions of ground and excited electronic states. More details in section 2.4. Adopted from refs [7-8].

The Franck-Condon principle leads us to the Stokes shift between absorption and emission. It is mainly due to the loss of excess vibrational energy (thermalization). If an exciton is excited to higher virbronic levels of S_1^v it relaxes to the lowest vibrational level of S_1 (internal conversion). Furthermore, it can decay into the higher vibrational levels of S_0. Of course, it needs to be mentioned that there maybe other reasons for Stokes shift such as energy transfer, solvent effects, aggregate formation etc.[7]

2.5 Singlet – triplet splitting

Another question arising from the Jablonski diagram is why the triplet level is lower in energy than the singlet level and what influences the size of splitting between singlet and triplet level? It is known that the Pauli exclusion principle states that two paired electrons of an excited state which are correlated to each other avoid collisions, minimize electron-electron repulsion yielding a lower energy state.

The energy of the singlet state E_S is given by[1]:

$$E_S = E_{gap} + J + K \qquad\qquad (2.2)$$

Where E_{gap} is the energy difference between the ground and excited state, J is the Coulomb interaction integral and K is the exchange interaction integral. The energy of triplet state E_T is given by[1]:

$$E_T = E_{gap} + J - K \qquad\qquad (2.3)$$

Coulombic repulsion just increases the energy of both states, whereas the exchange interaction increases the energy of a singlet state but decreases the energy of a triplet state[1]. Thus the splitting between singlet and triplet levels ($E_S-E_T= 2K$) depends on exchange interaction integral 2K which is proportional to the excited state and ground state wavefunction overlap (or in other words overlap between highest occupied molecular orbital-HOMO and lowest unoccupied molecular orbital-LUMO). The bigger this overlap the higher the probability of two electrons to occupy the same point in space hence the higher electon-electron correlation energy increasing singlet-triplet splitting.

2.6 Other types of excited states in organic materials

In the literature, one can find lots of conflicting descriptions of other types excited states excimers, exciplex, polarons etc. The descriptions outlined in this paragraph will be used throughout the thesis. As already, mentioned photoexcitation does not result in separate electron and hole charges as is the case of inorganic semiconductors. The result of photoexcitation in organic conjugated semoconductors is a bound hole and electron pair, which can have a spin multiplicity of 1 or 3, i.e. respectively called singlet or triplet excitons[9]. Injected electrons (or holes) into an organic film significantly distort the bonds of the organic molecules where the charge resides. This charge plus distortion in organic semiconductors is usually referred to as a polaron[9]. An excited state where two polarons (positive and negative) are bound by Coulombic forces but when their exchange interaction is negligible is called bound-polaron pairs. Therefore, this type of state is more easily affected by an applied field and can dissociate into free polarons. Furthermore, it is possible that electron can tunnel via a barrier into the singlet (or triplet) state and emit so called delayed fluorescence. Normally this type of fluorescence has the same spectrum as prompt fluorescence but much longer lifetime[2]. Sometimes bound polaron pairs are called geminate pairs[10]. Other states that can be formed in organic films are aggregates. This term is normally used to refer to a delocalized wavefunction over two or more polymer chain segments or molecules in a ground state. As this is a new ground state normally it is observed as an additional band in the absorption spectra as concentration of material in solution is increased and of course in a film in comparison with dilute solution. These states also sometimes are referred to as dimer states.

Exciplex states can also be created in organic films. These are also called charge transfer states as it is a Coulomb bound electron hole pair with a single wavefunction like of exciton, however, this wavefunction is asymmetrical in such a way, that the electron primarily resides on one chain or molecule whereas hole on another. Thus, the spatial overlap of electron and hole is very weak, meaning that the absorption oscillator strength generally is weak and this state is active in most cases only as excited state[9]. An analogous excited state is an excimer state where the difference from the exciplex is that the wavefunction is symmetrical in such a manner that neither of the chains or molecules holds any sign of the charge i.e. the particle is much more neutral than exciplex. However, it differs from an exciton as it can be localized over couple of chains or molecules, i.e. the spatial overlap can be bigger than in excitons and consequently the energy of this state is smaller. Excimers and exciplexes are interactions between ground state and excited state and the former is a dissociative state therefore excimers and exciplexes cannot be detected using absorption spectroscopy. Excimers, dimers and exciplexes can be very effective pathways of deactivation of excitons in organic films.

2.7 Spectral broadening

The simplest electronic system consists of an electronic ground state and an electronic excited state. Let us assume that ΔE determines the energy width of the electronic state during its lifetime of Δt and from Heisenberg uncertainty principle[11]:

$$\Delta E \Delta t \geq \hbar = h/(2\pi) \qquad (2.4)$$

The higher energy level ΔE_h will have the uncertainty associated with finite lifetime τ_h:

$$\Delta E_h \approx \frac{\hbar}{\tau_h} = \hbar * k_h . \qquad (2.5)$$

Where k_h is the radiative decay rate at this level. The same can be written for the lower energy level ΔE_l (see figure 2.4):

$$\Delta E_l \approx \frac{\hbar}{\tau_l} = \hbar * k_l \qquad (2.6)$$

The total effective energy width will be:

$$\Delta E = \hbar(k_h + k_l) \qquad (2.7)$$

This energy can also be expressed in terms of the frequency width of radiative decay:

$$\Delta E = h\Delta\nu \qquad (2.8)$$

The natural width $\Delta\nu$ of the radiative transition can be defined:

$$\Delta\nu = \frac{k_h + k_l}{2\pi} \qquad (2.9)$$

This can be applied not only to a single 'system' but also to the many equivalent 'systems' and for such systems, normally natural broadening produces a Lorentzian linewidth. The reason for this is that all electronic systems (assuming they make the same radiative transition) produce the same lineshape and the same width, which is the opposite to the inhomogeneous broadening (below).
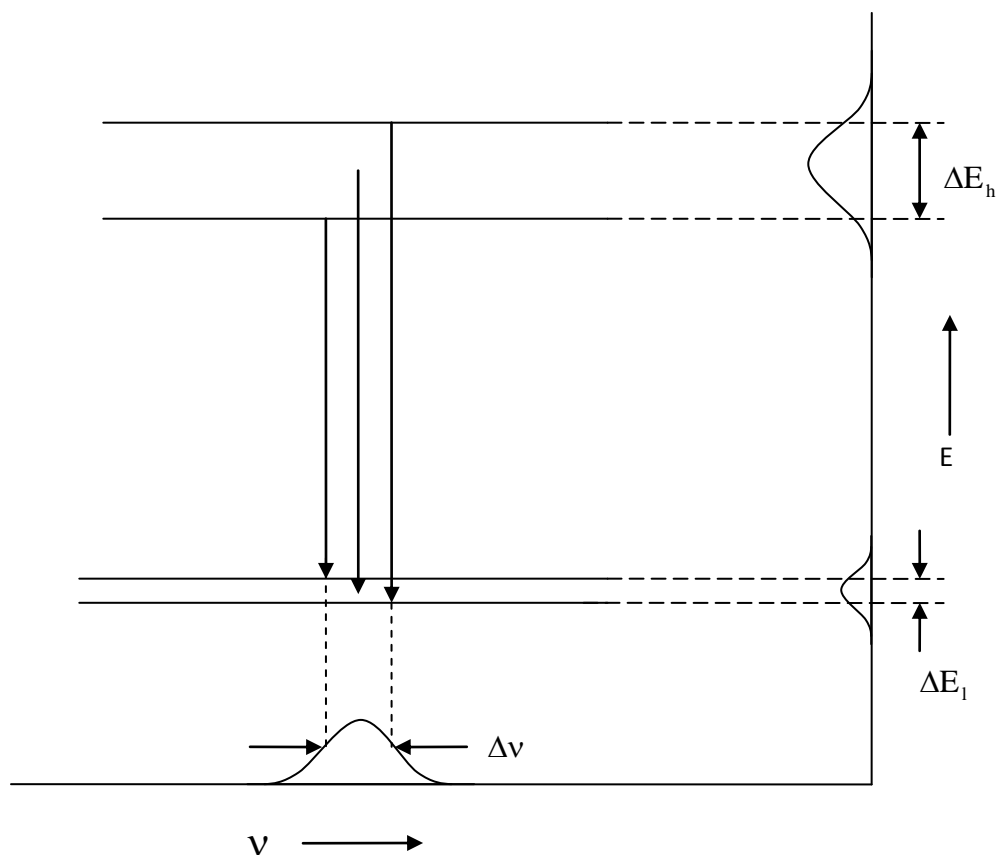
Figure 2.4 Schematic illustration of how the broadening of emission spectrum is formed. On the vertical axis broadened higher and lower energy levels of a molecule is depicted and it is shown how the transitions from higher level to lower level is reflected as a broadened frequency range in a recorded spectrum (horizontal axis). Adopted from ref[11].

2.8 Types of broadening

An increase in decay rate due to collisions with the surrounding medium, other atoms, or molecules, produces a broadening. In other words after interaction with the medium the excited state emits spontaneously. This normally produces the Lorentzian lineshape especially if this happens in the perfect crystal as most of the excited states are affected by the same amount of broadening.

Another type of broadening is not due to the shortening of the lifetime of the state but because of the dephasing of the radiating wave. When this process is dominant over other broadening mechanisms, it usually produces a Lorentzian lineshape.

The Doppler broadening is due to different velocities of molecules in gases which induces the red or blue shift in the wavelength of the moving atoms, molecules (and consequently excited states) thus increasing the linewidth. Normally it induces a Gaussian distribution[11].

Amorphous material broadening happens due to the energetical disorder in the material. Frozen glassy solids tend to have sites oriented differently and randomly towards each other. Thus, the energy of each site might be a bit different due to different local interactions (normally van der Waals forces) what leads to the creation of a Gaussian distribution of energies. The result normally is inhomogeneous broadening of spectra (Gaussian distribution)[11].

2.9 Energy transfer of excitations in conjugated organic molecules and films

Excited states, independently whether they are singlet or triplet excited states, can migrate in a film or can undergo energy transfer between two molecules. One trivial mechanism of transfer is self absorption. Nevertheless, there exist two other non trivial or radiationless transfer mechanisms that are very important in films (as well as in solutions). One of them is known as the resonant or Forster transfer and another as electron exchange or Dexter transfer.

The theory of Forster transfer is quite complex however here only the final equation which is relevant to experimentalists will be described. For a consistent approach, the reader is referred to the following papers [12-13].

Forster transfer is visualized at best when considering isolated donor D and acceptor A at a distance r (for example organic molecules in zeonex matrix at very low mass to mass concentrations). Thus, we can describe the Forster transfer rate $k_T(r)$ as[7]:

$$k_T(r) = \frac{Q_D \kappa^2}{\tau_D r^6} \left(\frac{9000(\ln 10)}{128\pi^5 N n^4} \right) \int_0^\infty F_D(\lambda)\alpha_A(\lambda)\lambda^4 d\lambda \text{, where}$$

$$\kappa^2 = (\cos\theta_T - 3\cos\theta_D \cos\theta_A)^2 \qquad\qquad (2.10)$$

Where Q_D is the quantum yield of the donor in the absence of acceptor, n is the refractive index of the medium, N Avogardo's number, τ_D is the lifetime of the donor in the absence of acceptor, $F_D(\lambda)$ is the corrected fluorescence intensity in the wavelength range λ to $\Delta\lambda$ with the total area under the emission curve normalized to unity, $\alpha_A(\lambda)$ is the exctinction coefficient of the acceptor which is typically in units of $M^{-1}cm^{-1}$ and κ^2 is a factor describing the relative

orientation in space of the donor and acceptor dipoles. θ_T is the angle between the emission transition dipole of the donor the absorption transition dipole of the acceptor, θ_D and θ_A are the angles between these dipoles and the vector joining the donor and the acceptor. Depending on dipole orientations κ^2 can range from 0 to 4 however as the 6th root is taken in calculations variations of κ^2 from 4 to 1 can give only 25 % error (for example in Forster radius calculations, see below). Usually κ^2 is assumed to be 0.67 when the largest error in calculated radius cannot be more than 35%. However if dipoles are perpendicular to each other ($\kappa^2 = 0$) then calculation results could have serious errors[7].

The transfer rate can be expressed in another way[7]:

$$k_T(r) = \frac{1}{\tau_D}\left(\frac{R_0}{r}\right)^6 \qquad (2.11)$$

Where

$$R_0^6 = \left(\frac{Q_D\kappa^2 9000(\ln 10)}{128\pi^5 N n^4}\right)\int_0^\infty F_D(\lambda)\alpha_A(\lambda)\lambda^4 d\lambda \qquad (2.12)$$

If the R_0 value is known, which is determined by the overlap of donor fluorescence and acceptor absorption spectra then the transfer rate can be calculated easily. From the equation 2.11 one can interpret R_0 as the distance where donor Forster transfer rate is equal to donor's decay rate i.e. meaning that half of the donor molecules decay radiatively or non-radiatively and the other half are Forster transferred to the acceptor.

Another important concept is the efficiency of Froster transfer:

$$E_F = \frac{k_T}{\tau_D^{-1} + k_T} \qquad (2.13)$$

2.13 equation tells the fraction of the absorbed molecules by the donor which is transferred to acceptor. For organic molecules R_0 is usually ~5 nm, indicating that this transfer is long range transfer. Forster transfer is more relevant to singlet singlet exciton transfer due to low absorption of triplet state. However, if molecules are close enough for example in solid films and if the wavefunctions of excited states overlap then they can interact via so called Dexter transfer[2]:

$$k_D = \frac{2\pi}{\hbar} |\beta_{DA}|^2 \int f_D(E) \, F_A(E) \, dE$$

where

$$f_D(E) = E^{-3} A(E) [\int E^{-3} A(E) dE]^{-1} \text{ and}$$

$$F_A(E) = E^{-1} \alpha(E) [\int E^{-1} \varepsilon(E) dE]^{-1}$$

(2.14)

where $|\beta_{DA}|^2$ is the exchange energy interaction between molecules, E is the energy, $f_D(E)$ and $F_A(E)$ are normalized phosphorescence spectrum of donor and normalized absorption spectrum of acceptor, respectively. $A(E)$ and $\alpha(E)$ are the emission and absorption curves of donor and acceptor, respectively. Dexter transfer could be visualized as simultaneous two electron transfer (or hole transfer in two molecule HOMOs an electron transfer in two molecule LUMOs)[14].

One could simplify all the above expressions to uncover the essence of both transfers in the following way as was done in a review about triplet states by Kohler *et al* [15]:

$$k_T \sim \frac{f_{od} f_{oa}}{R^6 \nu^2} J \text{ and } k_D \sim J \exp(-2R/L_{orb})$$

where

$$J = \int_0^\infty A(\nu) \alpha(\nu) d\nu \text{ with } \int_0^\infty A(\nu) d\nu = \int_0^\infty \varepsilon(\nu) d\nu = 1$$

(2.15)

R is the donor acceptor separation, L_{orb} is the effective average orbital radius of donor and acceptor sites, f_{od} and f_{oa} are oscillator strengths of donor and acceptor respectively, ν is in wavenumbers. The reason why k_D changes exponentially with donor acceptor distance comes from the fact that electron cloud densities usually decrease exponentially as the distance between electron and nucleus is increased. Normally Dexter transfer is active when molecules are in very close distance i.e. 1-1.5 nm. It is important to note that triplet transfer normally takes place via Dexter mechanism (electron exchange mechanism). Furthermore there were some attempts to express probability of triplet transfer via Dexter mechanism by the product of an electron transfer and a hole transfer probabilities, though one has to admit this view is oversimplified[14]. Nevertheless, this implies that triplet migration and transfer in organic solid films is conceptually very similar to charge transfer processes.

Finally, by comparing the Dexter equation the with Forster equation we can conclude the following. The rate of Forster transfer decreases as R^{-6} and the rate of exchange transfer ignoring stereoelectrical effects is proportional to $\exp(-2R/L_{orb})$[1]. The transfer rate of the dipole mechanism scales with the oscillator strength of the donor emission and acceptor absorption but

not for Dexter mechanism. For both types of mechanisms, the transfer rate depends on spectral overlap J (2.15).

2.10 Bimolecular transitions

Besides unimolecular transitions, at very high excitation densities bimolecular transitions can dominate the photophysics of organic films. Some of the most important are triplet-triplet annihilation, singlet-singlet annihilation and singlet-triplet annihilation.

Triplet-triplet annihilation might be a very relevant exciton depletion mechanism in films of organic molecules. One could describe it as triplet collision and annihilation of each other consequently producing some other species.

$$T_1 + T_1 \rightarrow T_n + S_0$$
or   (2.16)
$$T_1 + T_1 \rightarrow S_n + S_0$$
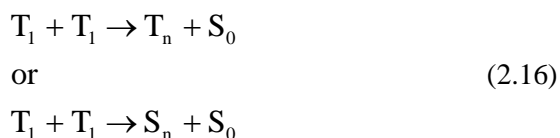
Thus, two triplets can create one triplet or one singlet. The probability of singlet creation is $1/9^{th}$ [15-16]. Here the intermediate creation of quadruplet states is ignored. The singlet exciton then can relax to S_1 and subsequently emit light. This delayed fluorescence emission though will have similar spectrum shape to that of prompt fluorescence emission but will have much longer lifetime. As already has been discussed, geminate pairs (bound hole-electron pairs) can give delayed fluorescence emission[10], however the latter scales linearly with initial excited state density whereas the former will depend upon the square of initial excited state population. TTA normally is realized as triplets migrate via Dexter transfer.

It is well known that singlets can be quenched by triplets and this process might reduce electroluminescence efficiency in OLEDs as well[17-18]. A bimolecular reaction where an excited singlet states meets with a triplet state and by annihilating, passes its energy to the triplet, exciting it to a higher triplet level, is called singlet-triplet annihilation:

$$S_1 + T_1 \rightarrow T_n + S_0$$ (2.17)

This mechanism is spin allowed and very similar to Forster transfer mechanism and depends on the overlap of singlet fluorescence spectrum with the triplet absorption to higher lying triplet states[1]. Triplet energy transfer to a singlet is not possible as the triplet transition to the singlet

ground state is forbidden. Another mechanism where a singlet transfers its energy to another singlet and excites it to a higher lying levels is as well possible and acts similarly as singlet – triplet transfer (via Forster mechanism). Singlet singlet annihilation like TTA leads to non-linear excitation dose dependency on the initial number of excitation states[18].

$$S_1 + S_1 \rightarrow S_n + S_0 . \qquad\qquad (2.18)$$

2.11 References

1.   N. J. Turro, *Modern Molecular Photochemistry*. (The Benjamin/Cummings Publishing Company, Inc, Menlo Park, California, 1978).

2.   M. Pope and C. E. Swenberg, *Electronic Processes in Organic Crystals*. (Oxford Univresity Press, New York, 1982).

3.   J. B. Birks, *The Photophysics of Aromatic Molecules*. (John Wiley & Sons Ltd, London, 1970).

4.   P. W. Atkins, *Molecular Quantum Mechanics*, Second Edition ed. (Oxford University Press, 1983).

5.   H. Yersin, *Highly Efficient OLEDs with Phosphroescent Materials*. (Wiley-VCH Verlag GmbH & Co. KGaA, Weinheim, 2008).

6.   Y. Kawamura, K. Goushi, J. Brooks, J. J. Brown, H. Sasabe and C. Adachi, Appl. Phys. Lett. 86 (7), 071104 (2005).

7.   L. R. Lakowicz, *Principles of Fluorescence Spectroscopy*. (Kluwert Academic / Plenum Pyblishers, New York, 1999).

8.   S. P. McGlynn, T. Azumi and M. Kinoshita, *Molecular Spectroscopy of Triplet State*. (Prentice-Hall Inc., Englewood Cliffs, N.J., 1969).

9.   G. Hadziioannou and G. G. Malliaras, *Semiconducting Polymers*. (Wiley-VCH Verlag GmbH & Co. KGaA, Weinheim, 2007).

10.   V. R. Nikitenko, D. Hertel and H. Bassler, Chem. Phys. Lett. 348 (1-2), 89-94 (2001).

11.   W. T. Silfast, *Laser Fundamentals*. (Cambridge Universtiy Press, 1996).

12.   D. L. Dexter, J. Chem. Phys. 21 (5), 836-850 (1953).

13.   T. Forster, Discussions of the Faraday Society (27), 7-17 (1959).

14.   G. L. Closs, M. D. Johnson, J. R. Miller and P. Piotrowiak, J. Am. Chem. Soc. 111 (10), 3751-3753 (1989).

15.   A. Kohler and H. Bassler, Mater. Sci. Eng. R-Rep. 66 (4-6), 71-109 (2009).

16.   J. Mezyk, R. Tubino, A. Monguzzi, A. Mech and F. Meinardi, Phys. Rev. Lett. 102 (8), 087404 (2009).

17.   Y. F. Zhang, M. Whited, M. E. Thompson and S. R. Forrest, Chem. Phys. Lett. 495 (4-6), 161-165 (2010).

18.   S. M. King, D. Dai, C. Rothe and A. P. Monkman, Phys. Rev. B 76 (8), 085204 (2007).

3 Energetic disorder influence on excited triplet state: theory, Monte Carlo simulations and experiment overview

3.1 Introduction

The description of excited states in conjugates molecules especially solid films has been actively disputed among researchers. One campus represented by scientists such as Su, Schrieffer and Heeger[1] have argued in favor of one dimensional semiconductor model i.e. a band model similar to inorganic materials. Indeed the electronic properties of materials like polyacetylene resembles band structure as described by Heeger[2-3]. However, others, mainly Movaghar, Bassler *et al* have shown that many other organic conjugate materials (polymers and small molecules) behave very differently[4-8]. The model they applied to the analysis of experimental results is based on strongly bound localized excited state electron-hole pairs, excitons. Sometimes this model is called the excitonic model. Due to van der Waals forces between molecules in the solid state, the interaction energies governing the exchange of excitons (and carriers) are relatively small[9]. They are comparable to the lattice vibration modes thus are scattered almost at every point; therefore, no coherent motion is present in these types of materials. Consequentially localization and incoherence excitonic transfer is modeled as single step hopping and the description of band theory is not very helpful[9]. In addition a large amount of experimental proof has been presented in favor of the excitonic model for such materials as benzophenone, polyfluorene and others[8, 10-16]. Thus the excitonic hopping model is adopted to analyze triplet exciton dynamics developed mainly by Movaghar, Bassler *et al* which is reviewed in the following chapters. Firstly theoretical results relevant to experiment interpretation will be reviewed and Monte Carlo simulations and experimental results of triplet dynamics performed so far will be shortly summarized.

One of the most important concepts in organic molecules is that of energetical disorder. The energy of the molecule in a film can be described by an energy matrix having diagonal and non-diagonal elements. Off diagonal elements are a measure of the strength of resonant interactions between molecule and its neighbors[9]. From their value, one can determine the rate at which excitons are exchanged between two resonant neighboring sites and how the rate depends on site separation. Obviously the differences in intersite separation in organic small molecule films affects those terms and consequently this creates so called off diagonal disorder i.e. the energy at each site will be slightly different[9]. Another type of disorder is diagonal, which is described by diagonal energy matrix elements. These diagonal elements indicate site energy when there

are no resonant interactions and it strongly depends on van der Waals forces (excitons) and/or polarization energy (charges). These terms depend on both intermolecular separations and intermolecular orientations consequentially on the structure of the film. Despite the fact that the effects of diagonal and off-diagonal disorders are quite difficult to separate in organic films, in single component systems mostly diagonal disorder dominates. This is because the site coupling between molecules are not very large in organic molecular films, thus the distribution of density of excited states mainly depends on van der Waals forces and polarization i.e. diagonal disorder[9]. This has been verified by experiment and very nicely presented in reviews [9, 17]. Further, it will be reviewed how disorder affects the density of state distributions of charges and excitons.

A simple model of distribution of site energy where sites are prone to intermolecular fluctuations is considered. The model itself is very nicely reviewed, together with the verification of its predictions (in vapor deposited polyacenes and poly(vinyl)carbazole) by Bassler *et al* [9] but originally it was suggested by Silinsh *et al[18]*. Because triplet transport is analogous to charges transport [19-20] description how charge energy distribution broadens due to diagonal disorder (charge DOS broadening) can be used to explain exciton (triplet exciton) DOS broadening.

According to the Haber-Born cycle, the excess positive P^+ and negative P^- charge in solids can be expressed as[9]:

$$P^+ = I_g - I_c$$
$$\text{and} \hspace{4cm} (3.1)$$
$$P^- = A_c - A_g$$

Where I_g is ionization potential of a molecule in gas phase, I_c ionization potential of the molecule in a solid, A_g electron affinity in gas phase and A_c electron affinity in solid phase. In solid A_c and I_c indicates conduction and valence bands. The polarization energy P_i of charge located at the molecule i can be written as:

$$P_i = \sum_{i \neq k} \frac{e^2 \alpha_{pol}}{2 r_{ik}^4}, \hspace{3cm} (3.2)$$

where α_{pol} is the poralizability of surrounding molecules, r – distance, e – elementary charge. Because of intermolecular separation, r, fluctuates, P also has to fluctuate. Further if the distance

distribution is random the distribution function for P_i must be random as well and it has to be a Gaussian[9]:

$$\frac{\Delta P_i}{P_i} \sim \sum_{i \neq k} \left(\frac{\Delta r_{ik}}{r_{ik}} \right) \qquad (3.3)$$

The width of Gaussian of polarization energy distribution is (root mean square standard deviation):

$$\sigma_P = \langle \Delta P \rangle \sim P \left(\left\langle \left(\sum_{i \neq k} \left(\frac{\Delta r_{ik}}{r_{ik}} \right) \right)^2 \right\rangle \right)^{0.5}$$

or $\qquad (3.4)$

$$\frac{\sigma_P}{P} \sim \left\langle \frac{\Delta r}{r} \right\rangle$$

where brackets $< >$ indicate average value and $<\Delta r/r>$ is the average fluctuation. The consequence of statistical disorder is to split both bands valence and conduction into a Gaussian distribution of states having the form:

$$N(E)dE = \frac{N_{eff}}{(2\pi\sigma_P^2)^{0.5}} \exp\left(-\frac{E_0^2}{2\sigma_P^2} \right) dE \qquad (3.5)$$

N_{eff} is the total density of states and equals the molecular density, E is energy (figure 3.1).

In this thesis, it is the exciton density of states (DOS) that is of interest. This has been very well described by Davydov[21]. Passing from gas phase to solvent phase and then to crystal phase assuming two molecules per unit cell both singlet and triplet levels split into two excitonic bands:

$$E(k) = E_g - D^{spl} - L_{11}(k) \pm L_{12}(k) \qquad (3.6)$$

where E_g is the gas excitation energy, D^{spl} is the gas crystal shift term arising from non-resonant interaction between excited molecule and unexcited molecules bath (polarization energies), $L_{11}(k)$ and $L_{12}(k)$ characterize resonance interactions between translationally equivalent and inequivalent molecules appropriately.

Let us suppose that gas crystal D^{spl} in amorphous materials becomes dependent on the van der Waals energies between unexcited and excited molecules in the medium with poralizability α_{pol} [9],

$$D_i^{spl} \sim \alpha_{pol} \sum_{i \neq k} r_{ik}^{-6} \qquad (3.7)$$

Equivalently as with charge polarization distribution the width of density of states:

$$\sigma_{D^{spl}} = \langle \Delta D \rangle \sim D^{spl} \left(\left\langle \left(\sum_{i \neq k} \left(\frac{\Delta r_{ik}}{r_{ik}} \right) \right)^2 \right\rangle \right)^{0.5}$$

or $\qquad (3.8)$

$$\frac{\sigma_{D^{spl}}}{D^{spl}} \sim \left\langle \frac{\Delta r}{r} \right\rangle$$
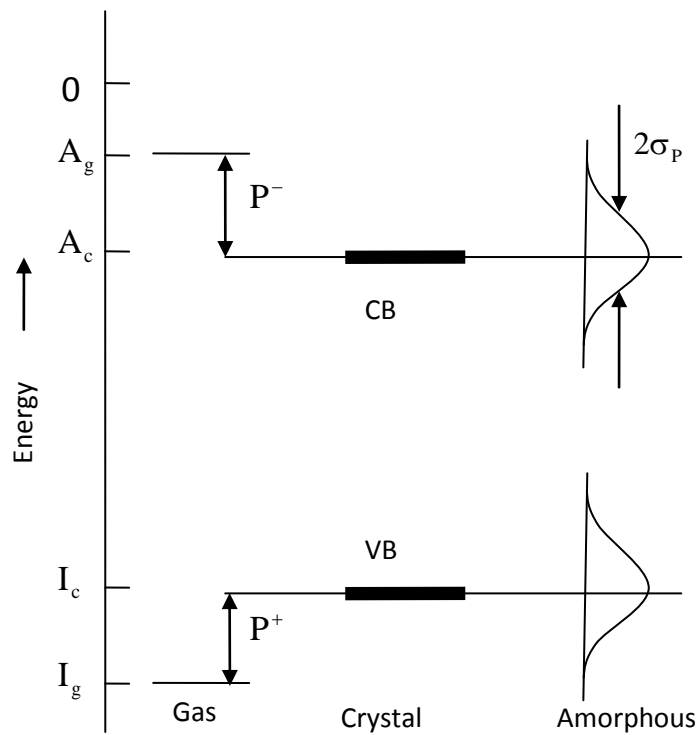
Figure 3.1. Schematic diagram of broadening of charge density of states with the change of phase of organic molecules. I_g is ionization potential of a molecule in gas phase, I_c ionization potential of the molecule in a solid, A_g electron affinity in gas phase and A_c electron affinity in solid phase. σ_P is energetic width of charge distribution. In solid A_c and I_c indicates conduction (CB) and valence bands (VB). Adopted from ref [9].
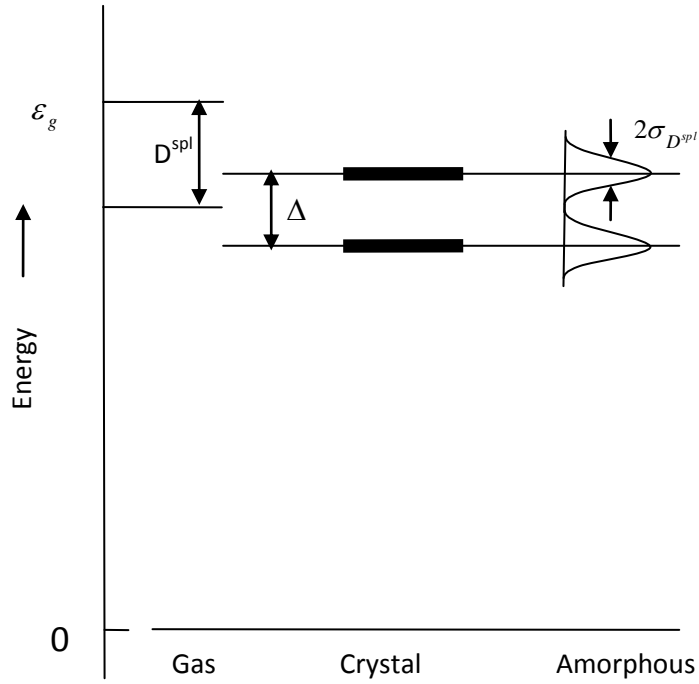
Figure 3.2. Schematic diagram of broadening of exciton density of states with the change of phase in organic molecules. Δ is Davydov splitting which equals to $2L_{12}(k\approx0)$, D^{spl} gas crystal shift term and $\sigma_{D^{spl}}$ is width of excitonic density of states. Adopted from ref [9].

The Gaussian distribution of states:

$$N\left(\Delta D^{spl}\right) = \frac{1}{(2\pi\sigma_{D^{spl}}^2)^{0.5}} \exp\left(-\frac{\Delta D^{spl2}}{2\sigma_{D^{spl}}^2}\right) \qquad\qquad (3.9)$$

The important implication of this is that the singlet (or triplet) energy density of states profile now has a Gaussian distribution. Further, the whole DOS distribution can be excited directly. Thus, the absorption profile should represent the broadening due to disorder.

Suppose at time t = 0 sites are randomly excited within the Gaussian DOS (figure 3.3) by a pulsed laser. At time 0 the average energy of the excited states is higher than k_BT (assuming a finite temperature). Then one can decompose triplet migration in organic disordered materials into an array of incoherent jumps between the localized energy states, which constitutes the density of states (DOS).
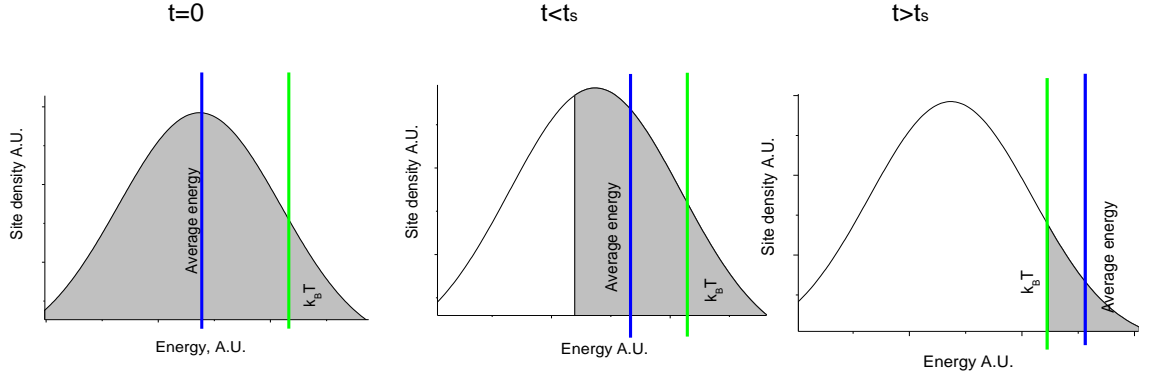
Figure 3.3. The population of the Gaussian DOS as the time lapses after pulsed excitation. The grey areas indicate the possible sites 'to-visit' for an exciton. As time lapses there is less and less grey area and so fewer sites possible to visit which translates into a nonlinear increase of site visiting and time dependent diffusion coefficient. t_s is time when average energy becomes equal to k_BT.

It was proven by experiment and Monte Carlo simulations[22-23] that after excitation (or after time 0), but before a time called the critical time t_s, triplet excitons migrate towards the lower energy tail of the (Gaussian) DOS, only executing downward jumps in energy (percolation) as the k_BT is too small to have any effect on the dynamics of the triplets. In other words, triplets are diffusing in a system due to percolation but not thermal hopping as k_BT is much smaller than the average triplet state energy. This regime is normally called the non-equilibrium dispersive regime as triplets move down the energy scale in such a way creating spectral dispersion. At a time t_s the average energy becomes equal to k_BT, which indicates that the diffusion due to percolation and diffusion due to thermal hopping are equal. Diffusion can be described by a quantity known as the diffusion coefficient which in turn could be described as the derivative of the mean square displacement $\langle \Delta R^2(t) \rangle$:

$$D = \frac{d\langle \Delta R^2(t) \rangle}{dt} \qquad (3.10)$$

The diffusion coefficient D is proportional to the hopping rate, $\nu(t)$, or the derivative of the number of new sites visited $N_s(t)$ over time[22, 24]:

$$D(t) \sim \nu(t) \sim \frac{dN_s(t)}{dt} \qquad (3.11)$$

After $t_{critical}$ thermal hopping becomes dominant in a system which makes the number of possible sites 'to-visit' at each time interval constant i.e.

$$\frac{dN_s(t)}{dt} = \text{const} \qquad (3.12)$$

and $D(t) \sim \nu(t) = \text{const}$. Then $N_s(t) \sim t$ meaning that the number of sites visited increases linearly with time, which describes classical diffusion. This is so called the quasiequilibrium regime (non-dispersive migration) – giving no further energy relaxation in the DOS.

The dispersive migration gives rise to a time-dependent diffusion coefficient because the number of new sites visited does not increase linearly with time. It is simple to visualize this from figure 3.3. The grey areas therein indicate the possible sites 'to-visit' for an exciton. As time lapses there is less and less grey area and so fewer sites possible to visit which translates into a nonlinear increase of site visiting and time dependent diffusion constant. This complicates the determination of the dynamics of triplets in amorphous organic films[6, 10, 12-14]. There have been some efforts to theoretically describe the migration of excited states in disordered materials[4-7]. Monte-Carlo (MC) simulations [22-23, 25] and experimental results using polymers and some small organic molecules[10, 12-15] showed that some of the theoretical considerations could be applied to the interpretation of experiments or calculations. Here, is outlined the theory that has been used in this thesis for triplet migration data analysis. The reader is referred to the original papers for a more rigorous approach[4-7].

3.2 Theory

Incoherent triplet exciton migration in organic materials is described by the Miller-Abraham equations[5],

$$\begin{aligned}
\nu_{ij} &= \nu_0 e^{-2\beta R_{ij}} e^{-(E_j - E_i)/kT}, E_i < E_j, \\
\nu_{ij} &= \nu_0 e^{-2\beta R_{ij}}, E_i > E_j,
\end{aligned} \qquad (3.13)$$

where ν_{ij} is triplet hopping rate, T - temperature, k - the Boltzmann constant, E - energy of the localized state, β is the inverse localization length, R_{ij} is the separation between two localized states, ν_0 denotes the attempt-to-jump frequency, which is in turn inversely proportional to the dwell time of an exciton t_0 at an energy site[7]:

$$t_0 = \frac{1}{\nu_0 6 e^{(-2\beta R_{ij})}} \qquad (3.14)$$

Neglect of the energy matching condition for downward jumps may be justified by low temperature studies of organic glasses, which suggest that energy dissipation does not limit the hopping rate[12]. This might be explained by the phonon rich spectrum in amorphous organic materials and strong electron-phonon coupling which facilitates relaxation[22].

As already mentioned the movement of excited states takes place within a DOS which has an assumed Gaussian distribution[9],

$$n(E) = \frac{1}{(2\pi\sigma^2)^{1/2}} e^{(-E^2/2\sigma^2)} \qquad (3.15)$$

σ being the width of the distribution.

After a laser pulse excitation, intersystem crossing from singlet to triplet manifold takes place, the initial population of triplets is equal to $[T_0]$ (initial condition at t = 0, $[T] = [T_0]$) which is then depopulated by monomolecular processes i.e. radiative decay at a rate k_r and non radiative decay rate k_{nr} as well as by bimolecular processes, for example, via triplet-triplet annihilation (TTA), rate k_{TT}[26]:

$$\frac{d[T]}{dt} = -(k_{nr} + k_r)[T] - k_{TT}[T]^2 \qquad (3.16)$$

where [T] denotes the triplet concentration function. Typically, the radiative lifetime of triplet excitons in these materials is very long, in the range of hundreds of miliseconds (especially at low temperatures), thus in most cases monomolecular processes can be neglected. Then one can solve for [T] considering k_{TT} being time independent to get

$$[T] = \frac{[T_0]}{(1 + k_{tt}[T_0]t)} \qquad (3.17)$$

and solve for k_{TT} being time-dependent to get

$$[T] = \frac{[T_0]}{1 + [T_0]\int k_{tt}(t)dt} \qquad (3.18)$$

If (3.17) is differentiated an expression for the delayed fluorescence signal arising from TTA can be written as

$$DF \sim \frac{d[T]}{dt} = k_{tt}[T_0]^2 \frac{1}{(1 + k_{tt}[T_0]t)^2} = k_{tt}[T]^2 \qquad (3.19)$$

From this, measurement of the time dependent DF decay signal will yield the diffusion coefficient D (from k_{TT}) since it can be expressed in this way[13]:

$$k_{tt} = 8\pi f_R R D \qquad (3.20)$$

where f_R is the fraction of triplets annihilated by encounter, and R the interaction radius.

However, it is not simple, if there is a time-dependent, dispersive diffusion coefficient, such as in equation (3.18). Unfortunately, in disordered materials, this is the case. As was mentioned above, triplet diffusion consists of two main regimes, at early times triplet excitons relax towards the low-lying energy sites in the Gaussian DOS. This regime is normally referred to as the non-equilibrium dispersive regime marked by a change of diffusion coefficient D(t) in time. Further, it needs to be said that, while in the dispersive non-equilibrium region the quantity DF~d[T]/dt follows a power law t^{-b} with an exponent close to -1. This is very unintuitive result, nevertheless, this has been confirmed with experiments and Monte Carlo simulations many times (see next section for more details) [13-14, 23]. After a certain time, this regime turns to a classical equilibrium non-dispersive regime, where the diffusion coefficient approaches the value D_∞. Then the exponent becomes –2, as one intuitively should expect for a bimolecular decay rate equation (3.16) and its solution (3.17). The transition time t_s between the two regimes strongly depends upon the available activation energy, and therefore upon temperature, and the expression it follows has been analytically derived using effective medium approximation techniques by Movaghar *et al* [4] and confirmed by the Monte Carlo (MC) calculations of Ries *et al* [22, 25]:

$$t_s(T) = t_0 e^{(c\sigma/k_b T)^2} \qquad (3.21)$$

where σ is the Gaussian density of states variance, c is a constant depending on dimensionality (0.67 in the 3D migration case), t_0 is the dwell time (jump time) for triplets if σ is 0 or if T approaches ∞, and k_B is the Boltzmann constant.

At very low temperatures or in materials having high energy disorder described by the disorder parameter $\sigma^* = \sigma/k_B T$ this transition time becomes infinitely long, i.e. the transport is always dispersive non-equilibrium and the diffusion coefficient depends on time. In other words, the triplets are trapped and the relaxation to the tail of DOS (equilibrium) takes an infinitely long time. Unfortunately it is not possible to cast this time dependent diffusion coefficient into any simple analytical expression and it heavily depends on the activation energy available i.e. temperature. There are a few analytical approximations [4-7] however the form of the density of states (Gaussian) makes this task difficult and most of the solutions are derived using limiting assumptions. For example Movaghar et al [6] succeeded in deriving the diffusion coefficient expression for highly disordered materials, i.e. when $T \rightarrow 0$ the condition $kT < 0.1\sigma$ is satisfied and when time approaches infinity:

$$D(t) \sim \frac{1}{t \ln(\nu_0 t)} \qquad (3.22)$$

The other parameter of interest for experimentalists is the peak energy of the DOS distribution needed to determine the non-relaxed triplet levels of the material. As was mentioned, the excited energy randomly distributed at first, migrates down towards the DOS energy tail in time thus preventing us from finding the real triplet energy level at near-zero times since in early times it is very hard to record very weak phosphorescence spectra. However, Richert et al [7] derived an expression describing how the peak energy of the triplet DOS (E_P) changes in the long time limit when $T \rightarrow 0$, under the condition $kT < 0.1\sigma$:

$$E_p \sim -\sigma(3\ln(\ln \nu_0 t))^{\frac{1}{2}} \qquad (3.23)$$

For example, this expression will enable us to find the unrelaxed triplet energy level of N,N'-diphenyl-N,N'-bis(1-naphthyl)-1,1'-biphenyl-4,4''-diamine (NPB), as the triplet levels which are normally measured at very late times after excitation are normally already in the tail of the DOS.

3.3 Monte Carlo simulations and experiments relevant to the thesis

There are a few published Monte Carlo simulations of triplet exciton transport in disordered materials[22-23, 25]. The most interesting for the purposes of this thesis is Monte Carlo simulations

of bimolecular exciton annihilation in energetically random hopping system by Scheidler *et al* [23]. The first principles of these simulations as well as main results are outlined below.

A cubic lattice with the 64x64x64 sites was taken and the lattice parameter was chosen to be 0.6 nm [23]. Random energies were assigned to the sites with Gaussian distribution (of the form of (3.15)) with Gaussian width of 42.4 meV. Then a certain number of excitations with infinite lifetime are generated simultaneously at time 0 at 0.3% and 1% of sites. They are allowed to execute hops within a sphere of radius to a six nearest neighbor sites to simulate Dexter type process. The jump rate was assumed to be of Miller-Abrahams type (of the form (3.13)). Computations were then made for different temperatures. The purpose of the simulation was to simulate bimolecular reactions among triplet excitations. They were considered to happen once two excitons encounter at the nearest neighbor sites. In the case of triplet excitations the total spin of S of the pair state can be either 0, 1 or 2 with appropriate probabilities of 1/9, 1/3 and 5/9. It was assumed that quintet states lead to scattering.

Simulated temporal decay of excitons as well as decay rate or in other words bimolecular decay of exciton annihilation (i.e. triplet-triplet annihilation leading to delayed fluorescence type process) at different temperatures are depicted in reference [23] figures 1 and 2. The main results from these simulations are that the triplet decay slope at very low temperatures is almost negligible and only at late times does the decay curve slightly. As temperature is increased, the decay approaches a power law with the slope -1. The delayed fluorescence decay rate at low temperatures follows the law with the slope of -1 whereas at high temperatures it approaches a power law with the slope of -2 as expected. The deviations of both phosphorescence and delayed fluorescence from expected behavior according to equations (3.17) and (3.19) at low temperatures regime is ascribed by authors to the fact that bimolecular annihilation coefficient is not constant and time dependent random walk or dispersive regime is dominant at low temperatures. Upon increase of temperature the regime turns to classical non-dispersive, which is the reason why then equations (3.17) and (3.19) can be used to explain the results.

Similar behavior is observed in experiments. For example, Hertel *et al*[14] and Rothe *et al*[13] looked into the triplet properties of polyfluorene polymers (films and solutions). The results are almost identical to the Monte Carlo simulations described above. Rothe et al. used the 3rd harmonic of a YAG laser and gated iCCD camera with a method of successively increasing gate and delay times described here in the experimental section (chapter 4) to record the decay of triplets and delayed fluorescence. Also, they used triplet pump probe experiments to probe triplet decay at earlier times. The results are in striking agreement with theoretical considerations and Monte Carlo simulations described above. Decay of delayed fluorescence in polyfluorene films at low temperatures follow power law with the slope ~-1 (ascribed by

authors to dispersive hopping) and approaches classically predicted regime with the slope ~-2 (non-dispersive-hopping) at higher temperatures. The form of triplet decay recorded at 15 K using transient absorption is similar to the one predicted by Monte Carlo simulations – in the initial time regions the decay is almost negligible - following a power law with the slope -0.04, whereas at later times it starts to decay exponentially. Almost identical results have been published by Hertel *et al*[14] using YAG laser excitation with the difference that they used integral method to record decays. In addition, Bassler *et al*[12] recorded temporal phosphorescence decay and time resolved spectra in benzophenone glass and concluded that triplet transport in organic glasses is dispersive and that the diffusion coefficient is time dependent at lower temperatures and at early times. All in all these examples in the literature demonstrate that in disordered materials such as polymers or amorphous organic films at low temperatures the dispersive hopping of excitons is dominating at early times and with an increase of thermal energy and consequentially thermally assisted hopping the turnover time between dispersive and non-dispersive classical triplet diffusion regime gradually increases.

3.4 References

1.   A. J. Heeger, S. Kivelson, J. R. Schrieffer and W. P. Su, Rev. Mod. Phys. 60 (3), 781-850 (1988).

2.   W. P. Su, J. R. Schrieffer and A. J. Heeger, Phys. Rev. B 22 (4), 2099-2111 (1980).

3.   W. P. Su, J. R. Schrieffer and A. J. Heeger, Phys. Rev. Lett. 42 (25), 1698-1701 (1979).

4.   M. Grunewald, B. Pohlmann, B. Movaghar and D. Wurtz, Philos. Mag. B-Phys. Condens. Matter Stat. Mech. Electron. Opt. Magn. Prop. 49 (4), 341-356 (1984).

5.   B. Movaghar, M. Grunewald, B. Ries, H. Bassler and D. Wurtz, Phys. Rev. B 33 (8), 5545-5554 (1986).

6.   B. Movaghar, B. Ries and M. Grunewald, Phys. Rev. B 34 (8), 5574-5582 (1986).

7.   R. Richert, H. Bassler, B. Ries, B. Movaghar and M. Grunewald, Philos. Mag. Lett. 59 (2), 95-102 (1989).

8.   U. Rauscher, H. Bassler, D. D. C. Bradley and M. Hennecke, Phys. Rev. B 42 (16), 9830-9836 (1990).

9.   H. Bassler, Phys. Status Solidi B-Basic Res. 107 (1), 9-54 (1981).

10.   R. Richert and H. Bassler, Chem. Phys. Lett. 118 (3), 235-239 (1985).

11.   J. Lange, B. Ries and H. Bassler, Chem. Phys. 128 (1), 47-58 (1988).

12.   R. Richert and H. Bassler, J. Chem. Phys. 84 (6), 3567-3572 (1986).

13.   C. Rothe and A. P. Monkman, Phys. Rev. B 68 (7), 075208 (2003).

14.   D. Hertel, H. Bassler, R. Guentner and U. Scherf, J. Chem. Phys. 115 (21), 10007-10013 (2001).

15.   V. Jankus, C. Winscom and A. P. Monkman, J. Phys.-Condens. Matter 22 (18), 185802 (2010).

16.   R. Richert, B. Ries and H. Bassler, Philos. Mag. B-Phys. Condens. Matter Stat. Mech. Electron. Opt. Magn. Prop. 49 (3), L25-L30 (1984).

17.   A. Kohler and H. Bassler, Mater. Sci. Eng. R-Rep. 66 (4-6), 71-109 (2009).

18.   A. Jurgis and E. A. Silinsh, Phys. Status Solidi B-Basic Res. 53 (2), 735 (1972).

19.   G. L. Closs, M. D. Johnson, J. R. Miller and P. Piotrowiak, J. Am. Chem. Soc. 111 (10), 3751-3753 (1989).

20.   D. Hertel and H. Bassler, ChemPhysChem 9 (5), 666-688 (2008).

21.   A. S. Davydov, Soviet Physics Jetp-Ussr 18 (2), 496-499 (1964).

22.   B. Ries, H. Bassler, M. Grunewald and B. Movaghar, Phys. Rev. B 37 (10), 5508-5517 (1988).

23.   M. Scheidler, B. Cleve, H. Bassler and P. Thomas, Chem. Phys. Lett. 225 (4-6), 431-436 (1994).

24.   G. Schonherr, R. Eiermann, H. Bassler and M. Silver, Chem. Phys. 52 (3), 287-298 (1980).

25.   B. Ries and H. Bassler, Phys. Rev. B 35 (5), 2295-2302 (1987).

26.   M. Pope and C. E. Swenberg, *Electronic Processes in Organic Crystals*. (Oxford Univresity Press, New York, 1982).

4 Experimental

4.1 Sample preparation

All samples were thermally evaporated using a commercial Kurt Lesker Spectros II deposition system (figure 4.1).

Figure 4.1 Kurt-Lesker Spectros deposition system. Taken from http://www.lesker.com.

It is computer controlled single 18" diameter x 36" high stainless steel chamber deposition system with a sliding door. Turbomolecular pumping gives a chamber a pressure of 1E-7 mbar vacuum. The system consists of 6 organic sublimation sources and 3 metal evaporation sources as depicted in figure 4.2. Substrate size can be up to 100 mm x 100 mm and there is the possibility to use different masks as 3 shelves are present where the occupation of each can be controlled manually from outside while the system is in vacuum. Windows 2000, Access 2000, Visual Basic 6 Professional Edition and Pentium IV industrial computer is used to control deposition, and "recipes" are created to perform standard procedures. By linking recipes, complete processes (almost) without interruption of the experimenter can be performed. Various control screens are used to configure the system and its deposition parameters. 3 thermal sources (for deposition of aluminum, lithium fluoride etc.) are separated in space from the organic evaporator sources and powered by thermal source controller and evaporated and controlled using Sigma deposition software. 400 Amps at 5 volts is the maximum current possible that can be used. OLED thermal sources are powered by low temperature controllers and controlled by Sigma software with a maximum temperature of up to 500 ºC. Thicknesses

are determined using quartz crystal film thickness monitors. One is used for all thermal sources, and one for each pair of 6 OLED sources. Thickness monitors were calibrated by evaporating organic material on silicon substrates with known silicon dioxide thickness (deposited in Engineering Department, Durham University). Then real organic material thickness was determined using Spectroscopic Ellipsometer VASE from J.A. Woollam Co., Inc with Cauchy function and/or Gaussian function modeling. Each organic material samples were calibrated using at least 4 different silicon dioxide thicknesses. As the absorption coefficient of the organic layer can be determined during the Cauchy or Gaussian function fitting process, extracted absorption coefficients were double checked with the ones determined using a UV-3600 Shimadzu or Lambda 19 from Perkin Elmer absorption spectrophotometer. Finally, the values were re-checked at least one more time after calibration again using ellipsometer and Cauchy modeling. All these steps assured the accuracy of the readings of evaporator thickness monitors.
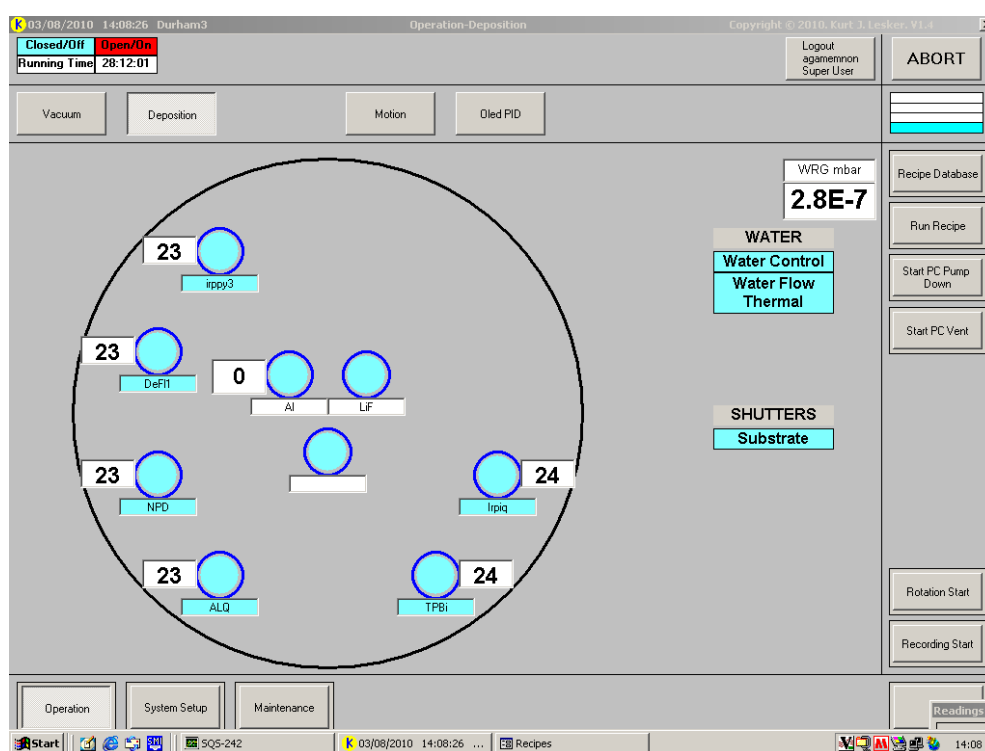
Figure 4.2 Kurt-Lesker Spectros deposition system, deposition window of software.

4,4-N, N′-dicarbazolyl-1,1′-biphenyl (CBP), N,N'-diphenyl-N,N'-bis(1-naphthyl)-1,1'-biphenyl-4,4''-diamine (NPB), Fac-tris(2-phenylpyridine) Iridium (III) (Ir(ppy)$_3$), Iridium (III) Tris(1-phenylisoquinoline) (Ir(piq)$_3$) were received from Eastman Kodak Corporation and used without further purification. All Eastman Kodak materials were vacuum sublimed. (1,1-bis((di-4-tolylamino)phenyl)cyclohexane (TAPC) was received from Sigma Aldrich and used without further purification. Thin films were evaporated using the rate of 2 Å per second (NPB, CBP, TAPC) or the rate of 0.5 Å per second (Ir(ppy)$_3$ and Ir(piq)$_3$), which was much higher than the 0.167 Å per second evaporation rate previously reported to yield films with high excimer

emission for NPB[1]. Sapphire or quartz substrates of 12 mm diameter have been used. Aluminum was evaporated at 1 Å per second rate.

4.2 Steady state spectra measurements

Steady state absorption spectra and excitation spectra of solutions and films were recorded using commercial UV/VIS spectrophotometer (Lambda 19 from Perkin Elmer or UV-3600 Shimadzu). Both spectrometers have a double beam photometric system and photometric range from -6 to 6 A. Resolution is ±0.1 nm and wavelength accuracy ±0.2 nm which is more than needed for recording normally broad spectra of disordered amorphous organic films. Photomultiplier tube detector was used to record UV/VIS spectra of materials reported in this thesis. Halogen and deuterium lamps were switched automatically using inbuilt motor to record spectra in visible or UV region appropriately.

Steady state luminescence emission was recorder using a commercial spectrofluorimeter (Fluorolog FL3-22 from Jobin Yvon). It consist of 450 W xenon light source, double excitation monochromator, sample compartment (90° excitation-emission geometry), double emission monochromator and photoncounting photomultiplier tube detector. Slits of both excitation and emission monochromators can be tuned to increase intensity (at the expense of resolution).

4.3 Time resolved nanosecond system setup
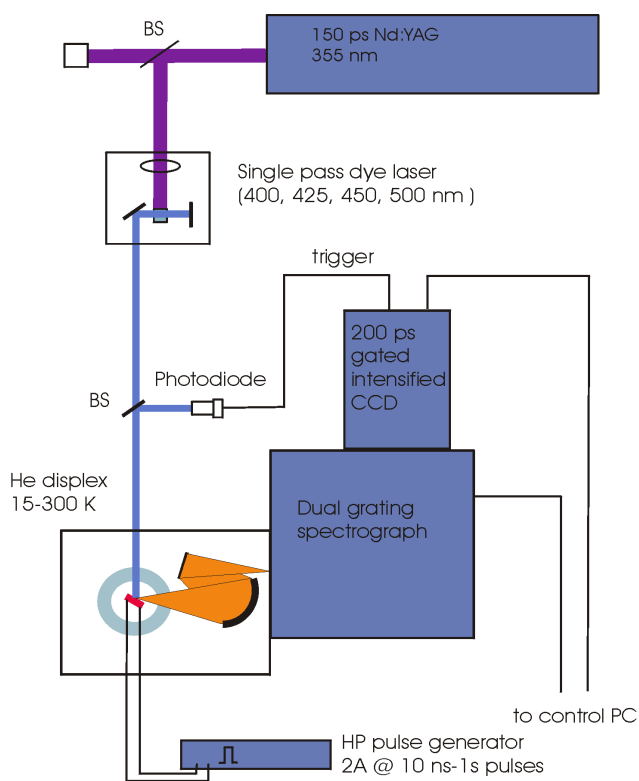
Figure 4.3 Time resolved gated luminescence setup. Sample in He duplex cryostat is excited with Nd:YAG 355 nm laser (or 450 nm dye laser). Dyes with other wavelengths are available if needed. Sample emission is then collected towards spectrograph entrance slit. At the exit slit of spectrograph iCCD camera collects spatially dispersed emission light. PC with software is used for iCCD and spectrograph control.

Gated luminescence and lifetime measurements were made using a system consisting of excitation source, pulsed Nd:YAG laser emitting at 355 nm (EKSPLA) or 450 nm single pass dye laser (Coumarin 450 from Exciton Inc.) pumped by the third harmonic of the Ekspla Nd:YAG laser. Samples were excited at a 45° angle to the substrate plane and the energy of each pulse could be tuned from 100 nJ up to few mJ per pulse (for Nd:YAG Ekspla laser) and up to 30 μJ for dye laser. Sometime another Nd:YAG laser from CryLas has been used which can achieve up to 30 μJ per 2ns length pulse. Emission was focused onto a spectrograph equipped with 300 lines/mm grating of 500 nm or 1000 nm base wavelength and detected on a sensitive gated iCCD camera (Stanford Computer Optics) with sub nanosecond resolution. The emitted light from the sample is dispersed by the spectrograph in space and falls onto 572x736 pixel iCCD at the exit port of the spectrograph. The horizontal pixel direction is calibrated to different wavelengths whereas vertical pixels are normally integrated as in most cases spatial distribution of emission was not important to the work done in this thesis. Camera and laser is

synchronized either by directing laser light via beamspliter onto photodiode which sends electrical signal to camera or by using electrical pulse from laser control block which normally is sent 1 μs before laser pulse emission. The intensity falling onto the detector could be increased by increasing the spectrograph entrance slit from ~0.1 mm to 2 mm at expense of resolution, or vice versa. Gated time resolved spectra were recorded using iCCD camera software 4 Picos where delay times after the trigger pulse and integration time (how long the shutter is open and light is collected) can be controlled to up to 0.1 ns accuracy. Decay measurements were performed by logarithmically increasing gate and delay times (see below). For low temperature measurements (down to 12 K) samples were placed in a cryostat and pumped to at least 1E-4 mbar vacuum. Samples were in at least 1E-4 mbar vacuum even when collecting data at room temperature. Optional HP generator for pulsed electrical excitation (2 ns to 1 s) can be attached.

Wavelength to pixel calibration and spectral resolution of system

Each iCCD pixel was assigned to a specific wavelength using CAL-2000 Mercury-Argon calibration light source (Ocean Optics) with many sharp peaks at known positions over all spectral range. A few pixels were assigned to the sharp peaks and linearly approximated for the pixels in between with accuracy of ~ ±1 nm estimated from variance of linear wavelength to pixel relation. For each spectrograph position (different wavelength region) another calibration was performed. Wavelength to pixel relationship was recalibrated every time after moving the iCCD camera and rechecked if the camera was not moved for a longer period of times. Occasionally it was rechecked using emission from well known organic materials e.g. polyfluorene[2]. The spectral resolution of the system was found by directing the 3rd harmonics of the Nd:YAG laser into spectrograph and consequentially iCCD and the value of 1 nm was found (full width at half maximum). This is more than theoretical resolution of the system (300 nm/736 pixels~0.4 nm) which is probably caused by iCCD not being exactly at the right angle to the spectrograph. However, 1 nm resolution is more than enough for systems having broad emission spectra studied here.

Intensity response calibration

Most of the components in this system (mainly spectrograph grating and iCCD camera) do not respond to the full wavelength range in the UV-VIS uniformly. Consequentially NIST traceable LS-1-CAL calibrated Tungsten-Halogen calibration light source (Ocean Optics) with known intensity profile was used to get the correction curve. Each recorded spectrum had to be multiplied by this curve. Different correction curve had to be derived for different grating positions and different entrance slit width of spectrograph.

Time resolution of system and calibration of zero time.

As the camera was synchronized with the laser by the electrical pulse coming from the Ekspla Nd:YAG laser control block, the zero time when the pulse arrives at the sample had to be determined. To do this, the Ekspla Nd:YAG laser beam (which is emitted ~ 1 μs after electrical pulse from the block) was directed onto the iCCD camera and the time resolved spectra with very short integration times (~ 0.5 ns) at delay times to cover the whole jitter region were recorded, integrated and then plotted (figure 4.4). A Gaussian function was fitted and the zero time was determined from the peak of Gaussian (in figure 4.4 case 964 ns is the time when the pulse arrives at the sample). After change of components (for example after changing cable length connecting laser control block and iCCD) a system zero point recalibration had to be made.
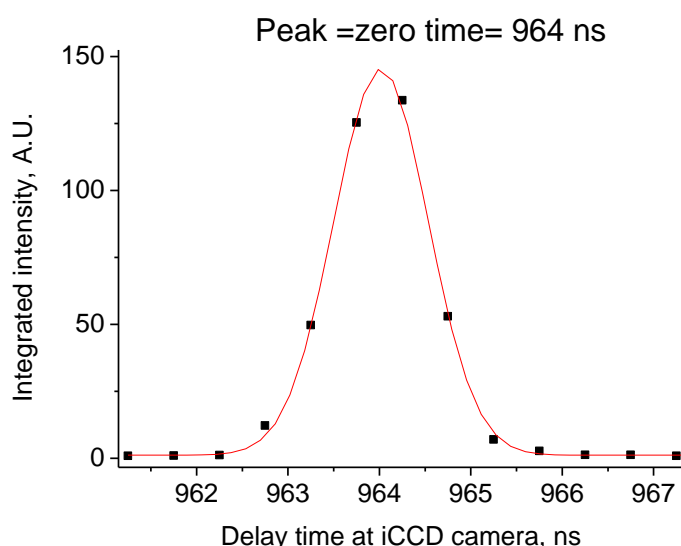
Figure 4.4 Zero time point determination of the spectrometer. Integrated time resolved spectra of the Ekspla Nd:YAG laser beam collected using 0.5 ns integration time and fitted with single Gaussian function. Peak of this Gaussian is the zero time of the system (i.e. the time when the pulse arrives at the sample).

Here a word needs to be said about the time resolution of the system. It obviously depends on the slowest component of the system. As the laser pulse length is 150 ps, and the delay time can be shifted by 0.1 ns and the smallest integration time of iCCD is 0.1 ns, the slowest component of the system is thus the electrical trigger jitter. From Gaussian fitting it is easy to determine that the full width at half maximum is 1.2 ns. This is the time resolution of the system.

Different integration time width calibration

Different camera integration times do not always result in a linear increase of recorded intensity. For example a 4 ns integration window does not necessarily record 10 times more intensity than a 400 ps integration window. This is especially true for small integration times up to ~10 ns. This can be tested experimentally using single wavelength continuous output diode laser and recording intensities at various integration times and dividing it by integration time. One should get approximately the same number for each integration time after this procedure if the system is linear (if normalized it should be 1). However as it is seen from figure 4.5 it is not the case and non-linearity below 7 ns is clearly present. Thus each decay curve recorded with dynamically increasing gate widths was multiplied by similar correction curves (see below).
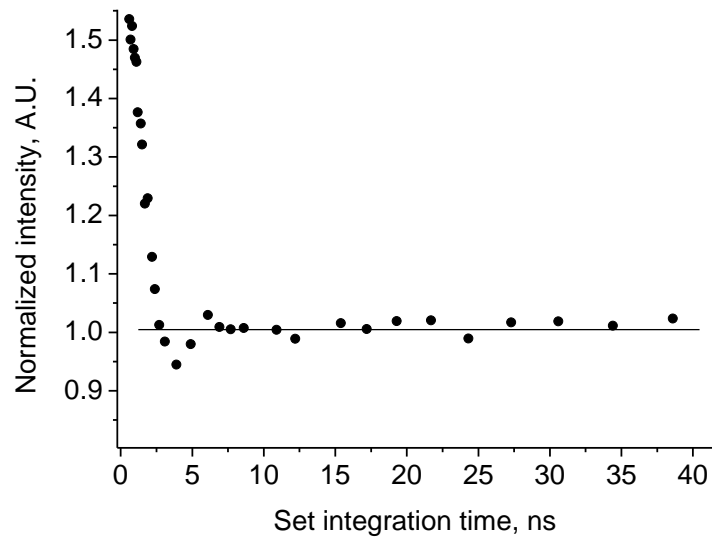
Figure 4.5 Experimental intensities of single wavelength continuous output laser diode recorded using different integration windows and divided by them. Non-linearity in region below ~ 7 ns is clearly present.

Decay curve recording with dynamically increasing delay times and integration windows

Decay measurements were performed by logarithmically increasing delayed and integration times[2]. This allows decay curves of up to 12 orders of time and intensity magnitude to be recorded. A set of delay times equally spaced in logarithmic scale have been chosen and time resolved spectra where taken with successively increasing integration window (not overlapping with the next delay time). Normally the integration time was chosen to be a tenth of the delay time as this was found to be the optimum between signal intensity and time resolution. Each

integrated spectra was scaled down appropriately by its integration time to get the real intensity according to the formula:

$$I_{tx}^{meas} \sim \int_{-\frac{t_x}{20}}^{\frac{t_x}{20}} I(t)dt \qquad (4.1)$$

where I_{tx}^{meas} is measured intensity at delay time t_x , and $I(t)$ is real intensity. The true intensity can be expressed as:

$$I(t) \sim \frac{I_{tx}^{meas}}{t_x} \qquad (4.2)$$

The validity of the method was checked by recording the decays of numerous samples at various time regions (CBP trap singlet decay in nanoseconds, $Ir(ppy)_3$ decay in microseconds, NPB triplet decay in millisecond) and comparing recorded decays with decay curves measured using regular method (using fixed integration time at various delay times without overlapping next delay time).

In practice, the decay curves are recorded in these steps. First of all the emission intensities for preset logarithmically increasing delay times t_x were taken with integration times equal to the tenth of delay times. This is simplified by using a self-written program. Then a background scan is taken and subtracted from emission intensities. Further, the spectra are integrated and divided by their integration times as well as multiplied by the correction curves.

It is important to emphasize that using dynamically increasing delay and gate times increase the dynamical range of the iCCD camera to ~12 orders of magnitude, whereas using fixing gate times it is not possible to achieve it. This type of method is very useful in recording power law type decays but not exponential ones as in the latter the increase of integration time is accompanied by large decease in time resolution. Thus in this theses both methods (using fixed integration time and dynamically increasing integration time) where used to record decay curves.

Ekspla Nd:YAG laser intensity fluctuations

The Ekspla Nd:YAG laser shot to shot fluctuation when averaging 100 shots per curve is ~10 %. Shot to shot fluctuation without averaging is even higher ~40%. This type of instability

could be easily overcome by integrating many shots in such a way to get good signal to noise ratio. However, the laser also exhibits mid-term (fluctuations with a period of ~10-20 minutes) instabilities of ~25 %. The only way to overcome this is to record decay curves few times and average them. Despite these drawbacks there is justification of using Ekspla Nd:YAG laser. First of all its high energy (up to few milijoules for 3rd harmonics) can pump a dye laser (Coumarin 450) to get redshifted 450 nm excitation very easily. The other laser used here, a Nd:YAG laser from CryLas Inc. can be more stable however highest energy per pulse is only 30 µJ. This is too low energy (or too time consuming) to pump Coumarin 450 dye. Furthermore, Ekspla YAG laser pulse is 150 ps in comparison for example with ~2 ns laser pulse of CryLas laser pulse. By using the latter time resolution of this home built spectrometer which is 1.2 ns would be decreased. Another useful feature of the Ekspla Nd:YAG laser is that it is possible to send electrical synchronization pulse to iCCD camera much earlier (microseconds) before laser pulse is emitted. This can be useful in certain cases, especially for fluorescence measurements, because the iCCD reacts to a trigger pulse in ~ 30 ns (transmits signal and opens the shutter) so if photodiode is used as a trigger this time is not accessible. In order to avoid this problem one can delay the optical beam by ~30 m however to do this in a safe manner is very cumbersome in practice. Overall, at the moment, these advantages offset the drawbacks of laser intensity fluctuations.

4.4 References

1.   P. A. Losio, R. U. A. Khan, P. Gunter, B. K. Yap, J. S. Wilson and D. D. C. Bradley, Appl. Phys. Lett. 89 (4) (2006).

2.   C. Rothe and A. P. Monkman, Phys. Rev. B 68 (7), 075208 (2003).

5 The photophysics of singlet, triplet and degradation trap states in CBP

5.1 Introduction

Before the examination of triplet transport in donor/spacer/acceptor systems a suitable spacer material had to be chosen. Only donor and acceptor should be excited with the picosecond laser pulse and then emission from the acceptor observed. Assuming the spacer absorption is negligible at the excitation wavelength, the donor triplet level is higher than the spacer triplet level and the latter is higher than the acceptor triplet level, the triplets should be transported via the donor/spacer interface to the spacer, travel in spacer and then transferred across the spacer/acceptor interface to the acceptor. Here it should emit and be detected. Hence emission from the acceptor should directly depend on the spacer layer thickness and triplet diffusion properties in this layer. Consequentially the spacer layer should satisfy the following requirements:

- It should have longer triplet lifetime of triplet than the donor and acceptor (preferably it should be much longer than the time during which triplets are transferred across the spacer layer).

- It should have a triplet level between ~2.4 eV and ~1.9 eV (thus should fluoresce in blue spectral region) assuming donor is a green-blue phosphorescent material (~2.43 eV) and acceptor is in the red (~1.92 eV). Then $E_{TDonor} > E_{TSpacer} > E_{TAcceptor}$.

- It should absorb at 355 nm (laser wavelength) however not at 450 nm (absorption at 355 nm excitation is needed to explore single layer properties and negligible absorption at 450 nm is needed to examine spacer in multilayer films).

- Time resolved luminescence photophysics should be as simple as possible – no trap states etc as this would complicate the analysis of results.

The first condition would be satisfied if donor and acceptor are heavy metal complexes, for example, well known iridium metal complexes Iridium (III) Tris(1-phenylisoquinoline) (Ir(piq)$_3$) and fac-tris(2-phenylpyridine) Iridium (III) (Ir(ppy)$_3$) [1] (short lived phosphorescent states due to heavy atom influence on spin-orbit coupling) and if the spacer is an organic molecule having long lived phosphorescence states for example archetype OLED materials 4,4-N, N′-dicarbazolyl-1,1′-biphenyl (CBP) or N,N'-diphenyl-N,N'-bis(1-naphthyl)-1,1'-biphenyl-4,4''-diamine (NPB) [2-7]. In this chapter the properties of CBP films will be examined whereas the following one will be devoted to unveiling the triplet properties in NPB films.
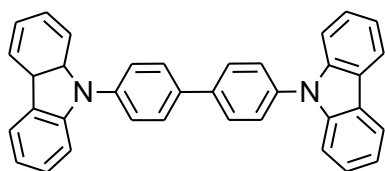
Figure 5.1 Chemical structure of 4,4-N, N′-dicarbazolyl-1,1′-biphenyl (CBP).

One of the most popular host materials used for red, yellow, green as well as blue emitters in OLEDs is CBP (figure 5.1)[8-11]. Triplet loss due to triplet annihilation is an issue in CBP and efforts have been made to explore triplet-triplet annihilation (TTA) decay rates in CBP by observing delayed fluorescence, in thin films, centered at 410 nm and 430 nm[7]. CBP triplet migration diffusion coefficients have been calculated using the information conveyed via delayed fluorescence decay[7]. However, in dilute solution the CBP fluorescence spectrum has peaks at 365 nm and 380 nm and one could not expect the singlet emission to shift to the red by such a large amount of energy just because of going from liquid to solid state. In addition, one can also find discrepancies among various research groups' measurements of optical properties of CBP film, especially for fluorescence and delayed fluorescence spectra [7, 12-18]. The question as to why people observe such a variety of steady state spectra of solid CBP is very intriguing. Some solid state spectra are reported with vibronic peaks at around 375 nm and 390 nm [13, 16-17] or only at around 390-400 nm[12, 14], whilst others report spectra with an additional peak at around 410 nm [15, 18] and some ascribe the bands at 410 nm and 430 nm (or 420 nm) to delayed fluorescence of CBP film [7, 15]. Though this material is widely used in devices, a literature review reveals that fundamental photophysical properties are still unclear. Hence in this chapter very unusual absorption, fluorescence, phosphorescence and delayed fluorescence properties of vacuum sublimed commercially available CBP is explored and discussed, how it is affected by ageing and UV light and the origin of the red shifted peaks at 410 nm and 430 nm is proposed. A step-by-step systematic approach is chosen to reveal the origins of emission from CBP films. First of all absorption and emission in various concentration solutions (toluene) is examined. Then films are evaporated and fluorescence, phosphorescence and delayed fluorescence properties at various temperatures are investigated with an expectation to find clues about the origins of previously unexplained variations in fluorescence and phosphorescence spectra.

5.2 Results

Absorption properties

First, the absorption dependence on concentration of CBP in toluene was measured. In figure 5.2 spectra of solutions with different concentrations are shown. The sharper peak at 295 nm

could be attributed to the carbazole moiety [19] and the broad region centered on 320 nm may be attributed to the π-π* transition. The region between 382 nm and 413 nm of higher concentrated solutions is depicted in figure 5.2b and a peak around 393 nm for highly concentrated solutions is seen, whereas for lower concentrations it is absent. Absorbance dependence on concentration at 340 nm and at 393 nm is linear. The absorption coefficient at 340 nm is approximately 23000 $M^{-1}cm^{-1}$ whereas at 393 nm ~16 $M^{-1}cm^{-1}$ that is about 1000 times smaller.
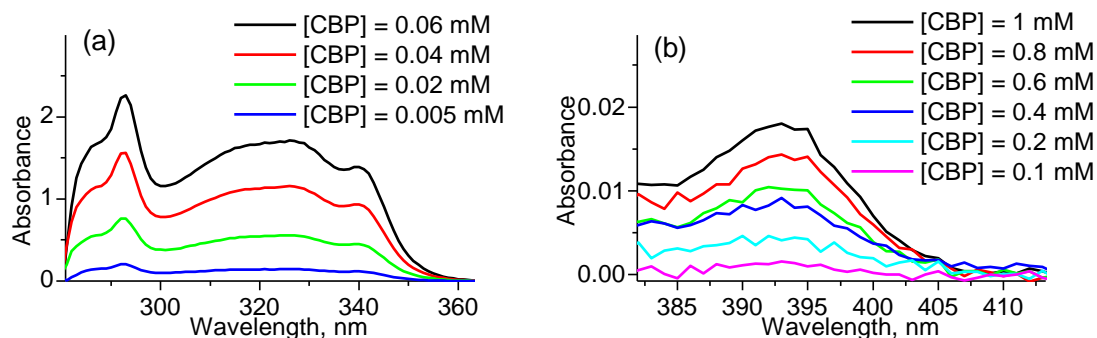
Figure 5.2 Absorption spectra of CBP in toluene of (a) low concentrated solutions in region between 280 nm and 360 nm and of (b) highly concentrated solutions in region between 382 nm and 413 nm. Square brackets around CBP is used as a sign indicating concentration.

Excitation and emission properties

The excitation spectra of CBP solutions confirm the findings about the 393 nm peak in absorption studies. The excitation spectrum (emission collected at 381 nm) of low concentration CBP solution (0.002 mM) has a broad band at about 320-330 nm (figure 5.3). As the concentration of CBP in solution is increased a new peak at 360 nm grows in. This is an artifact (due to inner filter effect) of the experimental setup as a result of the way light is collected (90 degrees between excitation and emission paths). But when the concentration is increased even more and the emission is collected at 468 nm, a new peak near 393 nm in the excitation profile is seen which is in agreement with the absorption spectrum.
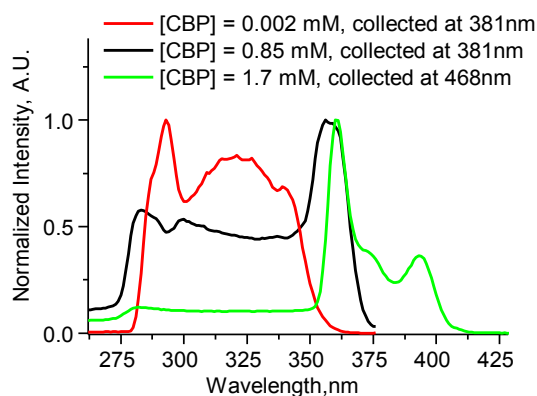
Figure 5.3 Normalized excitation spectra of CBP in toluene at various concentrations. Square brackets around CBP is used as a sign indicating concentration.

Emission studies as well show concentration dependent luminescence properties. At very low concentrations (0.002 mM) and exciting at 320 nm the CBP solution luminescence exhibits two peaks: at 365 nm and 380 nm (figure 5.4). Since the concentration is very low this has to be the emission from individual CBP molecules and these peaks are ascribed to CBP individual molecule singlet emission (singlet emission bands). When the concentration is increased up to 0.85 mM the emission band broadens. Two small bands growing around 404 nm and 424 nm and two new well resolved peaks out of those bands at 404 nm and 424 nm are observed when the concentration is increased up to 1.7 mM. These bands are termed LE (lower energy) bands further in the text. The overall intensity decrease with an increase of concentration may be the artifact of the measurement because of very high concentrations[20]. However the relative decrease of the peak at 365 nm in comparison to 380 nm cannot be due to such an artifact and it may indicate that CBP singlet emission is quenched in the higher concentrated solution by the state which absorbs at 393 nm and is reemitted via LE bands (recall figure 5.2b and compare with figure 5.4a).

The luminescence spectrum of thin film has four peaks and they are all red shifted by approximately 10 nm, which is reasonable. Two higher energy peaks at 374 nm and 392 nm in analogy to CBP in solution can be ascribed to CBP individual molecule singlet emission (singlet emission bands) and two lower energy peaks at 413 nm and 438 nm can be ascribed to LE (lower energy) bands. Most important is that the relative intensities of the LE bands (compared to singlet emission bands) in film is higher than the relative intensities of LE bands (compared to singlet emission bands) in solutions. This indicates that the species giving rise to the LE bands act as a quenchers of singlet excitons. Thus the more concentrated the solution, the higher the LE band relative intensity, being highest in a thin film. It is important to note that lifetime of LE bands in solid state are much longer ~7 ns (figure 5.5.) than the lifetime of peaks at 374 nm and 392 nm which according to the literature should be smaller than 1 ns[21] thus showing a different origin for these states. For the moment the reader's attention is drawn to this LE state

emission as in thin film the "delayed emission" from these states has been interpreted as a sign of triplet-triplet annihilation (TTA) and has been used to probe TTA and calculate diffusion coefficients in other CBP studies[7]. However as it is shown here, the species giving rise to these emission bands are different to the isolated CBP molecular species, and thus the LE emission is not delayed fluorescence arising from TTA from CBP triplet state.
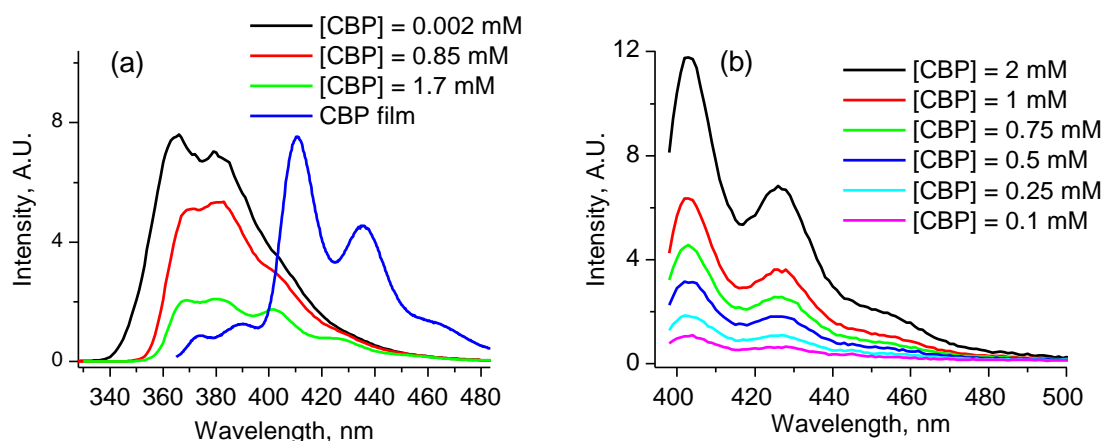
Figure 5.4 Steady state emission spectra of CBP in toluene at various concentrations at two excitation wavelengths (a) 320 nm and (b) 393 nm. When exciting at 393 nm spectrum intensity increases linearly (b). For comparison purposes CBP film photoluminescence spectrum in (a) is added (the intensity is offset for clarity). Square brackets around CBP is used as a sign indicating concentration.
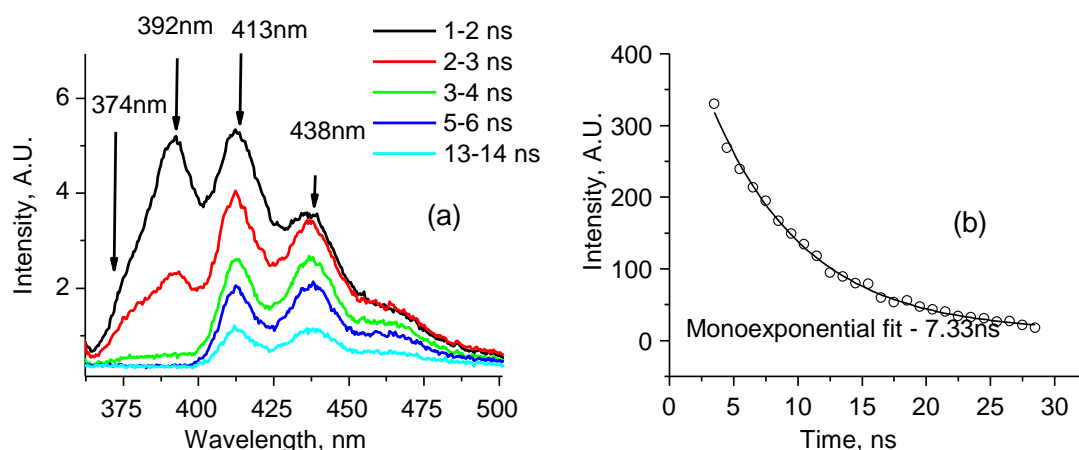
Figure 5.5 (a) Time resolved spectra of CBP film, thickness 250 nm, evaporation rate 0.5 A/s, measured at 12 K, excitation with YAG 3rd harmonics, camera opening and closing time after excitation are indicated. (b) Photoluminescence decay (open circles) of CBP film, intensity integrated from 405 nm to 460 nm. Black solid line corresponds to monoexponential fit.

To understand what gives rise to the LE features further measurements were made. The LE bands (404 nm and 424 nm in solution, or 413 nm and 438 nm in solid state) at first sight do not

look like excimer emission because normally in this case bands are structureless and much broader[5], whereas here, we see two well resolved features. It would be reasonable to think that these two peaks are due to dimer formation and the new peak arising in the absorption spectra at high concentrations further supports this. However, as already mentioned above, the absorbance at 393 nm has a linear dependence on concentration which excludes the dimer model. This has further been tested using fluorescence (exciting at the newly emerging absorption band at 393 nm, recall figure 5.2b), and the result is the same – LE band luminescence intensity increases linearly with the increase of concentration (figure 5.4b). Thus excimer or dimer as the species responsible for the LE features can be ruled out.

Effects of annealing and UV light on steady state spectra of CBP in solutions and films

One possible origin of LE states could be from degradation products of CBP, thus efforts were made to explore this. In a thorough study of CBP degradational mechanisms in devices and in thin films Kondakov *et al* [22] found that UV light can affect CBP. However, in this study there is no account of how the photophysical properties of this material changes when exposed to UV light. Here it is studied how steady state absorption, excitation and emission spectra of CBP in highly concentrated solutions and thin films are affected by UV light, with the hope to get some insight on the origin of LE bands. Degassed, highly concentrated samples ~1 mM were put under a UV lamp (8 W mercury lamp peaking at 365 nm). Absorption, steady state excitation and emission spectra were recorded after various periods of time under the UV lamp.
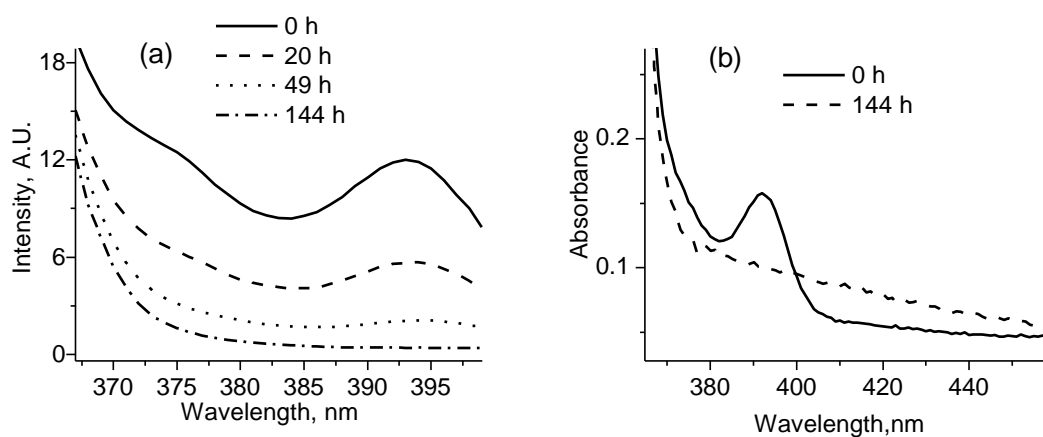
Figure 5.6 UV light effect on (a) excitation spectra (light collected at 404 nm) and (b) absorption spectra of 1mM CBP in degassed solution of toluene. Parameter is time in hours after exposure to UV light.
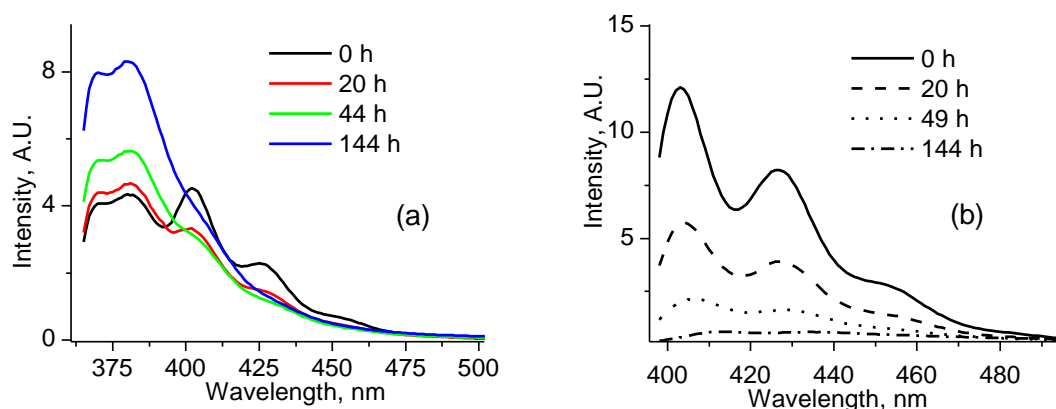
Figure 5.7 UV light effect on emission spectra of 1 mM CBP in degassed solution of toluene when excitation wavelength is (a) 355 nm and (b) 393 nm. Parameter is time in hours after exposure to UV light.

In the excitation and absorption spectra the peak at 393 nm diminishes with the increase of time under UV excitation (figure 5.6). The same tendency is seen in emission spectra where the LE bands gradually decrease and the singlet emission bands increase at the same time (figure 5.7). This again indicates, that the LE states act as quenchers of the singlet emission bands as the absorption band at 393 nm overlaps strongly with singlet emission bands. It is interesting to note that when exciting at 393 nm the LE band emission decreases exponentially with UV exposure time. The same tendency is seen when exposing thin films to UV light (figure 5.8). The relative decrease of intensity of the LE states is observed with the increase of UV exposure time. In this case one cannot completely extinguish these peaks with the UV irradiation probably due to lower UV penetration into film than into solution. The interpretation of this behavior and how it relates to the origins of LE is given in the discussion section of this chapter.
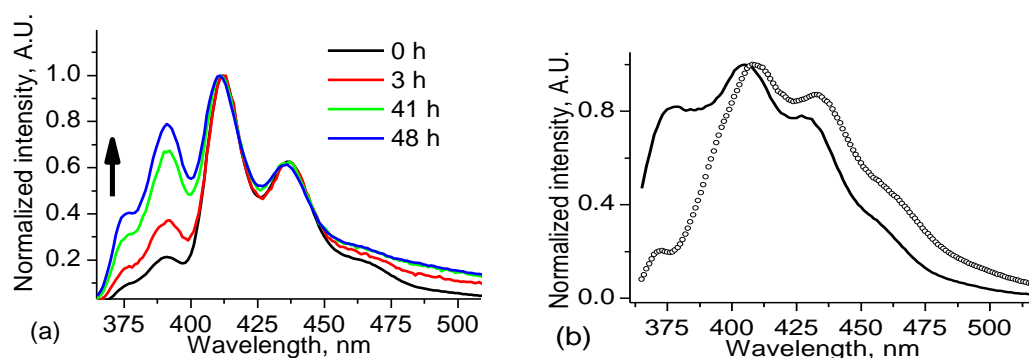
Figure 5.8 (a) Change of emission spectra of CBP thin film after exposure to UV light, excited at 355 nm. Arrow indicates the relative increase direction of peaks at 374 nm and 392 nm. Parameter is time in hours after exposure to UV light. (b) Change of emission spectra of CBP thin film capped with aluminum before heating (straight line) and after heating at 140 C° for 5 hours (open circles).

The effects of annealing on steady state spectra where also investigated. The fluorescence spectrum of a 100 nm thick CBP film capped with a 200 nm Al film has been recorded before and after annealing in nitrogen for 5 hours. The singlet emission peak at ~374 nm decreases in relation to the LE bands and the latter shifts to the red by ~4 nm (figure 5.8). Normally luminescence spectra tend to red shift for more ordered materials, such as would arise after annealing processes.

Triplet state of CBP

Further long lived states in CBP have been investigated in the same detail as short lived states. The triplet level (at the onset) of CBP in frozen toluene solution is located at 440 nm or 2.81 eV. Since the concentration of the measured solution was very low, in the range of 1 μM, the phosphorescence spectra recorded is of isolated molecules interacting only with the toluene solvent (figure 5.9).

Measurements of the triplet level of evaporated CBP were made (figure 5.9a red curve). The phosphorescence spectrum of CBP film has four features: at 497 nm, 532 nm, 560 nm, and 607 nm. All these spectral components have the same lifetime, however as will be shown later the states at 560 nm and 607 nm may have different origin to the real phosphorescence of the material. The triplet level (at the onset) of evaporated CBP on a quartz substrate is located at 475 nm (2.61 eV) which is redshifted in comparison to frozen solution phosphorescence measurements. The same CBP film samples were stored in an inert atmosphere and exposure to air was minimized. They were subsequently (figure 5.9a black curve) remeasured ~6 weeks after evaporation. The peaks at 497 nm and 532 nm are gone and all that is left are the features at 560 nm and 607 nm, both of which have the same lifetime.
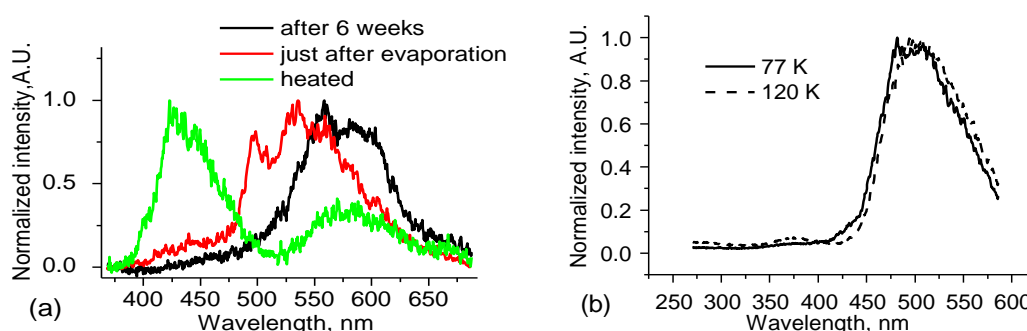
Figure 5.9 (a). Gated late emission spectra of evaporated CBP thin film, at 16K, film just after evaporation (we ascribe it to phosphorescence), the same film 6 weeks after evaporation and later heated at 381K for three hours. All spectra recorded 20 ms after excitation. (b). Phosphorescence spectra of degassed solution of CBP in toluene (1.7 μM) at two different temperatures recorded at least 5 ms after excitation.

Then the aged samples were heated for 3 hours at 381 K in a low vacuum approximately 10^{-2} mbar. The normalized gated late emission spectrum of the heated sample is plotted in figure 5.9a as a green curve. The intensity of features at 560 nm and 607 nm after heating decreased, but now one can observe a new band at around 420 nm while before heating it is clearly not present. Since it is observed 20 ms after excitation this could be ascribed to delayed fluorescence and this must imply higher triplet mobility after heating of the film. This delayed fluorescence is more likely to come from the LE states (at 413 nm and 438 nm in film) rather than singlet emission states (at 374 nm and 392 nm in film). Higher triplet mobility would also imply that more triplet excitons are caught in trap states in heated film, than in unheated and unaged film. It is likely that trap states are around the energies of 2.2 eV (560 nm), and 2.0 eV (607 nm). This is further supported by the observed temperature dependence of CBP triplet spectra (figure 5.10).
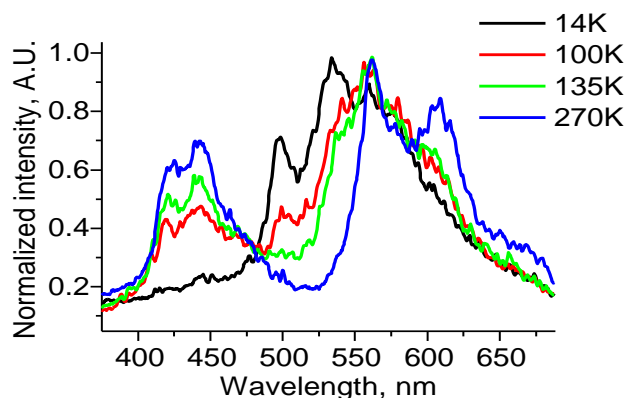
Figure 5.10 Temperature dependence of late emission spectra of evaporated fresh CBP thin film, thickness 250 nm. All spectra recorded 20ms after excitation.

At the higher temperatures (110 K-270 K) the higher mobility of triplets is probably present leads to more trap state emission at 2.2 eV (560 nm), and 2.0 eV (607 nm), while at low temperature, 14 K, virtually no delayed fluorescence is observed, i.e. low triplet mobility, and only phosphorescence emission from the states at 2.49 eV (497 nm) and 2.33 eV (532 nm) is present. Similar spectra delayed emission spectrum, measured at 125 K, having a peak at 560 nm (which was ascribed to CBP phosphorescence) and a peak at 420 nm (ascribed to delayed fluorescence from CBP triplet-triplet annihilation) have been presented by others [15], which in the discussion section is shown to be incorrect.

5.3 Discussion

The question as to why people observe such a variety of steady state spectra of solid CBP is very intriguing. Lets recall that some solid state spectra are reported with vibronic peaks at around 375 nm and 390 nm [13, 16-17] or only at around 390-400 nm [12, 14], whilst others report spectra with an additional peak at around 410 nm [15, 18] and some ascribe the bands at 410 nm and 430 nm (or 420 nm) to delayed fluorescence of CBP film [7, 15]. The formation of dimer or excimer species being responsible for the LE features at 413 nm and 438 nm has been ruled out, thus the other assumption is, that some degradation products are responsible for them. And indeed, this may be true, since Kondakov *et al* proposed degradation mechanism specifically for CBP [22] and suggested that degradation is due to breaking of the N-C bond between aryl and carbazolyl radicals. Density functional calculations, performed by them, showed that the dissociation of this bond should take place with an excitation energy of approximately 3.65 eV [22] which is close to singlet emission energy of ~3.4 eV (in solution). Taking into account other evidence [22] presented by this group, it is very likely that CBP degradation (which also occurs in OLEDs) takes place via the dissociation of this bond in the excited state. Kondakov's [22] HPLC/MS as well as ^{1}H NMR analysis of CBP in devices after device operation and of CBP films after their exposure to UV showed that one can detect an array of different molecules other than CBP present in the samples (figure 5.11) [22]. For example, they found that it could be carbazolyl, 4-(N-carbazolyl)biphenyl (BCP), or 3-carbazole-4,4'–bis(N-carbazolyl)biphenyl (3-CCBP) [22]. As it can be easily identified from molecular structures of the detected chemical products, those molecules can be formed if one has breakage of the N-C bond between aryl and carbazole radicals of CBP. It is very important to note that even the pristine samples could have these type of products if they were exposed to UV photons. As well, because of the innate nature of degradation mechanism they can easily appear during the measurement process when intense UV light is used for excitation. That is why such a variety of CBP film fluorescence and delayed fluorescence spectra have been recorded by others. So it is reasonable to assume that the quenching LE states observed here may have resulted from CBP dissociation due to this weak C-N bond over time. However, the species formed due to such degradation are themselves unstable because of the same C-N bond and after illumination with UV for a long enough time they photodegrade into non-emissive species, reducing the LE band emission.
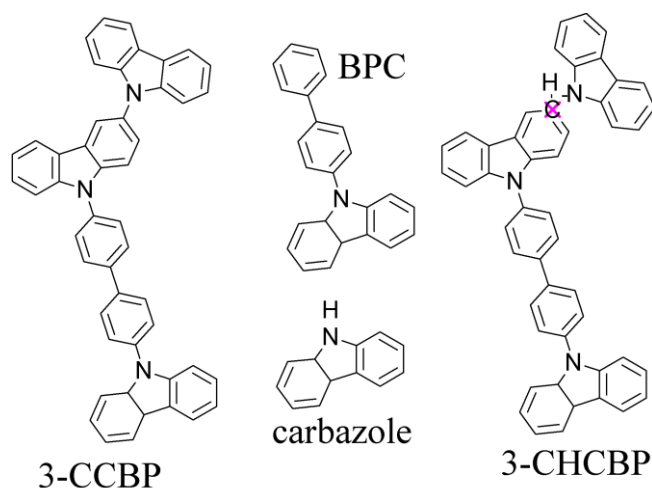
Figure 5.11 Chemical structures of possible degradational products (3-CCBP (3-carbazole-4,4'–bis(N-carbazolyl)biphenyl), carbazole and BPC (carbazolyl, 4-(N-carbazolyl)biphenyl)) as well as one proposed intermediate product 3-CHCBP, adopted from reference[22].

The other question is, where do the CBP triplet trap states at 560 nm and 607 nm come from? The most likely answer is that those trap states are triplet states from the same degradation species which are responsible for LE band emission i.e. it is triplet emission of degradational product. LE band peak energies in solid film are 3 eV (~413 nm) and 2.83 eV (~438 nm), and the difference between them is equal to 0.17 eV (see e.g. figure 5.4a blue curve). From figure 5.10, 270 K curve, the difference between peaks of trap state energies 2.21 eV (560 nm) and 2.04 eV (~607 nm) is as well 0.17 eV. Normally triplet emission bands are mirror image of the singlet band, which is the case this time. As a consequence the triplet trap states are related with the species producing the LE bands. In figure 5.12 a Jablonski diagram depicting the state levels for a thin film is given. From Fig. 5.4a it is clear that the vibronic spacing of CBP molecular singlet species in film is 0.16 eV i.e. a carbon double bond stretch mode. The peak energies 2.49 eV (497 nm) and 2.33 eV (532 nm) of CBP molecule triplets (the phosphorescence) is also 0.16 eV (figure 5.9a red curve). Now the behavior of late delayed emission in film at various temperatures becomes more clear (recall figure 5.10). At the higher temperatures (110 K-270 K) higher mobility of triplets gives more migration to the low concentrated triplet trap states and as a consequence more delayed fluorescence (from the traps) and more triplet trap state emission at 2.2 eV (560 nm), and 2.0 eV (607 nm) is observed. While at low temperature, 14 K, virtually no delayed fluorescence emission from LE species is observed, i.e. low triplet mobility so little population of triplet trap sites, and only genuine CBP phosphorescence emission from the states at 2.49 eV (497 nm) and 2.33 eV (532 nm) can be recorded. It is important to stress that no delayed fluorescence related to molecular CBP species (around 374 nm and 392 nm) has been observed. Again this is as expected because triplet mobility at low temperature is small so no triplet-triplet annihilation is present. This fits well with the late emission spectra results of heated or aged CBP. The increase of triplet mobility is

probably due to the change of conformation of the CBP crystallites (more ordered) during comparatively long storage time, or while the sample is heated during very short time. Indeed one expects a more ordered structure since the molecules have enough energy to reorient themselves into more favorable – ordered - positions. More ordered structure results in narrower width of triplet DOS, hence increased hopping rate of triplet excitons in a film. This results in an increased probability to reach a trap state even if the trap density is comparatively low as migrating excitons can easily find them. A more ordered structure also results in an increased annihilation rate, yielding those singlets responsible for delayed LE bands fluorescence. The red shift of steady state emission in the CBP films the after heating may too confirm that CBP becomes more ordered after exposure to higher temperatures.

The consequences of even small concentrations of traps in the material can have a crucial effect on the photphysical properties and OLED device performance. The increase of the emission intensity from trap sites looks similar to the effects of keto defects in polyfluorene[23], where one sees large increases of a lower energy, broad peak in solid state in comparison to solution and where the longer wavelength peaks acts as a luminescence quencher site via energy transfer mechanisms. The quenching is so effective that very large changes in emission color of the material may be observed as in CBP. Castex *et al*[24] observed the photodegradation under UV light illumination, of the carbazole derivative N,N-diethyl-3,3-bicarbazyl, causing the emergence of a new emission band between 400 nm and 500 nm. It was proposed that phototransformation may have occurred via formation of carbazolylium N-oxide species[24]. Those trap states may appear in the device after long enough operation or annealing, resulting in the decrease of electrophosphorescence efficiency seen by others[22]. Finally Giebink *et al* (figure 6 in ref[7]) used delayed fluorescence emission at 410 nm and 430 nm here ascribed to emission from trap states as the probe to examine triplet-triplet migration in CBP films. They used CBP neat film and subsequently sublimed CBP doped with Ir(ppy)$_3$ on top. They excited CBP neat film with short laser and observed decay dynamics of both Ir(ppy)$_3$ and CBP delayed fluorescence (at 410 nm and 430 nm) at different CBP neat film thicknesses and then used classical diffusion equations to extract information about triplet transport properties in CBP. Their assumption were that mostly neat CBP is excited and then triplets travel through neat CBP to CBP doped with Ir(ppy)$_3$ and are trapped on iridium complex ($T_{CBP} > T_{Ir(ppy)3}$). First of all they assumed that delayed fluorescence from LE species is delayed fluorescence from genuine CBP (which as proven here to be incorrect and should be at 375 nm and 390 nm). Further they did not account for triplet level from LE species (at 2.21 eV) which is lower than Ir(ppy)$_3$ triplet level (2.46 eV). Thus whole dynamics of triplet is different as $E_{TCBP} > E_{TIr(ppy)3} > E_{TLE\ species}$ and not $E_{TCBP} > E_{TIr(ppy)3}$ as assumed in their publication. Hence the physical modeling should be completely different and might give different results. This is a perfect illustration of the

importance of understanding photophysics of single layer films before creating more complicated structures.
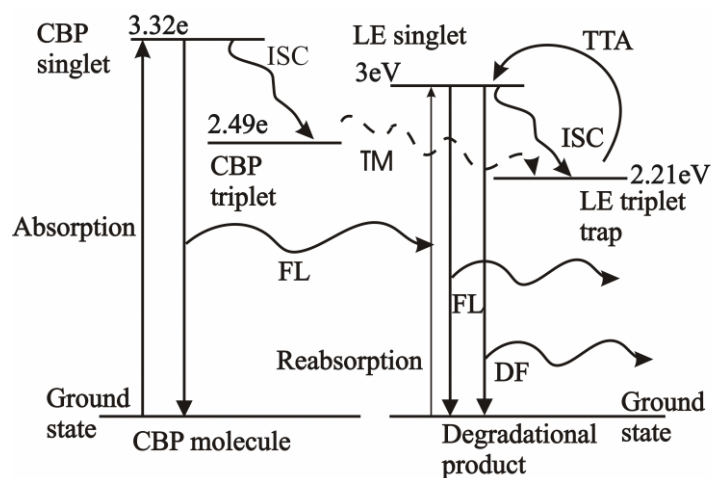
Figure 5.12 Proposed Jablonski diagram for CBP thin film. ISC stands for intersystem crossing, TM – triplet migration, TTA – triplet annihilation, LE – low energy bands. Levels are determined taking the peak energy of first vibronics (not the onsets).

5.4 Summary

CBP was characterized by steady state absorption, emission and excitation steady state as well as time resolved spectroscopies. Peaks at 295 nm (carbazole moiety) and 320 nm ($\pi - \pi^*$ transition) of CBP in toluene were observed by using steady state absorption spectroscopy. As the concentration of CBP in solution is increased a new absorption peak at 393 nm is observed. The same peak is present in the excitation spectrum of highly concentrated CBP solutions. Dilute CBP solution exhibits two peaks: at 365 nm and at 381 nm which are ascribed to (individual) molecule singlet emission whereas when the concentration is increased, two new bands at 404 nm and 424 nm emerge (LE peaks). In thin film CBP all these bands red shift including the LE bands which shift to 413 nm and 438 nm respectively. Experimental results as well as the variety of CBP fluorescence and delayed fluorescence spectra recorded by other research groups, show that conventionally used commercial CBP (even vacuum sublimed 'pristine' sample) is not very stable and probably dissociates into carbazolyl-type moieties over time. Under UV light, these degradation products themselves can be degraded and the corresponding peaks decrease considerably. The true triplet level (at the onset) of CBP in frozen solution is 2.81 eV (440 nm) and it red shifts (at the onset) in an evaporated CBP film to 2.61 eV (475 nm). Measurements show that annealing and aging affects phosphorescence emission by increasing the fraction emitting from trap states and/or delayed fluorescence from LE species. The delayed emission observed in CBP films by others and ascribed to delayed

fluorescence, is showed here to be not from the pure CBP film singlet emissive states but probably from the degradation product species. Chemical analysis performed by Kondakov *et al*[22] proved that CBP indeed is not very stable. HPLC/MS as well as ^{1}H NMR analysis of CBP in devices after device operation and of CBP films after their exposure to UV showed that one can detect an array of different molecules in the samples other than CBP such as carbazolyl, 4-(N-carbazolyl)biphenyl (BCP), or 3-carbazole-4,4'–bis(N-carbazolyl)biphenyl (3-CCBP)[22]. As it can be easily identified from molecular structures of detected chemical products, those molecules can be formed if one has breakage of N-C bond between aryl and carbazole radicals of CBP. Thus LE species as well as triplet trap states probably are related to these degradational products. These states, even if the concentration is very low, act as trap states and decrease the efficiency of CBP via exciton migration in film, especially of triplet states. The relatively long-lived emission intensity from these low energy triplet traps increases after annealing or aging. This chapter is concluded by stating that before looking into complex structures consisting of two or three layers photophysical properties of single layer films have to be examined well in order to avoid unnecessary mistakes when modeling triplet transport. Finally the triplet level of CBP (2.81 eV) is higher than needed (less than 2.43 eV).

5.5 References

1.   A. Tsuboyama, H. Iwawaki, M. Furugori, T. Mukaide, J. Kamatani, S. Igawa, T. Moriyama, S. Miura, T. Takiguchi, S. Okada, M. Hoshino and K. Ueno, J. Am. Chem. Soc. 125 (42), 12971-12979 (2003).

2.   L. Zou, V. Savvate'ev, J. Booher, C. H. Kim and J. Shinar, Appl. Phys. Lett. 79 (14), 2282-2284 (2001).

3.   M. A. Baldo and S. R. Forrest, Phys. Rev. B 62 (16), 10958-10966 (2000).

4.   V. Jankus, C. Winscom and A. P. Monkman, J. Phys.-Condes. Matter 22 (18), 185802 (2010).

5.   P. A. Losio, R. U. A. Khan, P. Gunter, B. K. Yap, J. S. Wilson and D. D. C. Bradley, Appl. Phys. Lett. 89 (4) (2006).

6.   V. Jankus, C. Winscom and A. P. Monkman, J. Chem. Phys. 130 (7), 074501 (2009).

7.   N. C. Giebink, Y. Sun and S. R. Forrest, Org. Electron. 7 (5), 375-386 (2006).

8.   Y. R. Sun, N. C. Giebink, H. Kanno, B. W. Ma, M. E. Thompson and S. R. Forrest, Nature 440 (7086), 908-912 (2006).

9.   B. J. Chen, X. W. Sun and K. R. Sarma, Mater. Sci. Eng. B-Solid State Mater. Adv. Technol. 139 (2-3), 192-196 (2007).

10.   M. A. Baldo, S. Lamansky, P. E. Burrows, M. E. Thompson and S. R. Forrest, Appl. Phys. Lett. 75 (1), 4-6 (1999).

11.   V. Adamovich, J. Brooks, A. Tamayo, A. M. Alexander, P. I. Djurovich, B. W. D'Andrade, C. Adachi, S. R. Forrest and M. E. Thompson, New J. Chem. 26 (9), 1171-1178 (2002).

12.   F. Li, M. Zhang, G. Cheng, J. Feng, Y. Zhao, Y. G. Ma, S. Y. Liu and J. C. Shen, Appl. Phys. Lett. 84 (1), 148-150 (2004).

13.   J. B. Yu, H. J. Zhang, L. Zhou, R. P. Deng, Z. P. Peng, Z. F. Li, L. S. Fu and Z. Y. Guo, J. Lumines. 122, 678-682 (2007).

14.   D. Schneider, T. Rabe, T. Riedl, T. Dobbertin, M. Kroger, E. Becker, H. H. Johannes, W. Kowalsky, T. Weimann, J. Wang and P. Hinze, Appl. Phys. Lett. 85 (11), 1886-1888 (2004).

15.   C. Adachi, M. A. Baldo and S. R. Forrest, J. Appl. Phys. 87 (11), 8049-8055 (2000).

16.   T. Z. Yu, W. M. Su, W. L. Li, R. N. Hua, B. Chu and B. Li, Solid-State Electron. 51 (6), 894-899 (2007).

17.   T. Tsuboi, H. Murayama, S. J. Yeh and C. T. Chen, Opt. Mater. 29 (11), 1299-1304 (2007).

18.   G. Ramos-Ortiz, Y. Oki, B. Domercq and B. Kippelen, Phys. Chem. Chem. Phys. 4 (17), 4109-4114 (2002).

19.   Q. Zhang, J. S. Chen, Y. X. Cheng, L. X. Wang, D. G. Ma, X. B. Jing and F. S. Wang, J. Mater. Chem. 14 (5), 895-900 (2004).

20.   L. R. Lakowicz, *Principles of Fluorescence Spectroscopy*. (Kluwert Academic / Plenum Pyblishers, New York, 1999).

21.   Y. Kawamura, H. Yamamoto, K. Goushi, H. Sasabe, C. Adachi and H. Yoshizaki, Appl. Phys. Lett. 84 (15), 2724-2726 (2004).

22.   D. Y. Kondakov, W. C. Lenhart and W. F. Nichols, J. Appl. Phys. 101 (2), 024512 (2007).

23.   S. I. Hintschich, C. Rothe, S. Sinha, A. P. Monkman, P. S. de Freitas and U. Scherf, J. Chem. Phys. 119 (22), 12017-12022 (2003).

24.   M. C. Castex, C. Olivero, G. Pichler, D. Ades and A. Siove, Synth. Met. 156 (9-10), 699-704 (2006).

6 Dynamics of triplet migration in films of NPB

6.1 Introduction

It was concluded in the previous chapter that it is very important to understand triplet dynamics in single layer films before constructing more complicated structures. In this chapter N,N'-diphenyl-N,N'-bis(1-naphthyl)-1,1'-biphenyl-4,4''-diamine (NPB), triplet dynamics will be examined in detail – triplet state statics, dispersive regime change to non-dispersive regime and thickness influence on triplet dynamics. NPB is perfect for this reason as its photophysical properties are understood well. Although formation of excimeric states has been reported[1] (after annealing or after evaporation at slower rates than 0.167Å per second) there is no evidence of other types of emissive trap states in NPB. It was chosen as a spacer layer candidate in this research due to its chemical stability, and consequently its consistent photophysical properties, in contrast to some other well-known hole transporters, such as 4,4-N, N'-dicarbazolyl-1,1'-biphenyl (CBP) (previous chapter). Some effort has already been put into elucidating triplet and triplet-triplet annihilation (TTA) properties of conjugated polymers[2-4] and small organic molecules[5-7]. For example Kalinowski *et al*[8] showed that plays a major role in the decrease of the quantum efficiency of electrophosphorecence in OLEDs. However, even for such archetypal transporters as already mentioned NPB , CBP or N,N'-diphenyl-N,N'-bis(3-methylphenyl)-(1,1'-biphenyl)-4,4'-diamine (TPD) extensively used in OLEDs there is very little known especially about dispersive triplet transport [9-11]. The morphological disorder present in these types of materials should give rise to both energetic and positional site distributions, that gives rise to dispersive transport and as a consequence, should give a time-dependent triplet diffusion coefficient what makes analytical treatment very complex[12-15]. Giebink *et al* [11] used time resolved spectroscopy to study triplet diffusion in CBP however there were no experimental results presented on the disorder of the system and the authors used the assumption that triplet migration is non-dispersive at higher temperatures. Indeed, there is no evidence presented throughout their publication showing the presence or absence of a dispersive regime of triplet migration at room temperature. Baldo *et al*[10] found evidence that triplet migration in tris(8-hydroxyquinoline) aluminum (Alq3) has dispersive nature even at room temperature; unfortunately, no detailed account on the dispersive triplet migration can be found in this publication. Thus, it turns out that dispersive transport is relevant in certain OLED materials at room temperature while in others the impact of it might be negligible. However, in most of the reports about triplet diffusion researchers tend to avoid the dispersive migration topic and exclude it without any experimental justification by confining themselves to a few ambiguous sentences[9-11]. In order to avoid this type of neglect, in this chapter, fundamental properties of

both transport regimes in NPB, dispersive and non-dispersive, will be unveiled - when and at what temperature the change between the two takes place and what is the overall mechanism of TTA. This chapter will begin with an overview of the basic triplet and singlet states of NPB film and determination of the origins of delayed fluorescence in NPB films. Then, dynamics of phosphorescence will be examined and properties of delayed fluorescence will be presented at various temperatures and in various migration regimes. Finally, the width of the density of states will be determined and the influence of film thickness on triplet dynamics will be presented.

6.2 Results and Discussions
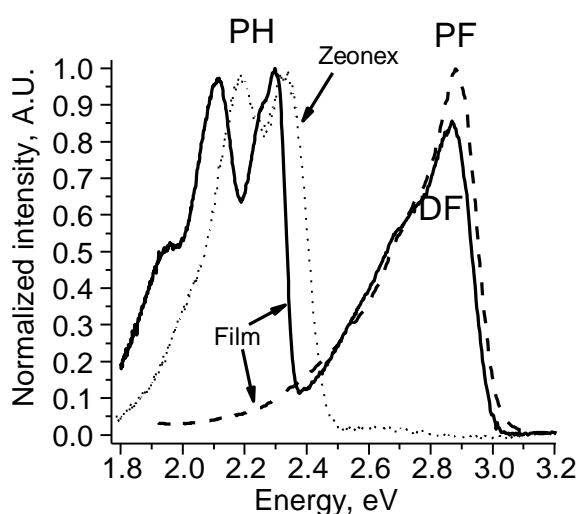
Figure 6.1 Prompt fluorescence-PF (dotted line), delayed fluorescence-DF (straight line) and phosphorescence-PH (straight line) spectra of evaporated NPB thin film and NPB in inert Zeonex matrix at dilute concentration (1E-4 weight-to-weight ratio-dotted line). Spectra are normalized to enable comparison since PF spectra intensity has much higher intensity than DF. PH and DF have been recorded 5 ms after excitation, and PF has been recorded during the first 10 ns after excitation. All spectra recorded at 12 K.

Prompt fluorescence (PF), delayed fluorescence (DF) and phosphorescence (PH) spectra of an evaporated NPB thin film are depicted in figure 6.1. The peak of DF and PF is at ~2.87 eV and first vibronic levels of PH are at ~2.29 eV which is similar to literature values[16]. The PH spectrum of NPB has been recorded in an inert matrix zeonex at very dilute concentrations (figure 6.1) which is blueshifted in comparison with film to ~2.35 eV. No DF has been observed from NPB in zeonex. The PH monoexponential lifetime of NPB in dilute zeonex was ~1 s at 14 K indicating very little non-radiative decay in this environment (compare with film below). Based on the DF and PH dependence on laser excitation pulse energy it can be concluded that the DF origin in films is non-monomolecular (figure 6.2).
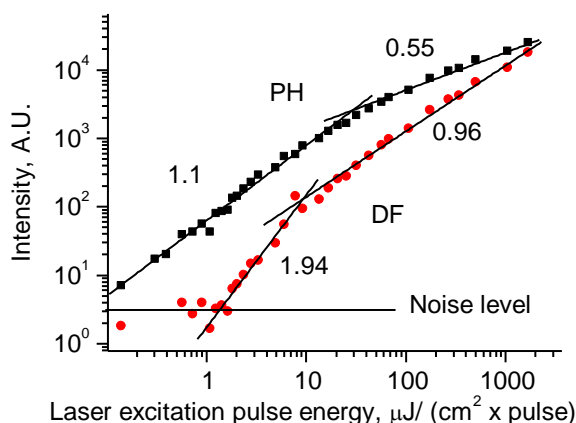
Figure 6.2 Delayed fluorescence-DF (circles) and phosphorescence-PH (squares) dependence on laser excitation pulse intensity of 250 nm NPB film at 12 K. PH and DF have been recorded 6 ms after excitation; gate time was 5 ms. Linear curves are fits to PH and DF with the slopes as indicated on the graph. Noise level is indicated as horizontal dark line in order to show that at very low excitation intensities DF is not observed and PH is already present.

Most of the noise in the graph comes from laser shot to shot fluctuations. Initially PH dependence on excitation intensity has a slope of 1.1 and DF has a slope of 1.94. At higher intensities PH follows the slope of 0.55 and DF follows the slope of 0.96. One would expect to get slopes 1 for PH and 2 for DF assuming that monomolecular decay is dominant. If bimolecular decay dominates the DF should be proportional to the initial excitation whereas the PH intensity should be proportional to the square root of the initial excitation. This is exactly what is observed. This type of excitation dose dependence of PH and DF has been already recorded in polyfluorene frozen solutions and films in refs[2-3, 17]. Furthermore the slope of the intensity increase of the DF is twice as large as that of PH which suggests a bimolecular character of delayed fluorescence emission. In addition to, an E-type DF origin can be safely rejected because the difference between the singlet level and triplet level is 0.55eV - much more than k_BT at room temperature. So it can be concluded that DF in NPB originates from triplet-triplet annihilation (TTA). In all further experiments the excitation pulse energy in the region where bimolecular decay is dominant were used.
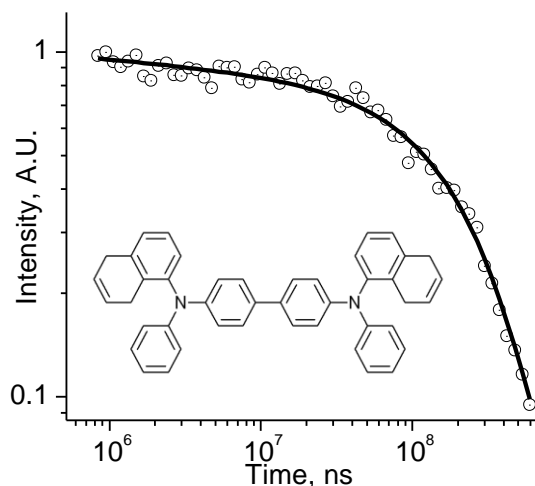
Figure 6.3 PH decay curve from a 250 nm NPB (structure drawn) film at 12 K in a log-log fashion. Black curve corresponds to fit of the form $t^a \exp(-t/t_1)$ with a=-0.04 and t_1 =243 ms. Interpretation can be found in text.

In figure 6.3 the decay curve of the phosphorescence is depicted in a log-log scale. The black curve fitted is proportional to $t^a \cdot \exp(-t/t_1)$ with an exponent a=-0.04 which is different from the expected value of -1 as in equation (3.17). A similar fit of PH decay of polyfluorene measured using time resolved photoinduced triplet absorption technique has been reported by Rothe *et al*[3] for a polyfluorene derivative and it has been ascribed to the manifestation of dispersive exciton migration when temperature approaches 0 K. The exponent a is of very small value, making it experimentally very difficult to observe this deviation from pure exponential law, thus more experiments were performed in order to show that the dispersive transport is present in this system.

PH decays vs time on a log-log scale for various temperatures are plotted in figure 6.4. It is clear that upon increasing the temperature the PH decay approaches a t^{-1} law, i.e. the non-dispersive regime for which equation (3.17) is valid. These results completely agree with the Monte Carlo (MC) simulations that can be found in reference [19]. The decays were recorded at late times after excitation, i.e. some 6, 7 orders of magnitude longer and it is impossible to infer from figure 6.4 how triplets behave at early times. This is of interest since the migration just after excitation should mainly determine the path length of the triplets' diffusion as well as TTA intensity. To gain more insight into triplet migration by using the PH signal is complicated due to the DF signal, which is much stronger at early times. In order to understand what is happening just after excitation one needs to carefully examine the dynamics of fluorescence states, mainly the dynamics of delayed fluorescence.
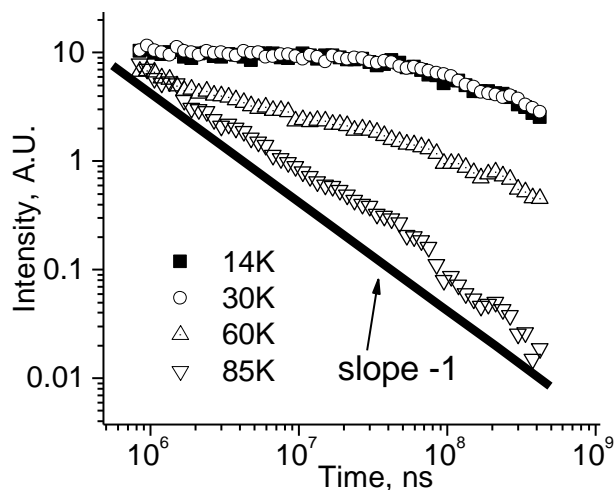
Figure 6.4 PH decay curves from a 250 nm film at various temperatures in log-log fashion. With an increase of temperature, the PH decay approaches t^{-1} i.e. the non-dispersive regime starts to dominate at late times. Straight line is a simulation of how t^{-1} non-dispersive TTA dominant PH decay would behave.

The prompt fluorescence lifetime at 12 K of a 250 nm NPB film is 3 ns (figure 6.5, fitted to dashed line), close to the reported values[20]. However, after ~40 ns the decay enters a power law regime with a slope of -0.96. For a non-dispersive equilibrium regime where TTA is dominant one should expect the slope of -2 (equation 3.19) which is not the case. The DF decay slope for a TTA dominated dispersive regime can be derived. According to equation (3.22) for highly disordered materials when T→0, D(t) is proportional to $1/[t \cdot \ln(v_0 t)]$ [14]. This in turn can be approximated as $D(t) \sim t^{-1.04}$ in the long time limit[18] and $k_{TT} \sim D(t)$. If as shown above triplet concentration decays as $t^{-0.04}$ (or is almost constant assuming DF does not significantly deplete the triplet resorvoir i.e. exponent is 0) and the exponents -1.04 (time dependent TTA coefficient) and -0.04 (or 0) are plugged into equation (3.19), DF then decays as $t^{-1.12}$ (or $t^{-1.04}$ again assuming triplet concentration is constant) which is close to the value obtained experimentally (-0.96). Scheidler et al using Monte Carlo simulations[19] have shown that in the dispersive triplet migration region PH should decay with power law having slope ~-0.04 (or is nearly constant i.e. slope is ~0 see ref[19]) and DF should decay with a power low having slope ~-1. In non-dispersive regime PH decay slope approaches -1 and DF decay slope approaches -2 that can easily be derived from equations (3.17) and (3.19). In addition, similar slopes (PH~-0.04 and ~DF -1) in the dispersive regime have been observed for conjugated polymers[2-3]. Thus resting upon theoretical evidence as well as Monte Carlo simulation and similar experimental observations, on could ascribe that TTA arising from dispersive migration is responsible for the power law with ~-1 slope (figure 6.5).
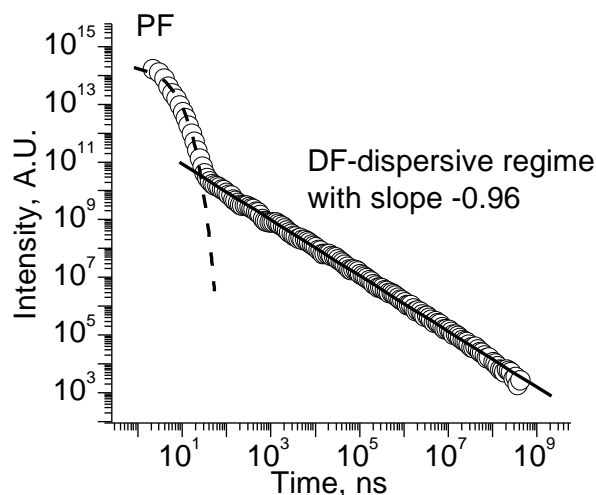
Figure 6.5 Decay curve of prompt and delayed fluorescence from a 250 nm film at 12 K. Dashed line corresponds to 3 ns exponential fit of PF; after ~ 40ns decay starts to follow the power law. This is the decay of DF, with a straight line fit in log-log scale with -0.96 slope.

The discrepancy between the expected (-1.12 or -1.04) and recorded (-0.96) slope values might arise from trap states outside the density of states (DOS) present in film as was suggested by Rothe *et al* [3]. The triplet trapping rate is hopping limited thus should have the same time dependence as the annihilation rate[5]. This means that triplet trapping and TTA could balance in time giving the similar power law time dependence however with slightly different slope. It is important to point out, that the curves, which have been recorded, come from inherent mobile NPB triplets in the NPB density of states. The PH spectra were intrinsic to NPB mobile triplets in NPB DOS peaking at ~ 2.3 eV[16]. No excimer emission emission was observed as in ref[1]. One would not expect to observe energy relaxation (see below, figure 6.11) from traps outside the density of states and power law decays from aggregates or traps outside the DOS. These decays should be of exponential form (mono, bi, or triexponential etc.). In addition, delayed fluorescence spectra from which DF decays were calculated were peaking at ~2.87 eV and this is genuine NPB singlet state emission[1].
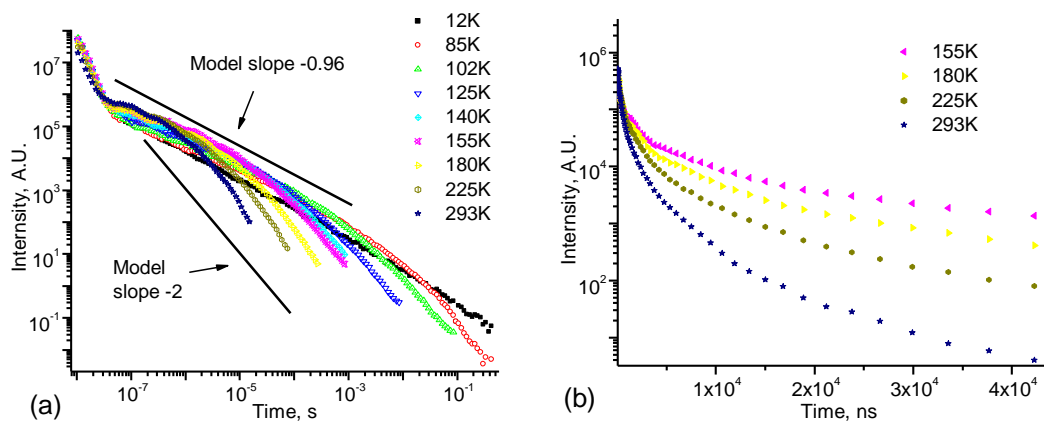
Figure 6.6 (a) Delayed fluorescence decay curves from a 250nm NPB film at various temperatures in log-log scale. (b) Decay curves at higher temperature in log-lin scale included with intent to show that the decays are far from exponential. Curves are not normalized.

In figure 6.6, delayed fluorescence decay curves at various temperatures are depicted in a non-normalized fashion. Each curve has been recorded with the same set of parameters enabling intensity comparison. It is clear from the graph that with increasing temperature the DF decay starts to divert from -0.96 slope and approaches classical -2 slope of a non-dispersive equilibrium triplet migration regime. The time at which the transition from the dispersive to the classical non-dispersive regime takes place is called the transition time t_s. In addition to this, around 100 ns to 800 ns with increase of temperature one can observe a gradual increase of DF intensity of slope ~-0.6 (figure 6.7). As can be inferred from figure 6.6 the same can be easily observed for the decays at higher temperatures up to room temperature. This might be an acceleration region as at higher temperatures more and more triplets can overcome barriers between different energy sites in the DOS. This increase of DF at early times has been mentioned in some reports with Monte Carlo calculations of exciton hopping as well been observed in polyfluorene [3, 19, 21]. However, in polyfluorene this early delayed fluorescence increases up to 130 K and then decreases after this temperature indicating that some other triplet deactivation process apart from TTA is turned on with increase in temperature[21]. This means that one could not make use of polyfluorene TTA in organic light emitting devices to extract light as has been done by Kodakov et al[22-23] or Murano et al[24]. NPB probably would be more suitable candidate for use in OLEDs where TTA is used to extract additional light as it has very efficient acceleration region up to room temperature.
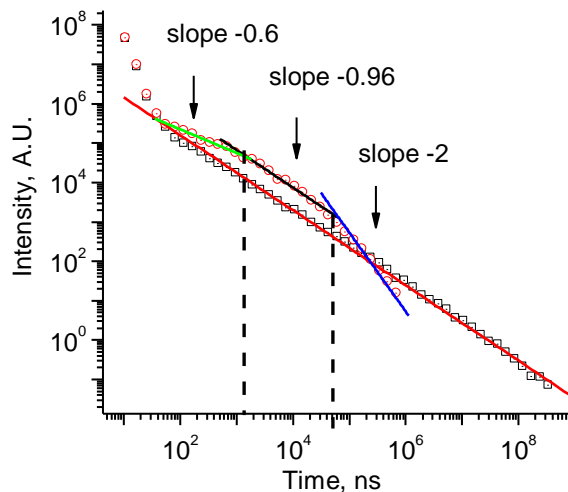
Figure 6.7 An example of three triplet migration regimes for DF decay curve at 140 K (circles) and their transition time indicated by dashed lines. Squares correspond to DF decay at 12 K included for comparison.

An example of how the transition times t_s can be determined is shown in figure 6.8. The dispersive regime slope has been determined by fitting 12 K temperature decay curve that in this case is - 0.96. At higher temperature, in this case at 155 K, curves tend to enter the -2 slope regime and exact time is found by the intersection of -2 and -0.96 slope curves (dashed line). The same is done for the 293 K curve. The transition time can be plotted versus the inverse square of temperature as shown in figure 6.9. One can fit a linear line in semi-ln scale and determine the DOS width, σ, according to equation (3.21), which for a 250 nm film equals to 42.9 meV. This value is very similar to values found for polyfluorene by Hertel *et al*[2] (36 meV) and by Rothe *et al*[3] (41 meV).

For benzophenone this value was found to be 45.88 meV [7]. Therefore, value of 43 meV is in the same range as already known experimentally determined DOS variances for other organic disordered materials. Further it is interesting to note that $k_B T$ at room temperature is ~ 25 meV which is almost half the DOS width. Thus, it suggests that even at room temperature it is possible to observe some relaxation towards the edge of the DOS i.e. at the beginning the transport will not be in equilibrium.
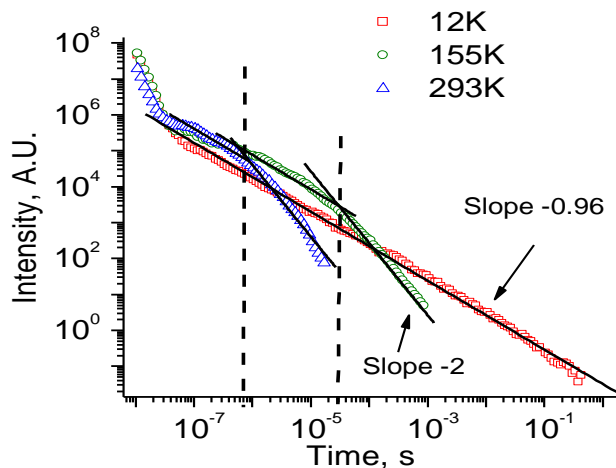
Figure 6.8 Example of how transition times t_s were determined from delayed fluorescence decay from NPB films using intersections of -0.96 and -2 curves. Linear fit with the slopes of -0.96 and -2 are shown as straight lines and indicated on the graph appropriately. Dashed lines denote the time value of intersection.

The intercept of the curve in figure 6.9 corresponds to a dwell time t_0 and in this case it is 253 ns. t_0 values of 70 ns and 55 ps for polyfluorene derivatives have been reported in Rothe *et al* [3] and Hertel *et al* [2], respectively. Both authors used equation (3.19) to analyze their data. However, the value of 55 ps was reported for the polyfluroene in frozen methyl tetrahydrofuran (MTHF) matrix between temperatures 100 K and 130 K. At these temperatures MTHF does not form a good glass, and it may crystallize, so it is reasonable that TTA has been accelerated by the solvent matrix[3].

Here a word needs to be said about the fitting of DF decay curves in a non-dispersive regime. Equation (3.19) was fitted, which is a simplified solution of equation (3.16). However, one could use the full solution of equation including monomolecular decay to fit instead[25]:

$$[T] = \frac{k_r + k_{nr}}{([k_r + k_{nr}]/[T_0] + k_{tt})e^{(k_r + k_{nr})t} - k_{tt}} \qquad (6.1)$$

k_r and k_{nr} are radiative and not radiative decay rates respectively, k_{tt} is triplet annihilation constant, [T] is triplet concentration and $[T_0]$ triplet concentration at time 0. Assuming that the PH intensity is proportion to the triplet concentration [T] and that DF is proportional to $[T]^2$ one could fit the squared equation (6.1) (similarly was done by Hertel *et al* [2]) to the non-dispersive decays of DF in order to determine the turnover time between dispersive and non-dispersive regime. Unfortunately it was not possible to simultaneously fit the square of equation (6.1) to

both dispersive and non-dispersive regions of the DF decay curves (or the fit is not physically meaningful with $k_r+k_{nr}<0$).
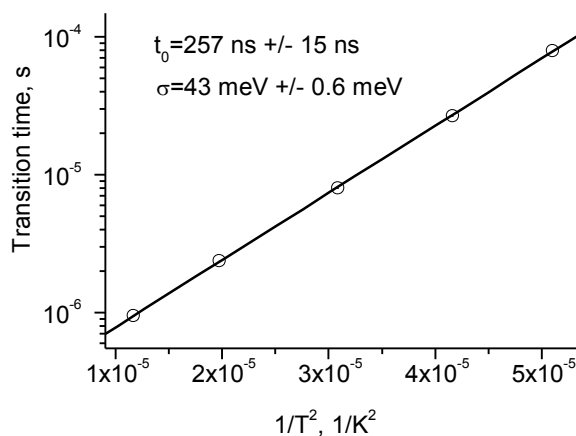
Figure 6.9 Transition times t_s plotted in semi-logarithmical fashion versus inverse squared temperature. Standard error of each transition time is ~2.5 % and is not seen on graph due to the presentation in a log scale.

In the non-dispersive regions at lower temperatures (of DF decay) the square of equation (6.1) does not fit as well as equation (3.17) and this probably reflects the fact that the monomolecular decay rate is very small at low temperatures. At higher temperatures especially at 293 K equation (3.17) could be fitted meaningfully and k_r+k_{nr} and k_{TT} determined, but only at the non-dispersive region of the curve. However, the transition times between dispersive and non-dispersive transition regimes at higher temperatures are similar irrespectively whether one fits equation (6.1) or equation (3.17) to the non-dispersive decay part of curves. Thus for the purpose of determining transitions times equation (6.1) is not more suitable than equation (3.17). Furthermore, in references 2 and 3 the authors used equation 3.17 instead of full solution to determine transition times in conjugated polymers and these systems are very similar to NPB – monomolecular decay of PH at low temperatures in the range of hundreds of milliseconds, triplet DOS in the range of 40 meV.
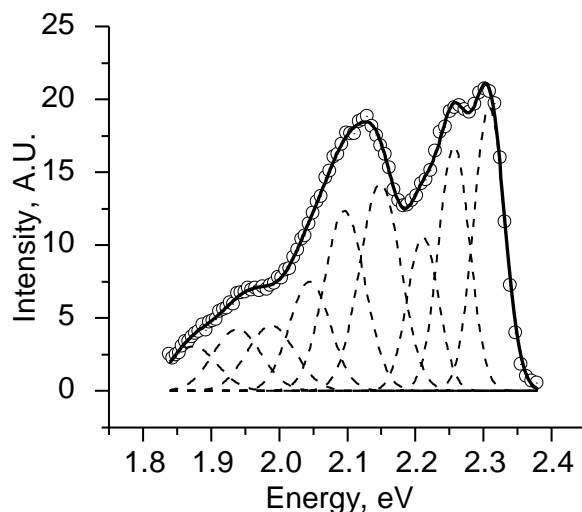
Figure 6.10 Phosphorescence spectrum of 250 nm NPB film recorded at least 100 ms after excitation at 12 K (black circles). Straight line represents 9 peak Gaussian fit, whereas dashed lines are 9 Gaussians fitted. Gaussian variance of the first vibronic band is 45 meV. For the process of fitting we refer to the text.

Another way to find the DOS variance and double check the results would be to fit a Gaussian of the form of equation (3.15) to the first vibronic levels of the phosphorescence spectrum. In the spectrum one can resolve three broad bands whereas in the first band two vibronic peaks can be seen. Since the first probable vibronic peak of the PH spectrum of NPB overlaps with the second, totally 9 Gaussian peaks of similar width have been used to fit the PH spectrum recorded at 12 K (figure 6.10). Fitting energies were based on the infrared and Raman spectra of NPB that can be found in refs [26-27]. The first peak at 2.308 eV (dashed line in figure 6.10) was assigned to the 0-0 band; the successive 8 vibronic bands are approximately 0.051 eV apart from each other. Indeed, there is an intense peak in the infrared spectrum around this energy[27] that has been assigned to CC torsion of naphthyl[26]. Also, referring to the same IR spectra one could infer, that every second peak (~0.096 eV apart) could be the CH wag of a naphthyl moiety. Both of those modes are ascribed to the out of plane rotations. Every third peak is 0.16 eV apart and in the IR spetrum[26] as well as in the Raman spectrum[27] this peak is clearly present. In both references it is assigned to CH bend, CN stretch and CCN bend of phenyl. These correspond to in-plane vibrations and are therefore more energetic. Clearly, they constitute a fingerprint of the three broad bands which are seen in figure 6.10.

All of these vibronic modes happened to be multiplies of around 0.05 eV and they are almost superimposed on one another, and thereby broadening the three bands even more as they successively overlap with each other. Thus, they are better resolved only in the first band. It is intuitive to claim that triplet states are localized around nitrogen atom and indeed the assignments made above only support this, since all in-plane and out-of-plane vibrations and

rotations are related to the near proximity of a nitrogen atom, i.e. naphthyl moiety or nitrogen atom itself. The resultant width of Gaussian fitted to the first vibronic band is ~45 meV, which is in agreement with σ ~43 meV.
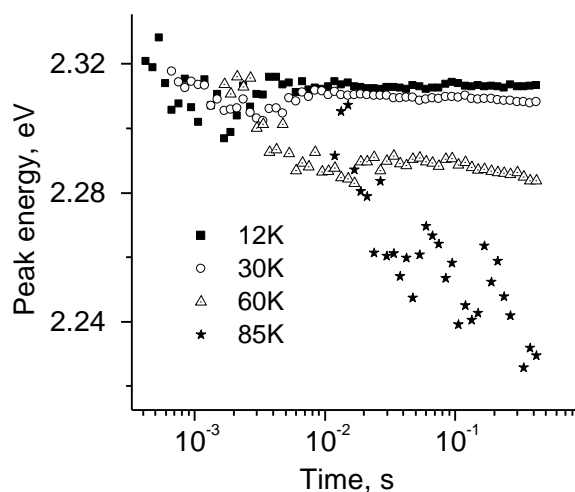
Figure 6.11 PH first vibronic peak change in time for 250 nm NPB film, at different temperatures. The peak determined by Gaussians fittings to PH spectra.

In addition, freezing-in effect of PH peak energy has been observed, which is another manifestation of the non-equilibrium effect in highly disordered materials (figure 6.11 and references [3, 15]). The higher the disorder parameter (the lower the temperature) the longer the time it takes for the relaxation of triplet energy. For a temperature of 12 K, the peak energy of PH relaxes to 2.31 eV only in the first 100 ms, while for 85 K in the same time it relaxes up to ~2.22 eV. This clearly shows the quasi detrapping of triplets at higher temperatures due to thermally activated hopping thus enabling them to relax earlier and consequently the transition time from dispersive to non-dispersive regime should take place earlier for higher temperature decays.

When T approaches 0 K, the PH peak energy change should follow equation (3.23). In this way it is possible to find the peak of the first PH vibronic band at time = 0 (i.e. triplet level at time = 0 s). In figure 6.12, the peak energy of the PH spectra of a 250 nm NPB film at 12 K as a function of time on a lnln scale is depicted ($k_b T/\sigma$ =0.02<0.1 for this temperature is much smaller than required so one can apply equation (3.23) safely).
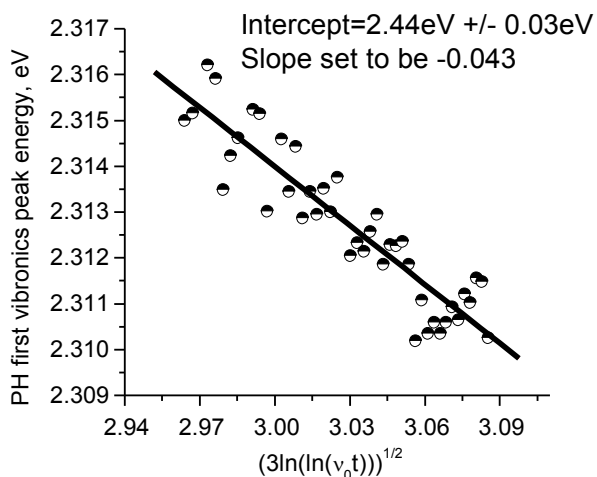
Figure 6.12 First vibronic peak of PH spectrum at 12 K plotted vs. a ln ln time scale. Straight line linear is fit to data, slope set to be -0.043, intersecting ordinate axis at 2.44 eV ± 0.03 eV.

ν_0 has been chosen to be such that the slope would fit to -0.043 eV and then the ordinate intercept was calculated to be 2.44 eV ± 0.03 eV. This value is much higher than the triplet value for NPB (2.28 eV) published elsewhere[16], and that determined (~2.3 eV) from phosphorescence spectra above. Similar discrepancies have been observed for polyfluroene triplet level[3]. But the higher triplet energy for polyfluorene at time zero determined in a similar way by authors of reference [3] agrees well with what has been determined experimentally by pulse radiolysis energy transfer measurements which yields the equivalent t = 0 s unrelaxed triplet energy [3, 28]. Thus it is probable, that the determined triplet levels E_T (which are normally detected from a phosphorescence spectrum at later times) for other disordered materials, small molecular glasses or conjugated polymer [10, 16], are lower than at time = 0 s, E_{T0}. Indeed, it is highly possible since normally phosphorescence spectra by most groups are recorded in long time limit when up to 5-6 decades of time have lapsed. This allows triplet excitons to relax to the energy tail of the DOS and thus most of the triplet levels E_T might be lowered in comparison to their true value E_{T0} and for energy transfer the key value might be E_{T0} not E_T.
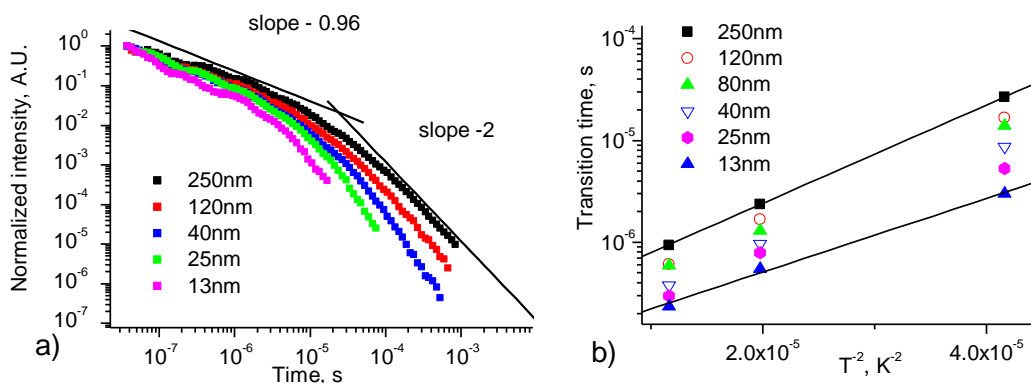
Figure 6.13 a) DF decay of NPB at 155 K for various thickness films in log-log scale. Straight lines correspond to linear fits with the slopes -0.96 and -2. b) Transition times t_s plotted in semi-logarithmical fashion versus inverse squared temperature for NPB films having different thicknesses. The results of linear fits (intercepts and density of state variance) at each thickness are in table 6.1. Straight black lines are drawn for visualization of different slopes.

The same set of experiments has also been repeated for different thickness of NPB films, an example of DF decay curves for 155 K is shown in figure 6.13. The thinner the film, the faster the dispersive regime changes to a non-dispersive classical triplet migration regime; 13 nm film having the fastest transition time. One should expect a change of t_0 and probably σ with the change of thickness. It is seen from the figure 6.13 and table 6.1 that this is the case. The thinner the film, the smaller the slope and intercept (exciton dwell time) in the semi-log graph of t_s indicating that with the decrease of thickness, surface effects (surface states) tend to become more important to triplet dynamics. First, surface effects clearly have a huge effect on the dwell time by decreasing it from 257 ns for a 250 nm film (table 6.1) to the value of 95 ns for a 13 nm film, which is already close to polyfluorene value of 70 ns[3].

The DOS width decreases with the decrease of thickness by approximately 13% if one goes from a 250 nm film to a 13 nm film (figure 6.14). If one plots DOS variance against thickness of film one gets a 1/thickness dependence, with the DOS variance saturating after a certain thickness, indicating that surface states no longer affect the TTA decay, and as a consequence DOS calculations. The DOS width approaches the asymptotic value of 43 meV (figure 6.14). However, for thinner films surface effects might have some significance by decreasing this value. This could be the consequence of a Gaussian distribution of energies of excited states. The reason for this type of distribution in organic crystals and glasses is statistical local fluctuations of the polarization energy of a charge carrier and/or the van der Waals energy of excitons[29]. The polarization energy of charge or van der Waals energy of excitons near the

93

surface is clearly different from the polarization energies in the bulk, since near to the surface there is an absence of polarizable medium from the vacuum side. The thinner the film, the more the triplet exciton distribution is determined by energies of surface sites, i.e. the smaller statistical fluctuations of near surface states determine the smaller density of states distribution. As well, it is possible that the bulk morphology is changing with the change of thickness. These might not be the only reasons of a change of the DOS width with the change of thickness. Another reason could be simply the decrease of the number of possible states with the decrease of one of the dimensions (thickness). Although it is very difficult to quantify it, if one decreases the volume by sufficient amount it is possible that the DOS decreases by the virtue of the decrease of number of possible excitonic states. Though this seems a plausible reason for the decrease of the DOS width, the former explanation is preferred by the author of this thesis; further experiment described below supply more evidence towards the first hypothesis of surface state effects.

Table 6.1 Intercept, t_0 and slope (density of states variance σ) for NPB films having different thicknesses.

Thickness, nm	Intercept, ns	Slope, σ
250	260	42.9
120	180	42.6
80	170	41.9
40	120	41.4
30	114	40.0
25	108	39.5
13	95	37.1
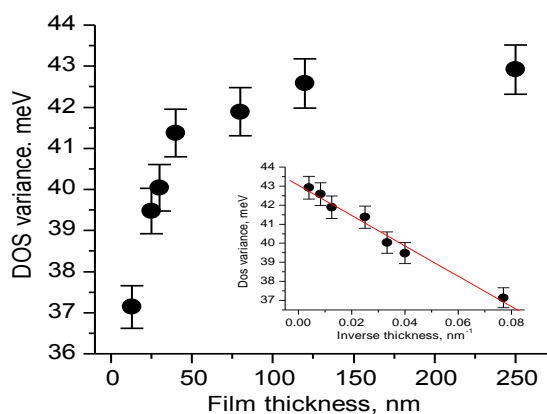
Figure 6.14 Triplet DOS variance plotted against thickness of NPB film. The resultant curve follows reciprocal function law and approaches asymptotic value of 43 meV. Inset: the linear fit of the DOS variance vs inverse thickness.

Repeating the experiments described above for NPB films with a 33 nm $Ir(piq)_3$ film on top of each NPB film we observe a different dependence of the DOS width with the decrease of thickness of NPB film. In bilayer films at very small thicknesses NPB triplet DOS width is smaller than DOS width of single layer NPB films (figure 6.15). These results show that an $Ir(piq)_3$ film, instead of vacuum, changes the local statistical fluctuations of surface states (as well as DOS distribution). This is another fact confirming that the main reason for a change in DOS with thickness being due to a surface state effect rather than the decrease of total possible density of states as discussed above. Of courses this is not conclusive evidence as it has been done only with one material, and further experimental evidence need to be collected, for example, using other materials, but the change of DOS width when another material is on top of NPB nicely fits with surface state effect hypothesis.

The dwell time dependence on thickness changes after the addition of an $Ir(piq)_3$ layer as well (figure 6.15). For very thick films above 100 nm the $Ir(piq)_3$ layer dwell time does not change whereas for thinner films, especially below 50 nm, the dwell time, is significantly decreased for an $NPB/Ir(piq)_3$ film complex in comparison with an NPB/vacuum film. This decreased dwell time shows that there is movement or diffusion of triplets from NPB film to the $Ir(piq)_3$ film. This will be discussed in the following chapters.
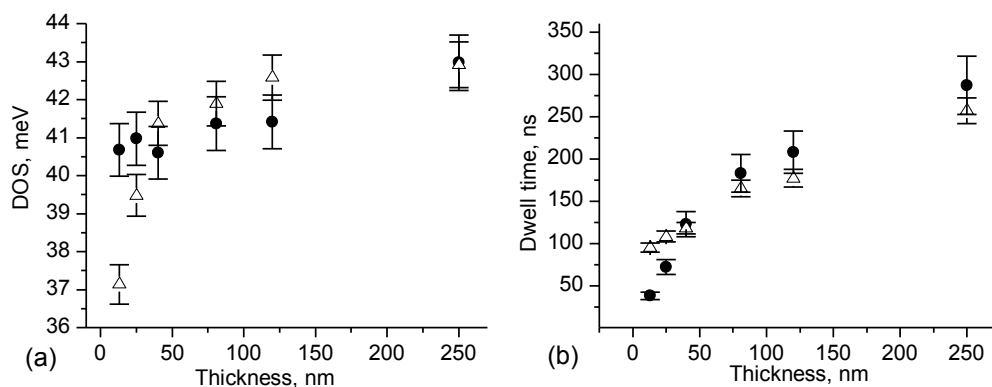
Figure 6.15 Triplet DOS width (a) and dwell time (b) plotted against thickness of NPB film in NPB/Ir(piq)$_3$ bilayer film (black circles). The NPB/Ir(piq)$_3$ was excited from NPB side and Irpiq thickness in bilayer all the time was 33nm. For comparison, the DOS variance of NPB film only is plotted as triangles.

6.3 Conclusions

Triplet migration properties of NPB thin films have been studied. The phosphorescence lifetime at 12 K was determined to follow not an exponential decay law but $t^a \cdot \exp(-t/t_1)$ law with an exponent a equal to -0.04. Intensity dependencies of PH and DF suggest that DF in NPB films is from triplet-triplet annihilation (TTA). The triplets of NPB films decay in a similar fashion to that which has been predicted theoretically, as well as by Monte Carlo simulations and it follows the same pattern as was determined experimentally for conjugated polymers. At first, the dispersive non-equilibrium regime with the slope -0.96 prevails, whereas later it turns to classical -2 slope for a non-dispersive equilibrium regime. From the turning points between the two regimes at various temperatures, the variance of Gaussian triplet density of states has been determined for various film thicknesses. It approaches an asymptotic value of 43 meV for infinite thickness, which possibly is the real DOS variance for an NPB film in which surface states do not have any importance. However, for thinner films for example of 13 nm, the DOS variance decreases to ~37 meV. After evaporating Ir(piq)$_3$ film on top, DOS does not decrease so significantly as for the single layer NPB film on its own and is almost constant, indicating that a poralizable medium near the NPB surface has an impact for NPB DOS variance. This means that thickness dependence can be ignored if NPB films are topped with another layer however if single layer films are examined the change of DOS should be taken into account. Furthermore, the results demonstrated that for high excitation doses even at room temperature the dispersive regime is still present for some time (~ few hundreds of nanoseconds, actual number depending on thickness). Whether it has to be taken in account depends on the times scales at which triplet dynamics are studied. For example, if multilayer films are studied and

triplet diffusion through the spacer layer takes place in microseconds range classical diffusion equations safely could be applied. However if this time decreases to few hundreds of nanoseconds it is wise to take into account presence of dispersive regime or if this is not possible interpret data carefully (i.e. assume that diffusion coefficient in classical diffusion equations is averaged). Finally, unrelaxed triplet level of the NPB thin film at zero time has been determined (the peak of the first vibronic band of PH spectrum) which is 2.44 eV - slightly higher than was determined from late gated phosphorescence spectra, but which should be considered when describing energy transfer processes between NPB and a dopant. Again whether it is better to use this unrelaxed value or the relaxed value when investigating triplet transfer it depends on time scales when triplet transfer takes place and what is the actual physical environment – whether the NPB is doped into another film, or a dopant is doped into NPB or NPB is neighboring another layer for example Ir(ppy)$_3$. The final conclusion of this chapter is that NPB is much more suitable spacer layer than CBP due to the reason that no emissive traps are found. As well excimer (dimer) formation can be controlled and triplet dynamic properties can be easily examined.

6.4 References

1.   P. A. Losio, R. U. A. Khan, P. Gunter, B. K. Yap, J. S. Wilson and D. D. C. Bradley, Appl. Phys. Lett. 89 (4) (2006).

2.   D. Hertel, H. Bassler, R. Guentner and U. Scherf, J. Chem. Phys. 115 (21), 10007-10013 (2001).

3.   C. Rothe and A. P. Monkman, Phys. Rev. B 68 (7), 075208 (2003).

4.   U. Rauscher, H. Bassler, D. D. C. Bradley and M. Hennecke, Phys. Rev. B 42 (16), 9830-9836 (1990).

5.   J. Lange, B. Ries and H. Bassler, Chem. Phys. 128 (1), 47-58 (1988).

6.   R. Richert and H. Bassler, Chem. Phys. Lett. 118 (3), 235-239 (1985).

7.   R. Richert and H. Bassler, J. Chem. Phys. 84 (6), 3567-3572 (1986).

8.   J. Kalinowski, W. Stampor, J. Mezyk, M. Cocchi, D. Virgili, V. Fattori and P. Di Marco, Phys. Rev. B 66 (23) (2002).

9.   S. Reineke, K. Walzer and K. Leo, Phys. Rev. B 75 (12), 125328 (2007).

10.   M. A. Baldo and S. R. Forrest, Phys. Rev. B 62 (16), 10958-10966 (2000).

11.   N. C. Giebink, Y. Sun and S. R. Forrest, Org. Electron. 7 (5), 375-386 (2006).

12.   M. Grunewald, B. Pohlmann, B. Movaghar and D. Wurtz, Philos. Mag. B-Phys. Condens. Matter Stat. Mech. Electron. Opt. Magn. Prop. 49 (4), 341-356 (1984).

13.   B. Movaghar, M. Grunewald, B. Ries, H. Bassler and D. Wurtz, Phys. Rev. B 33 (8), 5545-5554 (1986).

14.   B. Movaghar, B. Ries and M. Grunewald, Phys. Rev. B 34 (8), 5574-5582 (1986).

15.   R. Richert, H. Bassler, B. Ries, B. Movaghar and M. Grunewald, Philos. Mag. Lett. 59 (2), 95-102 (1989).

16.   H. Yersin, *Highly Efficient OLEDs with Phosphroescent Materials*. (Wiley-VCH Verlag GmbH & Co. KGaA, Weinheim, 2008).

17.   C. Rothe and A. Monkman, Phys. Rev. B 65 (7), 073201 (2002).

18.   B. Ries and H. Bassler, Journal of Molecular Electronics 3, 12-24 (1987).

19.   M. Scheidler, B. Cleve, H. Bassler and P. Thomas, Chem. Phys. Lett. 225 (4-6), 431-436 (1994).

20.   Y. Kawamura, H. Yamamoto, K. Goushi, H. Sasabe, C. Adachi and H. Yoshizaki, Appl. Phys. Lett. 84 (15), 2724-2726 (2004).

21.   C. Rothe, R. Guentner, U. Scherf and A. P. Monkman, J. Chem. Phys. 115 (20), 9557-9562 (2001).

22.   D. Y. Kondakov, J. Appl. Phys. 102 (11), 114504 (2007).

23.   D. Y. Kondakov, J. Soc. Inf. Disp. 17 (2), 137-144 (2009).

24.   S. Murano, G. He, D. Pavicic, U. Denker, C. Rothe, M. Hofmann, A. Werner and J. Birnstock, in *The 7th Int. Conf. on Electroluminescence of Molecular Materials and Related Phenomena* (Dresden, Germany, 2008).

25.   G. Dicker, M. P. de Haas and L. D. A. Siebbeles, Phys. Rev. B 71 (15), 155204 (2005).

26.   M. D. Halls, C. P. Tripp and H. B. Schlegel, Phys. Chem. Chem. Phys. 3 (11), 2131-2136 (2001).

27.   T. Sugiyama, Y. Furukawa and H. Fujimura, Chem. Phys. Lett. 405 (4-6), 330-333 (2005).

28.   A. P. Monkman, H. D. Burrows, L. J. Hartwell, L. E. Horsburgh, I. Hamblett and S. Navaratnam, Phys. Rev. Lett. 86 (7), 1358-1361 (2001).

29.   H. Bassler, Phys. Status Solidi B-Basic Res. 107 (1), 9-54 (1981).

7 Phosphorescent state properties of heavy metal iridium complexes - case study of Ir(ppy)₃ and Ir(piq)₃

7.1 Introduction

In chapter 7 properties of iridium heavy metal complexes, which will be used in multilayer structures, are overviewed. These materials have been chosen due to the short triplet lifetime and the fact that the triplet state is emissive at room temperature (unlike NPB or CBP, chapters 5 or 6). Mainly photophysical properties of *fac* - tris(2-phenylpyridine) iridium ($Ir(ppy)_3$) is overviewed and new experimental findings unveiling triplet exciton dynamics in $Ir(ppy)_3$ films are presented. Triplet exciton properties of Iridium (III) Tris(1-phenylisoquinoline ($Ir(piq)_3$) are investigated. Comprehension of triplet dynamics in $Ir(ppy)_3$ and $Ir(piq)_3$ films is relevant as it could facilitate the interpretation of multilayer film experiment data (chapter 9).

7.2 Literature overview of Ir(ppy)₃ photophysical properties

$Ir(ppy)_3$ is very widely used in phosphorescent organic light emitting diodes (PHOLEDs)[1-4]. Normally it is used as a dopant in a host material because in neat film form it exhibits substantial concentration quenching of photoluminescence quantum efficiency (PLQY)[5]. It is very important to explain the physics behind the decrease of PLQY in neat films as this knowledge could be used to chemically modify $Ir(ppy)_3$ in order to reduce concentration quenching. Also the decrease of PLQY in films should depend on triplet exciton dynamics thus explanation of the former should shed some light on the latter. A few publications have already attempted to do this and they will be summarized below. The review will start with general static properties of absorption and emission spectra.
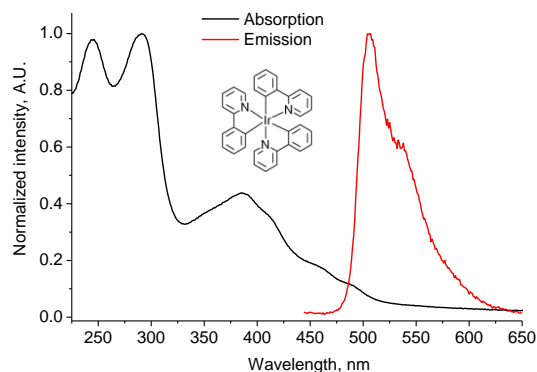
Figure 7.1 Absorption spectrum of Ir(ppy)$_3$ (structure drawn) evaporated neat film and emission spectrum of Ir(ppy)$_3$ doped in zeonex (1E-4 weight to weight ratio).

In heavy metal iridium complexes the phosphorescence spectra (figure 7.1) of the ligand centered $^3(\pi$-$\pi^*)$ transition is more structured than the phosphorescence spectra of the ³MLCT transition which is broad and featureless. This is the case in the iridium metal complex Ir(ppy)$_3$. The absorption spectrum shoulders of Ir(ppy)$_3$ in toluene (and dichloromethane) at 450 nm and 480 nm have been assigned to S$_0$→^{3}MLCT transition while peaks at 385 nm and 405 nm have been assigned to S$_0$→^{1}MLCT transition [6-7]. This is in line with assignments of the Ir(ppy)$_3$ thin film absorption spectrum recorded by Tsuboi *et al*[8] whereby peaks at 386 nm and 406 nm were assigned to S$_0$→^{1}MLCT transition and peaks at 485 nm and 452 nm were assigned to S$_0$→^{3}MLCT transition. Two intense bands at 284 nm and 242 nm have been assigned to ligand transitions[8].

Colombo *et al*[6] observed two types of phosphorescent bands in Ir(ppy)$_3$ embedded in a poly(methyl methacrylate) (PMMA) matrix. One peaking at ~510 nm was assigned to ³MLTC transition (lifetime ~2μ at room temperature) and another band appearing at ~455 nm after cooling the sample to 9 K was assigned to $^3(\pi$-$\pi^*)$ transition. When temperature is decreased Ir(ppy)$_3$ essentially becomes embedded in a more rigid matrix and molecules do not have enough time to stabilize hence the phosphorescent ³MLTC transition blueshifts with the decrease of temperature. At extremely low temperatures in certain regions of sample the lowest excited states blueshifts to such an extent that its ³MLTC energy level is aligned with $^3(\pi$-$\pi^*)$ state and the latter becomes emissive. As PMMA is amorphous and energetical disorder is present, this happens only in certain specific regions of sample whereas in other regions PMMA is less rigid and crystalline thus ³MLTC transition is still lowest state and both of the transitions are seen in spectrum.

101

Yersin *et al[9]* purified Ir(ppy)$_3$ by recristalization from DMSO and/or acetonitrile in an inert atmosphere. A purity of more than 99.99% was achieved. The emission spectrum of this single Ir(ppy)$_3$ crystal substantially deviates from one in solution or in PMMA. First of all the highest peak is at 545 nm (shift of ~35 nm in comparison with Ir(ppy)$_3$ in dilute PMMA matrix). This is reasonable as normally emission spectra redshifts in solid films. However, another shoulder at the blue side of the PL spectrum (~507 nm) is present which has been assigned by Yersin *et al* to be due to irregularities in the crystal structure due to systematic twining. They conjecture that the peak at 545 nm is from the bulk whereas the blueshifted shoulder is emission from crystal domain interfaces which have different electronic structures. They indeed observed the change of blue energy shoulder emission intensity with the change of position of the same sample. This rejects the possibility that this shoulder is due to $^3(\pi\text{-}\pi^*)$ transition in Ir(ppy)$_3$ observed by Colombo *et al* but redshifted in solid (it has been recorded at 9 K whereas all spectra by Yersin *et al* has been recorded at room temperature).

Zero field splitting in Ir(ppy)$_3$

It is well known that heavy metal complexes due to spin-orbit coupling exhibit so called triplet energy level zero-field splitting (triplet energy level splitting in the absence of a magnetic field). Yersin *et al[10]* recorded decay times of Ir(ppy)$_3$ dissolved in tetrahydrofuran at temperatures between 1.2 K and 300 K and fitted their dependence on temperature with the equation 7.1 assuming that 3 zero-field splitting substates exists:

$$k_{therm} = \frac{k_1 + k_2 e^{-\Delta E_{2,1}/k_B T} + k_3 e^{-\Delta E_{3,1}/k_B T}}{1 + e^{-\Delta E_{2,1}/k_B T} + e^{-\Delta E_{3,1}/k_B T}} \qquad (7.1)$$

where $\Delta E_{2,1}$ and $\Delta E_{3,1}$ are energy differences between appropriate substates, T is temperature, k_1, k_2 and k_3 are decay rates of 3 substates, k_{therm} is averaged decay rate, k_B is Boltzmann constant.

It was concluded by Yersin *et al[10]* that 3 substates are present each of them having substantial ^{3}MLTC character. A theoretical investigation based on time dependent density functional theory by Hay *et al[11]* concludes the same. Determined lifetimes of the 3 sublevels are τ_1=145 μs, τ_2=11 μs, τ_3=750 ns. Energy levels between appropriate states are $\Delta E_{2,1}$ =13.5 cm^{-1} and $\Delta E_{3,1}$=83 cm^{-1} (figure 7.2). Nevertheless one has to be careful with evaluation of zero-field splitting and decay times as it depends on the matrix and even individual sites in the same matrix.

III

8.7

meV

II

1.6 meV

I

$\tau(III)=$

145μs

$\tau(II)=$

11μs

$\tau(I)=$

0.75μs

0
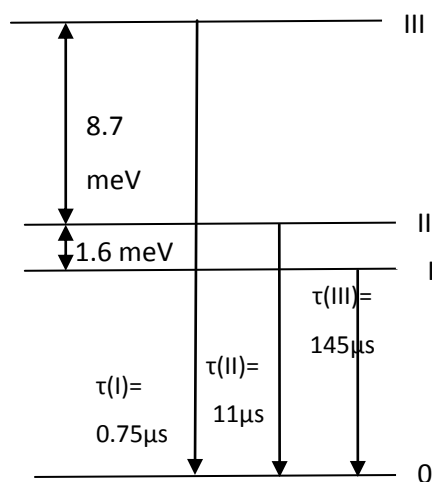
Figure 7.2 Energy level diagram and decay times of Ir(ppy)$_3$ dissolved in tetrahydrofuran. Adopted from reference [12].

At sufficiently high temperatures all 3 substates equilibrate lifetime of which can be calculated using formula[12]:

$$\tau_{therm} = 3\left(\frac{1}{\tau_1} + \frac{1}{\tau_2} + \frac{1}{\tau_3}\right)^{-1} \qquad (7.2)$$

Using the values of Ir(ppy)$_3$ from figure 7.2 one arrives at the equilibrated value of approximately 2.1 µs which is very close to reported triplet state decay values for Ir(ppy)$_3$ at room temperature (2 µs) [7]. Equilibrated lifetime value at room temperatures is mainly governed by spin-lattice relaxation processes whereby the transition between substates is followed by simultaneous transfer of excess energy to lattice vibrations. There are 3 different processes of spin lattice relaxation (SLR), namely the direct, the Orbach and the Raman process (figure 7.3).
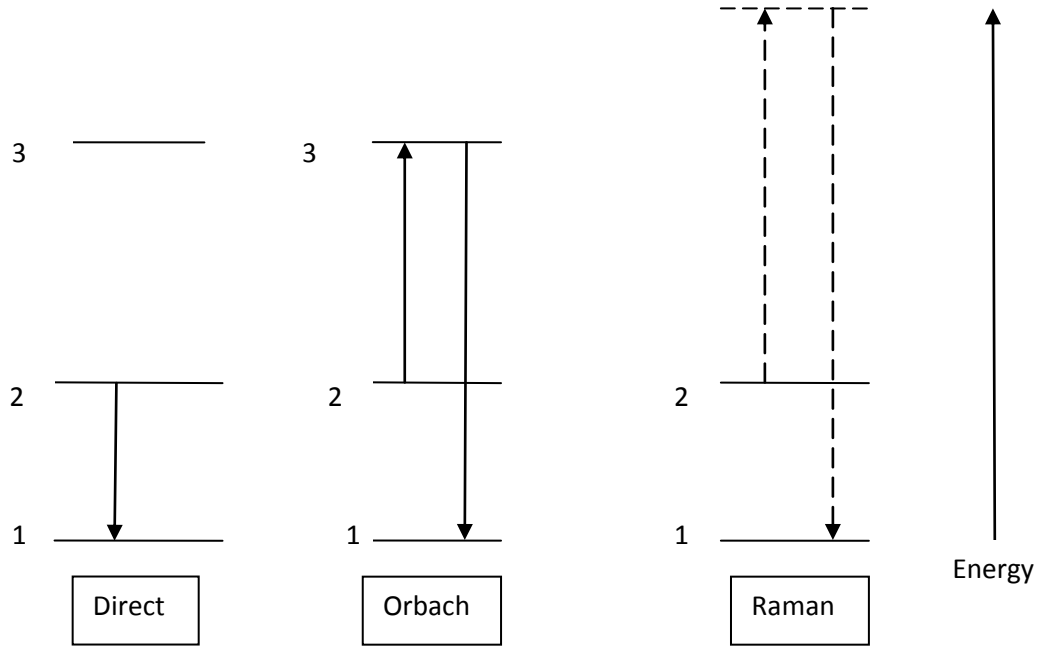
Figure 7.3 Types of spin lattice relaxation (SLR) processes. Adopted from reference [7]. More details in text.

Relaxation from substate 2 to substate 1 (figure 7.3) may occur via a direct process when one phonon is transmitted to lattice. Rate of SLR via direct process can be described as follows[7]:

$$k_{2,1}^{SLR}(\text{direct}) = \frac{3}{2\pi\hbar^4\rho v^5}\left|\langle 2|V|1\rangle\right|^2 (\Delta E_{2,1})^3 \coth(\Delta E_{2,1}/2k_B T) \qquad (7.3)$$

where ρ is density of the matrix material, v the average velocity of sound in the matrix, and k_B is Boltzmann constant. V is the perturbation caused by lattice phonon modes, which couples electronic states 1 and 2. This process does not depend on temperature heavily. At higher temperatures the Orbach process can facilitate the relaxation. A phonon of energy $\Delta E_{3,2}$ is absorbed while phonon of energy $\Delta E_{3,1}$ is emitted and the exciton relaxes from state 2 to state 1. Approximate expression for Orbach process can be written as[7]

$$k_{2,1}^{SLR}(\text{Orbach}) = \text{const}\cdot(\Delta E)^3 e^{-\Delta E/k_B T} \qquad (7.4)$$

The Orbach process vanishes as T→0 K and ΔE →0 cm^{-1}. The Raman process is a two phonon scattering process via intermediary state[7]:

$$k_{2,1}^{SLR}(\text{Raman}) = RT^n \qquad (7.5)$$

where R is a constant and n is equal to 5 or 7. Normally for organo-transition metal complexes this constant is 5[13]. It has to be mentioned that the Orbach process is usually more effective if substate 3 is present. If it is not present the Raman process becomes dominant.

Triplet exciton properties in Ir(ppy)₃ neat films

Although photophysical properties of Ir(ppy)$_3$ doped into hosts and Ir(ppy)$_3$ neat films have been widely studied[9, 14-17], unfortunately, there is no unified opinion on the reasons behind the decrease of PLQY in Ir(ppy)$_3$ films. The proposed reasons of the decrease of PLQY (in comparison with Ir(ppy)$_3$ dispersed in matrix) are contradicting – from concentration quenching[5], triplet-triplet annihilation[15] to efficiency loss due non-radiative sites[17] or radiative less efficient aggregate/excimer states[15-16]. In the literature the PLQY values of neat films ranging from 1% to 27% are published which is not reassuring and leaves the author of this thesis even more puzzled[16-20]. PLQY values of Ir(ppy)$_3$ films, evaporation parameters and references are summarized in table 7.1.

Table 7.1 Quantum yield values of Ir(ppy)$_3$ films found in literature[18].

Quantum Yield of Ir(ppy)$_3$ film	Film parameters
1 %[18]	65 nm thick, sublimed, no pressure
3 %[19]	100 nm thick sublimed, 1E-3 Pa
29 %[20]	300 nm sublimed, no pressure reported
6% (with 30% mer ratio in film)[20]	300 nm sublimed, no pressure reported
26 %[17]	300 nm sublimed, no pressure reported
12 %[16]	no thickness reported, 1E-6 Torr and rate 0.1-0.5 nm/s sublimed

Holzer *et al*[18] extracted values of triplet-triplet annihilation constants in neat fac-Ir(ppy)$_3$ film, CBP doped with 7.9 wt% fac-Ir(ppy)$_3$ and polystyrene doped with 1 wt%, 4 wt% and 8 wt% of fac-Ir(ppy)$_3$ (Table 7.2). An interesting fact is that the triplet-triplet annihilation constant of the neat film is 25% lower than of CBP doped with 7.9 wt% Ir(ppy)$_3$ and quantum yields are 0.01 and 0.61 appropriately. Intuitively one would expect the opposite relationship for TTA constant especially having in mind the initial triplet concentration in both samples are 1E19 and 3.2E17 cm^{-3} appropriately. There is no explanation proposed by authors but possibly trapping of triplet excitons in aggregates, non-emissive sites etc. due to more effective hopping in films is more efficient than in Ir(ppy)$_3$ doped in matrices. It acts as an additional exciton de-activation pathway thus TTA is decreased and is not as important as for Ir(ppy)$_3$ doped in matrices.

Another source of this non-intuitive result could be that the authors have not included triplet trap states in CBP (2.21 eV< 2.43 eV Ir(ppy)$_3$ triplet level)[21] in their modeling.

The TTA coefficient for 1 wt% in polystyrene is higher than the TTA coefficient for a neat film; again this is an unexpected result as the number of initial triplet excited states differ by around 3 orders of magnitude (higher for neat film)[18]. The average distance calculated by the authors between excited states in neat film is 4.8 nm. The average distance calculated by the authors between 1 wt% Ir(ppy)$_3$ molecules doped in polystyrene is 4.7 nm whereas the distance between excited states should be much higher as clearly not all molecules absorb photons. Furthermore, the Dexter transfer between these molecules in doped film is inhibited as they are apart from each other by more than the Dexter transfer distance which is ~ 1 nm normally[22]. These questions, however, remained unanswered by the authors of the publication. The following two scenarios might explain these discrepancies. One of them is that in doped film TTA takes place via Forster transfer, not Dexter as assumed by the authors, so it should be modeled using different equations as in ref[23] . Indeed both Leo *et*[23] *al* and Kawamura *et al*[5] discovered that the Forster process can be dominant when PtOEP is doped in CBP and when Ir(ppy)$_3$ is doped in CBP. Another scenario could be that the authors miscalculated the initial intensities by not accounting for hole-burning process which can occur in films, thus lowering the extinction coefficient[24-26] (more on this in chapters 8 and 9).

Another intriguing result presented in this paper is that TTA coefficient decreases with an increase of concentration of Ir(ppy)$_3$ in polystyrene. Forrest *et al*[27] found very similar results for PtOEP doped in Alq$_3$ and ascribed it to poor triplet confinement. Unfortunately one could not use the same justification in this case as triplets are confined very well in a polystyrene matrix. A summary of TTA coefficients of Ir(ppy)$_3$ in different host environments published by Holtzer *et al*[18] is presented in table 7.2.

Tsuboi *et al*[15] studied neat Ir(ppy)$_3$ and used numerical calculations based on 3 triplet sublevel states and an excimer state model (totally 4 state model) to fit the experimental data. Good agreement was achieved between the simulation and experiment indicating that apart from 3 sublevels states another state exists which influences triplet exciton dynamics. Other results of their research was that the quantum efficiency of Ir(ppy)$_3$ film increases from 300 K to 125 K, and then decreases from 125 K to 5 K. They found that the decays of phosphorescence are multi-exponential and the lifetimes of each increases with decrease of temperature. Tsuboi *et al*[15] suggest that concentration quenching in Ir(ppy)$_3$ films are partly due to excimer formation (4th state) and partly due to triplet-triplet annihilation and polaron pair annihilation. Indeed, they observed very broad band Ir(ppy)$_3$ film emission spectra (~600 nm), which was attributed to excimer emission. Their results show that initial Ir(ppy)$_3$ triplet exciton number is only 68% of

absorbed photons. They claim triplet-triplet annihilation is responsible for this and the decrease of PLQY in Ir(ppy)$_3$ films. They concluded that neither Dexter, nor Forster energy transfer could be responsible for the quenching in Ir(ppy)$_3$ films by stating that the overlap between emission and excitation spectra of neat film at 10 K is small. There are conflicting reports and Kawamura et al[5] claim that Forster transfer is responsible for energy transfer and concentration quenching in Ir(ppy)$_3$ molecules doped in CBP.

Table 7.2. Triplet-triplet annihilation constants and PLQY of Ir(ppy)$_3$ in different environments found by Holtzer et al[18].

Material Parameter	Neat film	CBP 7.9 wt%	Polystyrene 1Wt%	Polystyrene 4wt%	Polystyrene 8wt%
PLQY %	1	61	92	85	82
Initial triplet concentration, cm^{-3}	1E19	3.2E17	2.6E16	7.9E16	2.6E17
TTA coefficient, cm^3/s	1.2E-10	1.6E-10	7.7E-10	1.3E-10	0.62E-10

Kalinowski et al[28] as well worked on photophysical properties of Ir(ppy)$_3$ films. They determined TTA constants and diffusion coefficients of Ir(ppy)$_3$ neat film by illuminating films with continuous laser light and recording film emission intensity at different excitation energies and used the following steady state equations to fit data[28]:

$$\alpha' I_{exc} - \frac{[T]}{\tau} - \gamma_{TT}^{eff}[T]^2 - \sigma_c I_{exc}[T] = 0 \qquad (7.6)$$

where $\alpha' = \frac{(1-e^{-\alpha d})}{d}$ with α being exponential absorption coefficient and d is thickness of film. I_{exc} is excitation intensity, τ is intrinsic lifetime and σ_c is the effective cross section of photionization of triplet excitons. γ_{TT}^{eff} is effective annihilation constant which is a summation of single-singlet annihilation and triplet-triplet annihilation constants. Using the solution of (7.6) Kalinowski et al got good fit to the data. However after modification of the model by accounting for non-emissive sites authors got much better fit to data. γ_{TT}^{eff} for this updated model was 2.7E-12 cm^3/s. Two main conclusions have been made by the authors - that

photoionization does not occur in Ir(ppy)$_3$ films (assuming σ is 0 does not decrease the quality of fit) and that non-radiative sites exists in Ir(ppy)$_3$ films.

Kobayashi *et al*[17] studied neat Ir(ppy)$_3$ film decay using a model with radiative decay from all 3 substates and 1 non-emissive state where non-radiative decay dominates. Kobayashi *et al* used the following equations to fit their experimental data[17]:

$$\frac{d[T]}{dt} = -\sum_{i=1}^{4} k_i [t]_i$$

$$[t]_i = [t]_1 \exp\left(-\frac{E_i}{k_B T}\right)$$

$$(7.7)$$

[T] is the number of triplet excitons, k_B is Boltzmann constant, $[t]_i$ is the population of i state, E_i is the energy difference between the i state and lowest state. The decay rate of triplet excitons and photoluminescence quantum yield could be expressed in this way[17]:

$$k_{obs} = \frac{k_1 + k_2 e^{-E_2/k_B T} + k_3 e^{-E_3/k_B T} + k_4 e^{-E_4/k_B T}}{1 + e^{-E_2/k_B T} + e^{-E_3/k_B T} + e^{-E_4/k_B T}}$$

$$PLQY = \frac{k_1 + k_2 e^{-E_2/k_B T} + k_3 e^{-E_3/k_B T} + k_4 e^{-E_4/k_B T}}{k_1 + k_2 e^{-E_2/k_B T} + k_3 e^{-E_3/k_B T} + k_4 e^{-E_4/k_B T}}$$

$$(7.8)$$

Where k_{obs} is the observed decay rate which was obtained by fitting single exponential to the data, PLQY – photoluminescence quantum yield.

They fitted equations (7.8) to the experimental data - decays and quantum yields - of neat Ir(ppy)$_3$ film versus temperature. They reject triplet-triplet annihilation as the main quantum efficiency decrease mechanism because its influence should decrease with the decrease of triplet lifetime thus quantum efficiency should increase. However, it is not the case as above 150 K the triplet lifetime decreases rapidly whereas the relative PLQY decreases. Further, they rejected the idea of a non-radiative decay channel from the triplet sub-states as the mechanism responsible for decrease of PLQY. They support this by citing Hager and Crosby[29-30] who claim that intensity dependence of ruthenium complexes where each substate had non-radiative decay channel monotonically decreased as temperature decreased whereas Kobayashi et al[17] observed the opposite (intensity level at room temperature is ~40% in comparison with highest intensity at ~125 K). They conclude that the decrease of the PLQY in Ir(ppy)$_3$ is due to the higher lying state (photons are lost during the absorption process as this state absorbs photons). In this publication it is proposed that the non-radiative state (predicted to be 121 meV higher than lowest triplet sublevel and having 3 ns non-radiative decay) is a higher lying ^{3}(d-d*) or ^{3}(π-π*)

state. They point out that Karatsu *et al*[31] proposed that in *mer*-Ir(ppy)$_3$ bond breaking via photoexcitation in higher lying ^{3}(d-d*) or ^{3}(π-π*) states can cause isomerisation and non-radiative decay. This could be feasible in *fac*-Ir(ppy)$_3$ as well. Tsuboi *et al*[15] proposed that this higher lying state is actually an excimer, and 121 meV is the activation energy required to form an excimer again creating a contradiction.

Table 7.3. Estimated lifetimes and energy differences in neat Ir(ppy)$_3$ films.[15]

State i	$\tau_i = (1/k_i)$	E_i, meV
1	66 µs	---
2	12 µs	2.45
3	0.20 µs	21.5
4	3.2 ns	121

In another publication Kobayashi *et al*[20] studied photoluminescence properties of facial- and meridional- Ir(ppy)$_3$ in thin films. Firstly, they observed that with an increase of meridional isomer ratio in films the spectra redshifts, thus *mer*- Ir(ppy)$_3$ have redshifted spectrum in comparison with *fac*- Ir(ppy)$_3$. Further from time resolved spectra they deduced that meridional isomer has a peak at ~580 nm (facial isomer at ~530 nm) and it appears at later times after excitation i.e. mer isomer has longer lifetime. The quantum efficiency of *fac*- Ir(ppy)$_3$ was found to be 29% while with a mixture of 30% meridional isomer it decreased to 6%. They conjecture that Dexter type energy transfer process dominates in these films (again opposite to what Tsuboi *et al*[15] concluded in their publication). Further if only 1% of mer isomer is present in films they project that quantum efficiency would be reduced from 92% of Ir(ppy)$_3$ in CBP to 87%.

Samuel *et al*[16] studied Ir(ppy)$_3$ and its cored dendrimers in solution and films. They concluded that in Ir(ppy)$_3$ films photoluminescence is quenched due to energy transfer to quencher sites. The rate of the energy transfer to quenching sites is 9.2E6 s^{-1} in Ir(ppy)$_3$ films, 0.8E6 s^{-1} for first generation dendrimer films, and 0.5E6 s^{-1} for second generation dendrimer films (more bulky). Decreasing quenching rate indicates that bulky dendrimer ligands inhibit energy transfer to quenching sites. According to authors the Dexter transfer rate should be of the order of 1E8-1E9 s^{-1}, so one could infer that migration via a few Ir(ppy)$_3$ sites is involved until the capture of the exciton in the trap. They calculate that the quencher species present at ~560 nm has a radiative lifetime by an order of magnitude higher than the monomolecular Ir(ppy)$_3$ species thus oscillator strength of quenching species is by an order of magnitude lower. As this has been observed for interchain aggregates in conjugated polymers before, they propose that aggregate type species might be responsible for quenching. This is confirmed by AFM images of Ir(ppy)$_3$ film where rod like aggregated structures are observed in films. However, they do not reject

other origins of traps such as weakly emissive isomer or impurity present at low concentration. They observe 12% PLQY in Ir(ppy)$_3$ films, and >22% in first generation dendrimers of Ir(ppy)$_3$ and >31% in second generation of dendrimers which is a clear manifestation of energy transfer inhibition and subsequent quenching in traps.

To summarize:

- There is at least one further 4th state (apart from 3 triplet sublevel states) present in Ir(ppy)$_3$ films. There are several proposal about the origins of those trap states. Some people claim it is non-radiative state (Kalinowski *et al*[28] – lower lying non-radiative state and Kobayashi *et al*[17] higher lying non-radiative state), some researchers claim it is radiative state (aggregate, excimer, or mer isomer, Samuel *et al*[16], Tsuboi *et al*[15], Kobayshi *et al*[20] respectively).

- There are conflicting reports about the reasons of the decrease of photoluminescence quantum yield in Ir(ppy)$_3$ neat films in comparison with dilute films. Some researchers claim that TTA is partly responsible for this[15] while others - that TTA plays no any role[17]. Kobayashi *et al*[17] conclude that main reason for decrease of QY is higher lying non-radiative state and claims that non-radiative decay pathway in 3 sub-level states could not be responsible for this. Others claim that aggregate/excimer formation is responsible for quenching[15-16] and that no Dexter or Forster transfer participates in this (i.e. no triplet migration)[15]. Kawamura *et al* proved otherwise, by showing that Forster transfer is responsible for concentration quenching[5]. From the publication by Samuel *et al*[16] the conclusion could be made that triplet migration to trap sites (aggregate, impurities or isomer) is mainly responsible for the decrease of PLQY in films.

- Reported photoluminescence quantum yield values of Ir(ppy)$_3$ films vary from 1% to 29%.

- People observe different PL spectra of neat Ir(ppy)$_3$ films. The spectrum of neat film observed by Kalinowski *et al*[28] at ~515 nm and a shoulder at 545 nm whereas Ir(ppy)$_3$ neat film PL spectrum observed by Samuel *et al*[16] has one broad band peaking at ~530 nm. Similar spectrum to the latter one has been observed by Kobayashi *et al*[16, 20].

Clearly this literature review shows that the photophysics in films of Ir(ppy)$_3$ is very complex and despite lots of attempts to shed some light on it is still unclear. There are few questions which still need to be answered by experiments:

- Why two type of steady state emission Ir(ppy)$_3$ neat film spectra are reported in literature – one peaking at 515 nm and another at ~530 nm?
- What is the reason of quantum yield variation among the reported Ir(ppy)$_3$ film values?

- How many emissive (non-emissive) states there are in Ir(ppy)$_3$ neat films and what is their origin? What would be the Jablonski diagram of observed Ir(ppy)$_3$ states in film?
- Finally what is the main reason for decrease of PLQY in Ir(ppy)$_3$ films in comparison with PLQY of doped Ir(ppy)$_3$?

7.3 Results and Discussions. Ir(ppy)$_3$

Steady state properties of Ir(ppy)$_3$ neat films
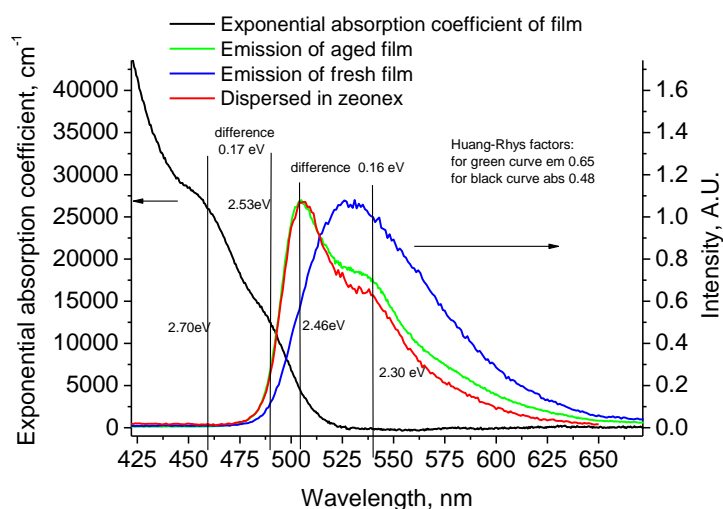
Figure 7.4 Absorption coefficient of Ir(ppy)$_3$ film (black) and emission spectra of Ir(ppy)$_3$ embedded in zeonex matrix at 1E-4 mass to mass ratio (red), fresh neat Ir(ppy)$_3$ film (blue) and aged film kept in nitrogen for a month (green).

In figure 7.4 absorption and emission spectrum of neat Ir(ppy)$_3$ film is depicted. Absorption spectrum shoulders of Ir(ppy)$_3$ at 459 nm and 490 nm could be assigned to $S_0 \rightarrow {}^3MLCT$ (see above). Spectrum of Ir(ppy)$_3$ imbedded into zeonex have a main peak at ~504 nm which in line with previous observation (section above) can be ascribed to ${}^3MLCT \rightarrow S_0$ transition. A smaller vibronic shoulder is at 540 nm. The difference between absorption and emission vibronic peaks is ~0.17 eV which is normally observed among most of the organic compounds and could be ascribed to carbon double bond vibration. The Huang-Rhys factor (ratio of 0th vibronics with 1st vibronics) is as well very similar (~0.5) for both emission and absorption spectra. This is emission from individual molecules (the concentration of Ir(ppy)$_3$ in zeonex is 1E-4 mass to mass ratio).

111

Emission spectrum of evaporated Ir(ppy)$_3$ neat film redshifts to ~530 nm and broadens in comparison with that of Ir(ppy)$_3$ embedded in a dilute zeonex matrix. After keeping this sample for 1 month in nitrogen atmosphere the spectrum becomes similar to the one of Ir(ppy)$_3$ in a dilute zeonex matrix. These two types of spectra are observed by other research groups. The spectrum of neat film observed by Kalinowski et al[28] is very similar to aged spectrum with peak at ~515 nm and a shoulder at 545 nm whereas Ir(ppy)$_3$ neat film PL spectrum observed by Samuel et al[16] and Kobayashi et al[17, 20] is very similar to fresh film spectrum with one broad peak at ~530 nm. It is probable that in freshly evaporated samples of Ir(ppy)$_3$, molecules are in energetical disorder which is determined by local crystal fields in the amorphous arrangement, hence the broader emission. One might anticipate that with time, at room temperature, this will slowly anneal to a more stable arrangement of crystal fields and the most stable facial isomer, with less disorder, thus leading to the spectrum of the aged Ir(ppy)$_3$. Lower energetical disorder will be proven to exist in aged Ir(ppy)$_3$ films in comparison with fresh films (see below).

Time resolved spectra analysis of fresh and aged Ir(ppy)$_3$ neat films
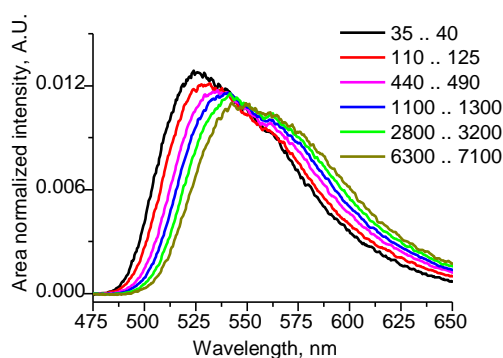
Figure 7.5 Fresh Ir(ppy) $_3$ film area normalized time resolved spectra at various times after excitation at 155 K; between 475 nm and 650nm. Camera opening and closing times indicated in the legend are in nanoseconds. No clear isoemissive point present.

Further, time-resolved emission spectra of fresh evaporated Ir(ppy)$_3$ film at various temperatures have been recorded and then normalized by area. The existence of an isoemissive point in area normalized time resolved spectra has been proven to show that two and only two emissive species exist in the system [32]. There is no isoemissive point in fresh films at a temperature of 15 K (not shown), 155 K or 293 K (figures 7.5 and 7.6). In aged film an isoemissive point is not observed at 15 K however unlike in fresh sample it already can be recorded at 155 K and at 293 K (figures 7.7, 7.8 and 7.9) that indicates the existence of two and only two emitting species (peaking at 530 nm and 600 nm). This coincides well with the species discovered by Samuel et al[16] (~560 nm) and Tsuboi et al[15] (600 nm) and ascribed to

aggregate/excimer emission. Another interpretation could be that it is *mer* – Ir(ppy)$_3$ emission (peaking at 580 nm Kobyashi *et al*[20]). Here in this thesis these species will be called 'trap 1' emission. These results indicate that either after aging more aggregates (or mer isomers) are created or that the structure becomes more ordered and hopping rate is increased thus the aggregate trap species are more quickly populated. The latter option is preferred as if the former is true more aggregate (or meridional isomer) emission in steady state spectrum of aged Ir(ppy)$_3$ film should be observed in comparison with the fresh which is not the case (section above).
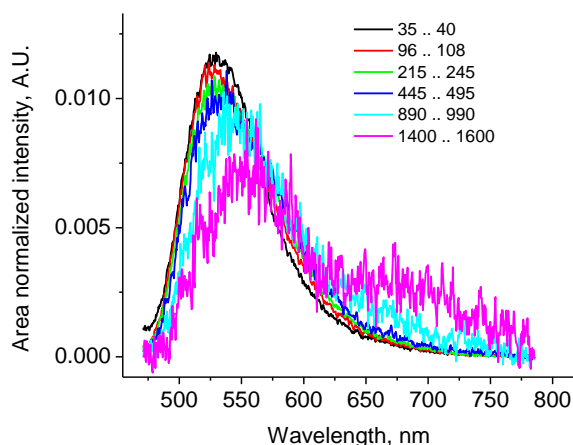
Figure 7.6 Fresh Ir(ppy)$_3$ film area normalized time resolved spectra at various times after excitation at 293 K; between 475 nm and 650nm. Camera opening and closing times indicated in the legend are in nanoseconds. No isoemissive point present.

In addition, at 15 K in neither films – aged or fresh – emission from possible aggregates (~600 nm) is observed which shows that the main absorbing species in films are Ir(ppy)$_3$ molecules where excitons are trapped at low temperatures as hopping is decreased due to lack of thermal energy. As well isoemissive point is absent in both films at 15 K so trap 1 sites (or meridional sites) clearly are populated via energy migration enhanced by thermal energy at higher temperatures and not direct laser excitation.
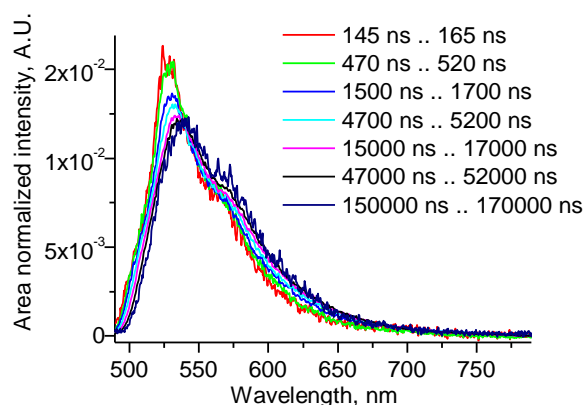
Figure 7.7 Aged Ir(ppy)$_3$ film area normalized time resolved spectra at various times after excitation at 15 K. Camera opening and closing times indicated in legend are in nanoseconds. No clear isoemissive point present.
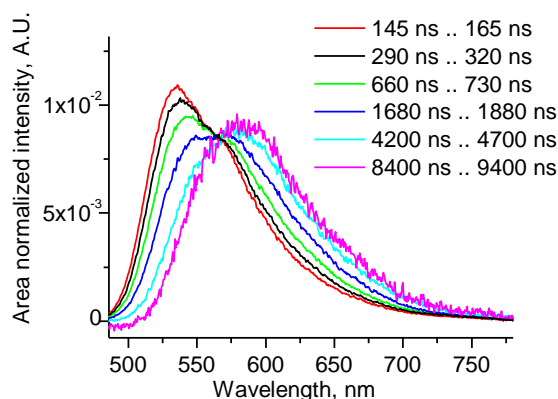
Figure 7.8 Aged Ir(ppy)$_3$ film area normalized time resolved spectra at various times after excitation at 155 K. Camera opening and closing times indicated in the legend are in nanoseconds. Isoemissive point is present and indicate presence of two and only two emissive species – one peaking at ~525 nm another at 600 nm.

The existence of triplet exciton migration in the density of triplet states of fresh films of Ir(ppy)$_3$ is supported by the peak energy dynamics with time (figure 7.10 below). For most temperatures triplet energy relaxation follows a logarithmic law until a certain time when the peak reaches a minimum and then instead of staying at this equilibrium peak energy, it starts to increase again. The higher the temperature the shorter time it takes to start blue shifting. Please see below sections for more discussions on blue shift as in this section the discussion will be concentrated on migration before it takes place.
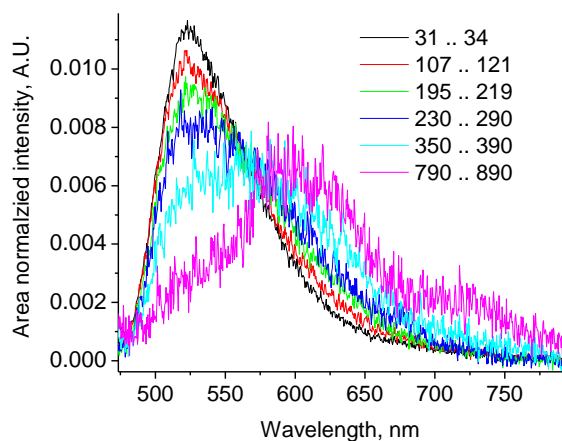
Figure 7.9 Aged Ir(ppy)$_3$ film area normalized time resolved spectra at various times after excitation at 293 K. Camera opening and closing times indicated in the legend are in nanoseconds. Isoemissive point is present and indicate presence of two and only two emissive species – one peaking at ~525 another at 600 nm.

No large scale changes of the shape of fresh Ir(ppy)$_3$ time-resolved spectra have been observed. The proportionality to log(t) indicates, that energy migration in a fresh films is of a non-equilibrium dispersive manner[33-34]. Similarly as was proven for NPB after each triplet hop the probability to visit other sites decreases as after each energetically downward hop the higher energy sites are not available for visit in the absence of enough thermal energy hence hopping rate decreases, which is proportional to the diffusion constant. The width of triplet density of states could be inferred from figure 7.10 black curve which is ~100 meV (2.42 eV- 2.31 eV - 10 meV). The DOS was calculated subtracting the highest state at 15 K from the lowest state at 15 K and further subtracting 10 meV triplet zero-field splitting (figure 7.2) as due to this splitting, peak shift can be observed which essentially is not due to the broadening of density of states. As expected Ir(ppy)$_3$ DOS is broader than the density of states of polymer films (e.g. polyfluorene[34]) and small host type molecule films (e.g. NPB-chapter 6). This comes from the fact that more states in heavy metal complex molecule films have substantial charge transfer character. Metal to ligand charge transfer states are more susceptible to polarization of surrounding material resulting in a bigger spread of energy, hence broader DOS. From figure 7.10b the triplet DOS in aged film can be calculated to be ~60 meV (highest triplet peak value-lowest triplet peak value – 10 meV). This indicates, as already predicted above, that energetical disorder decreases in aged samples in comparison with the fresh ones hence the hopping rate increases and more trap sites can be occupied (main reason why trap 1 emission is observed).
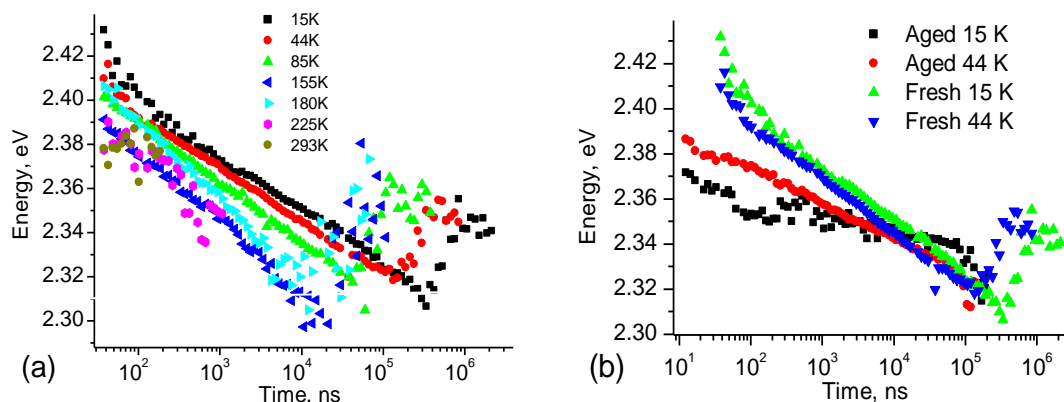
Figure 7.10 (a) Fresh Ir(ppy) $_3$ film phosphorescence peak shift in time at various temperatures in lin-log scale. Peak positions were determined by fitting 3 Gaussians to the time resolved PH spectra of Ir(ppy) $_3$ film. (b) Comparison of fresh and aged films peak shift in time at low temperatures.

Emission from other types of states in Ir(ppy)₃ films

In addition to trap 1 trap states (or mer isomer state) at ~580-600 nm in fresh films at room temperature another type of emission at ~700 nm was observed (figure 7.11). To the best of author's knowledge this has not been published elsewhere yet and in this thesis it will be called trap 2 emission. The origins of this emission is difficult to predict, the only characteristic is that it can be recorded ~ 3-4 μs after excitation at room temperature and that its oscillator strength is many orders of magnitudes smaller in comparison with the oscillator strength of genuine Ir(ppy)₃ emission. Nevertheless it might be important to take it into account when doing time resolved spectroscopy on multilayer structures as will be shown in successive chapters.
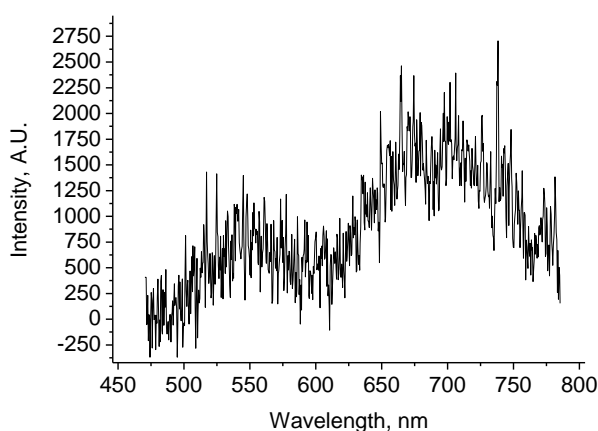
Figure 7.11 Spectrum of pure Ir(ppy)₃ film in between 4μ and 4.5 μs. ~700 nm new peak appears named here as trap 2 state emission.

116

Another two types of emission have been detected at 14 K in time resolved spectra that could not be ascribed neither to genuine Ir(ppy)$_3$ ^{3}MLCT $\rightarrow$S$_0$ phosphorescence, nor to trap 1 type emission and trap 2 state emission (figure 7.12). One of them peaks at ~430 nm (recorded at 10 ns after excitation) and another at ~466 nm (recorded at few milliseconds after excitation). The 466 nm late times emission could be the same as emission of Ir(ppy)$_3$ in PMMA matrix which was recorded by Colombo *et al*[6] and ascribed to emission from ^{3}(π-π*) state of phenylpyridine ligand.

The short times 430 nm emission has not yet been reported in the literature. Steady state room temperature spectrum of 4-phenylpyridine gives emission at 430 nm so it is reasonable to suggest that this short lived emission comes from phenylpyridine ligand state having singlet character (figure 7.12). Another option could be that this is singlet ^{1}MLCT $\rightarrow$S$_0$ emission as Hay[11] calculated it to be of a similar energy. Clearly both of these states - short lived and long lived- are excited directly with laser as they are observed at 15 K when triplet migration is very slow and emission from migration populated traps should be negligible.
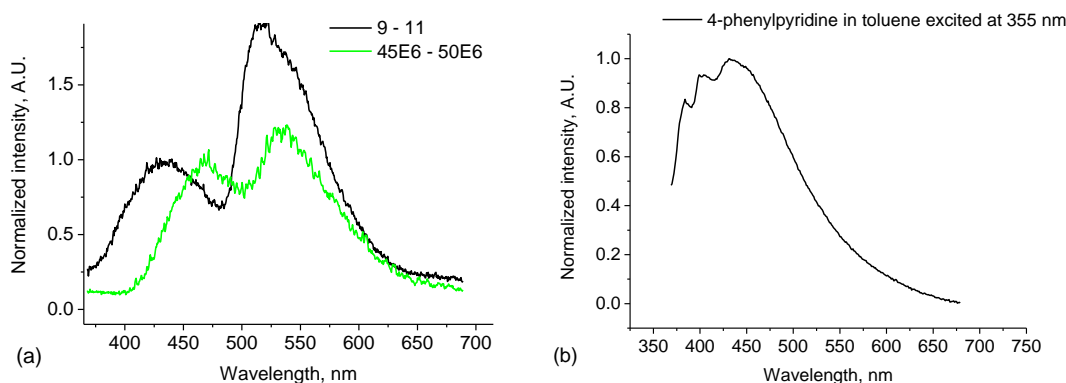
Figure 7.12 (a) Time resolved spectra of fresh Ir(ppy)$_3$ film emission at 15 K excited at 355 nm. Time in nanoseconds is indicated. (b) Steady state emission spectrum of 4-phenylpyridine in toluene excited at 355 nm.

Here it must be noted that neither energy migration nor other type of traps discussed here have been observed in Ir(ppy)$_3$ doped in zeonex and just genuine Ir(ppy)$_3$ emission peaking ~510 nm has been recorded at all temperatures as demonstrated in figure 7.13. Proposed diagram of states in Ir(ppy)$_3$ film is shown in figure 7.14.
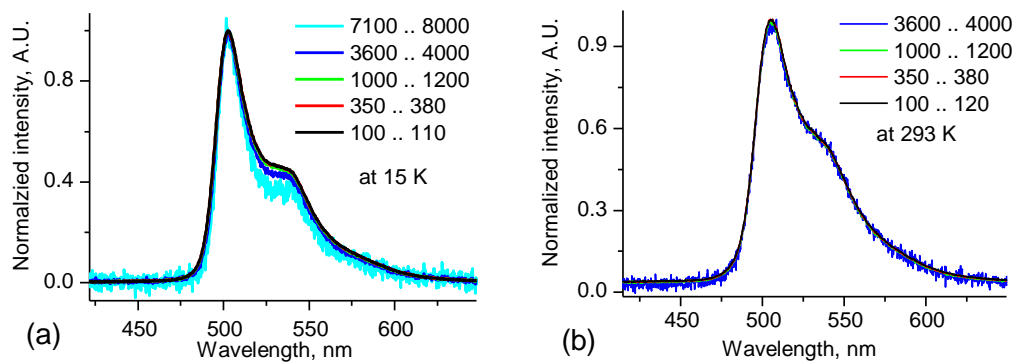
Figure 7.13 Ir(ppy)$_3$ in zeonex phosphorescence peak at various times after excitation at 15k (a) and at 293 K (b). Camera opening and closing times indicated in the legend are in nanoseconds.

2.88 eV ———————— 430 nm state having substantial singlet character (this thesis)

2.66 eV ————————— 450 nm phenylpyridine state having substantial triplet character ($^3\pi-\pi^*$ Colombo *et al* and this thesis)

2.55 eV ———————— Non-radiative state having singlet character (Kobayshi *et al*)

Energy

60 meV

110

Aged

Ir(ppy)$_3$

2.43 eV

2.34 eV

Fresh

Ir(ppy)$_3$

Type 1 Trap State. mer-Ir(ppy)$_3$ or aggregate

2.14 eV ————

trap (Tsuboi *et al*, Kobayashi *et al*, Samuel *et al*

1.77 eV ————

Type 2 Trap

State (this thesis)

S_0 —————————————————————————

Figure 7.14 Proposed diagram of states in Ir(ppy)$_3$ films. Not drawn to scale.
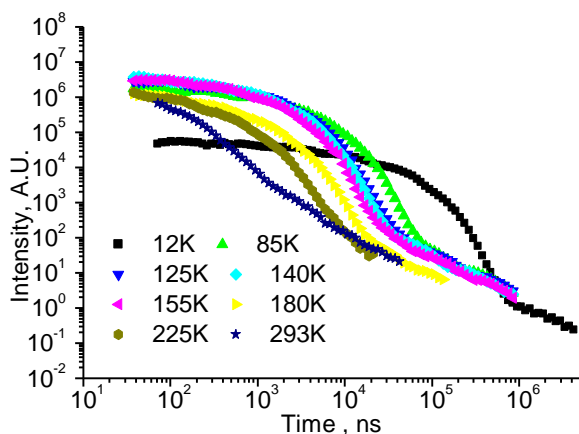
Figure 7.15 Decay curves of phosphorescence in 20 nm Ir(ppy) $_3$ fresh film at various temperatures in log-log scale (12 K to 293 K). Excitation energy ~ 25 µJ per pulse with 450 nm laser.

In figure 7.15 decays of Ir(ppy)$_3$ film at various temperatures are shown. Decay at each temperature could be divided into two parts – an exponential region (cascade like region) and power law region (straight line with slope -1 in log-log scale). Exponential region could be fit with 3 exponents at lower temperatures (12 K) and 2 exponents at higher temperatures. Exponential decay region coincides with the downgrade in energy (dispersive energy migration). Power law region coincides with a blue shift in energy as shown for decay at 12 K in figure 7.16 below. This is valid for decays at higher temperatures with the difference that the turning point between exponential and power law (or between peak energy downward migration and blue shift) takes place at earlier times, compare figures 7.16 and 7.17 (for 44 K it is at 150 µs whereas at 12 K 330 µs). The power law decay with the slope -1 and the simultaneous blue shift (figure 7.18) also has been observed in aged sample, however not in Ir(ppy)$_3$ doped in zeonex.
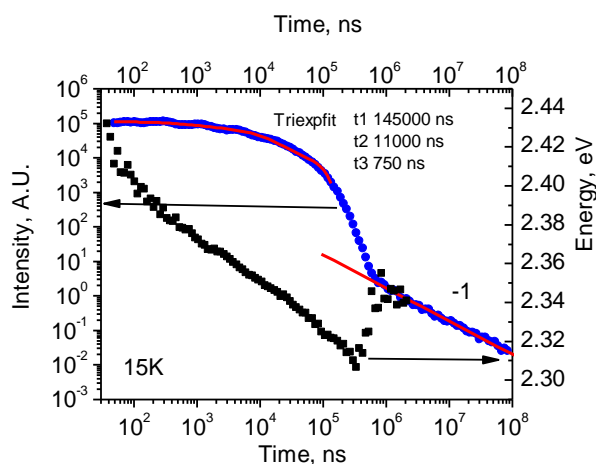
Figure 7.16 Fresh Ir(ppy)$_3$ film phosphorescence peak shift in time at various temperatures in lin-log scale and decay of phosphorescence in 20nm Ir(ppy)$_3$ film at 15 K in log-log scale. Straight lines are triexponential fit (100 ns to 100000 ns), and linear fit having slope -1 (600μs to 100ms). Peaks were determined by fitting 3 Gaussians to the PH time resolved spectra of Ir(ppy)$_3$ film. Excitation energy ~ 25 μJ per pulse with 450 nm laser.
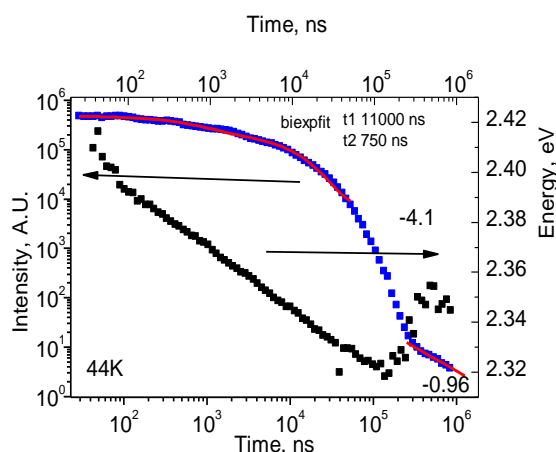
Figure 7.17 Fresh Ir(ppy)$_3$ film phosphorescence peak shift in time at various temperatures in lin-log scale and decay of phosphorescence in 20 nm Ir(ppy)$_3$ film at 44 K in log-log scale. Straight lines are biexponential fit (100 ns to 60 μs), and linear fit having slope -1 (400 μs to 1 ms). Peaks were determined by fitting 3 Gaussians to the PH time resolved spectra of Ir(ppy)$_3$ film. Excitation energy 25 μJ per pulse with 450 nm laser.
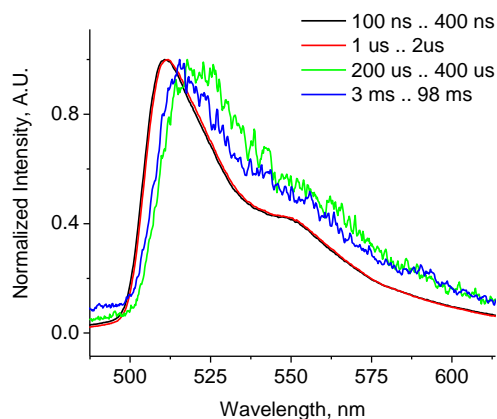
Figure 7.18 Time resolved spectra of aged Ir(ppy)$_3$ film (was kept in nitrogen atmosphere for 2 months) at 15 K. Parameters are gating times. At late times when power law with the slope -1 is present (3 ms to 98 ms) spectrum blueshifts in comparison with earlier times spectrum when exponential decay region is dominant (200us .. 400 us).

Decays shown in figure 7.15 quantitatively are very similar to the ones recorded by Kobayashi *et al*[17] (see review section above). Kobayashi *et al*[17] fitted single exponent function to these decays and assumed that in the initial time domain non-exponential decay prevails (despite the fact that three or two exponents can actually be fit to all decays). Kobayashi *et al*[17] ascribed the initial time region where decay is 'non-exponential' to the fact that in these time regions the thermalization of sublevel states have not been completed thus concentration of triplet excitons in higher states decreases much more rapidly because of two processes acting - thermalization and radiative decay. The values obtained by fitting decays in figure 7.15 in the same way as Kobayshi *et al*[17] are comparable with the fits by them: at 15 K, the decay recorded here is 43 μs (Kobayashi *et al*[17] 40 μs), at 33 K is 29 μs (30 μs), at 54 K~18 μs (15-20 μs), at 125 K~2.7 μs (2-3 μs). Kobayashi *et al*[17] did not observed the power law part of the decay. Thus as the decays presented here are almost identical to the ones in the Kobayashi *et al* publication, the same conclusions could be drawn – 3 radiative substates and 1 non-radiative short lived higher lying state exists in Ir(ppy)$_3$ films (figure 7.14).

There are few hypotheses of the origins of the -1 slope decay. The first one is that it could be exponential law violation observed by Rothe *et al*[35] in conjugated polymers and organic molecules and theoretically predicted by Khalfin[36]. However all the decays observed by Rothe *et al* obeyed power laws with slopes from -2 to -4 but not -1.

Another option could be that this decay originates from triplet-triplet annihilation. As shown in chapter 3 if triplet-triplet annihilation is the dominant exciton depletion decay mechanism, triplet concentration should decay following the slope -1 (assuming non-dispersive transport):

$$[T] = \frac{[T_0]}{(1 + k_{tt}[T_0]t)} \qquad\qquad (7.9)$$

If -1 slope emission arises from monomolecular type decay (for example if it is simple phosphorescence) emission intensity dependence on initial excitation energy density should follow slope 1 in log-log scale assuming that monomolecular decay is dominant, and if bimolecular decay dominates, this intensity should be proportional to the square root of initial excitation density. The exponential region intensity dependence on excitation energy density follows the slope 1 in log-log scale and the power law - follows the slope 1.37, that indicates that monomolecular type decay is responsible for both exponential part and power law part of Ir(ppy)$_3$ decay in films (figure 7.19).

If -1 slope emission arouse from bimolecular type decay, emission intensity dependence on excitation energy density should follow slope 2 in log-log scale assuming that monomolecular decay is dominant mechanism, and if bimolecular decay dominates, this intensity should follow slope 1 in log-log scale. Clearly neither exponential, nor power law parts of Ir(ppy)$_3$ decay follow slope 2 in log-log scale (figure 7.19). In addition exponential and power law regimes have intensity dependence on initial excitation energy density follow power laws with exponents 1 or 1.37 (respectively) from very low energies (~1μJ/cm2). At these energies triplet-triplet annihilation (bimolecular mechanism) could not be the dominant exciton depletion mechanism as normally it starts to be such at much higher fluxes (100 μJ/cm2) see e.g. Hertel *et al*[37], Rothe *et al*[34] and Monkman *et al*[38]. Thus bimolecular type mechanism influence on exponential part of decay and power law part of decay is minimal.

Decay with slope -1 could arise from geminate pair recombination as well and this type of emission has already been observed in polymers. Firstly Bassler *et al*[39] observed that geminate pair emission dependence on excitation energy density is a power law with exponent ~1 what is quite close to here recorded exponent 1.37 (figure 7.19). In addition, triplets originating from geminate pair recombination decay in time with the slope close to -1 as was simulated using Monte Carlo methods and shown experimentally by Bassler *et al*[39-41].
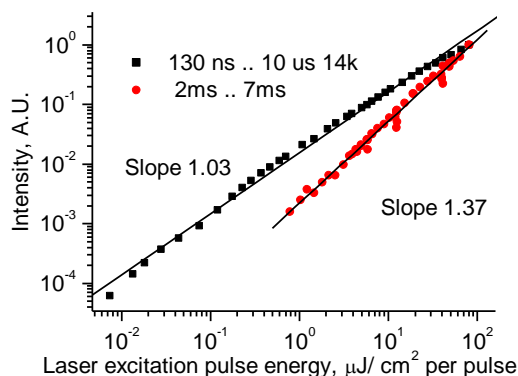
Figure 7.19 Intensity dependence on laser excitation energy of 20 nm Ir(ppy)$_3$ film at various delay and gate times representing 2 parts of the decay regions– triexponential (130 ns .. 10 μs) shown as squares and region with the slope -1 (2ms .. 7 ms) shown as circles. Black curves are just a guide to an eye having slopes 1.03 and 1.37 in log-log plot. Excited with 355 nm laser.

However there is some evidence against geminate pair recombination. Firstly Kalinowski *et al*[28] by analyzing decays of Ir(ppy)$_3$ films at high excitation doses, concluded that charge separation based recombination is very unlikely. Secondly, in order to separate exciton into a free charge carriers one needs ~1 eV excess above the absorption threshold[42] which is 2.48 eV (500 nm) for Ir(ppy)$_3$ (see figure 7.1). Slope -1 decay in Ir(ppy)$_3$ films has been recorded when exciting with two wavelengths 355 nm (3.49 eV) and 450 nm (2.76 eV) with an expectation to see that intensity of the slope -1 decay in relation to exponential part decay will decrease when exciting with 355 nm (more charge separation will result in less -1 slope emission if it arises from geminate pair recombination). This is not the case and it is even opposite as shown in figure 7.20. After excitation with 355 nm laser, power law region increases in intensity in respect to exponential part in comparison with the curve excited at 450 nm and the intensity. This is not what would be expected if the slope -1 arose from geminate pair recombination (this ratio should increase).

Let us assume that long lived states at ~2.66 eV (figure 7.14) in Ir(ppy)$_3$ films with very long lifetime are populated independently after laser excitation. Some of these excitons are stored until Ir(ppy)$_3$ emission dyes away sufficiently and then are fedback to the Ir(ppy)$_3$ molecules at very long times. Then slope -1 emission intensity dependence on excitation dose should be ~1 which is the case. In addition, after changing excitation wavelength to 355 nm it is reasonable to expect increase in the intensity of -1 slope decay in respect to the exponential part with the condition that at this wavelengths these states have larger absorption coefficient then genuine Ir(ppy)$_3$ molecules.

A summary of possible origins of -1 slope decay and experimental results supporting or rejecting the hypothesis is presented in table 7.4.
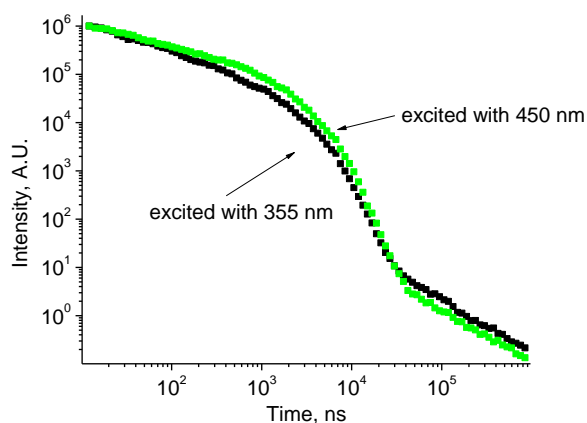
Figure 7.20 Decay of phosphorescence in 20 nm Ir(ppy) $_3$ film at 85K in log-log scale. Excited with two different wavelengths – 355 nm and 450 nm. Slope -1 decay intensity in respect to exponential decay region, increases after exciting with 355 nm.
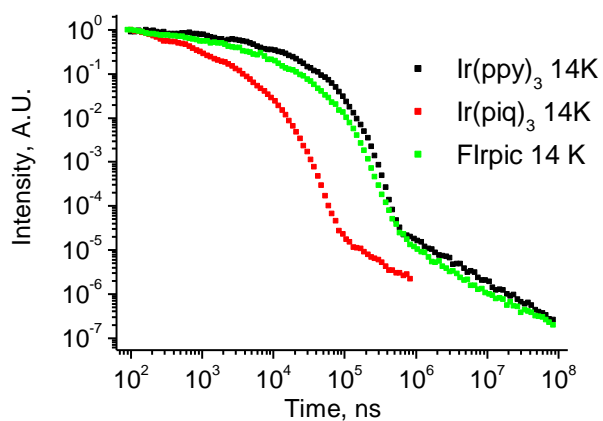
Figure 7.21 Decay of phosphorescence in Ir(ppy) $_3$, Ir(piq)$_3$ and FIrpic films at 14 K in log-log scale. -1 slope is present in the decays of all materials. Triplet sublevel splitting are Irppy 83.5 cm^{-1} [10], FIrpic 39-76 cm^{-1} [43], Ir(piq)$_3$ 44-66 cm^{-1} [44].

Table 7.4. Summary of possible origins of -1 slope decay and experimental results supporting or rejecting the hypothesis

Origin hypothesis	Experimental evidence which would support hypothesis	Experimental results
Non-exponential violation	Power law slope after exponential region with the slope from -2 to -4[34].	Slope -1.
TTA	Excitation dose dependence follows power law with exponent 2 at low intensities (see above for discussion0	Exponent is 1.37 even at very low energy intensities.
Geminate pairs	Excitation dose dependence follows power law with exponent 1.	Exponent is 1.37.
	Decay vs. time follows power law with exponent -1[39-41].	Exponent is -1.
	Exciting 1 eV (355 nm) above absorption edge should decrease slope -1 decay intensity in comparison with exponential region intensity – separate geminate pairs.	Exciting 1 eV (355 nm) above absorption edge increased slope -1 intensity in comparison with exponential region intensity.
Energy transfer from long lived higher lying states	Proof of existence of higher lying state.	Higher lying long lived emissive state exists – figure 7.14 above.
		Increase in intensity of slope -1 in relation to exponential region intensity after exciting with 355 nm does not prove it to be incorrect (see discussion above)

Despite that there is no firm evidence supporting any origins of -1 slope decay it is interesting to note that this type of decay has been observed not only in Ir(ppy)$_3$ films but also in FIrpic (Bis(4,6-difluorophenylpyridinato-N,C2)picolinatoiridium) and Ir(piq)$_3$ which indicates that this is common to the whole group of iridium based materials. To the best of author's knowledge, this is the first time this type of decay has been reported in films of iridium heavy metal complexes.

Finally a few words needs to be said about origins of PLQY loss in Ir(ppy)$_3$ neat films in comparison with the Ir(ppy)$_3$ doped in CBP or other matrix[5, 18]. Based on the experiments performed by other researchers and throughout the work of this thesis, the conclusion can be made that PLQY decreases due to the triplet exciton migration to the lower lying trap sites (trap 1 and trap 2) and due to direct absorption by higher energy sites and later non-radiative decay from there. It can be supported by the fact that with an increase of temperature the hopping rate increases (shown here figure 7.10 for example) and it takes a shorter time to reach the bottom of density of states. Temperature increase is analogous to an increase in concentration from hopping point of view. Hence with an increase of concentration from Ir(ppy)$_3$ doped in CBP or other matrix to neat Ir(ppy)$_3$ film population of trap states increases and larger part of all exciton population is trapped therein. It is very probable that these sites have lower PLQY. For example meridional isomer is less efficient than facial isomer emission[20] and aggregate sites in most cases have lower oscillator strength and are less efficient (e.g. reference [18]). Consequentially aged and fresh Ir(ppy)$_3$ neat film samples should have different PLQY values due to different exciton migration properties (aged Ir(ppy)$_3$ -> smaller disorder -> faster hopping -> more trap sites populated -> lower PLQY). Then one can readily understand the origins of different PLQY values (1 % to 29%) published in literature. Further triplet-triplet annihilation should be rejected as the main reason for decrease of PLQY as shown in figure 7.19 both regimes − exponential and power law – even at low excitation doses follow a power law with an exponent 1 and does not follow power law with an exponent 2 what would indicate the bimolecular origins of decay. Finally Tsuboi *et al*[15] findings that initial Ir(ppy)$_3$ triplet exciton number is only 68% of absorbed photons and the proof of existence of higher lying states (figure 7.14) supports the hypothesis that some photons are lost during initial direct excitation to higher lying energy states which are probably less efficient then genuine Ir(ppy)$_3$ ^{3}MLCT$\rightarrow$S$_0$ emission.

7.4 Results and Discussions. Ir(piq)$_3$
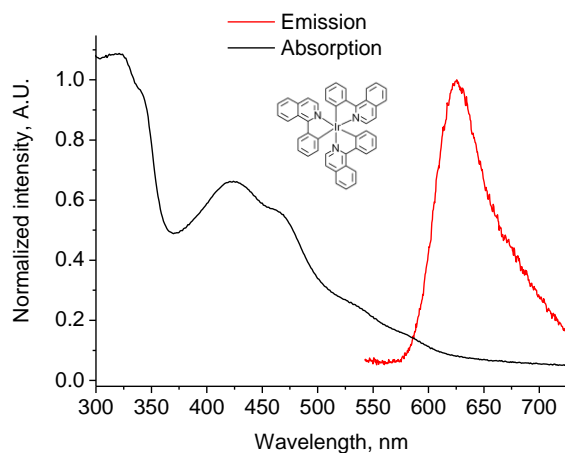
Figure 7.22 Absorption spectrum of Ir(piq)$_3$ (structure drawn) film and emission spectrum of 10% Ir(piq)$_3$ doped in NPB.

Absorption and emission spectra of Ir(piq)$_3$ is shown in figure 7.22. In analogy with Ir(ppy)$_3$ two small features at 540 nm and 585 nm could be ascribed to $S_0 \rightarrow {}^3$MLCT transitions, those at 426 nm and 468 nm to $S_0 \rightarrow {}^1$MLCT and absorption below 350 nm with transitions related to ligands[7]. Emission is peaking at 624 nm with a shoulder at 679 nm. It could be ascribed to ^{3}MLCT $\rightarrow S_0$ transition as the difference with the $S_0 \rightarrow {}^3$MLCT vibronics is 0.18 eV whereas between ^{3}MLCT $\rightarrow S_0$ vibronics is 0.16 eV which is close to that already observed in Ir(ppy)$_3$, 0.17 eV carbon-carbon double bond. Triplet excitation dynamics in Ir(piq)$_3$ is very similar to the one in Ir(ppy)$_3$. First of all triplet state of Ir(piq)$_3$ consists of three substates at zero-magentic field. The approximate ranges of energy difference between sublevels of Ir(piq)$_3$ dissolved in tetrahydrofuran are: $\Delta E_{2,1}$=8-9 cm^{-1} and $\Delta E_{2,1}$=46-66 cm^{-1}. Emission decay times of Ir(piq)$_3$ are τ_1=58 - 65 μs, τ_2=7 - 10 μs, τ_3= 500 - 600 ns[44]. Using formula 7.2 an equilibrated value can be calculated to be between 1.4 μs and 1.7 μs. Experimentally the lifetime of Ir(piq)$_3$ in dilute toluene solution have been determined to be 750 ns[7]. In analogy with Ir(ppy)$_3$ emission, a short lived higher lying energy state (2.88 eV) and long lived higher energy state (2.61 eV) has been observed too. Finally, lower lying trap states ~ 700 nm in Ir(piq)$_3$, at higher temperatures appear at later times then genuine emission (~200 ns after excitation) have been recorded, which in analogy to Ir(ppy)$_3$ could be ascribed to aggregate emission.
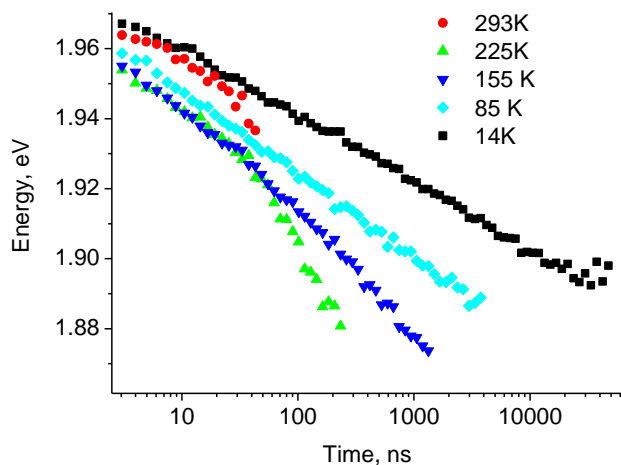
Figure 7.23 Fresh Ir(piq)$_3$ film phosphorescence peak shift in time at various temperatures in lin-log scale. Peak positions were determined by fitting Gaussians to the time resolved PH spectra.
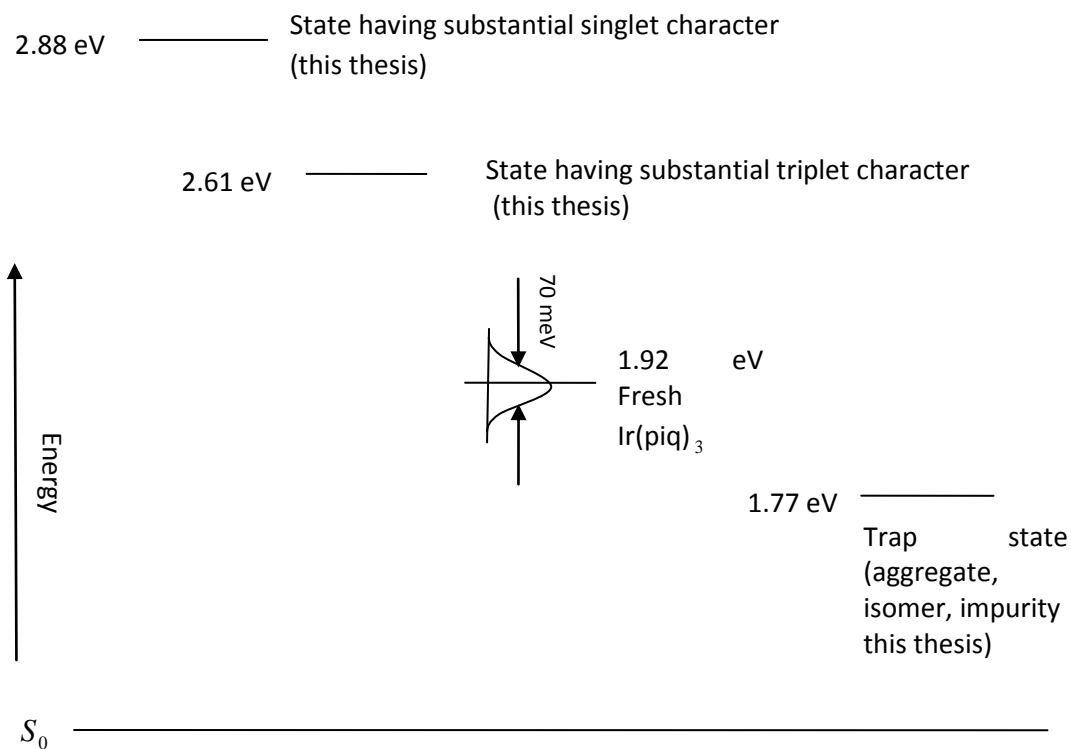
Figure 7.24 Proposed diagram of states in Ir(piq)$_3$ films. Drawn not to scale.

Migration of triplet states is proportional to log(t) and this indicates (figure 7.22), that energy migration is of a non-equilibrium dispersive manner[33-34]. Triplet density of states has width of ~70 meV (1.97 eV – 1.89 eV – 0.008 eV) slightly smaller than in Ir(ppy)$_3$ fresh films. Power law decay with slope -1 also has been recorded at most temperatures the origins of which could be similar to Ir(ppy)$_3$. The diagram with proposed states in Ir(piq)$_3$ films is shown in figure 7.24.

7.5 Conclusions

In this chapter, by using time-resolved spectroscopy it was shown that in neat Ir(ppy)$_3$ films triplets migrate in the density of states similarly as in other organic sublimed films or polymers. A decay in Ir(ppy)$_3$ neat films have been observed (with the slope -1) which to the best of authors knowledge has not been published in the literature before. In addition, this type of decay is observed in neat films of FIrpic and Ir(piq)$_3$ showing that it is characteristic not only to Ir(ppy)$_3$ but also other Iridium metal complexes. It was discovered that similar to CBP (chapter 5), aged films exhibit change in conformational order. Thus, in order for experiments to be repeatable one needs to use only fresh films (just after evaporation). Finally based on a literature review and new experimental evidence, a new triplet and singlet energy level diagram for Ir(ppy)$_3$ films is proposed. Similar analysis has been preformed with Ir(piq)$_3$ films. Fresh Ir(ppy)$_3$ and Ir(piq)$_3$ films have DOS width of approximately 100 meV and 70 meV respectively, which to the best of authors knowledge was determined for the first time. Dispersive migration at room temperature in Ir(piq)$_3$ lasts for ~30 ns seconds (figure 7.22) thus interpretation of diffusion and triplet-triplet annihilation quenching constants if classical diffusion equations is used for modeling should be very careful.

7.6 References

1.   M. A. Baldo, S. Lamansky, P. E. Burrows, M. E. Thompson and S. R. Forrest, Appl. Phys. Lett. 75 (1), 4-6 (1999).

2.   C. L. Lee, K. B. Lee and J. J. Kim, Appl. Phys. Lett. 77 (15), 2280-2282 (2000).

3.   T. X. Zhou, T. Ngo, J. J. Brown, M. Shtein and S. R. Forrest, Appl. Phys. Lett. 86 (2), 021107 (2005).

4.   Z. W. Liu, M. G. Helander, Z. B. Wang and Z. H. Lu, Org. Electron. 10 (6), 1146-1151 (2009).

5.   Y. Kawamura, J. Brooks, J. J. Brown, H. Sasabe and C. Adachi, Phys. Rev. Lett. 96 (1), 017404 (2006).

6.   M. G. Colombo, T. C. Brunold, T. Riedener, H. U. Gudel, M. Fortsch and H. B. Burgi, Inorg. Chem. 33 (3), 545-550 (1994).

7.   A. Tsuboyama, H. Iwawaki, M. Furugori, T. Mukaide, J. Kamatani, S. Igawa, T. Moriyama, S. Miura, T. Takiguchi, S. Okada, M. Hoshino and K. Ueno, J. Am. Chem. Soc. 125 (42), 12971-12979 (2003).

8.   T. Tsuboi and M. Tanigawa, Thin Solid Films 438, 301-307 (2003).

9.   J. Breu, P. Stossel, S. Schrader, A. Starukhin, W. J. Finkenzeller and H. Yersin, Chemistry of Materials 17 (7), 1745-1752 (2005).

10.   W. J. Finkenzeller and H. Yersin, Chem. Phys. Lett. 377 (3-4), 299-305 (2003).

11.   P. J. Hay, Journal of Physical Chemistry A 106 (8), 1634-1641 (2002).

12.   H. Yersin, *Highly Efficient OLEDs with Phosphroescent Materials*. (Wiley-VCH Verlag GmbH & Co. KGaA, Weinheim, 2008).

13.   H. Yersin and J. Strasser, Coordination Chemistry Reviews 208, 331-364 (2000).

14.   N. Nabatova-Gabain, Y. Wasail and T. Tsuboi, Current Applied Physics 6 (5), 833-838 (2006).

15.   T. Tsuboi and N. Aljaroudi, Opt. Mater. 30 (9), 1375-1381 (2008).

16.   J. C. Ribierre, A. Ruseckas, I. D. W. Samuel, S. V. Staton and P. L. Burn, Phys. Rev. B 77 (8), 085211 (2008).

17.   T. Kobayashi, N. Ide, N. Matsusue and H. Naito, Japanese Journal of Applied Physics Part 1-Regular Papers Brief Communications & Review Papers 44 (4A), 1966-1969 (2005).

18.   W. Holzer, A. Penzkofer and T. Tsuboi, Chem. Phys. 308 (1-2), 93-102 (2005).

19.   Y. Kawamura, K. Goushi, J. Brooks, J. J. Brown, H. Sasabe and C. Adachi, Appl. Phys. Lett. 86 (7), 071104 (2005).

20.   N. Ide, N. Matsusue, T. Kobayashi and H. Naito, Thin Solid Films 509 (1-2), 164-167 (2006).

21.   V. Jankus, C. Winscom and A. P. Monkman, J. Chem. Phys. 130 (7), 074501 (2009).

22.   N. J. Turro, *Modern Molecular Photochemistry*. (The Benjamin/Cummings Publishing Company, Inc, Menlo Park, California, 1978).

23.   W. Staroske, M. Pfeiffer, K. Leo and M. Hoffmann, Phys. Rev. Lett. 98 (19) (2007).

24.   S. Volker, Annual Review of Physical Chemistry 40, 499-530 (1989).

25.   R. Bauer, W. J. Finkenzeller, U. Bogner, M. E. Thompson and H. Yersin, Org. Electron. 9 (5), 641-648 (2008).

26.   Y. V. Romanovsko and H. Bassler, J. Lumines. 113, 156-160 (2005).

27.   M. A. Baldo, C. Adachi and S. R. Forrest, Phys. Rev. B 62 (16), 10967-10977 (2000).

28.   J. Kalinowski, J. Mezyk, F. Meinardi, R. Tubino, M. Cocchi and D. Virgili, J. Appl. Phys. 98 (6), 063532 (2005).

29.   G. D. Hager, R. J. Watts and G. A. Crosby, J. Am. Chem. Soc. 97 (24), 7037-7042 (1975).

30.   G. D. Hager and G. A. Crosby, J. Am. Chem. Soc. 97 (24), 7031-7037 (1975).

31.   T. Karatsu, T. Nakamura, S. Yagai, A. Kitamura, K. Yamaguchi, Y. Matsushima, T. Iwata, Y. Hori and T. Hagiwara, Chemistry Letters 32 (10), 886-887 (2003).

32.   A. S. R. Koti, M. M. G. Krishna and N. Periasamy, Journal of Physical Chemistry A 105 (10), 1767-1771 (2001).

33.   S. C. J. Meskers, J. Hubner, M. Oestreich and H. Bassler, Chem. Phys. Lett. 339 (3-4), 223-228 (2001).

34.   C. Rothe and A. P. Monkman, Phys. Rev. B 68 (7), 075208 (2003).

35.   C. Rothe, S. I. Hintschich and A. P. Monkman, Phys. Rev. Lett. 96 (16), 163601 (2006).

36.   L. A. Khalfin, Soviet Physics Jetp-Ussr 6 (6), 1053-1063 (1958).

37.   D. Hertel, H. Bassler, R. Guentner and U. Scherf, J. Chem. Phys. 115 (21), 10007-10013 (2001).

38.   V. Jankus, C. Winscom and A. P. Monkman, J. Phys.-Condens. Matter 22 (18), 185802 (2010).

39.   A. Gerhard and H. Bassler, J. Chem. Phys. 117 (15), 7350-7356 (2002).

40.   V. R. Nikitenko, D. Hertel and H. Bassler, Chem. Phys. Lett. 348 (1-2), 89-94 (2001).

41.   B. Ries and H. Bassler, Journal of Molecular Electronics 3, 12-24 (1987).

42.   C. Rothe, Phd thesis, Durham University, 2004.

43.   A. F. Rausch, M. E. Thompson and H. Yersin, Inorg. Chem. 48 (5), 1928-1937 (2009).

44.   T. Fischer and H. Yersin, Unpublished data (2009).

8 Overview of triplet transport dynamical properties' determination.

8.1 Introduction

The first organic light emitting diode (OLED) developed at Eastman Kodak laboratory by Tang and VanSlyke[1] in 1987 consisted only of two organic layers - hole transporter and fluorescent emitter sandwiched between anode and cathode. Since then OLED device architectures have become more complex[2-5] as engineers used additional layers to improve the efficiency of devices for example via achieving better charge balance or increasing electron/hole injection. In recent years, phosphorescence in addition to fluorescence has been used in OLEDs in order to overcome the fundamental triplet to singlet formation ratio on charge of recombination[6-9]. In addition, very complex white OLED structures have been demonstrated recently where different types of triplet or singlet excitons are harvested away from the recombination zone[10-12]. In both types of devices harvesting is based on exciton diffusion where triplet or singlet excitons are transferred either via Forster or Dexter transfer towards the desired direction. As this type of devices has reached fluorescent tube efficiency[13], it is believed to be one of the most promising architectures, which could enable OLEDs to be used in lighting applications extensively. One of the most important parameters for materials used in these type of devices is the exciton diffusion coefficient, as from its value one could infer how far and how long excitons can move in device structure and whether material is suitable to be used in one or another device architecture. However there are lots of other parameters which have to be adjusted such as triplet and singlet levels, highest occupied molecular orbital (HOMO) and lowest unoccupied molecular orbital (LUMO) levels, electron mobilities. Besides, the material has to be sublimable (or spincoatable if it is polymer) and cheap and easy to synthesize if one wanted to use it in manufacturing. Thus, OLED engineers would definitely like to have a variety of organic films having different triplet diffusion coefficients in order to create efficient white device architectures. Finally, not only in the OLED community exciton transport is important. Organic solar cells researchers could be interested in these properties as well. In organic solar cells exciton transport plays a crucial role as created excitons tend to diffuse before charge separation takes place[14-15]. This diffusion could be used to harvest excitons to dopants or thin layers where charge separation could take more efficiently. Finally lots of aspects of triplet transport have not been investigated at all for example transfer through interface and it is interesting for fundamental reasons. Consequentially determination of thin film exciton diffusion coefficients and triplet properties in general has come under the spotlight in recent years [9, 16-18]. Thus here

first, a review will be presented on how one could determine triplet properties - diffusion coefficients, triplet-triplet annihilation constants and diffusion length of excitons - in organic thin films. It must be emphasized that this review does not intend to evaluate each method in scrupulous detail. The goal is to evaluate whether general assumptions are appropriate for the work intended to be performed throughout the course of this thesis. Thus most of the mathematical derivations are skipped and only the main assumptions, initial and final equations are analysed. In some cases only initial assumptions and equations or only final results are investigated. This will help to understand how to proceed with multilayer structure experiments and how to model triplet dynamics in these structures. Further it will help to identify potential problems and ways to deal with it.

8.2 Exciton transport in acene crystals

One of the first reviews on the determination of diffusion coefficients in organic films can be found in the book written by Pope and Swenberg[19]. During the sixties most of the work in this area has been done with acene crystals such as anthracene. Avakian and Merrifield[19] were one of the first people to report direct determination of triplet diffusion coefficient of anthracene. They illuminated anthracene crystals with continuous laser light through a Ronchi ruling (grating) thus creating parallel sections of exciton distribution in material. They expected to see a change in delayed fluorescence intensity from triplet-triplet annihilation due to the diffusion of excitons to the covered grating sections. They used grating widths ranging from 8.5 to 51 microns. By attenuating light in such a way that triplet-triplet annihilation could be ignored in comparison to monomolecular decay, they used following equation to fit their results:

$$\frac{d[T(t, x)]}{dt} = 0 = D \frac{\partial^2 [T(t, x)]}{\partial x^2} - k_1 [T(t, x)] + \alpha I_0 \qquad (8.1)$$

where, [T] is triplet concentration, k_1 - monomolecular decay rate constant, α - absorption coefficient, t - time, x - distance and I_0 is intensity of incident light. The total delayed fluorescence photon flux emitted from the crystal is then proportional to the integral of $[T(t,x)]^2$ over the crystal length (solution to equation 8.1). The photon flux finally is expressed in this way:

$$\Phi / \Phi_\infty = 1 - \frac{3}{4\xi} + (1 + \frac{3}{2\xi}) * e^{-2\xi} + ... \qquad (8.2)$$

where $\xi = \dfrac{x_0}{\sqrt{2}L}$, x_0 is grating linewidth, L is diffusion length and Φ_∞ is the value of Φ for a grating with $x_0 \gg L$. Hence, after plotting delayed fluorescence photon flux against the ruling width it is possible to determine the diffusion length from the slope. The observed diffusion length was ~10 microns from which one could infer a diffusion constant of approximately 1E-4 cm^2/s.

Later they their expanded experiment by using a chopper in order to record the build up and decay of fluorescence intensity. The diffusion coefficient determined in this way was found to be 2E-4 cm^2/s in the ab plane of the anthracene crystal[20].

Kepler *et al*[21] setup another experiment to determine diffusion constants of anthracene crystals. In the first one they studied luminescence decay dependence on crystal thickness after excitation with laser. They used the following equation as a starting point:

$$\frac{d[T(t,x)]}{dt} = D\frac{\partial^2[T(t,x)]}{\partial x^2} - k_1[T(t,x)] - k_{TT}[T(t,x)]^2 \qquad (8.3)$$

where k_{TT} is triplet-triplet annihilation constant. Under weak illumination the decay rate of triplet excitons becomes much stronger than triplet-triplet annihilation. Then term $k_{TT}[T(t,x)]^2$ can be ignored and equation is solved to get:

$$[T(t,x)] = \frac{4}{\pi}n_0\sum_{k=0}^{\infty}\frac{1}{2k+1}\exp\left\{-\left[k_1 + \frac{(2k+1)^2\pi^2 D}{L^2}\right]t\right\}\sin\left(\frac{2k+1}{L}\pi x\right) \qquad (8.4)$$

The authors state that after time longer than $0.005\dfrac{L^2}{D}$ equation (8.3) approaches

$\dfrac{d[T(t,x)]}{dt} = -k_1'[T(t,x)]$ with solution $[T(t,x)] = (4/\pi)n_0 e^{-k_1' t}\sin(\pi x/L)$ where

$k_1' = k_1 + \pi^2 D/L^2$ and L is crystal thickness. Thus by measuring decay times for different thickness crystals and plotting them against inverse squared thickness authors determined the diffusion constant from the slope. For various types of anthracene crystals Kepler *et al*[21] got diffusion coefficients ranging from 4E-3 cm^2/s to 0.7E-2 cm^2/s. It is interesting to note that the authors conclude that exciton diffusion is not hopping based but can be better described using band model opposite to Avakian and Merrifield.

Another method used to analyze energy transport in molecular crystal is the picosecond transient-grating method first reported by Salcedo et al[22]. An interference pattern is produced by two time coincident laser beams and a third one is used as a probe beam. This pattern changes in time due to both finite exciton lifetime and exciton diffusion. The characteristics of exciton motion is reflected in time dependence of the pattern. More details can be found elsewhere[22].

As can be seen from the above discussion the diffusion length of most molecular crystals are in the range of microns meaning that diffraction gratings or absorption properties of film can be used to analyze transport due to large exciton travel distances. However, in most of the present OLEDs or organic solar cells amorphous films are used rather than molecular crystals. As these films are more disordered it is intuitive to expect that diffusion lengths will be much smaller - even in the range of tenths of nanometers. This means that the above methods cannot be be used to infer the diffusion coefficients thus new ones had to be devised.

Table 8.1 Diffusion coefficients of some organic crystals. Adopted from Pope et al[19].

Material	Diffusion coefficient in aa plane ($\times$ 1E-4 cm^2/s)	Diffusion coefficient in bb plane ($\times$ 1E-4 cm^2/s)	Diffusion coefficient in c'c' plane ($\times$ 1E-4 cm^2/s)
Triplet excitons			
Naphthalene	0.33	0.27	-
Anthracene	1.5	1.8	<0.12
Tetracene	-	40	-
Pyrene	0.3	1.25	0.3
Trans-stylbene	0.09	0.7	-
Singlet excitons			
Naphthalene	2		0.5
Anthracene	30		
Tetracene	400		

8.3 Exciton transport analysis by using OLED type structures

Forrest et al[17] evaporated OLED type structures ITO/NPB/Alq$_3$/Alq$_3$:8% PtOEP/Alq$_3$/MgAg with different length aluminum tris(8-hydroxy-quinoline) (Alq$_3$) spacer layers between the recombination zone (Alq$_3$) and the phosphorescent zone consisting of the 2,3,7,8,12,17,18-octaethyl-21H,23H-porphine platinum(II) (PtOEP) doped in Alq$_3$ layer. Here NPB stands for (N,N′-bis-(1-naphthyl)-N,N′-diphenyl-1,1′-biphenyl-4,4′-diamine) and ITO for indium tin oxide. Short 200 ns voltage pulses where applied to the devices and electroluminescence (EL)

transients were recorded with the streak camera. They used the following equation to fit triplet exciton flow transients of these devices:

$$\frac{d\varphi}{dt} = -\frac{\varphi}{\tau} + D_T \frac{d^2\varphi}{dx^2} \qquad (8.5)$$

Where φ is triplet exciton flow. Triplet exciton flows were calculated from EL transients by deconvoluting the phosphorescent decay of PtOEP. The authors observed that given the single diffusion coefficient value it is impossible to reproduce both the sharp initial increases in the PH and long tails using the solution of equation (8.5). This clearly is a signature of dispersive transport at room temperature.

Nevertheless from fits they obtained $D_T = 8 \pm 5E-8$ cm^2/s cm^2/s and exciton lifetime $\tau = 25 \pm 15$ µs. Using this diffusion length expression

$$L_D = \sqrt{D\tau_H} \qquad (8.6)$$

a diffusion length of 14 ± 9 nm was calculated. They compare that to previously published singlet-exciton diffusion coefficients in Alq$_3$ $D_S = 1.2 \pm 0.8E-5$ cm^2/s and $D_S = 2.6 \pm E-4$ cm^2/s [17]. In this experiment they ignored triplet-triplet annihilation.

In another publication Baldo *et al*[16] used stacked OLED devices consisting of ITO/NPB/Dopant:Host/BCP/ Alq$_3$/MgAg and applied short electrical excitation pulse of 200 ns to create transient EL. They fitted the solution of the following equation to the data:

$$\frac{d[T(t)]}{dt} = -\frac{[T(t)]}{\tau} - \frac{1}{2}k_{TT}[T(t)]^2 + \frac{J}{qd} \qquad (8.7)$$

where [T] is triplet concentration, k_{TT}-triplet-triplet annihilation constant, J-current density, q-charge, d is the thickness of exciton formation zone. Also they excited the same dopant:host systems with short laser pulse and recorded photoluminescence decay from these films. More experiments with light excitation used to determine triplet properties can be found in the section below as these results are included here for the reasons of comparison with electric excitation. For simplicity Baldo *et al*[16] assumed that *only* dopant triplets (!) participate in triplet-triplet annihilation. This assumption is very unreasonable as guest concentration used are from ~1% to ~16% and at these concentrations the majority of the triplets will be created on the host (host will absorb most exciting light). Further they assume that each TTA reaction outcome is a loss

of one triplet and a gain of one triplet (that is where fraction ½ comes in equation (8.7)) which can be questioned as in most references[19, 23-25] there is assumption that $1/9^{th}$ of TTA events creates a singlet state.

Luminescence intensity, proportional to the solution of equation 8.7 can be written:

$$L(t) = \frac{L(0)}{\{1 + [T(0)]k_{TT}\tau / 2\}e^{t/\tau} - [T(0)]k_{TT}\tau / 2} \quad , \quad (8.8)$$

assuming that luminescence intensity is linearly proportional to the concentration of excited states. L(0) is intensity at time 0.

They fitted equation (8.8) to EL and PL decay curves (transients) and extracted TTA coefficients and lifetimes for the following systems - PtOEP in CBP, PtOEP in Alq_3 and $Ir(ppy)_3$ in CBP.

For the PtOEP in CBP system k_{TT} was independent on whether EL or PL excitation where used to extract it. The lifetimes extracted from EL measurements were smaller by ~25% assigned by the authors to the quenching of excitons by metal cathode in the EL device. Authors did not observe any dependence on initial triplet population. However they observed that τ decreases and k_{TT} increases with an increase of PtOEP concentration in the host. This might be probably due to an increase of aggregate sites with increase of concentration and subsequent quenching of excited states hence shorter lifetime. Forrest et al[16] conjecture that k_{TT} increases because of percolation among clustered or adjacent molecules. The lifetime of triplets determined from PL is ~110 μs, from EL ~65 μs (8% PtOEP:CBP). $k_{TT}/2$ increases from ~8E-15 cm^3/s at 1% PTOEP concentration to 1.5E-14 cm^3/s at 16% PtOEP concentration at initial triplet population of 1E18 cm^{-3}.

The observed dynamics of TTA constants is different for 6% PtOEP: Alq_3 structure. $k_{TT}/2$ decreases from ~6E-13 cm^3/s to 4E-14 cm^3/s with an increase of initial triplet exciton concentration from ~4E16 cm^{-3} to 1E19 cm^{-3}. In addition to as PtOEP concentration in Alq_3 increases, the lifetime also increases as well (from ~16 μs when PtOEP concentration is 1%, to ~33 μs when PtOEP concetration is 16%). However $k_{TT}/2$ decreases from 1.5E-13 cm^3/s at 1% to 5E-14 at 16%. Both of those effects, according to the authors, are manifestations of poorer triplet confinement of PtOEP in Alq_3 in comparison with CBP.

In the 8% $Ir(ppy)_3$:CBP case the authors where not able to fit the above equation to EL transient decay and where able to fit biexponential decay only. They assume that this might have been

due to some Ir(ppy)$_3$-CBP interactions as this system posses overlap between host and guest energies. As previously shown in this thesis trap species are present in CBP (chapter 5) with lower triplet level than Ir(ppy)$_3$, introducing another pathway for triplet deactivation, hence more complicated biexponential decay dynamics should arise.

Unfortunately there is a problem with the determination of exciton diffusion properties using electrical excitation. This is exciton-polaron quenching[9, 26-27] which might skew triplet diffusion properties (TTA as well) as it is complicated to separate these two effects. The author of this thesis holds opinion that it should be more useful first to unveil triplet dynamical properties unperturbed with charge effects and only then investigate triplet transport 'in situ' in OLEDs.

8.4 Diffusion constant determination by using photocurrent spectrum analysis

Matsusue *et al* [28] used steady state photocurrent spectra to determine the diffusion lengths of triplet excitons. They sandwiched FIrpic doped CBP between indium tin oxide (ITO) and gold electrodes. Then they illuminated the films through ITO side with steady state monochromatic light and recorded steady state photocurrent spectra. Initially photocurrent is given by

$$I_p = D\left(\frac{dn}{dx}\right)_{x=0} = \frac{\alpha\theta I_0}{\beta^2 - \alpha^2} \frac{\beta(e^{\beta L} - e^{-\alpha L}) + \beta(e^{-\beta L} - e^{-\alpha L}) + \alpha(e^{-\beta L} - e^{\beta L})}{e^{-\beta L} - e^{\beta L}} \tag{8.9}$$

where θ is the quantum efficiency of exciton generation by illumination light, α is the absorption coefficient, I_0 is the incident light flux, L is the film thickness, and $\beta = 1/\sqrt{D\tau}$ is the reciprocal exciton diffusion length and τ is exciton lifetime. They assumed that exp(-βL) was much smaller than 1 hence the equation becomes:

$$\frac{1}{I_p} = \frac{1 + \beta/\alpha}{\theta I_0 e} \tag{8.10}$$

To satisfy the latter condition the samples used were 2.5 microns thick. Then they plotted $1/I_p$ found from steady state photocurrent spectrum versus reciprocal absorption coefficient $1/\alpha$ and from the slope determined $\beta = 1/\sqrt{D\tau}$. For the case of 3.5% and 7% FIrpic doped into CBP the diffusion lengths are 250 nm and 310 nm appropriately. These lengths are much longer than for 3.5% and 7% Ir(ppy)$_3$ doped into CBP determined using the same method which are 21 nm and 50 nm appropriately[29]. If the triplet lifetime is known, it is easy to calculate diffusion constant

using $L = \sqrt{D\tau}$. It is interesting to note that triplet exciton diffusion lengths are so different for the different dopants. It is probably due to the fact that triplet exciton are scattered from Firpic dopant whereas they are more likely to be trapped on Ir(ppy)$_3$.

Yang *et al*[30] used steady state photocurrent spectra of Alq$_3$ and N,N'-diphenyl-N,N'-bis(3-methylphenyl)-(1,1'-biphenyl)-4,4'-diamine (TPD) sandwiched between ITO and aluminum to analyse exciton transport. Exciton density , n(z) at a distance z from the illumination can be given by:

$$n(z) = \frac{\alpha\theta I_0}{\beta^2 - \alpha^2}\left[\left(\frac{e^{\beta L} - e^{-\alpha L}}{e^{-\beta L} - e^{\beta L}}\right)e^{-\beta z} - \left(\frac{e^{-\beta L} - e^{-\alpha L}}{e^{-\beta L} - e^{\beta L}}\right)e^{\beta z} + e^{-\alpha z}\right] \quad (8.11)$$

where θ is the quantum efficiency of exciton generation by illumination light, α is the absorption coefficient, I_0 is the incident light flux, L is the film thickness, and $\beta = 1/\sqrt{D\tau}$ is the reciprocal exciton diffusion length, D is diffusion coefficient and τ is exciton lifetime.

At z=0 the current density j=-De(dn/dz) is given by

$$j_s = \frac{\alpha\theta I_0 De}{(\beta^2 - \alpha^2)}\frac{2\beta - e^{-\alpha L}(\beta e^{-\beta L} + \beta e^{\beta L} - \alpha e^{-\beta L} + \alpha e^{\beta L})}{e^{-\beta L} - e^{\beta L}} \quad (8.12)$$

At z=L it is given by:

$$j_A = \frac{\alpha\theta I_0 De}{(\beta^2 - \alpha^2)}\frac{\beta(e^{\beta L} - e^{-\alpha L}) + \beta(e^{-\beta L} - e^{-\alpha L}) + \alpha(e^{-\beta L} - e^{\beta L})}{e^{-\beta L} - e^{\beta L}} \quad (8.13)$$

Both of those currents contribute to the spectra of photocurrent, however with different amounts (see reference [30] for more details). Thus the authors used the following equation to fit the steady state photocurrent spectra:

$$J = (1 - x_s)j_A + x_s j_s \quad (8.14)$$

x_s describes the contribution of j_s current in total photocurrent. Total current change with a change of excitation wavelength (as absorption coefficient changes). They changed x_s in order to get the best fit to experimental data and deduced diffusion coefficients D=1.53E-3 cm^2/s for TPD and D=4E-5 cm^2/s for Alq$_3$. The lifetimes used where 1.89 ns for TPD and 16 ns for Alq$_3$.

The biggest problem with the determination of triplet transport constants using the photocurrent method is charge transport dispersivity[31]. Also polaron-exciton annihilation is likely to have substantial impact to the exciton and charge dynamics in these type of structures[9, 26-27].

8.5 Thin film structures and optical excitation for the determination of exciton transport properties

Another way to extract diffusion coefficients was devised by Fushimi *et al*[32]. They fabricated/synthesized heterostructured films with tris(2,2'-bipyridine)ruthenium(II) moieties as phosphorescence emitter (Ru) and with ferrocene (Fc) moieties used as phosphorescence quenchers introduced into a polycarbonate copolymer (Fc_{21}/Ru_x). The subscript here indicates molar fraction of moiety in the polycarbonate copolymer. They used simple one-dimensional diffusion equation to fit the decay of Ruthenium phosphorescence:

$$\frac{d[T(x,t)]}{dt} = D\frac{\partial^2[T(t,x)]}{\partial x^2} \qquad (8.15)$$

[T] here is triplet exciton concentration. Under the boundary conditions [T(x,0)]=[T_0], [T(L,t)]=0 and $\left[\frac{\partial[T(t,x)]}{\partial x}\right]_{x=0} = 0$ authors solved equation (8.15):

$$[T(x,t)] = [T_0] - [T_0]\sum_{n=0}^{\infty}(-1)^n\left[\text{ercfc}\left\{\frac{(2n+1)L-x}{2\sqrt{Dt}}\right\} + \text{ercf}\left\{\frac{(2n+1)L+x}{2\sqrt{Dt}}\right\}\right] \qquad (8.16)$$

Intensity of different thickness films with ruthenium moieties after illumination with laser light can be expressed as:

$$I_{total} = \int_0^{\infty}I_0(t)\int_0^L[T(x,t)]dxdt \qquad (8.17)$$

The $I_0(t)$ is the decay curve of phosphorescence of polymer ruthenium films in the absence of quenching ferrocene moities at the top of film and L is thickness of films. Then one can plot the intensities for different thickness films and fit to the equation (8.17). The authors' measured diffusion coefficients are <1E-7 cm^2/s , 7E-6 cm^2/s and 2E-5 cm^2/s for Fc$_{21}$/Ru$_4$, Fc$_{21}$/Ru$_{12}$, Fc$_{21}$/Ru$_{18}$ appropriately. They used at least 4 different thicknesses for each film (from ~ 15 nm

to ~ 55 nm) to check whether the fit to equation (8.17) is good. It is clear from the results that with increase of the concentration of Ru in polycarbonate matrix there is an increase in diffusion coefficient hence energy harvesting is increased. The disadvantage of the mathematics used here is that only diffusion term is used without monomolecular decay and triplet-triplet annihilation which obviously must be taken into account especially under high excitation power densities. Also polycarbonate is not a good representation of a conjugated material.

Leo *et al*[9] as well used photoluminescence decay (PL decay) to find the triplet-triplet annihilation (TTA) constant values. They recorded decay from 4,4′,4″-tris(N-carbazolyl)-triphenylamine (TCTA) doped with Ir(ppy)$_3$ and NPB doped with Ir(piq)$_3$ films. The equation

$$\frac{d[T(t)]}{dt} = -\frac{[T(t)]}{\tau} - \frac{1}{2}k_{TT}[T(t)]^2 \qquad (8.18)$$

can be solved and expressed via the light intensity of decay assuming concentration is proportional to the intensity of decay as:

$$L(t) = \frac{L(0)}{\{1 + n_{ex}(0)k_{TT}\tau/2\}e^{t/\tau} - n_{ex}(0)k_{TT}\tau/2} \qquad (8.19)$$

and fitted to the PL decay of films. Here L(t) is light intensity and L(0) light intensity at 0 time. k_{TT} and τ for TCTA: Ir(ppy)$_3$ were found to be 3+/-2E-12 cm^3/s and 1.58 µs respectively, and for NPB:Ir(piq)$_3$ were found to be 1.4+/-0.6E-12 cm^3/s and 1.10 µs respectively. They varied initial exciton density from ~8E16 to 9E18 cm^{-3} and used the averaged values of annihilation constant and lifetimes. They did not find any correlation between excitation density and annihilation constant or lifetime. Intretingly the extracted exciton polaron quenching by Leo *et al*[9] is slightly smaller than TTA indicating that TTA contributes more to the decrease of efficiency in PHOLEDs. This is another reason why triplet diffusion properties are very important to understand.

It is also very important to mention that by using PL decay of PtOEP doped in CBP Leo *et al*[33] concluded that not only multistep Dexter type transfer in a host can take place in doped amorphous films but also single step Forster type transfer can occur among heavy metal ligand dopants. The authors extracted triplet-triplet annihilation constants for this type of transfer. They used equation (8.18) for data analysis, but with the following single step transfer annihilation constant expression

$$k_{TT}(t) = \frac{2}{3}\pi R_0^3 \sqrt{\frac{\pi}{\tau t}} \qquad\qquad (8.20)$$

The time dependence in equation (8.20) is explained by Leo *et al*[34]. This explanation is based on T. Forster publication [35] . Forster considered a model whereby donor molecule is surrounded by acceptor molecules. For a single donor molecule decay rate is a sum of its natural decay rate plus all energy rates to surrounding acceptor molecules. Summing up and averaging all the donor molecules leads to the time dependent donor population which after few algebraic actions can be expressed as equation (8.20). Then equation (8.18) is solved to get

$$[T(t)] = \frac{[T(0)]e^{-t/\tau}}{1 + \frac{2}{3}\pi^2 \frac{1}{2}[T(0)]R_0^3 \mathrm{erf}(\sqrt{\frac{t}{\tau}})} \qquad\qquad (8.21)$$

and fitted to PL decay. R_0 is Forster radius (2.12), and τ is the lifetime. The PtOEP concentration in CBP was 1.8 mol %. Initial excitation densities used were 1.1E19 cm^{-3} and 2.4E18 cm^{-3}. As the $k_{TT}(t)$ is time dependent for Forster type annihilation it is not possible to extract single TTA coefficient value. Leo *et al* tried to fit multistep transfer to the decay and found $k_{TT}(t)$ =9E-15 cm^3/s and $k_{TT}(t)$ =8.5E-15 cm^3/s. However, the fit residues clearly show that single step model gives much better description of the processes taking place in these films.

Holzer *et al* explored properties of Ir(ppy)$_3$ neat film and Ir(ppy)$_3$ doped in CBP and polystyrene films at various concentrations. They used photoluminescence decays and fitted the solution of equation (8.18) to their data[36]. The values they found are listed in table 8.2. These results have already been discussed in chapter 7. Here it only can be summed up that it makes very little sense that TTA constant in neat Ir(ppy)$_3$ film is smaller in 1% Ir(ppy)$_3$: polystyrene (PS) film and TTA constant in 1% Ir(ppy)$_3$:PS film is smaller than in 4% Ir(ppy)$_3$:PS film which is smaller than in 8% Ir(ppy)$_3$:PS films.

Table 8.2. Tripelt-triplet annihilation constants found by Holtzer et al[36].

Parameter/ material	Neat film	CBP 7.9 wt%	Polystyrene 1Wt%	Polystyrene 4wt%	Polystyrene 8wt%
Initial triplet concentration, cm^{-3}	1E19	3.2E17	2.6E16	7.9E16	2.6E17
Triplet-triplet annihilation constant, cm^3/s	1.2E-10	1.6E-10	7.7E-10	1.3E-10	6.2E-11

There are difficulties if considering triplet properties determination using laser or light excitation instead of electrical, especially using the assumptions outlined above. First is the absence of triplet diffusion term in the equation. Another is that there is no mention in these publications about how intersystem crossing yield is determined when calculating initial exciton density. In all of them initial *triplet* exciton densities are not fitted but calculated and without knowing intersystem crossing yield of the host materials it is not very easy task to estimate it especially for non-heavy metal complexes. Hence triplet-triplet annihilation constant errors could easily reach orders of magnitude. Another source of error could come from the assumption that only dopant triplets are considered participating in triplet-triplet annihilation. For example, Baldo et al[16] (section above) investigate a CBP: 4% PtOEP system after excitation with a pulsed laser and assumes that all excitons are generated on CBP then all of them are transferred to the singlet of PtOEP and they intersystem cross to the PtOEP triplet state. There is a possibility that triplets intersystem cross from CBP singlet to CBP triplet what is not considered at all nor proven to be incorrect in their publication. Finally in equation (8.18) there is an unjustified choice of the ½ factor in front of TTA constant. The authors assume that two annihilating triplets always create 1 triplet and do not create any singlet state which clearly in most systems not the case[19, 23-25]. A similar assumption is made in the Leo et al[9] publication. They investigate 10% Ir(piq)$_3$ doped in NPB and assume that Ir(piq)$_3$ triplet (acceptor A) annihilates by interacting with NPB triplet (donor-D), $^3D^* + {}^3A^* \rightarrow {}^1D + {}^3A^*$. Again Leo et al[9], similarly as Forrest et al[16], assume that only acceptor triplets participate in TTA reaction. As in Forrest et al[16] case this is unjustified because after excitation with the laser, NPB (consists larger part of molecules in the system) absorbs more photons than Ir(piq)$_3$ and NPB triplets must interact and annihilate before being transferred to Ir(piq)$_3$. This is supported by the fact that delayed fluorescence was still observed in time resolved spectra which was recorded throughout the course of this thesis.

Forrest *et al*[37] in the publication in Journal of Applied Physics use spectrally resolved photoluminescence quenching as a way to determine exciton diffusion lengths. Organic film (thickness from 200 nm to 600 nm) is evaporated on quartz substrate. Then a quencher (having much lower triplet or singlet level) or blocking layer (having much higher triplet or singlet level) is evaporated on top of organic films and monochromatic source is directed onto this structure. A wavelength dependent exciton distribution is generated in this way. The boundary conditions near the exciton blocking or quenching layer are $\frac{\partial n(0)}{\partial x} = 0$ or $n(x = 0) = 0$ appropriately. For thick films $n \rightarrow 0$ near the substrate organic material interface. The exciton distribution is then described by the one dimensional rate equation[37]:

$$\frac{L_D}{\tau} \frac{\partial^2 n(x)}{\partial x} - \frac{n(x)}{\tau} + \frac{I_0 \alpha}{\cos(\theta_\lambda)} \exp\left(\frac{\alpha x}{\cos(\theta_\lambda)}\right) = 0, \qquad (8.22)$$

where

$$\theta_\lambda = a\sin\left(\frac{n_2}{n_3} a\sin\left[\frac{\sin\theta_0}{n_2}\right]\right) \qquad (8.23)$$

and the first term describes diffusive transport, the second describes natural decay of excitons, the last term is the exciton generation rate. n is excited state concentration, I_0 is the incident photon flux, α is the absorption coefficient, and θ_λ is the incidence angle at organic material blocking layer interface, subscript λ indicating the dependence of different wavelength refraction through the blocking or quenching layer. θ_0 is the angle of incidence, n_2 is the index of refraction of the quenching layer, and n_3 is the index of refraction for the organic layer.

By comparing the PL intensity of the sample with the blocking layer to the sample with the quenching layer they obtained the normalized quenching ratio η:

$$\eta(\alpha) = \frac{PL_B(\alpha)}{PL_Q(\alpha)} = \frac{\int_0^\infty n_B(x, \alpha)dx}{\int_0^\infty n_Q(x, \alpha)dx} \qquad (8.24)$$

The authors solved for n(x) in equation (8.22) and by rearranging get an expression:

$$\eta(\alpha) = \frac{\alpha(\lambda)L_D}{\cos(\theta_\lambda)} + 1 = \alpha'(\lambda)L_D + 1 \qquad\qquad (8.25)$$

They plotted $\frac{PL_B}{PL_Q}$ versus $\alpha'(\lambda)$ and extracted the diffusion length from the slope. This is valid only if there is no energy transfer between the organic film and the quenching layer. If Forster transfer cannot be ignored one has to modify equation 8.22 as follows:

$$L_D \frac{\partial^2 n(x)}{\partial x} - \frac{n(x)}{\tau} + \frac{I_0\alpha}{\cos(\theta_\lambda)}\tau\exp\left(\frac{\alpha x}{\cos(\theta_\lambda)}\right) - n(x)\left[\rho_A\int\left(\frac{R_0^6}{R(x)^6}\right)dA\right] = 0,$$

$$(8.26)$$

where Forster transfer rate is integrated over all quenching interface area A, R_0 is Forster radius, $R(x)$ is the distance from a point in the film to any molecule within quenching layer, and ρ_A is the number of quenching molecules per unit area. Equation 8.26 can be rewritten:

$$L_D \frac{\partial^2 n(x)}{\partial x} - \frac{n(x)}{\tau} + \frac{I_0\alpha}{\cos(\theta_\lambda)}\tau\exp\left(\frac{\alpha x}{\cos(\theta_\lambda)}\right) - n(x)\rho_A\frac{2\pi}{5}\frac{R_0^6}{x^4} = 0, \qquad (8.27)$$

Both equations can be solved numerically and then as previously $\frac{PL_B}{PL_Q}$ plotted versus $\alpha'(\lambda)$ to yield the slope i.e. diffusion length L_D.

The main findings from these results are that the presence of the stacking and dimers affects diffusion coefficients to a large extent. Triplet excitons normally have lower diffusivities than singlets however diffusion lengths among the explored materials are very similar due to the effect of longer triplet lifetime. Also it is interesting that the same group in another publication[38], again using this method demonstrated that exciton diffusion length in PTCDA increases with an increase of crystalline order in films. They concluded that in these cases diffusion losses are mainly due to the non-radiative losses at grain boundaries.

Table 8.3. The diffusivity values extracted by the coworkers using diffusion length and natural lifetime of each material. PTCDA = perylene-3,4,9,10-tetracarboxylic-3,4,9,10-dianhydride), DIP = di-indenoperylene,SubPC = boron subphthalyocyanine, PtOEP = Pt(II) Octaethylporphine.

Material	Exciton	Lifetime (ns)	Diffusivity D (cm^2/s)
NPB	S	3.5	0.7E-4
CBP	S	0.7	40E-4
SubPc	S	<1	>6.4E-4
PTCDA	S	3.2	3.4E-4
DIP (upright)	S	1.8	15E-4
DIP (flat)	S	1.8	26E-4
PtOEP	T-monomer	800	0.041E-4
PtOEP	T-dimer	2800	0.00061E-4

Kalinowski *et al*[39] determined TTA constants and diffusion coefficients of Ir(ppy)$_3$ pure film and of Ir(ppy)$_3$ doped films. They illuminated films with continuous laser light and recorded film emission intensity at different excitation energies and used the solution to equation 7.6 to fit data:

$$[T(I_{exc})] = \left\{ \left[\left(\frac{1}{\tau_0^2} + \sigma I_{exc} \right) + 4\alpha' \gamma_{TT}^{eff} I_{exc} \right]^{1/2} - \left(\frac{1}{\tau_0} + \sigma_c I_{exc} \right) \right\} / 2\gamma_{TT}^{eff} \qquad (8.28)$$

Then relative phosphorescence yield can be calculated as:

$$\frac{Y}{Y_0}(I_{exc}) = \frac{[T(I_{exc})]/I_{exc}}{[T(I_{exc})]/I_{exc}(I_{exc} < I_{crit})} \qquad (8.29)$$

where I_{exc} is excitation intensity and I_{crit} is the critical excitation intensity. At this intensity level exciton kinetics changes from first order to second. Then Kalinowski *et al*[39] fitted the above equation to experimental data of pure Ir(ppy)$_3$ film (normalized intensity dependence on excitation energy). The best fit was achieved when γ_{TT}^{eff} =1.3E-12 cm^3/s considering σ =0 and τ =300 ns. Assuming R=1 nm (intermolecular spacing) D=5.2E-7 cm^2/s (using equation 3.20). Further Kalinowski *et al*[39] modified the model by accounting for non-emissive radiative sites and have got much better fit to data. γ_{TT}^{eff} for this model was twice as large, 2.7E-12 cm^3/s.

The disadvantage of this method is that triplet absorption coefficient needs to be known and its determination for organic materials without heavy atoms is not an easy task. Thus for example using this method to determine TTA constants of NPB could be a cumbersome experiment. Further they do not include a diffusion term in their calculations.

Giebink *et al*[18] study triplet diffusion migration in organic material CBP using it as a neat spacer layer capped with doped CBP. They doped CBP with two materials namely $Ir(ppy)_3$ and iridium(III) bis(2-phenyl-quinolyl-NC²') acetylacetonate (PQIr). They observed both delayed luminescence from spacer layer as well as phosphorescence from doped layer and used the following equations for fitting:

$$\frac{d[T_H(t,x)]}{dt} = D\frac{\partial^2[T_H(t,x)]}{\partial x^2} - \frac{[T_H(t,x)]}{\tau_T} - k_{TT}[T_H(t,x)]^2$$

$$\frac{d[S_H]}{dt} = -\frac{[S_H]}{\tau_S} + \frac{1}{2}k_{TT}[T_H(t)]^2$$

$$\frac{d[T_H(t,x)]}{dt} = D\frac{\partial^2[T_H(t,x)]}{\partial x^2} - k_{TT}[T_H(t,x)]^2 - (k_{TG} + \frac{1}{\tau_T})[T_H(t,x)]$$

$$\frac{d[T_G]}{dt} = -\frac{[T_G]}{\tau_g} + k_{TG}[T_H]$$

(8.30)

Here $[T_H]$ is host (neat) layer triplet exciton concentration, $[T_G]$ is guest triplet exciton concentration, $[S_H]$ is host layer singlet exciton concentration (arising from triplet-triplet annihilation), τ_T is host triplet lifetime, τ_G is guest triplet lifetime, τ_s is host singlet exciton lifetime, k_{TG} is host guest triplet transfer rate. They used the COMSOL package (finite element method) to solve these equations and fitted it to the phosphorescence (PH) and delayed fluorescence (DF) decay curves. There are a few issues with their approach. First they ignored the trap species present in CBP (chapter 5). Even in their paper[18] one can see emission from singlet trap species (compare spectra in chapter 5 and their paper[18] in figure 6 – they considered this to be emission from CBP) meaning that triplet traps are present at ~ 2.21 eV. This is much lower than triplet energy of dopant $Ir(ppy)_3$ (2.4 eV) meaning that a back transfer from this dopant to CBP trap has to be considered. Similar argument is valid for PQIr dopant. Their fitting results are as follows:

$$D(cm^2/s) = 1.4 \pm 0.3E - 8$$

$$k_{TT}(cm^3/s) = 1.6 \pm 0.4E - 14$$

$$[T_{H0}](cm^{-3}) = 7 \pm 2E17$$

$$\tau_H(ms) = 14 \pm 8$$

$$k_{TG}(s^{-1}) = 0.8 \pm E7 \text{ for Irppy}$$

$$k_{TG}(s^{-1}) = 0.5 \pm 0.2E7 \text{ for PQIr}$$

where $[T_{H0}]$ is triplet exciton concentration at time 0. Then using the relation

$$k_{TT} = 8\pi fRD \qquad\qquad (8.31)$$

they calculated at what distance TTA takes place with 100 % efficiency (f=1) which is R=0.455 nm in this case. Here f is triplet-triplet annihilation probability when triplets are at a certain distance R, D is the diffusion constant. The effective diffusion length can be calculated using formula 8.6 which is 25 nm for CBP when accounting for TTA. Assuming TTA is negligible Giebink *et al[18]* calculated it to be 140 nm (not explained how though in the paper). According to them this is similar to tris(8-hydroxy-quinoline) (Alq$_3$) case when with TTA Alq$_3$ L_D=14 nm and assuming it is negligible - 140 nm. Another finding by this group was that they doped the spacer layer with high gap triplet layer material to act as a scatter center and with an increase of its concentration found the simultaneous decrease of annihilation constant and diffusion coefficient. Fitting is not perfect in the initial regions of decay (e.g. figure 3, 4 and 5 in ref[18]) possibly indicating some dispersive behavior of triplet transport. Finally in this paper transfer between two different layers has not been captured and it is possible that at the interfaces physics might be of different kind.

It is important to mention a problem which is valid for all experiments were homogeneous pulsed laser excitation is used to create excited states. Namely, a laser pulse is homogenous and it is absorbed by an inhomogeneoulsy broadened thin film which consists of numerous homogenous profiles (figure 8.1)[40]. A process called hole-burning could occur [40-41], see figure 8.1. The hole-burning mechanisms could be divided into two categories – persistent hole burning and transient hole burning[41]. Persistent hole burning mechanisms are divided into photochemical hole burning and non-photochemical hole burning. As the name implies photochemical hole burning occurs via photochemical processes when intramoleculer reaction occurs in the dopant or intermolecular reaction occurs between the dopant and the host. Non-photochemical hole burning occurs mostly in amorphous systems after excitation with a homogeneous width laser, slight local environment rearrangement seems to take place. Transient hole burning occurs when an excited state is transferred through the state of interest to

a metastable state[40]. In addition to this, saturation of excitations in homogeneous linewidth could take place.

A linewidth of Ekspla YAG laser used in this thesis is less 0.1 cm^{-1}. Haarer *et al*[42] investigated H$_2$Pc/PMMA (free base phorphin in polymethylmethacrylate) and obtained homogeneous widths of 0.34 cm^{-1} (4.2K), 0.5 cm^{-1} (10K) 0.85 cm^{-1} (15K) and 6.5 cm^{-1} (50K). Clearly at room temperature these widths must be much higher as Volker *et al* deduced that homogeneous linewidths of organic amorphous glasses increases with $T^{1/3}$ or even T^{2} [40]. Assuming other amorphous organic materials behave in a similar manner, the homogeneous width of the laser should be much smaller even than the homogeneous widths of the organic film absorption. Further there are studies claiming that with an increase of laser power the widths of burnt holes increases[41]. The CW laser power used in those studies was from 0.4 µW/cm^2 to 45 mW/ cm^2 and holes were burnt for all of these power densities. The laser power used here (in order to create high triplet exciton densities) are in the range of 1 MW/cm^2. Similar powers were used by Rothe *et al*[43]. Giebink *et al*[18] used powers not smaller above 0.1 MW/cm^2 considering the most conservative calculations as exact pulse length is not reported. Leo *et al* uses power densities at ∼ 0.03 MW/cm^2. Thus it is highly probable that the hole burning process is existent during these experiments. Also it is likely that all transitions in homogeneous linewidth are saturated. Hence a problem arises to calculate the absorbed number of photons.
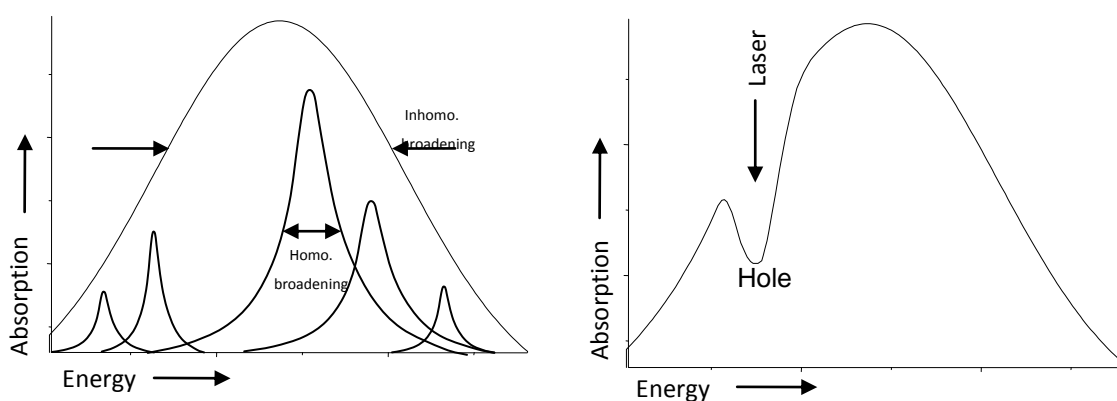
Figure 8.1 Left. Inhomogeneous broadening of absorption profile is shown which is superposition of homogeneously broadened transitions. Right. Hole burnt after excitation with homogeneously broadened laser is shown

8.6 Summary

Architectures of recently published efficient white OLED multilayer devices based on singlet and triplet harvesting present lots of challenges for material engineers. There are many parameters which need to be adjusted among them triplet and singlet diffusion properties. The main parameters characterizing triplet diffusion, assuming non-dispersive exciton migration, are the diffusion constant, triplet-triplet annihilation constant and exciton diffusion length. Having in mind that the exciton harvesting path to get efficient white OLEDs is very promising, there is little wonder that in recent years, research in diffusion properties of excitons has been revived and novel methods to determine them devised. Here, the main of techniques are reviewed, and modeling and fitting guidelines enabling to evaluate their advantages and drawbacks are presented. There are few methods to determine diffusion properties and constants. Firstly one could use double or multilayer structures with sensing layers and pulsed or steady-state excitations to construct an exciton transport experiment. Further, there is an option to analyze exciton transport 'in situ' in OLED devices by changing the width of spacer layer and by using electrical excitation. Although the latter method is more close to the real conditions, unfortunately other process such as triplet-polaron annihilation takes place in these type of structures thus it is possible that exciton diffusion properties might be skewed. Hence fundamental properties of triplet transport might not be understood properly which is one of the aims of this thesis. In the former type of experiments despite the fact that the structures and type of excitation (optical opposed to electrical) are further from practice, genuine diffusion properties might be uncovered which might help to understand the role of triplet-polaron role in OLEDs later when genuine triplet transport properties are understood well. Diffusion coefficient determination using photocurrent spectrum might be a viable alternative and most probably it could be useful in uncovering exciton migration role in solar cells. The methods used in the sixties and seventies to determine the constants of crystal would not be so useful in modern OLED or Solar Cell materials mainly due to different sizes of samples and higher level of disorder in these materials. Finally, before trying to extract the diffusion parameters one should make sure that the material of interest exhibits dispersive exciton transport features or whether they can be neglected and if not how extracted parameters should be interpreted.

The following problems during the investigation of triplet transport could be identified and should be considered:

- If using OLED type structures one has to be careful and evaluate exciton-polaron annihilation[9, 26-27].

- If using OLED type structures one has to be careful in applying current and charge transport equations as charge transport was shown to be dispersive even at room temperature[31].

- If using OLED type structures one has to use excitation pulses having shorter length than OLED charging times[16].

- Determination of initial triplet exciton densities in film structure after optical excitation (PL) can be difficult as in most cases the intersystem crossing yield is unknown. This could be overcome by using heavy –metal complexes where intersystem crossing yield is close to unity.

- Determination of initial triplet exciton densities in film structure after optical excitation (PL) can be difficult due to the fact that the laser pulse is normally homogeneously broadened whereas absorption profile of most organic materials is inhomogeneously broadened (which is many orders of magnitude larger) [40-42]. Saturation of all excitations in homogeneous linewidth also could occur.

- When simulating experiments one has to be cautious with the fact that dispersive exciton transport might be prevalent in amorphous organic films and especially one has to be cautious with the interpretations with extracted triplet transport constants (diffusion coefficient, triplet-triplet annihilation constant)[44]

- If use of classical diffusion equations is unavoidable (for example time dependence of diffusion constant is unknown) it is advisable to use all terms i.e. diffusion term, monomolecular decay term and bimolecular decay terms as neglect of any of them might skew the results.

- Before creating and performing experiments with multilayer structure it is important to investigate each material one by one in order to determine all possible trap states, excimer, or aggregate states. This will guarantee that all emission observed from multilayer films is identified and assigned to appropriate species and that equations used in simulations are set correctly.

- Finally transfer through interface has not been investigated and experimentally captured yet despite the fact that it could heavily influence triplet transport between layers.

In this thesis optical excitation of multilayer non-doped structures has been chosen despite the difficulties in determining initial triplet concentration. The main reason for this is the absence of any processes related to charge transfer (after electrical excitation), possibility to determine genuine triplet transport properties and possibility to capture triplet transport via interfaces (no doping!). As properties of single layer material films are already known (chapters 5,6,7), the type of structures and excitation type has been chosen and main possible problems are identified.

8.7 References

1. C. W. Tang and S. A. Vanslyke, Appl. Phys. Lett. 51 (12), 913-915 (1987).

2. S. A. VanSlyke, C. H. Chen and C. W. Tang, Appl. Phys. Lett. 69 (15), 2160-2162 (1996).

3. L. S. Hung and C. H. Chen, Mater. Sci. Eng. R-Rep. 39 (5-6), 143-222 (2002).

4. M. Pfeiffer, K. Leo, X. Zhou, J. S. Huang, M. Hofmann, A. Werner and J. Blochwitz-Nimoth, Org. Electron. 4 (2-3), 89-103 (2003).

5. S. M. Tadayyon, H. M. Grandin, K. Griffiths, P. R. Norton, H. Aziz and Z. D. Popovic, Org. Electron. 5 (4), 157-166 (2004).

6. M. A. Baldo, S. Lamansky, P. E. Burrows, M. E. Thompson and S. R. Forrest, Appl. Phys. Lett. 75 (1), 4-6 (1999).

7. M. A. Baldo, D. F. O'Brien, Y. You, A. Shoustikov, S. Sibley, M. E. Thompson and S. R. Forrest, Nature 395 (6698), 151-154 (1998).

8. T. X. Zhou, T. Ngo, J. J. Brown, M. Shtein and S. R. Forrest, Appl. Phys. Lett. 86 (2), 021107 (2005).

9. S. Reineke, K. Walzer and K. Leo, Phys. Rev. B 75 (12), 125328 (2007).

10. Y. R. Sun, N. C. Giebink, H. Kanno, B. W. Ma, M. E. Thompson and S. R. Forrest, Nature 440 (7086), 908-912 (2006).

11. G. Schwartz, S. Reineke, T. C. Rosenow, K. Walzer and K. Leo, Adv. Funct. Mater. 19 (9), 1319-1333 (2009).

12. M. E. Kondakova, J. C. Deaton, T. D. Pawlik, D. J. Giesen, D. Y. Kondakov, R. H. Young, T. L. Royster, D. L. Comfort and J. D. Shore, J. Appl. Phys. 107 (1), 014515 (2010).

13. S. Reineke, F. Lindner, G. Schwartz, N. Seidler, K. Walzer, B. Lussem and K. Leo, Nature 459 (7244), 234-238 (2009).

14. W. A. Luhman and R. J. Holmes, Appl. Phys. Lett. 94 (15), 153304 (2009).

15. Y. Shao and Y. Yang, Adv. Mater. 17 (23), 2841-2844 (2005).

16. M. A. Baldo, C. Adachi and S. R. Forrest, Phys. Rev. B 62 (16), 10967-10977 (2000).

17. M. A. Baldo and S. R. Forrest, Phys. Rev. B 62 (16), 10958-10966 (2000).

18. N. C. Giebink, Y. Sun and S. R. Forrest, Org. Electron. 7 (5), 375-386 (2006).

19. M. Pope and C. E. Swenberg, *Electronic Processes in Organic Crystals*. (Oxford Univresity Press, New York, 1982).

20. V. Ern, P. Avakian and R. E. Merrifield, Physical Review 148 (2), 862-867 (1966).

21. R. G. Kepler and A. C. Switendick, Phys. Rev. Lett. 15 (2), 56-59 (1965).

22. J. R. Salcedo, A. E. Siegman, D. D. Dlott and M. D. Fayer, Phys. Rev. Lett. 41 (2), 131-134 (1978).

23. D. Y. Kondakov, J. Appl. Phys. 102 (11), 114504 (2007).

24.   J. Mezyk, R. Tubino, A. Monguzzi, A. Mech and F. Meinardi, Phys. Rev. Lett. 102 (8), 087404 (2009).

25.   J. Birks and S. P. McGlynn, *Organic Molecular Photophysics*. (John Wiley & Sons, Bristol, 1973).

26.   D. Hertel and K. Meerholz, J. Phys. Chem. B 111 (42), 12075-12080 (2007).

27.   F. X. Zang, T. C. Sum, A. C. H. Huan, T. L. Li, W. L. Li and F. R. Zhu, Appl. Phys. Lett. 93 (2), 023309 (2008).

28.   N. Matsusue, S. Ikame, Y. Suzuki and H. Naito, J. Appl. Phys. 97 (12), 123512 (2005).

29.   N. Matsusue, S. Ikame, Y. Suzuki and H. Naito, Ieice Transactions on Electronics E87C (12), 2033-2038 (2004).

30.   C. L. Yang, Z. K. Tang, W. K. Ge, J. N. Wang, Z. L. Zhang and X. Y. Jian, Appl. Phys. Lett. 83 (9), 1737-1739 (2003).

31.   D. Hertel and H. Bassler, ChemPhysChem 9 (5), 666-688 (2008).

32.   T. Fushimi, A. Oda, H. Ohkita and S. Ito, J. Phys. Chem. B 108 (49), 18897-18902 (2004).

33.   W. Staroske, M. Pfeiffer, K. Leo and M. Hoffmann, Phys. Rev. Lett. 98 (19), 197402 (2007).

34.   E. Engel, K. Leo and M. Hoffmann, Chem. Phys. 325 (1), 170-177 (2006).

35.   T. Forster, Z. Naturforsch. (A 4), 321 (1949).

36.   W. Holzer, A. Penzkofer and T. Tsuboi, Chem. Phys. 308 (1-2), 93-102 (2005).

37.   R. R. Lunt, N. C. Giebink, A. A. Belak, J. B. Benziger and S. R. Forrest, J. Appl. Phys. 105 (5), 053711 (2009).

38.   R. R. Lunt, J. B. Benziger and S. R. Forrest, Adv. Mater. 22 (11), 1233-1236 (2010).

39.   J. Kalinowski, J. Mezyk, F. Meinardi, R. Tubino, M. Cocchi and D. Virgili, J. Appl. Phys. 98 (6), 063532 (2005).

40.   S. Volker, Annual Review of Physical Chemistry 40, 499-530 (1989).

41.   H. P. H. Thijssen and S. Volker, Chem. Phys. Lett. 120 (6), 496-502 (1985).

42.   A. R. Gutierrez, J. Friedrich, D. Haarer and H. Wolfrum, Ibm Journal of Research and Development 26 (2), 198-208 (1982).

43.   C. Rothe and A. P. Monkman, Phys. Rev. B 68 (7), 075208 (2003).

44.   A. Kohler and H. Bassler, Mater. Sci. Eng. R-Rep. 66 (4-6), 71-109 (2009).

9 Triplet excitons in multilayer structures: dynamical properties in neat films, transfer through an interface between two layers and determination of diffusion properties – experiments and simulations.

A decade after Tang *et al[1]* managed to make an organic light emitting device (OLED) based on tris(8-hydroxyquinolato) aluminum (Alq$_3$), devices based on efficient phosphorescence emission started to appear[2-5] and interest in the properties of triplet excitons in amorphous organic materials[6-10] was triggered. Phosphorescent white emitting OLEDs (WOLEDs) has been designed which can reach fluorescence tube efficiency[11]. Very recently Forrest *et al[12]* and later Leo *et al[13]* presented another approach to making use of non-emissive triplet states which caused this interest to grow further. They use triplet harvesting, an approach where triplets created by recombination of charges in one layer hop through interfaces and are trapped on different color emissive heavy metal dopants in other organic layers which emit efficiently. This technological approach to make WOLEDs could revolutionize the lighting industry in supplying very efficient devices with much wider color mixing and rendering options than the present widely used fluorescent tubes. However, much work still needs to be done in improving WOLEDs, mainly in understanding triplet transfer between the layers and controlling it with high precision. Numerous studies analyzing triplet exciton dynamics in single layer amorphous organic films have been published already [6-10] . Unfortunately, there are no published studies on triplet movement through interfaces between thin amorphous layers. Although there were a few studies where multilayer structures have been used to determine triplet properties (diffusion constants, triplet-triplet annihilation constants, details in chapter 8, the dynamics of triplets excitons across an interface have not been captured experimentally. Despite the fact that transfer of excitons across the interface will be a major controlling factor in efficient triplet harvesting within WOLEDs, this has been overlooked. Furthermore, it is generally accepted that simple exothermic triplet transfer between bulk states of two amorphous films occurs (assuming one of them is of much higher triplet energy than the other). Here it is proposed that this is not always the case and that intermediate interface states are involved and triplet dynamics is elucidated at the interface of two neat amorphous layers in section 9.1. In these studies a layer with high triplet energy (~2.35 eV) N,N'-diphenyl-N,N'-bis(1-naphthyl)-1,1'-biphenyl-4,4''-diamine (NPB) and a layer with low triplet energy (~1.96 eV) Iridium (III) tris(1-phenylisoquinoline) (Ir(piq)$_3$) are evaporated and it is shown that triplet transfer between them does not occur as a straightforward exothermic exciton transfer.

The mechanism allowing triplet harvesting to happen is the difference between singlet and triplet exciton diffusion lengths. For example, one scheme places the fluorescent blue material at the recombination zone with the phosphorescent green and red complexes doped in subsequent layers separated by interlayers within the diffusion length of triplet excitons, but which are much further than diffusion length of singlet excitons[13]. Thus a good understanding of triplet state dynamics and diffusion properties is of crucial importance for improving PHOLEDs and Hybrid OLEDs further. Hence in section 9.2, time resolved gated optical spectroscopy is used and multilayer structures are evaporated to extract information about triplet migration. The main goal of this experiment is to show that triplets can be transferred via optically inactive (no absorption of the excitation light) spacer layer from the donor layer to acceptor layer. NPB is sandwiched in between donor, *fac* - tris(2-phenylpyridine) iridium ($Ir(ppy)_3$) and an acceptor $Ir(piq)_3$ thin films. Donor and acceptor are excited at 450 nm, which is absorbed only by donor and acceptor but not NPB. During their lifetime triplet excitons migrate from donor to acceptor via the NPB layer and by changing the NPB thickness, the change in the decay dynamics of acceptor $Ir(piq)_3$ can be followed. By drawing on the experimental results of section 9.2 triplet transfer across interface in this structure is discussed.

Finally chapter 9 is concluded with section 9.3 were a different approach to triplet diffusion modeling is presented (compare with the ones reviewed in chapter 9) which includes interface effects and it is shown, that complicated triplet transfer through interface and between layers can be reliably modeled using relatively small number of parameters. Diffusion and triplet-triplet annihilation constants obtain during the simulation are compared with the literature values.

9.1 Triplet exciton interface trap states in bilayer films of NPB and Ir(piq)$_3$
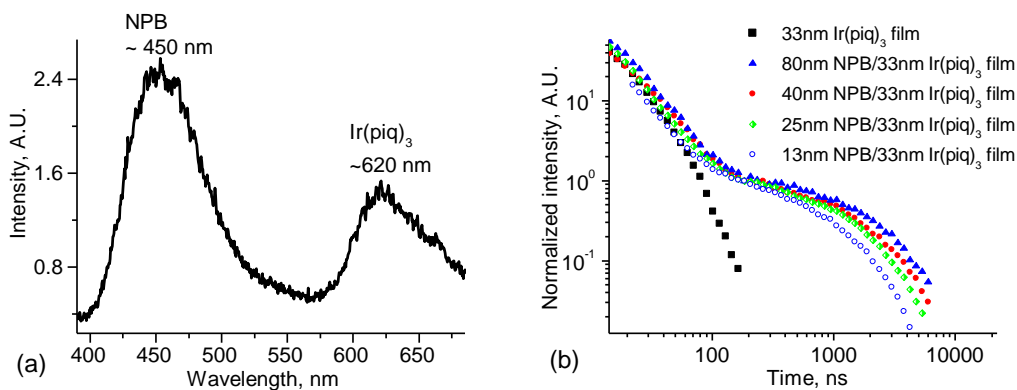
Figure 9.1 (a) Time resolved spectrum of bilayer sapphire/33 nm Ir(piq)$_3$/25 nm NPB film, recorded from 370 ns to 410 ns after excitation. 9b) Influence of different thicknesses of NPB on the decay of an Ir(piq)$_3$ film (measured at 620 nm) in bilayer sapphire/Ir(piq)$_3$/NPB films. The thickness of NPB is varied while the Ir(piq)$_3$ thickness is kept 33 nm. Excited at NPB side with 355 nm light, recorded at 293 K. For comparison purposes the decay of a 33nm Ir(piq)$_3$ film is included.

Triplet decays of Ir(piq)$_3$ in sapphire/Ir(piq)$_3$/NPB bilayer films have been recorded where the Ir(piq)$_3$ thickness has been kept constant (33 nm) while the thickness of NPB has been changed (13 nm, 25 nm, 40 nm, 80 nm). NPB was directly excited with the 355 nm laser (exponential absorption coefficients ~164380 cm-1 for NPB and ~101760 cm-1 for Ir(piq)$_3$ at 355 nm - extracted using spectroscopic ellipsometry with Cauchy modeling). In figure 9.1a the time resolved spectrum of sapphire/33 nm Ir(piq)$_3$/25 nm NPB film is shown. The emission from NPB delayed fluorescence, peaking at ~ 450 nm is observed[14] along with emission of Ir(piq)$_3$ phosphorescence, peaking at ~620 nm[15]. The decays of Ir(piq)$_3$ in bilayer films, as well as the single layer Ir(piq)$_3$ film, are depicted in figure 9.1b. It is evident from the graph that the single layer Ir(piq)$_3$ film decays almost completely within the first 200 ns whereas the NPB topped films have a tail of very unconventional form after 200 ns which decays monoexponentially. This tail is ascribed to Ir(piq)$_3$ emission arising from triplets transferred from the NPB layer, whereas the emission up to ~200 ns is ascribed to emission primarily from directly excited bulk Ir(piq)$_3$ layer within the sapphire/Ir(piq)$_3$/NPB bilayer film. The thinner the NPB layer the smaller the reservoir of NPB triplet excitons which add to the initially excited Ir(piq)$_3$ layer. Therefore, the monoexponential lifetime of the tail decreases with the decrease of NPB thickness - for 80 nm thickness it is 2031 ns, for 40 nm – 1763 ns, for 25 nm – 1411 ns, for 13nm – 1084 ns. Triplet excitons are transferred from the NPB to the Ir(piq)$_3$ due to the long

lifetime of triplets in NPB (chapter 8). The bulk triplets of the Ir(piq)$_3$ rapidly decay (as seen in the pure Ir(piq)$_3$ film), but the triplets from NPB continue to be feed into the interfacial Ir(piq)$_3$ sites, over a much longer time giving rise to this monoexponential decay.
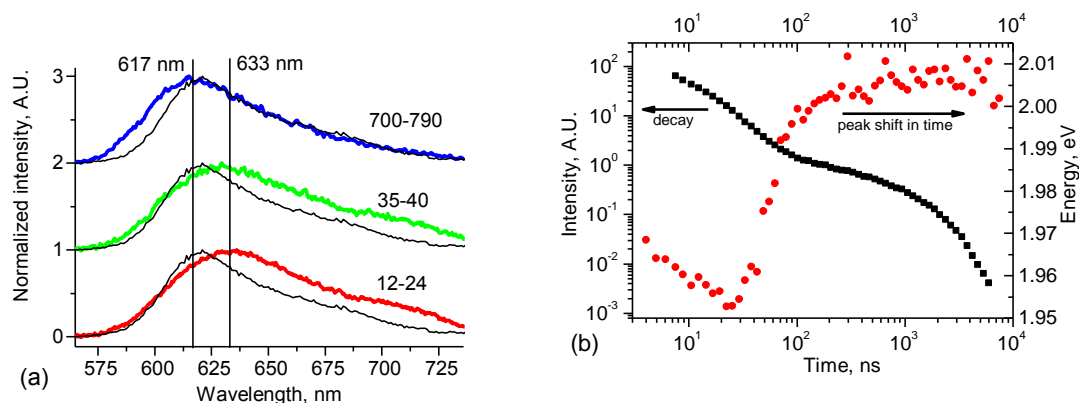
Figure 9.2 (a) Time resolved spectra of sapphire/33 nm Ir(piq)$_3$/13 nm NPB bilayer film (thick lines) and steady state emission spectrum of 10% Ir(piq)$_3$: NPB (thin lines). The parameters shown are camera opening and closing times in nanoseconds. Recorded at room temperature. (b) Peak shift (circles) and decay (triangles) of Ir(piq)$_3$ layer in a bilayer sapphire/33 nm Ir(piq)$_3$/13 nm NPB film.

In figure 9.2a time resolved emission spectra of Ir(piq)$_3$ from a sapphire/33 nm Ir(piq)$_3$/13 nm NPB bilayer film is shown and in figure 9.2b the peak as a function of time in comparison with intensity change is presented. In the initial 200 ns the peak shifts from ~ 1.97 eV to 1.95 eV. This can be ascribed to energy relaxation in the triplet density of states (chapter 7); similar relaxation has been observed in other disordered films (chapter 8). By considering the fact that the single 33 nm layer Ir(piq)$_3$ film also emits at this region (figure 9.3) this emission, with a peak at ~1.96 eV, could be ascribed as that from bulk Ir(piq)$_3$ states, created by direct 355 nm laser excitation. After ~200 ns the peak energy monotonically shifts to *higher* energies (up to ~2.00 eV). This coincides in time with the monoexponential decay tail and it is not observed in a single layer Ir(piq)$_3$ film where emission comes from bulk states. The emission at ~2.00 eV could be ascribed to be from interface sites of Ir(piq)$_3$. Emission from Ir(piq)$_3$ at ~2.00 eV is observed up to ~10 μs indicating that triplets from the NPB reservoir do not migrate through the Ir(piq)$_3$ interface sites into the Ir(piq)$_3$ bulk – they are effectively trapped at the interface sites. The largest possible Ir(piq)$_3$-NPB triplet energy difference calculated from experimental results is 0.39 eV i.e. 2.35 eV (NPB in zeonex spectrum) minus 1.96 eV (bulk Ir(piq)$_3$ spectrum), the smallest triplet energy difference is 0.29 eV i.e. 2.29 eV (NPB bulk triplet spectrum) minus 2.00 eV (isolated Ir(piq)$_3$ spectrum), see chapters 6 and 7 for more details. Whatever value is taken, simple exothermic transfer could be expected between the bulk states of the two layers. However this is not the case as can be inferred from figure 9.2b and it is evident that triplets are energetically trapped at Ir(piq)$_3$ interface sites and that an activation energy is involved for the

158

triplets to escape to bulk Ir(piq)$_3$ states. This final process is not observed in this experiment and indicates that this barrier is much higher than 0.026 eV (data has been recorded at 293 K) and that interface sites of Ir(piq)$_3$ therefore play the main role in triplet energy transfer between the bulk NPB and Ir(piq)$_3$ states. Careful examination of time resolved spectra in figure 9.2a also shows that the blue shift after ~200 ns is also accompanied by a change in the spectral band shape. The red emission tail is lost, yielding effectively a band shape indicative of isolated Ir(piq)$_3$ not bulk material (compare with thin line steady state emission spectra of 10% Ir(piq)$_3$ doped into NPB). This indicates that the interface is not abrupt but consists of a thin layer of Ir(piq)$_3$ doped in NPB, yielding isolated Ir(piq)$_3$ molecules. One can then readily realize the origin of the barrier into the bulk Ir(piq)$_3$. Similar time resolved spectra and energy peak vs time behavior has also been observed for sapphire/33 nm Ir(piq)$_3$/25 nm NPB, sapphire /33 nm Ir(piq)$_3$/40 nm NPB and sapphire/33 nm Ir(piq)$_3$/80 nm NPB bilayer films.
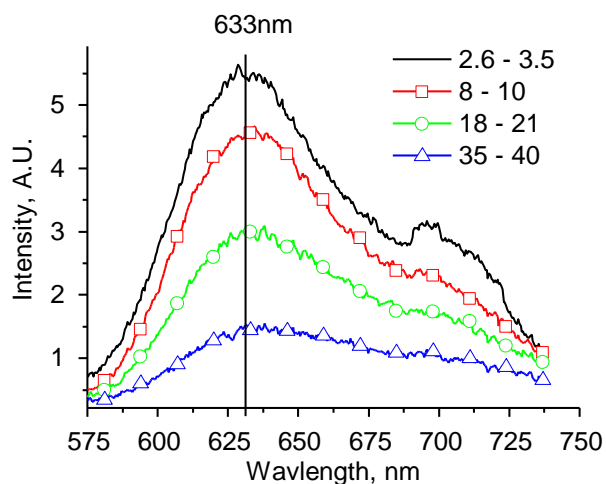
Figure 9.3 Time resolved spectra of a neat 33 nm Ir(piq)$_3$ single layer film. Parameter is camera opening and closing times in nanoseconds. Recorded at room temperature. At earlier times ~710 nm 2nd order of laser at 355 nm is observed.

In conclusion it can be said that evidence of triplet trapping in the Ir(piq)$_3$ interface states between NPB and Ir(piq)$_3$ layers has been presented. This experiment show that the widely accepted view that transfer between layers having two different triplet energy levels is governed by a simple exothermic process is not always correct. It is shown here that triplets from the donor NPB are mainly trapped at the interface sites of Ir(piq)$_3$ and are not directly transferred into the bulk states of Ir(piq)$_3$ and should be considered when modeling triplet dynamics in multilayer films. Indeed, models of the type of processes described here will be particularly important in designing optimum transfer into the bulk states behind such interfaces. Hopefully these findings will encourage more experimental, computational and theoretical research on triplet movement in interfaces between two amorphous organic layers as it not only may be

important to device physicists but also could open a new chapter in understanding of this physical phenomenon.

9.2 Triplet energy transfer across an NPB interlayer between Ir(ppy)₃ and Ir(piq)₃ structure
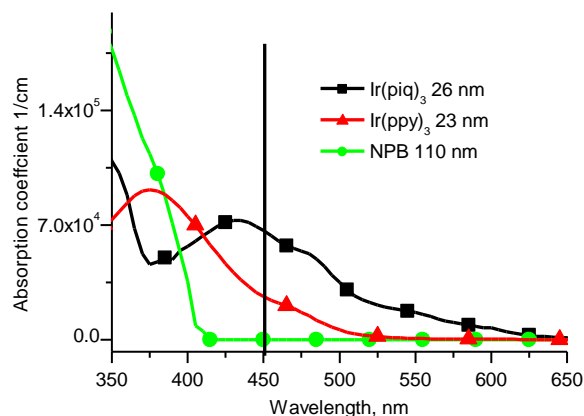
Figure 9.4 Exponential absorption coefficients of Ir(ppy)$_3$, Ir(piq)$_3$ and NPB films. Determined using ellipsometry measurements and Cauchy point-by-point or Gaussian function fitting.

Films consisting of five layers namely Ir(ppy)$_3$ 5 nm/NPB x nm/Ir(piq)$_3$ 5 nm/ TAPC (1,1-bis((di-4-tolylamino)phenyl)cyclohexane 100 nm/ Aluminum 200 nm, x being the thickness of NPB which was varied from 0 nm to 20 nm, have been evaporated on sapphire substrate in the order of naming. 450 nm pulsed laser light has been directed onto the surface of Ir(ppy)$_3$ layer expecting that part of it will be absorbed by Ir(ppy)$_3$ and another part by Ir(piq)$_3$. NPB does not absorb any light at 450 nm (figure 9.4), so it should act as an inter layer between the Ir(ppy)$_3$ donor and Ir(piq)$_3$ acceptor. TAPC has negligible absorption at 450 nm[16] and 2.9 eV triplet level[17] and has been used as an organic capping layer and thick spacer layer between Ir(piq)$_3$ and aluminum layer which acts as a capping layer against oxygen and water. Effectively only 3 layers are participating in photophysical processes. The main reason why triplets should be transferred from Ir(ppy)$_3$ to NPB to Ir(piq)$_3$ is the triplet level gradient ($E_{TIr(ppy)3} > E_{TNPB} > E_{TIr(piq)3}$, figure 9.5) and triplet concentration gradient from Ir(ppy)$_3$ to NPB (no absorption in NPB). Another factor in favor of transfer is longer triplet lifetime in NPB than in Ir(piq)$_3$ that leaves plenty of time for them to travel in between donor and acceptor and be detected in the latter. Namely, monomolecular decay lifetime of Ir(ppy)$_3$ and Ir(piq)$_3$ triplet states in N$_2$ saturated dilute toluene solutions at room temperature are 2 µs and 0.74 µs appropriately[15]. Monomolecular decay lifetime of NPB triplets in a film is ~2.5 µs at room temperature which was indirectly extracted from the simulation of triplet migration in NPB films (section 9.3 below). Other references report shorter monomolecular lifetime of dilute Ir(ppy)$_3$ dispersed in CBP (1.3 µs)[18] and longer monomolecular decay lifetime of Ir(piq)$_3$ dispersed in NPB (~ 1.1

161

μs)[8]. Whatever values are taken from literature monomolecular lifetime of both heavy metal complexes at room temperature in films will be even shorter than in dilute solution or matrix (due to additional concentration quenching, migration to trap sites etc. see e.g. ref by Kawamura *et al*[18] or chapter 7) by at an order of magnitude in comparison with NPB monomolecular 2.5 μs lifetime in film.
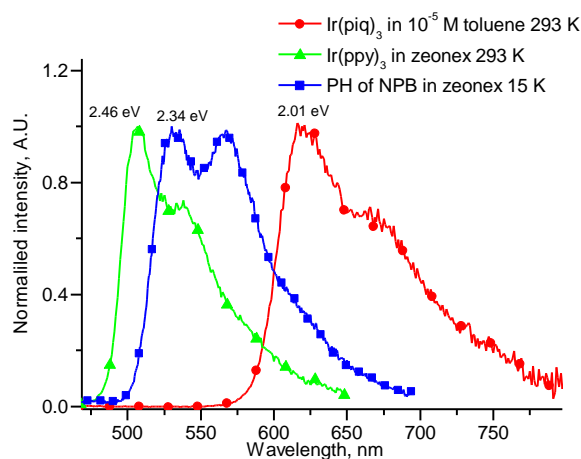
Figure. 9.5 Phosphorescence spectra of Ir(ppy)$_3$ and NPB in zeonex and Ir(piq)$_3$ in dilute toluene solution. Triplet levels are ~2.46 eV for Ir(ppy)$_3$, ~2.34 eV for NPB and ~2.01 eV for Ir(piq)$_3$.

In figure 9.6 time resolved spectra of sapphire/Ir(ppy)$_3$ 5 nm/NPB 2.5 nm/Ir(piq)$_3$ 5 nm/TAPC 100 nm/Al 200 nm film as an example is shown. At ~540 nm Ir(ppy)$_3$ emission is observed (normalized at the peak of this emission) and at earlier times intrinsic Ir(piq)$_3$ emission peaking at 630 nm is observed. At later times (1 μs) peak at ~700 nm starts to appear which could be ascribed to trap species already detected in single layer films of Ir(ppy)$_3$ and Ir(piq)$_3$ (chapter 7). Thus in order to record intrinsic Ir(piq)$_3$ decays rather than decays from trap species, spectra were integrated between 600 nm and 625 nm and all emission appearing after 1000 ns was considered to be coming from the trap species. Here it becomes clear how relevant the information extracted from single layer film experiments is and that it is essential for the interpretation of data from multilayer films.
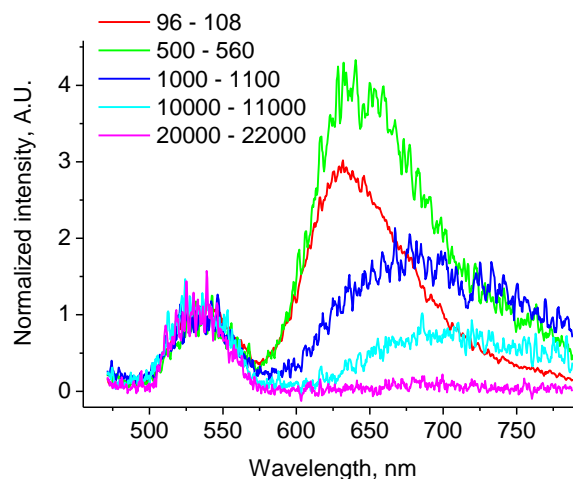
Figure 9.6 Spectra of sapphire/ Ir(ppy)$_3$ 5nm/NPB 2.5 nm/ Ir(piq)$_3$ 5nm/TAPC 100nm/Al 200nm film. All curves are normalized to 1 at 529 nm to enable comparison. Excited at Ir(ppy)$_3$ side with 450nm pulsed laser, recorded at 293K. Ir(piq)$_3$ emission integrated between 600 and 625nm. At very late times peak at ~700nm starts to appear which is not genuine Ir(piq)$_3$ emission, see chapter VII for more details on this type of emission.

In figure 9.7 the decay of Ir(piq)$_3$ layer from sappire/Ir(ppy)$_3$ 5 nm/NPB x nm/ Ir(piq)$_3$ 5 nm/TAPC 100 nm/Al 200 nm films is depicted. In the initial 100-200 ns the decay is similar for all trilayer films independent of spacer thickness. This is much longer than the excitation pulse length (~ few nanoseconds as 450 nm dye laser was used). However, it is clear from the graph that as the thickness of the spacer layer increases the tail of Ir(piq)$_3$ decay also increases, indicating that it takes longer for the triplets to arrive to the Ir(piq)$_3$. Further, even though initial decay is of multiexponential (or non-exponential) character, the tail after ~200 ns obeys a monoexponential law (figure 9.7b). This may be interpreted to be due to the delay of triplets traveling through the NPB layer before reaching Ir(piq)$_3$ and consequently having longer effective lifetime. It is interesting to note that the fitted monoexponential lifetime of the tails of Ir(piq)$_3$ decay depends linearly on spacer thickness (not shown). Similar decay behavior of the "detector" layer has already been observed in bilayer sapphire/Ir(piq)$_3$/NPB films (acceptor/donor) when exciting NPB with 355 nm laser light (section 9.1). It was concluded that the initial multiexponential decay comes from the directly excited Ir(piq)$_3$ layer and that triplets arriving from NPB are trapped at interface sites of Ir(piq)$_3$ and do not migrate directly to the bulk states of Ir(piq)$_3$. Here it is analysed how triplets behave in donor/spacer/acceptor case.
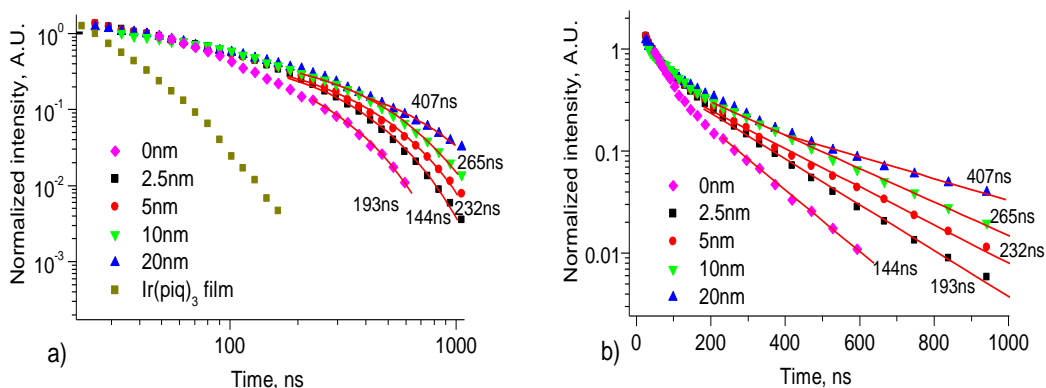
Figure 9.7 Influence of different thickness NPB on the decay of $Ir(piq)_3$ in an sapphire/$Ir(ppy)_3$ 5 nm/NPB x nm/ $Ir(piq)_3$ 5 nm/TAPC 100 nm/Al 200 nm film in a log-log representation (a) and in log-lin representation (b). Excited at $Ir(ppy)_3$ side with 450 nm pulsed laser, recorded at 293K. $Ir(piq)_3$ emission integrated between 600nm and 625nm. Intensity is normalized. Lines are fits to long lived decays and the lifetime of long lived $Ir(piq)_3$ emission on each curve is indicated in ns. Parameter indicated is NPB thickness.

The peak energy of $Ir(piq)_3$ in a multilayer films decreases from 1.97 eV to 1.95 eV in the first 10 ns and follows log(t) law (figure 9.8). Downwards migration in energy and proportionality to log(t) of peak energy signals about dispersive migration in a first few tens of ns[9, 19] (chapter 7). After this, the peak energy stays on average at ~1.95 eV from ~100 ns to ~ 1000 ns independent of the thickness of NPB. For comparison peak change in time of 33 nm $Ir(piq)_3$ single layer neat film is included which decreases in energy from ~1.97 eV at 5 ns to 1.95 eV at ~30 ns after excitation. In this multilayer film case no blueshift of $Ir(piq)_3$ spectra after energetical relaxation has been observed as in bilayer films case (compare figures 9.3b and 9.8). In section 9.1 $Ir(piq)_3$ emission from bilayer films at ~1.95 eV has been assigned to the bulk triplets whereas from states at 2.0 eV to interface triplets, thus emission from $Ir(piq)_3$ in multilayer films in all time regions is from bulk $Ir(piq)_3$ sites. Reasons of the unexpected absence of interface sites in these multilayer films are discussed at the end of this section.

That emission in $Ir(piq)_3$ acceptor after ~100-200 ns is coming not from the directly excited bulk states, but from triplets which are starting to arrive from $Ir(ppy)_3$ via NPB to $Ir(piq)_3$ bulk states can be concluded from figure 9.9a. In this figure the decay of $Ir(piq)_3$ in a multilayer samples (with NPB=5 nm and NPB=0 nm) is portrayed together with peak shift in time. From 10 ns to 100 ns peak energy migration downwards in time is observed which could be ascribed to the dispersive energy migration of directly excited states as already discussed in section 9.1.
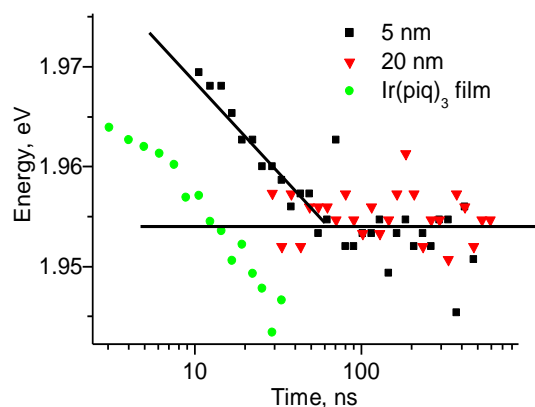
Figure 9.8 Peak energy shift in time resolved Ir(piq)$_3$ emission from 3 layer sapphire/ Ir(ppy)$_3$ 5 nm/NPB x nm/Ir(piq)$_3$ 5 nm/TAPC 100 nm/Al 100 nm film where x as indicated is 5 nm and 20 nm. Peak energy shift of neat single layer 33 nm Ir(piq)$_3$ film is included. Emission is predominantly from bulk species. Similar Ir(piq)$_3$ peak energy relaxation is observed for multilayer films with 0 nm, 2.5 nm, and 10 nm NPB thicknesses but is omitted here for clarity.
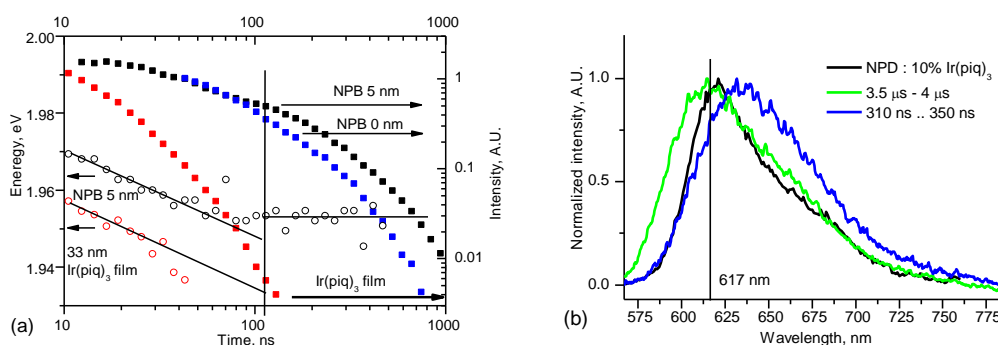
Figure 9.9 (a) Ir(piq)$_3$ peak energy variation in time and decays of Ir(piq)$_3$ layer from sapphire/Ir(ppy)$_3$ 5 nm/NPB x nm/ Ir(piq)$_3$ 5 nm/TAPC 100 nm/Al 200 nm films (where x is 0 nm and 5 nm) and single layer 33nm neat Ir(piq)$_3$ film. Horizontal arrows denotes different NPB thickness or film curves and their appropriate scales and black lines is just a guide to an eye. (b) Comparison of Ir(piq)$_3$ time resolved spectra in multilayers films sapphire/ Ir(ppy)$_3$ 5 nm/NPB 5 nm/Ir(piq)$_3$ 5 nm/TAPC 100 nm/Al (blue) and sapphire/Ir(piq)$_3$ 10 nm/NPB 20 nm/ Ir(ppy)$_3$ 25 nm (green) with steady state spectrum of 10% Ir(piq)$_3$ doped in NPB. Please note the sequence of evaporation. Gating time is indicated for blue and green curves.

Around 100 ns energy peak stabilizes at ~ 1.95 eV and this coincides well with the start of the differences between 5 nm and 0 nm NPB layer thickness in multilayer films. Clearly up until 100 ns decay comes from direct excitation (plus maybe small amount of triplets already arriving from Ir(ppy)$_3$ via NPB) while after 100 ns mainly species arriving from Ir(ppy)$_3$ is recorded. Compare with the 33 nm Ir(piq)$_3$ curve decay as well – directly excited triplets should have all decayed after ~100 ns. Figure 9.9a reasserts that the interface between NPB and Ir(piq)$_3$ in these

structures is of different type in comparison with the bilayer film structures described in section 9.1. Here triplets from Ir(ppy)$_3$ reservoir via NPB are transferred straight to the bulk of Ir(piq)$_3$ and no interface sites emitting at 2 eV are observed at any times.

All the above is supported by the shapes of time resolved spectra (figure 9.9b). The long wavelength tail in time resolved spectra of Ir(piq)$_3$ from sapphire/Ir(ppy)$_3$ 5 nm/NPB 5 nm/Ir(piq)$_3$ 5 nm/TAPC 100 nm/Al films recorded at ~330 ns after excitation (i.e. emission comes from Ir(ppy)$_3$ reservoir via NPB) is broader and does not follow the tail of Ir(ppy)$_3$ doped in NPB film spectrum i.e. it comes from the bulk sites and excitons are not trapped at the NPB/Ir(piq)$_3$ interface unlike in sapphire/Ir(piq)$_3$/NPB films in section 9.1. Why interface between the same material layers behaves in such a different way? The answer to this is hidden in the sequence of the layer deposition. In bilayer sapphire/Ir(piq)$_3$/NPB films NPB was evaporated on top of the Ir(piq)$_3$, whereas in sapphire/Ir(ppy)$_3$/NPB/Ir(piq)$_3$/TAPC/Al films Ir(piq)$_3$ was evaporated on top of the NPB. Ir(piq)$_3$ molecules are heavier and larger than NPB thus when evaporated on top of NPB they cannot percolate through. Whereas if NPB is evaporated on top of Ir(piq)$_3$, smaller and more mobile NPB molecules percolate through the sieved-like layer of Ir(piq)$_3$ in such a way creating interfacial semi-doped layer. This does not depend much on the thickness of layers or on the fact that another Ir(ppy)$_3$ layer is evaporated on NPB/Ir(piq)$_3$ and can be demonstrated by comparing Ir(piq)$_3$ time resolved spectrum at ~4 µs from sapphire/Ir(piq)$_3$ 10 nm/NPB 20 nm/Ir(ppy)$_3$ 25 nm multilayer films where NPB was evaporated on top of Ir(piq)$_3$ and Ir(ppy)$_3$ on top of NPB (figure 9.9b). This spectrum resembles the Ir(piq)$_3$ spectra of bilayer sapphire/Ir(piq)$_3$/NPB films (at late times) and steady state 10% Ir(piq)$_3$ doped into NBP, but not the multilayer film spectra analysed in this section (compare figures 9.9b and figure 9.2a).

To conclude, by using sublimed sapphire/Ir(ppy)$_3$ 5 nm/NPB x nm/Ir(piq)$_3$ 5 nm/TAPC 100 nm/Al 200 nm multilayer layer films with different NPB thicknesses it was showed that one could easily create structures were triplets are transferred from donors to acceptors. This structure is excited with 450 nm pulsed laser light from Ir(ppy)$_3$ side and a change is observed in the decay of Ir(piq)$_3$ with the decrease of NPB spacer layer thickness. In the first ~100-200 ns the decay of Ir(piq)$_3$ is of multiexponential character whereas after it follows monoexponential law. For 0 nm NPB layer thickness the lifetime of this monoexponential decay is 144 ns, 2.5 nm – 193 ns, 5 nm – 232 ns, 10 nm - 265 ns, 20 nm - 407 ns. Ir(piq)$_3$ decays and time resolved spectra peak analysis show that monoexponential emission decay arises due to emission from the triplet reservoir in Ir(ppy)$_3$ which arrive to Ir(piq)$_3$ via the NPB. In this case not unlike in bilayer sapphire/Ir(piq)$_3$/NPB systems triplets are not trapped in the interface and can be transferred straight to the bulk states of Ir(piq)$_3$. Finally here it is proven that by changing the sequence of evaporation of layers one can avoid creation triplet interface sites. This can

determine whether triplets are transferred from higher triplet energy layer to lower one or whether they are trapped in the interface.

9.3 Triplet exciton interface trap states in bilayer films of NPB and Ir(piq)$_3$ – simulations confirming experiments.

It is possible to get a more quantitative description of triplet transport in bilayer or multilayer systems by not only extracting such parameters as the diffusion constant as has been done, for example, by Giebink *et al* [20]or Reineke *et al*[8], but also demonstrating the energy-trapping behavior in the Ir(piq)$_3$ at the interface. Bilayer sapphire/NPB/Ir(piq)$_3$ systems has been chosen to do modeling as experimentally it was shown to have interface trapping. The simulation software has been programmed in Pascal by Professor Chris Winscom from Brunel University. The author of this thesis contributed by participating in discussions about the choice of equations and in decision making process about the parameters to be used, as well suggested which parameters can be ignored and what values or ranges should be chosen for various constants i.e. in modeling process.

A model based on classical rate diffusion equations has been used to understand the physics behind triplet exciton transport and interface trapping in the sapphire/ Ir(piq)$_3$/NPB bilayer system. Taking into account the overview presented in chapter 8 and its conclusions it has been chosen to include diffusion term, bimolecular annihilation term and monomolecular decay term. Here very high excitation powers have been directed on samples thus bimolecular term could not be neglected. Further the diffusion term had to be included as transfer from one layer to another is demonstrated by experimental results which indicate directional triplet movement.

At this point it needs to be mentioned that triplet migration in NPB (and in Ir(piq)$_3$) films at room temperature was found to have dispersive character (chapters 6 and 7). However, here classical rate equations appropriate to non-dispersive character will be used. Firstly, the dispersive regime in NPB at room temperature lasts for a few hundred of nanoseconds (as can be found in chapter 6) which is not accessible experimentally in this case, as only directly excited emission from Ir(piq)$_3$ film up until ~300 ns is observed. Consequently it is hard to detect dispersive migration in the experiment described in section 9.1. As well, the lifetime of NPB film triplets at room temperature could be expected to be at least in the range of a few microseconds (for example could be approximately derived from delayed fluorescence decays found in chapter 6) and dispersive migration should last only for a fraction of this lifetime. Further, it is probable that dispersively migrating triplets do not travel far into the NPB layer as they annihilate much more strongly than in non-dispersive region because TTA coefficient

should be higher until it reaches its equilibrium non-dispersive value[21]. In other words due to the high initial exciton concentration in the dispersive region migration is triplet-triplet annihilation dominated rather than directional diffusion dominated. Thus dispersive triplet migration exists only for a small fraction of total triplet travel time and distance to Ir(piq)$_3$, so it can be approximated as classical non-dispersive in the whole range. Finally, despite of all the above justifications of ignoring dispersive migration regime, one has to take care when interpreting the diffusion and TTA coefficients found using classical diffusion equation and have in mind that in initial time regions it might be larger. Hence the one extracted here should be viewed as averaged over the whole time range and evaluation of the distance triplet has traveled during set time especially just after excitation should be avoided. Nevertheless these extracted averaged diffusion constants could be useful in comparing general (averaged) triplet transport properties of two different materials.

Each layer is considered to be a "box" with an area of 1 cm^2 and specified thicknesses, L_{NPB} and L_{PIQ}, respectively. Here subscript or superscript PIQ means Ir(piq)$_3$. In line with experiment 4 NPB thicknesses with 1 Ir(piq)$_3$ thickness were analysed. The boxes were divided into small elements, dx, of about one monolayer thick, the length of which was considered to be 1 nm. At the interface of the two layers, the last monolayer of NPB, and the adjacent first monolayer of Ir(piq)$_3$ are treated separately. Consequentially due to the new terms the penultimate layer of NPB and the second layer of Ir(piq)$_3$ had to be treated separately as well. In order to include interface traps which in experimental 9.1 and 9.2 sections was shown to be due the diffusion of NPB molecules into Ir(piq)$_3$ layer during the sublimation, the model includes exchange of NPB and Ir(piq)$_3$ sites taking place between the bordering NPB and Ir(piq)$_3$ monolayers. Initial S_1 - S_0 absorption during laser excitation (using extinction coefficient from figure 9.4 above), with subsequent ISC, was used to establish the initial T_1 exciton densities in each element of the NPB, Ir(piq)$_3$, and their interfacial region. As was shown in chapter 8 determination of initial triplet concentration in literature is described very vaguely and unclearly. In order to avoid this type of ignorance here it is explained in details how we calculated the initial *triplet* exciton concentration.

The 355 nm laser pulse is directed onto sample having the photon density of 6.4E14 photons/cm^2 in a plane normal to the beam. The length of the beam is 200 ps, which is negligibly small compared with the hundreds of nanosecond time scales studied here. As the beam was incident at 45° to the upper surface of NPB layer the amount of light reflected from NPB surface, and not entering the sample was accounted for using Fresnel equations. Similarly, the amount of light reflected from the substrate surface back through the layers was accounted for. NPB and Ir(piq)$_3$ refractive indexes are too similar to consider the reflection from this interface to be substantial. The ISC quantum yield for Ir(piq)$_3$ can be estimated to be

approximately 1 as it is heavy metal complex. Photoluminescence quantum efficiency of NPB films is 29% hence largest possible amount of created triplet state is 71 %[22]. However clearly it is hardly possible that all of this 71 % excitons, which are not emitted as fluorescence, participate in intersystem crossing to triplet state as competing processes such as non radiative decay should take place in NPB (because singlet lifetime is quite long in NPB ~3 ns see chapter 6). In addition, it is reasonable that some singlets participate in an energy transfer and are trapped in quenching sites, for example excimer state found to be formed in NPB[14]. Hence a range 0.25 - 0.45 for triplet intersystem crossing was considered to be reasonable. It is important to draw reader's attention that in most of Leo *et al*[8] and Forrest *et al*[6] publications it was considered that initial *triplet* concentration is known (thus in this way getting rid of one fitting parameter) . However in these publications it is not disclosed how ISC was determined leaving the author of this thesis very puzzled. It is not an easy task to determine ISC and complicated techniques using a femtosecond laser system has to be used for this[23].

Unfortunately this is not the only problem in determining initial triplet excitation. Since the excitation laser wavelength bandwidth (0.1 cm^{-1}) was narrower than the inhomogeneous (I) and homogeneous (H) widths of the absorption bands, the ratio (H/I) of the homogeneous to inhomogeneous absorption was a parameter affecting the total number of photons absorbed in the sample. Again, although in most previous publications[6, 8] narrow bandwidth lasers have been used to excite amorphous materials having broad inhomogeneous absorption profile this has been ignored. Here this is accounted for and the initial triplet exciton densities throughout the two layers were established using H/I characteristics, together with the S_1- S_0 absorption coefficients for NPB and Ir(piq)$_3$, and their estimated ISC quantum yields. For example the accuracy of the bimolecular quenching rate constants obtained by fitting will be directly dependent on the precision, with which the initial triplet densities are estimated, and these are crucially dependent on the estimated H/I ratio (and ISC quantum yields too).

The H/I ratio in amorphous organic materials at room temperature is undocumented and it is very hard to determine. There are few papers by S. Volker and R. Sylbey detailing work on homogeneous/ inhomogeneous broadening calculations by using photochemical hole burning spectroscopy. Part of their findings was already introduced in chapter 8 and here it is discussed more extensively. Volker *et al*[24] studied hole burning in organic glasses in the temperature range between 1 and 20 K. It was found that homogeneous linewidths of organic glasses depend on $T^{1.3}$ in this range [24-25]. At higher temperature some authors found that the dependence is T^2 [25-26]. Haarer *et al*[27] investigated glassy H$_2$Pc doped into PMMA (free base phorphin in polymethylmethacrylate) and got homogeneous widths of 0.34 cm^{-1} (4.2 K), 0.5 cm^{-1} (10 K) 0.85 cm^{-1} (15 K) and 6.5 cm^{-1} (50 K). At room temperature with $T^{1.3}$ this extrapolates to 67 cm^{-1}, and with T^2 to 234 cm^{-1}. One could assume this is the sort of range to be expected for

amorphous organics investigated here. Inhomogeneous width of Ir(piq)$_3$ is ~ 2380 cm^{-1} (full width at half maximum), so using the above ranges and Ir(piq)$_3$ inhomogeneous emission width the H/I ratio range is 0.028 -0.098. A similar range can be deduced for NPB. Recently, Yoshikawa *et al*[28] investigated homogeneous linewidths at 300 K in differently sized single wall nanotubes. They measured homogeneous linewidths from 9 to 14 meV (i.e. 70 - 112 cm^{-1}) for single wall nanotube diameters in the range 0.8 to 1.2 nm. These values are at room temperature and is in the same range with estimations from the numbers of Haarer *et al*[27]. Hence during the simulation approximately the above ranges were the starting point used in H/I linewidth determination. Here it needs to be said that in the single layer 33 nm Ir(piq)$_3$ film PL decay experiment, equally good fits to the data could be obtained with H/I =0.015, 0.030, 0.060 yielding k_{TT}^{PIQ} values of 4.7·10^{-11}, 3.3·10^{-11}, 2.3·10^{-11} cm^{3}s^{-1} , respectively (see below for simulation and modeling details). In the 2-layer structures, in which 4 different thicknesses of NPB are explored, different initial triplet densities are produced in both layers. This has the advantage that by requiring that TTA bimolecular annihilation constants k_{TT}^{NPB} and k_{TT}^{PIQ} (more details on determination of these constants below) be the same for all NPB thicknesses, a very precise fix of the unknown H/I and ISC parameters based on the root mean square error (RMSE) of the simulated vs. experimental data can be achieved. In this way H/I ratios of 0.014 for NPB and 0.030 for Ir(piq)$_3$ and an ISC quantum yield of 0.36 for NPB were found to deliver the smallest RMSE's.

The densities of triplet states determined in a manner above in the different dx elements were then allowed to change with time according to the equations described below. Classical diffusion equations with monomolecular and bimolecular triplet decay terms within the NPB and Ir(piq)$_3$ layers, can be expressed in the following way:

$$0 < x \le L_{NPB} - dx, [T_{PIQ}] = 0 \text{ and}$$

$$\frac{d[T_{NPB}(x,t)]}{dt} = D_{NPB} \cdot \frac{d^2[T_{NPB}(x,t)]}{dx^2} - k_1^{NPB} \cdot [T_{NPB}(x,t)] - k_{TT}^{NPB} \cdot ([T_{NPB}(x,t)])^2 \quad (9.1a)$$

$$L_{NPB} + dx \le x \le L_{NPB} + L_{PIQ}, [T_{NPB}] = 0 \text{ and}$$

$$\frac{d[T_{PIQ}(x,t)]}{dt} = D_{PIQ} \cdot \frac{d^2][T_{PIQ}(x,t)]}{dx^2} - k_1^{PIQ} \cdot [T_{PIQ}(x,t)] - k_{TT}^{PIQ} \cdot ([T_{PIQ}(x,t)])^2 \quad (9.1b)$$

Equations 9.1 are valid in all dx elements except in L_{NPB} and L_{NPB}+dx. [$T_{NPB}(x,t)$], [$T_{PIQ}(x,t)$] are the densities of triplet exciton states (cm^{-3}) in an element dx at depth x from the upper NPB surface at time t, respectively for NPB and Ir(piq)$_3$. D_{NPB}, D_{PIQ} (cm^{2}s^{-1}) are the NPB and Ir(piq)$_3$ exciton diffusion constants, k_1^{NPB}, k_1^{PIQ} (s^{-1}) are the total monomolecular triplet decay and

quenching rate constants, for NPB and Ir(piq)$_3$, respectively, and k_{TT}^{NPB}, k_{TT}^{PIQ} (cm^{3}s^{-1}) are the total bimolecular triplet decay rate constants for NPB and Ir(piq)$_3$ respectively.

Interfacial transfer from the last element of the NPB layer (x = L$_{NPB}$) to the first element of the Ir(piq)$_3$ layer (x = L$_{NPB}$+dx) takes account of the processes involved in the relatively large exothermic – and irreversible – change (very large triplet energy difference ~0.39 eV, chapters 6 and 7). Also it is assumed that there is a small fractional penetration, f , of Ir(piq)$_3$ molecules (sites) into the last monolayer of NPB, and an equal complementary penetration of NPB molecules (sites) into the first monolayer of Ir(piq)$_3$. The new terms replace the normal diffusion and decay terms between the L$_{NPB}$-dx, L$_{NPB}$, L$_{NPB}$+dx and L$_{NPB}$+2dx elements across the interface. Different kinetic paths are summarized in the figure 9.10.
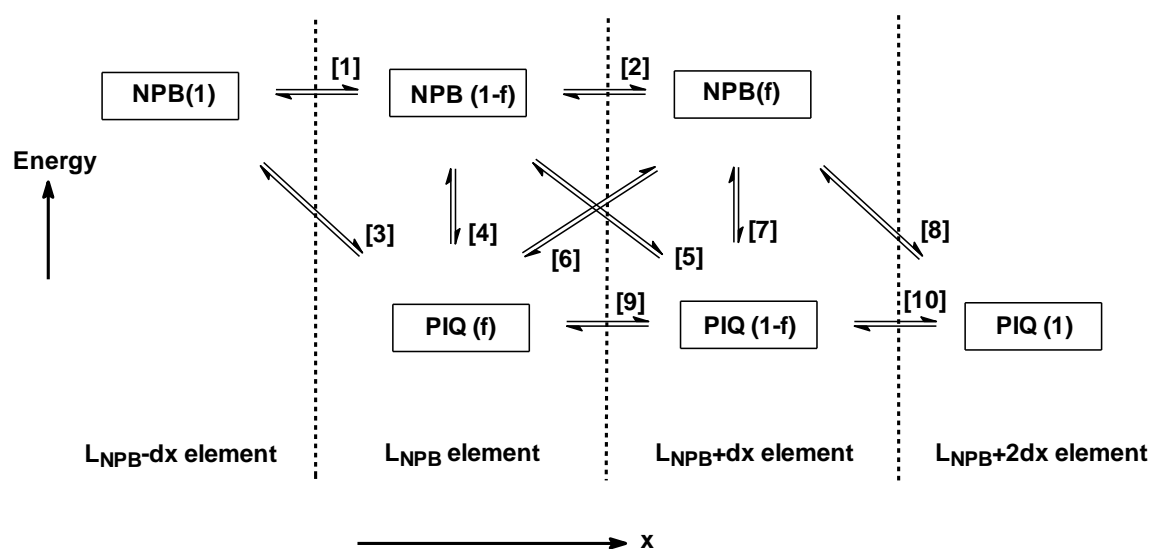
Figure 9.10 Mixing of NPB and Ir(piq)$_3$ molecules in the last monolayer of NPB (L$_{NPB}$ element) and the first monolayer of the Ir(piq)$_3$ (L$_{NPB}$+ dx element) is depicted. Consequentially the elements L$_{NPB}$-dx and L$_{NPB}$+2dx are affected. Transport across the interface occurs via processes 1 to 10. 1, 2 represent attenuated diffusion between the NPB sites and 9, 10 similarly for the Ir(piq)$_3$ sites. Processes 3 to 8 represent the exothermic equilibria between NPB and Ir(piq)$_3$. The fraction, f, represents the mixing between the neighboring monolayers of Ir(piq)$_3$ and NPB across the interface (figure is courtesy of Professor Chris Winscom).

Each process happening at neighboring NPB and Ir(piq)$_3$ monolayers as well as the successive monolayers from each side is numbered from 1 to 10. The forward-going rates (from NPB to Ir(piq)$_3$ or following the x direction in figure if transfer is between same type of molecules) are marked as A$_1$, A$_2$,...A$_{10}$, and the reverse-going rates (from Ir(piq)$_3$ to NPB or opposite to x direction in figure if transfer is between same type of molecules) are marked B$_1$, B$_2$, ...B$_{10}$. Processes 1 and 2 account for the attenuated diffusion between NPB sites and processes 9 and 10 attenuated diffusion between the Ir(piq)$_3$ sites. Processes 3 through 8 account for the

adsorption-desorption process between the NPB and Ir(piq)$_3$ sites in the same monolayers or in between neighboring monolayers. For the L$_{NPB}$-dx element of the neat NPB layer, and the L$_{NPB}$+2dx element of the Ir(piq)$_3$ layer, several terms in addition to the ones in equations 9.1a and 9.1b is included:

$$\frac{d[T_{NPB}(L_{NPB}-dx,t)]}{dt} \text{ additional terms to 9.1a are } +B_1+B_3-A_1-A_3$$
$$\frac{d[T_{PIQ}(L_{NPB}+2dx,t)]}{dt} \text{ additional terms to 9.1b are } +A_8+A_{10}-B_8-B_{10}$$

(9.2)

Only small exchange of NPB for Ir(piq)$_3$ sites (0<f<0.01) is expected, so the monomolecular decay term in dilute Ir(piq)$_3$ guest/NPB host compositions in element L$_{NPB}$ can be anticipated to exist with the rate k_T^{PIQ}. k_T^{PIQ} can be viewed as the isolated Ir(piq)$_3$ decay rate for example in dilute toluene solution (740 ns)[15]. In the L$_{NPB}$+dx element Ir(piq)$_3$ bulk monomolecular decay is taken (k_1^{PIQ}). For the NPB sites in both of these elements, it is assumed that the monomolecular decay is dominated by the transfer process contained in the relevant A- and B-terms (i.e. they are considered to be the main quenching mechanisms of natural triplet decay). The lifetime of dilute NPB in zeonex at 14 K was more than 1 s hence at room temperature it should be very long due to the lack of spin orbit-coupling as in Ir(piq)$_3$. Despite this, for completeness, the negligible isolated NPB molecule triplet decay rate, k_T^{NPB} is included in the L$_{NPB}$ and L$_{NPB}$+dx element. Diffusion terms are ignored and all the terms in L$_{NPB}$ and L$_{NPB}$+dx elements are:

$$\frac{d[T_{NPB}(L_{NPB},t)]}{dt} = -k_T^{NPB} \cdot [T_{NPB}(L_{NPB,t})] - k_{TT}^{NPB} \cdot [(T_{NPB}(L_{NPB},t))]^2 +$$
$$+A_1+B_2+B_4+B_5-B_1-A_2-A_4-A_5$$

(9.3a)

$$\frac{d[T_{NPB}(L_{NPB}+dx,t)]}{dt} = -k_T^{NPB} \cdot [T_{NPB}(L_{NPB}+dx,t)] - k_{TT}^{NPB} \cdot ([T_{NPB}(L_{NPB}+dx,t)])^2 +$$
$$+A_2+B_6+B_7+B_8-B_1-A_6-A_7-A_8$$

(9.3b)

$$\frac{d[T_{PIQ}(L_{NPB},t)]}{dt} = -k_T^{PIQ} \cdot [T_{PIQ}(L_{NPB},t)] - k_{TT}^{PIQ} \cdot ([T_{PIQ}(L_{PIQ},t)])^2 +$$
$$+A_3+A_4+A_6+B_9-B_3-B_4-B_6-A_9$$

(9.3c)

$$\frac{d[T_{PIQ}(L_{NPB}+dx,t)]}{dt} = -k_T^{PIQ} \cdot [T_{PIQ}(L_{NPB}+dx,t)] - k_{TT}^{PIQ} \cdot ([T_{PIQ}(L_{NPB}+dx,t)])^2 +$$
$$+A_5+A_7+A_9+B_{10}-B_5-B_7-B_9-A_{10}$$

(9.3d)

The rates are equal to:

$A_1 = (1\text{-}f)\, k_D^{NPB}\, \{[T_{NPB}(L_{NPB}\text{-}dx,\, t)] - [T_{NPB}(L_{NPB},\, t)]\};$ $\quad B_1 = -A_1$

$A_2 = f\,(1\text{-}f)\, k_D^{NPB}\, \{[T_{NPB}(L_{NPB},\, t)] - [T_{NPB}(L_{NPB}+dx,\, t)]\};$ $\quad B_2 = -A_2$ $\qquad$ (9.4)

$A_9 = f\,(1\text{-}f)\, k_D^{PIQ}\, \{[T_{PIQ}(L_{NPB},\, t)] - [T_{NPB}(L_{NPB}+dx,\, t)]\};$ $\quad B_9 = -A_9$

$A_{10} = (1\text{-}f)\, k_D^{PIQ}\, \{[T_{PIQ}(L_{NPB}+dx,\, t)] - [T_{PIQ}(L_{NPB}+2dx,\, t)]\};$ $\quad B_{10} = -A_{10}$

where $k_D^{NPB} = D_{NPB}/dx^2$, $k_D^{PIQ} = D_{PIQ}/dx^2$ (s^{-1}).

k_D^{NPB} arises from the following approximation

$$\frac{d^2[T(x,t)]}{dx^2} \approx \frac{\dfrac{\{[T(x+dx,t)] - [T(x,t)]\}}{dx} - \dfrac{\{[T(x,t)] - [T(x-dx,t)]\}}{dx}}{dx} \qquad (9.5)$$

for a monolayer dx. If multiplied by the diffusion constant D the second order derivative can be approximated as

$$D\frac{d^2[T(x,t)]}{dx^2} \approx k_D\{[T(x+dx,t)] - [T(x,t)]\} - k_D\{[T(x,t)] - [T(x-dx,t)]\} \qquad (9.6)$$

where $k_D = D/dx^2$ for an element dx. Hence the discrete A_1, A_2 and A_9, A_{10} terms are expressed as in 9.4. Transfer involving both NPB and Ir(piq)$_3$ molecules can be written:

$A_3 = (1/6)\, U_3\, k_A\, [T_{NPB}(L_{NPB}\text{-}dx,t)];$ $B_3 = (1/6)\, V_3\, k_A\, \exp(-\Delta E/k_B T)\, [T_{PIQ}(L_{NPB},\, t)]$

$A_4 = (2/3)\, U_4\, k_A\, [T_{NPB}(L_{NPB},t)];$ $B_4 = (2/3)\, V_4\, k_A\, \exp(-\Delta E/k_B T)\, [T_{PIQ}(L_{NPB},\, t)]$

$A_5 = (1/6)\, U_5\, k_A\, [T_{NPB}(L_{NPB},t)];$ $B_5 = (1/6)\, V_5\, k_A\, \exp(-\Delta E/k_B T)\, [T_{PIQ}(L_{NPB}+dx,\, t)]$

$A_6 = (1/6)\, U_6\, k_A\, [T_{NPB}(L_{NPB}+dx,t)];$ $B_6 = (1/6)\, V_6\, k_A\, \exp(-\Delta E/k_B T)\, [T_{PIQ}(L_{NPB},\, t)]$

$A_7 = (2/3)\, U_7\, k_A\, [T_{NPB}(L_{NPB}+dx,t)];$ $B_7 = (2/3)\, V_7\, k_A\, \exp(-\Delta E/k_B T)\, [T_{PIQ}(L_{NPB}+dx,\, t)]$

$A_8 = (1/6)\, U_8\, k_A\, [T_{NPB}(L_{NPB}+dx,t)];$ $B_8 = (1/6)\, V_8\, k_A\, \exp(-\Delta E/k_B T)\, [T_{PIQ}(L_{NPB}+2dx,\, t)]$

$$(9.7)$$

where k_A (s^{-1}) is the rate at which the NPB triplets are "adsorbed" by the Ir(piq)$_3$ sites exothermically. The reverse process is attenuated by a Boltzmann factor where ΔE is the energy difference between the NPB and Ir(piq)$_3$ triplet states. It was chosen to be 0.39 eV. No

173

substantial difference has been observed in root mean square error between simulations and experimental results if this difference was chosen to be 0.29 eV. k_B is Boltzman constant and T is temperature. The numerical factors 1/6 and 4/6 account for the different directions from which transfer can take place. U and V factors account for the availability of sites to which transfer can take place, where N_{PIQ} is the total number of Ir(piq)$_3$ sites available in a dx element which is exclusively Ir(piq)$_3$, and similarly N_{NPB} for NPB sites. :

$$U_3 = U_4 = U_6 = 1 - \frac{[T_{PIQ}(L_{NPB}, t)]}{fN_{PIQ}}$$

$$U_5 = U_7 = 1 - \frac{[T_{PIQ}(L_{NPB} + dx, t)]}{(1-f)N_{PIQ}} \qquad (9.8)$$

$$U_8 = 1 - \frac{[T_{PIQ}(L_{NPB} + 2dx, t)]}{N_{PIQ}}$$

and

$$V_3 = 1 - \frac{[T_{NPB}(L_{NPB} - dx, t)]}{N_{NPB}}$$

$$V_3 = V_5 = 1 - \frac{[T_{NPB}(L_{NPB}, t)]}{(1-f)N_{NPB}} \qquad (9.9)$$

$$V_6 = V_7 = V_8 = 1 - \frac{[T_{NPB}(L_{NPB} + dx, t)]}{fN_{NPB}}$$

Reasonable starting positions were adopted for unknown rate constants (chapter 8) and then refined to get the best fit to experimental results (figure 9.11 and 9.12). All four decay curves were fitted with single set of parameters. The quality of fit was evaluated using root mean square error (RMSE) of simulation versus experimental points in log-log plot. Simulated versus experimental data RMSE's were in the range 0.029 – 0.048 for bilayer films. For Ir(piq)$_3$ single layer sample (0nm NPB) the fit was worse RMSE=0.075. This could happen due to dispersive triplet migration at very short times which could be expected in this system (chapter 7 and 8). Further it is presented in chapter 7 that heavy metal complexes have spin-selective sublevels (0 field splitting) and it can be found in the literature that that populating and depopulating processes of these sublevels in organic materials can be spin-selective[29-31]. However in amorphous materials random hopping will essentially remove any spin – sublevel selectivity and sublevel population will be equalized. This will be strengthened by the conventional spin-lattice relaxation processes at room temperature already overviewed in chapter 7. Under conditions at which the bilayer films were studied these processes are happening fast enough to

consider population and depopulation rates to be averaged especially at times longer than 200 ns. However this might not be the case for single layer Ir(piq)$_3$ film decay data as it was recorded at very early times. Hence if departure from spin-averaged character would be taken into account at very short time scales better fitting probably could be achieved.

The experiment shown in figure 9.11 has been performed throughout 4 orders of magnitude in time. Simulation covering this range was performed by a finite element approach, where each order of magnitude was subdivided into 100 logarithmically proportional elements. Each of these elements was further linearly subdivided into a number of elements, such that no time element was greater than one half or less than 1/20, of the lifetime of the fastest individual process in the longest and shortest time elements, respectively. Each curve in the log-log representation of figure 9.11 consists of two cascade-like features. The faster part of curve remains constant with the change of NPB thickness and follows the path of the decay of a single 33 nm layer of Ir(piq)$_3$ in the absence of NPB. It is clearly the result of the decay of directly excited Ir(piq)$_3$ and its quenching as was already shown experimentally in section 9.1. The slower component of those curves representing the different thicknesses of an additional NPB layer, results from the diffusion-controlled percolation of excitons stored in the NPB layer up to, and through, the NPB/Ir(piq)$_3$ interface.

Monomolecular and bimolecular Ir(piq)$_3$ constants have been obtained independently by fitting 33 nm Ir(piq)$_3$ neat single layer experimental decays. Activation energy needed for triplet transfer from Ir(piq)$_3$ to NPB was taken to be the triplet energy difference between these materials (0.39 eV). As already mentioned if this difference was taken slightly smaller (0.29 eV see section 9.2) no substantial differences in simulation results have been observed.

The most critical parameters were the NPB and Ir(piq)$_3$ diffusion constants, the monomolecular and bimolecular NPB triplet decay in the bulk and the fractional NPB/Ir(piq)$_3$ site-exchange at the interface, and the transfer rate, k_a. Using a single set of the parameters, good agreement with the bilayer experiments is obtained for all of the different NPB thicknesses. Inclusion of both monomolecular and bimolecular terms in the neat NPB and Ir(piq)$_3$ layers were essential to achieve acceptable simulation profile and good agreement with experimental points. Trapping at surface sites between Ir(piq)$_3$ and sapphire has been considered and modeled as well, however, no substantial difference was observed. Consequentially this has been considered to be negligible.
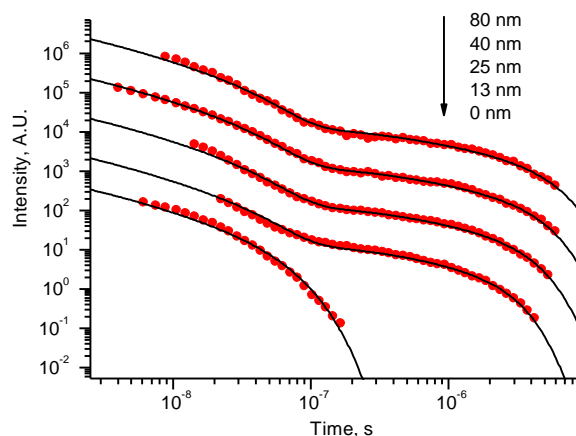
Figure 9.11 The overall simulation of the curves arising from different (black curves) sapphire/NPB x/Ir(piq)$_3$ simulations. Parameter is NPB thickness. Experimental points, as red closed circles, are included for comparison. The values used here were: $k_1^{NPB} = 4.0 \times 10^5$ s^{-1}, $k_{TT}^{NPB} = 6.2 \times 10^{-13}$ cm^3 s^{-1}, $D_{NPB} = 2.4 \times 10^{-5}$ cm^2 s^{-1}, $k_1^{PIQ} = 3.75 \times 10^7$ s^{-1}, $k_{TT}^{PIQ} = 3.3 \times 10^{-11}$ cm^3 s^{-1} and $D_{PIQ} = 1.7 \times 10^{-5}$ cm^2 s^{-1}. The NPB/Ir(piq)$_3$ interface characteristics were: f=0.002, $k_a = 9.10^{-1}$ cm s^{-1}, $E_a = 0.39$eV.
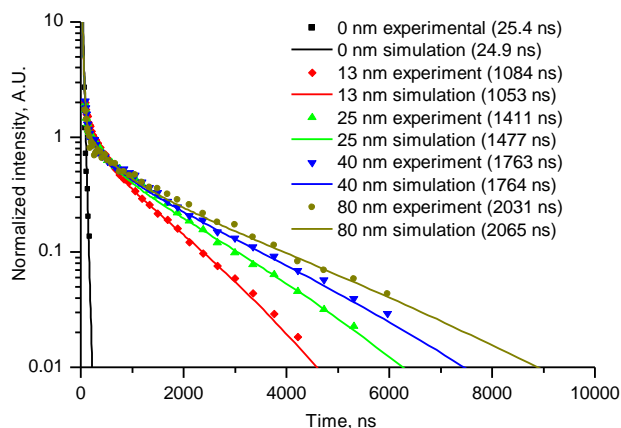
Figure 9.12 The simulation (straight lines) of the intensity vs. time behavior in a log-lin scale of the slower part of the decay for the different thicknesses of the NPB layer. The single parameter set described in figure 9.11 has been used, and the experimental data points are overlaid for comparison. The lifetimes of the experimental and the calculated curves are presented in the legend for comparison. The corresponding pairs of lifetimes for each thickness are derived from a least squares fit between 7.10^{-7} s and the last experimental time point. In the 0 nm case, the times used were between 7.10^{-8} s and the last experimental time point.

The effective decay lifetimes of the slower feature are each reproduced to within 5% of their experimental values (figure 9.12). In summary, directly excited Ir(piq)$_3$ decays through normal triplet decay and bulk quenching processes to a point where the rate of arrival of excitons from the NPB reservoir starts to balance this rate of disappearance from the Ir(piq)$_3$. The resultant decay then has a pseudo first order behavior, and is quantitatively predicted by the diffusion

176

model described. Finally analysis of the triplet densities at times $>10^{-7}$s show that more than 50% of the excitons reaching the interface reside in the interface trap sites again showing agreement with experimental results.

At the first sight many more parameters are used in this modeling than in previously published results on triplet transport and review in chapter 8 (3 parameters by Leo *et al and* Forrest *et al*)[6, 8]. However more diligent analysis shows this is not the case. For the Ir(piq)$_3$, the monomolecular triplet decay lifetime (k_T^{PIQ}) at room temperature for isolated molecules in dilute toluene deaerated solution is 740 ns[15]. This value was used as k_T^{PIQ}. There are thus six important parameters arising from the main equations 9a and 9b. k_1^{PIQ} and k_{TT}^{PIQ} can be obtained directly and independently from the Ir(piq)$_3$ monolayer decay experiments. ΔE is known from the triplet energies of NPB and Ir(piq)$_3$. The two remaining, f and k_A, are taken as parameters of the model. Hence if using the monolayer and dilute Ir(piq)$_3$ data, the model reduces to just six key parameters: k_1^{NPB}, k_{TT}^{NPB}, D_{NPB}, D_{PIQ}, f and k_A for the bilayer modeling. Furthermore both Leo *et al*[8] and Forrest *et al*[6] analysed doped systems and ignored triplet-triplet annihilation in the host and assumed that only guest (!) triplets participate in annihilation. Indeed then, fewer parameters are needed to be accounted for however this simplification cannot be justified. First of all there are many more host molecules than guest and TTA in host should take place even before triplets are localized on the guest as guest concentrations investigated by the authors were very small from 1% to 15 %. Also, guest saturation effects depending on host-guest transfer rates and concentration and time scales analysed might take place. These effects were not discussed in mentioned publications. Both of those groups ignore triplet diffusion term in their studies. In summary equations are simplified to such an extent that physical model validity is questionable. Finally one has to pay attention to the fact that Leo *et al*[8] and Forrest *et al*[6] analysed much simpler systems – doped films instead of more complicated bilayer films with and interface sites investigated here. Giebink *et al*[20] used 4 parameters in their experiments (chapter 8). They accounted for the diffusion term, however their structures were simpler - without interface traps that requires the two additional parameters f and k_a to be added. Furthermore, CBP triplet lifetime at room temperature was determined by measuring triplet decay from 5 K to 140 K and then extrapolated to obtain 14 ms. Unfortunately it is not explained what decay vs temperature relationship they used for extrapolation and why. As it was shown in chapter 6 with NPB it is extremely difficult to determine any triplet lifetime dependence on temperature due to dispersive manner of triplet migration at low temperatures. In addition, the exponential triplet lifetime in the dispersive regime does not have any meaning as at certain temperatures it can follow a power law decay (chapter 6). Again it is not shown or explained in their publication how the lifetime for example at 100 K was determined. Clearly, the obtained CBP triplet lifetime at room temperature might be at least an order of magnitude larger or smaller than the true CBP triplet lifetime consequentially the constants obtained by

Giebink *et al*[20] as well might be by a few orders of magnitude off. If they considered this to be a parameter, 5 of them would have been used in their simulations.

Finally at this point is the time to compare diffusion constants extracted during the work of this thesis with the ones found in literature.

Table 9.1 Comparison of singlet exciton diffusion coefficients found in literature. PTCDA = perylene-3,4,9,10-tetracarboxylic-3,4,9,10-dianhydride), DIP = di-indenoperylene,SubPC = boron subphthalyocyanine, PtOEP = Pt(II) Octaethylporphine.

Material (singlets)	Diffusion coefficient cm^2/s	Material (singlets)	Diffusion coefficient cm^2/s
Naphthalene in aa plane	2E-4 [32]	PTCDA	3.4E-4 [33]
Naphthalene in c'c' plane	0.5 E-4 [32]	DIP (upright)	15E-4 [33]
Anthracene in aa plane	30 E-4 [32]	DIP (flat)	26E-4 [33]
Tetracene in aa plane	400E-4 [32]	TPD	15.3E-4 [34]
NPB	0.7E-4 [33]	Alq$_3$	0.4E-4 [34], 0.12E-4 [7], 2.6E-4 [7]
CBP	40E-4 [33]	SubPc	>6.4E-4 [33]

In this thesis singlet diffusion constants were not dealt with, nevertheless it is useful to compare various values found in the literature (table 9.1). Singlet diffusion constants of CBP and TPD are very similar to diffusion constants of anthracene crystal. Alq$_3$ and NPB values are similar to the ones of naphthalene crystal. This is quite an unexpected result as one would expect smaller diffusion coefficients in less ordered amorphous NPB, CBP and Alq$_3$ films.

Comparing NPB and Ir(piq)$_3$ triplet diffusion constant values obtained here with the values in table 9.3 is evident that they are in the range of naphthalene or pyrene constants in a similar way as singlet diffusion constants of amorphous materials are similar to those of more ordered crystals. Triplet diffusion values determined by Forrest *et al*[6, 20, 33] (CBP, Alq$_3$, PtOEP dimer) are ~3 orders of magnitude lower than the ones determined in this thesis. Indeed, the difference is substantial; however, as already discussed in chapter 8 there are lots of unclear points in the CBP diffusion constant determination including the neglect of CBP trap states in the modeling as well as the unjustified way of CBP triplet lifetime determination (see above). Shortcomings

of Alq$_3$ diffusion constant determination[7] also were discussed in chapter 8. First, triplet-triplet annihilation was not accounted for and second, determination was made in an OLED type structure using electrical excitation implying that polaron-triplet annihilation might take place. PtOEP monomer diffusion constant is not in such a big discrepancy with Ir(piq)$_3$, - ~ 4 times smaller, which, considering very different methods used to determine them (chapter 8) is not in bad agreement. Comparison of PtOEP monomer with PtOEP dimer implies that dimerisation and stacking can decrease the diffusion constant by a few orders of magnitude. Hence ~2 orders of magnitude discrepancy between PtOEP dimer diffusion constant and Ir(piq)$_3$ (monomer) diffusion constant is reasonable.

As discussed in the paragraph about diffusion constants, similarly, one should be careful in evaluating the validity of CBP TTA constant determined by Giebink *et al*[20] (table 9.2). Further 7% Ir(ppy)$_3$:TCTA, 20% Ir(piq)$_3$:NPB, 8% PtOEP:CBP and 8% PtOEP:Alq$_3$ TTA constants (table 9.2) were determined assuming that only guest triplets participate in triplet-triplet annihilation despite the fact that the hosts molecules occupies a large part of these systems (in most cases more than 90%). TTA constant of doped films also might be different to those in neat film because of the fact that the dopant might either scatter or trap triplets hence skew the results. Thus at the moment in the literature only one amorphous OLED material value, that of Ir(ppy)$_3$ neat film, determined by Kalinowski *et al*[35] can be compared to the ones determined here. This value is an order of magnitude smaller than the one determined for Ir(piq)$_3$ film, and around four times larger than the one determined for NPB films. Having in mind very different methods of determination this could be considered to be in a good agreement.

Table 9.2 Comparison of TTA constants found in literature (only values extracted using PL excitation is presented)

Material (triplets)	TTA constants, cm^3/s	Material (triplets)	TTA constants, cm^3/s
CBP triplet	1.6E-14[20]	8% PtOEP:CBP	3.6E-14[6]
7% Ir(ppy)$_3$:TCTA	3E-12[8]	8% PtOEP:Alq$_3$	From ~1.2E-12 cm^3/s to 8E-14 cm^3/s with a decrease of exciton density from ~6E16 cm^{-3} to 1E19 cm^{-3} [6]
20% Ir(piq)$_3$:NPB	1.4E-12[8]	NPB	6.2E-13 [this thesis]
Ir(ppy)$_3$	2.7E-12[35]	Ir(piq)$_3$	3.3E-11 [this thesis]

Table 9.3 Comparison of triplet exciton diffusion coefficients found in literature. PtOEP = Pt(II) Octaethylporphine. Fc_{21}/Ru_x stands for heterostructured films with tris(2,2'-bipyridine)ruthenium(II) moieties as phosphorescence emitter and with ferrocene moieties used as phosphorescence quenchers in a polycarbonate copolymer. The subscript here indicates molar fraction of moiety in percentage in the copolymer.

Material (triplets)	Diffusion coefficient, cm^2/s	Material (triplets)	Diffusion coefficient, cm^2/s
Naphthalene in aa plane	0.33E-4[32]	Trans-stylbene in bb plane	0.7E-4[32]
Naphthalene in bb plane	0.27 E-4[32]	PtOEP T-monomer	0.041E-4[33]
Anthracene in aa plane	1.5 E-4[32]	PtOEP T-dimer	0.00061E-4[33]
Anthracene in bb plane	1.8 E-4[32]	CBP	0.00014E-4[20]
Anthracene in c'c' plane	<0.12 E-4[32]	Alq$_3$	0.0008E-4[7]
Tetracene in bb plane	40 E-4[32]	Fc$_{21}$/Ru$_4$	<0.001E-4[36]
Pyrene in aa plane	0.3E-4[32]	Fc$_{21}$/Ru$_{12}$	0.07E-4 [36]
Pyrene in bb plane	1.25E-4[32]	Fc$_{21}$/Ru$_{18}$	0.2E-4 [36]
Pyrene in c'c' plane	0.3E-4[32]	Ir(piq)$_3$	0.17E-4 [this thesis]
Trans-stylbene in aa plane	0.09E-4[32]	NPB	0.24E-4 [this thesis]

9.4 References

1. C. W. Tang and S. A. Vanslyke, Appl. Phys. Lett. 51 (12), 913-915 (1987).

2. C. Adachi, M. A. Baldo, M. E. Thompson and S. R. Forrest, J. Appl. Phys. 90 (10), 5048-5051 (2001).

3. V. Adamovich, J. Brooks, A. Tamayo, A. M. Alexander, P. I. Djurovich, B. W. D'Andrade, C. Adachi, S. R. Forrest and M. E. Thompson, New J. Chem. 26 (9), 1171-1178 (2002).

4. M. A. Baldo, D. F. O'Brien, Y. You, A. Shoustikov, S. Sibley, M. E. Thompson and S. R. Forrest, Nature 395 (6698), 151-154 (1998).

5. T. X. Zhou, T. Ngo, J. J. Brown, M. Shtein and S. R. Forrest, Appl. Phys. Lett. 86 (2), 021107 (2005).

6. M. A. Baldo, C. Adachi and S. R. Forrest, Phys. Rev. B 62 (16), 10967-10977 (2000).

7. M. A. Baldo and S. R. Forrest, Phys. Rev. B 62 (16), 10958-10966 (2000).

8. S. Reineke, K. Walzer and K. Leo, Phys. Rev. B 75 (12), 125328 (2007).

9. C. Rothe and A. P. Monkman, Phys. Rev. B 68 (7), 075208 (2003).

10. D. Hertel, H. Bassler, R. Guentner and U. Scherf, J. Chem. Phys. 115 (21), 10007-10013 (2001).

11. S. Reineke, F. Lindner, G. Schwartz, N. Seidler, K. Walzer, B. Lussem and K. Leo, Nature 459 (7244), 234-238 (2009).

12. Y. R. Sun, N. C. Giebink, H. Kanno, B. W. Ma, M. E. Thompson and S. R. Forrest, Nature 440 (7086), 908-912 (2006).

13. G. Schwartz, S. Reineke, T. C. Rosenow, K. Walzer and K. Leo, Adv. Funct. Mater. 19 (9), 1319-1333 (2009).

14. P. A. Losio, R. U. A. Khan, P. Gunter, B. K. Yap, J. S. Wilson and D. D. C. Bradley, Appl. Phys. Lett. 89 (4), 041914 (2006).

15. A. Tsuboyama, H. Iwawaki, M. Furugori, T. Mukaide, J. Kamatani, S. Igawa, T. Moriyama, S. Miura, T. Takiguchi, S. Okada, M. Hoshino and K. Ueno, J. Am. Chem. Soc. 125 (42), 12971-12979 (2003).

16. J. Kalinowski, G. Giro, M. Cocchi, V. Fattori and P. Di Marco, Appl. Phys. Lett. 76 (17), 2352-2354 (2000).

17. K. Goushi, R. Kwong, J. J. Brown, H. Sasabe and C. Adachi, J. Appl. Phys. 95 (12), 7798-7802 (2004).

18. Y. Kawamura, K. Goushi, J. Brooks, J. J. Brown, H. Sasabe and C. Adachi, Appl. Phys. Lett. 86 (7), 071104 (2005).

19. S. C. J. Meskers, J. Hubner, M. Oestreich and H. Bassler, Chem. Phys. Lett. 339 (3-4), 223-228 (2001).

20.   N. C. Giebink, Y. Sun and S. R. Forrest, Org. Electron. 7 (5), 375-386 (2006).

21.   B. Ries, H. Bassler, M. Grunewald and B. Movaghar, Phys. Rev. B 37 (10), 5508-5517 (1988).

22.   Y. Kawamura, H. Yamamoto, K. Goushi, H. Sasabe, C. Adachi and H. Yoshizaki, Appl. Phys. Lett. 84 (15), 2724-2726 (2004).

23.   C. Rothe, S. M. King and A. P. Monkman, Phys. Rev. Lett. 97 (7), 076602 (2006).

24.   S. Volker, Annual Review of Physical Chemistry 40, 499-530 (1989).

25.   H. P. H. Thijssen, R. v. d. Berg and S. Volker, Journal de Physique Colloque C7 supplement no 10 (Tome 46), page C7- 363 (1985).

26.   D. Haarer and R. Silbey, Physics Today 43 (5), 58-65 (1990).

27.   A. R. Gutierrez, J. Friedrich, D. Haarer and H. Wolfrum, IBM Journal of Research and Development 26 (2), 198-208 (1982).

28.   K. Yoshikawa, R. Matsunaga, K. Matsuda and Y. Kanemitsu, Appl. Phys. Lett. 94 (9), 093109 (2009).

29.   C. J. Winscom and A. H. Maki, Chem. Phys. Lett. 12 (2), 264 (1971).

30.   C.J.Winscom, K.P.Dinse and K.Mobius, Proceedings of the XIXth Congress Ampere, Heidelberg 413 (1976).

31.   Z. G. Soos, J. Chem. Phys. 51 (5), 2107 (1969).

32.   M. Pope and C. E. Swenberg, *Electronic Processes in Organic Crystals*. (Oxford Univresity Press, New York, 1982).

33.   R. R. Lunt, N. C. Giebink, A. A. Belak, J. B. Benziger and S. R. Forrest, J. Appl. Phys. 105 (5), 053711 (2009).

34.   C. L. Yang, Z. K. Tang, W. K. Ge, J. N. Wang, Z. L. Zhang and X. Y. Jian, Appl. Phys. Lett. 83 (9), 1737-1739 (2003).

35.   J. Kalinowski, J. Mezyk, F. Meinardi, R. Tubino, M. Cocchi and D. Virgili, J. Appl. Phys. 98 (6), 063532 (2005).

36.   T. Fushimi, A. Oda, H. Ohkita and S. Ito, J. Phys. Chem. B 108 (49), 18897-18902 (2004).

10 General conclusions

Throughout the course of this thesis the following work has been completed. CBP was characterized by absorption, emission and time resolved spectroscopies. It was discovered that trap states exist in CBP with peaks at 413 nm and 438 nm in film fluorescence spectra and at 560 nm and 607 nm in film phosphorescence spectra. Measurements show that annealing and aging affects phosphorescence and fluorescence emission by increasing the fraction emitting from trap states. These trap states are probably the result of the degradation product.

Triplet migration properties of NPB thin films have been studied. It was proven here that dispersive exciton migration is prevalent in NPB films at a range of temperatures including room temperature. The width of Gaussian triplet density of states has been determined for various NPB film thicknesses. This varies from 37 meV for 13 nm thickness film to 43 meV for 250 nm thickness films. If $Ir(piq)_3$ is evaporated on top, the triplet DOS is almost constant, indicating that a poralizable medium near the NPB surface has an impact for NPB DOS. Unrelaxed triplet level of the NPB thin film at zero time has been determined which is 2.44 eV. The final conclusion is that NPB is much more suitable spacer layer than CBP due to the reason that no emissive traps are found, excimer (dimer) formation can be controlled and triplet dynamic properties can be easily examined and understood.

In chapter 7 $Ir(ppy)_3$ and $Ir(piq)_3$ films were characterized using time-resolved spectroscopy. It was shown that in neat $Ir(ppy)_3$ and $Ir(piq)_3$ films triplets migrate in the density of states. Fresh $Ir(ppy)_3$ and $Ir(piq)_3$ films have triplet DOS widths of approximately 100 meV and 70 meV respectively which was determined for the first time. A decay in $Ir(ppy)_3$ neat films have been observed (with the slope -1) which has not been published in the literature before. In addition, this type of decay is observed in neat films of FIrpic and $Ir(piq)_3$ showing that it is characteristic not only to $Ir(ppy)_3$ but also other Iridium metal complexes. It was discovered that aged $Ir(ppy)_3$ films exhibit change in conformational order. Finally, based on a literature review and new experimental evidence, a new triplet and singlet energy level diagram for $Ir(ppy)_3$ films is proposed.

Further bilayer sapphire/$Ir(piq)_3$/NPB films have been investigated. Unconventional decays having two "cascade" like features have been observed from $Ir(piq)_3$. The faster part of the decay (up to ~200 ns) is not changing with the change of NPB thickness and is the same as the decay of a single layer 33 nm $Ir(piq)_3$ film. This is the result of the decay of directly excited $Ir(piq)_3$. The slower parts of the decay are different for each NPB thickness, resulting from diffusion controlled triplet migration in NPB towards NPB/$Ir(piq)_3$ interface. These parts decay

monoexponentially and the lifetimes decrease with the decrease of NPB thicknesses - for 80 nm thickness it is 2031 ns, for 40 nm – 1763 ns, for 25 nm – 1411 ns, for 13nm – 1084 ns. Triplets from the donor NPB are mainly trapped at the interface sites of Ir(piq)$_3$ and are not directly transferred into the bulk states of Ir(piq)$_3$ and should be considered when modeling triplet dynamics in multilayer films.

In addition, sapphire/Ir(ppy)$_3$ 5 nm/NPB x nm/Ir(piq)$_3$ 5 nm/TAPC 100 nm/Al 200 nm multilayer layer films with different NPB thicknesses have been investigated. It was shown that one could easily create structures were triplets are transferred from donors to acceptors via optically inactive spacer layer. Ir(piq)$_3$ decays from these structures have been analysed and explained. In the first ~100-200 ns the decay of Ir(piq)$_3$ is of multiexponential character whereas after it follows monoexponential law. For 0 nm NPB layer thickness the lifetime of this monoexponential decay is 144 ns, 2.5 nm – 193 ns, 5 nm – 232 ns, 10 nm - 265 ns, 20 nm - 407 ns. Again similarly to bilayer films the initial part of the decay comes from directly excited Ir(piq)$_3$. Ir(piq)$_3$ decays and time resolved spectra peak analysis show that monoexponential emission decays arise due to emission from triplets arriving from Ir(ppy)$_3$ reservoir via NPB to Ir(piq)$_3$. In this case not unlike in bilayer sapphire/Ir(piq)$_3$/NPB systems triplets are not trapped in the interface and can be transferred straight to the bulk states of Ir(piq)$_3$. This is due the fact that the sequence of evaporation is different.

Finally mathematical model based on classical diffusion equations was created in conjunction with Professor Chris Winscom where interface trap states are included. Computer simulations performed by Professor Chris Winscom using this model agree well with Ir(piq)$_3$ decays from bilayer sapphire/Ir(piq)$_3$/NPB films. Triplet exciton diffusion and triplet triplet annihilation constants were determined for NPB ($k_{TT}^{NPB} = 6.2 \times 10^{-13}$ cm^3 s^{-1}, $D_{NPB} = 2.4 \times 10^{-5}$ cm^2 s^{-1}) and Ir(piq)$_3$ ($k_{TT}^{PIQ} = 3.3 \times 10^{-11}$ cm^3 s^{-1}, $D_{PIQ} = 1.7 \times 10^{-5}$ cm^2 s^{-1}) . Monomolecular decay constants for NPB ($k_1^{NPB} = 4.0 \times 10^5$ s^{-1}) and Ir(piq)$_3$ films ($k_1^{PIQ} = 3.75 \times 10^7$ s^{-1}) were found as well. Analysis of the triplet densities at times later than 100 ns shows that more than 50% of the excitons reaching the interface reside in the interface trap sites again agreeing with experimental results.

The main reason why these experiments were done is that interest in triplet exciton dynamics has increased throughout the last few years. This is because of the fact that phosphorescent light emitting diodes (PHOLED) have attracted significant research effort and interest recently. Further, hybrid organic light emitting diodes (OLED) were developed where a blue fluorescent dye is used together with phosphorescent emitters. It was demonstrated that these devices can achieve high efficiencies. In these devices triplets are harvested by making use of their diffusion properties. However creating these structures is extremely complicated due to large number of layers and the fact that other properties such as electron/hole mobilites, HOMO and LUMO

levels should be adjusted simultaneously. Thus it would be useful for device engineers to know triplet diffusion properties in the same way as they can know HOMO and LUMO levels or electron mobilities before trying out the material in the device. Unfortunately triplet diffusion has not been well characterized and understood in amorphous organic films and more importantly between the layers in these films. There has been some pioneering efforts to do this, however as it was shown here, in chapter 8 and chapter 9, still lots of research needs to be done in order to understand triplet diffusion in amorphous films properly. Most of the investigations of triplet dynamics in doped films are oversimplified and there is little research done on triplet migration (without charge being involved) between the neat layers and across the interfaces. After this is thoroughly understood then it would be easier to perceive what influence charge can impose on triplet exciton dynamics in OLEDs.

The starting point in this systematic study was to understand triplet migration dynamics in single layer films. It was shown in chapter 5 how important trap states can be in films. Indeed even small amounts of traps can influence triplet exciton dynamics to such an extent that the majority of film fluorescence and phosphorescent spectra is dominated by light coming from trapped triplets. If they are not identified, incorrect modeling and final conclusions about triplet dynamics can be made. Further in chapter 7 the abundance of states in iridium metal complex films was shown. Emission from these states was observed in spectroscopic investigations of multilayer films too (chapter 9) and as their origins were known, this trap emission could easily be identified and accounted for (or avoided). This again confirmed that before investigating complex structure it is extremely important to determine photophysical properties of single layer films. All small molecule films investigated in this thesis – NPB, CBP, $Ir(ppy)_3$, $Ir(piq)_3$ - had trap states which together with triplet exciton migration could be one of the main sources of the decrease of PLQY in films. Having very efficient triplet migration will result in efficient population of existing trap states in films leading to lower PL quantum yield in comparison to equivalent material where exciton migration is inhibited. This was already shown for charge iridium complexes and confirmed again here. Thus OLED (or solar cells) engineers will have to make trade-offs between efficient triplet harvester and efficient emitter.

Another issue related to amorphous disordered materials is the dispersivity of triplet exciton migration. This, as discussed in chapter 6, can influence triplet migration not only at low temperatures but also at room temperatures. As was shown by other workers in polymer films and here in small molecule films this dispersive migration results in time dependent diffusion 'constants' which in turn translates into time dependent bimolecular annihilation 'constants'. Interestingly for the first time here triplet density of states width of iridium heavy metal complex film has been determined. As expected it is broader than the density of states of polymer films (e.g. polyfluroene) and small host type molecule films (e.g. NPB). This comes

from the fact that more states in heavy metal complex molecule films have substantial charge transfer character. Metal to ligand charge transfer states are more susceptible to polarization of surrounding material resulting in a bigger spread of energy, hence broader DOS. Unfortunately, so far, diffusion constant time dependence arising due to this broad density of states has not been cast into any expression despite substantial effort by a few researchers. Thus classical diffusion equations cannot be modified to account for dispersive migration and have to be used as it is – with time-independent diffusion (and TTA) constant. Then caution needs to be taken when interpreting the results as those constants reflects the averaged over time properties of triplet migration (averaged D and k_{tt}) and their values at different points in time might be slightly different. Nevertheless these values can give a general idea of triplet exciton migration properties in films despite the existence of dispersive migration. It needs to be said that the triplet-triplet annihilation constant k_{TT} at some instances may not be dependent on time even if dispersive regime is prevalent. k_{TT} constant used in classical diffusion equations accounts for both diffusion and triplet-triplet annihilation (assuming equation (3.20) $k_{TT} = 8\pi f_R RD$ is valid). If triplet annihilation is diffusion controlled then k_{TT} essentially has a similar physical meaning as the diffusion coefficient and is dependent on time if the dispersive regime is prevalent. However if the triplet annihilation constant represents the annihilation probability i.e. probability that two triplets nearby will annihilate is small then k_{TT} essentially is time independent even if dispersive transport is dominant in the system.

The implication of NPB triplet trapping in interface sites from Ir(piq)$_3$ layer is that triplets cannot be harvested (transferred to the bulk) if such interfaces exist. More surprisingly in chapter 9 it was shown why these type of interface trap sites are created and that this depends on such a simple technical parameter as sequence of layer evaporation. If less massive NPB molecules are evaporated on top of Ir(piq)$_3$ film, then they sieve through the larger and more massive molecules of Ir(piq)$_3$, hence creating a doped-like interface layer. If the evaporation sequence is reversed interface states are not observed as heavier and larger Ir(piq)$_3$ cannot penetrate into NPB films. This finding might be very interesting to OLED engineers as they could use this effect to inhibit triplet transfer from higher triplet layer to lower triplet layer in OELD structures where it is needed. Finally it is interesting from a fundamental point of view as up to now these quasi interfaces in amorphous films has not been investigated so far (apart from exciplex formation between neighboring layers).

From interface physics work has been moved towards triplet transfer physics whereby three layer experiments proved that structures can be created where triplets are transferred from donor to acceptor via optically inactive spacer layer. Furthermore the method used here is so sensitive that 3 layer structures having spacer layer thickness of 2.5 nm and 5 nm could be easily distinguished from the unconventional shaped decay having two cascade features. From the

graphs in chapter 9 it is clearly seen that even differences between 0 nm and 1 nm spacer thicknesses in these structure could be resolved if this two cascade shaped decay is used as an indicator. Indeed this type of accuracy is remarkable and could be used to analyse triplet dynamics across the thinnest spacer layers.

The model described here could be particularly important in designing optimum triplet transfer into the bulk states behind the interface states. This model is probably more comprehensive that all others so far published in the literature. Closer inspection of previous literature models can unveil that this is in part due to the fact that here the system is more complicated in comparison with dopant:hosts systems studied previously. As well in the majority of models in literature unjustified assumptions are made, for example, that only dopant triplets annihilate while dopants are present only less than 10% in the host. In this way one can get rid of a few parameters but simultaneously invalidates the physical situation under investigation.

Despite the fact that a considerable amount of work has been done in considering all of the aspects of this model, it could (and should) be improved in the future. First of all the accuracy of the determination of initial triplet concentration could be enhanced. One has to admit that in both cases - in this thesis and in literature - intersystem crossing yield (ISC) determination of non-heavy metal materials such as NPB or CBP could induce some errors in further calculations. This could be avoided if intersystem crossing yields could be measured more accurately or if heavy metal complexes are used as donor layer (ISC~1). Indeed ISC of some polymers have already experimentally measured however very complicated femtosecond ground state recovery technique had to be used. This is an area where more work should be done as ISC is an important parameter not only for the subjects studied in this thesis. Furthermore efforts should be put into more accurate determination of homogeneous linewidths of investigated materials (and consequentially hole burning or saturation effects of homogeneous linewidths). Very little work has been done so far in this area especially using modern archetype OLED materials studied here. If this could be evaluated more accurately then initial density of excitations in a film could be determined more precisely.

One could summarize all the above as follows when trying to do research on triplet dynamics in multilayer structures using optical time resolved spectroscopy. First of all single layer materials should be diligently investigated before putting them into structures in order to determine possible trap states, Jablonski diagrams and density of states widths. Then it should be determined whether in these single layer films dispersive migration is prevalent in order to know how to interpret diffusion and TTA constants later. Careful investigation should be done on interface trap states as these can act as triplet traps even from higher energy triplet materials to lower. Finally appropriate donor and acceptor systems as well as exciting laser has to be

chosen in order to create 3 layer donor/spacer/acceptor system where spacer is optically inactive and $E_{Tdonor} > E_{Tspacer} > E_{Tacceptor}$. It is preferred that donor and acceptor are heavy metal complexes where ISC yield ~1. Finally a model developed with interface trapped states can be used to extract diffusion and annihilation constants which on average could predict triplet exciton dynamics in these films.

11 List of publications

Publications resulting from work contained in this thesis:

Chapter 5:

V. Jankus, C. Winscom, and A. P. Monkman, "The photophysics of singlet, triplet, and degradation trap states in 4,4-N,N'-dicarbazolyl-1,1'-biphenyl," J. Chem. Phys. 130 (7) (2009).
(contributon: performed all experiments and wrote manuscipt)

Chapter 6

V. Jankus, C. Winscom, and A. P. Monkman, "Dynamics of triplet migration in films of N, N '-diphenyl-N, N '-bis(1-naphthyl)-1,1'-biphenyl-4,4 "-diamine," J. Phys.-Condes. Matter 22 (18) (2010).
(contributon: performed all experiments and wrote manuscipt)

Chapter 9

V. Jankus, C. Winscom, and A. P. Monkman "Triplet exciton interface trap states in bilayer films of NPB and Ir(piq)$_3$", Phys. Rev. B (submitted).
(contributon: performed all experiments, participated in modeling process and wrote part of manuscript)

Chapter 9

V. Jankus, C. Winscom, and A. P. Monkman "Triplet energy transfer across an NPB interlayer between Ir(ppy)$_3$ and Ir(piq)$_3$ structure", (in preparation).
(contributon: performed all experiments, participating in modeling process and wrote part of manuscript)

Other publications by the author:

Rothe, C. J. Chiang, <u>V. Jankus</u>, K. Abdullah, X. S. Zeng, R. Jitchati, A. S. Batsanov, M. R. Bryce, and A. P. Monkman, "Ionic Iridium(III) Complexes with Bulky Side Groups for Use in Light Emitting Cells: Reduction of Concentration Quenching," Adv. Funct. Mater. 19 (13), 2038-2044 (2009).
(contributon: performed luminesence decay experiments)

S. U. Pandya, K. C. Moss, M. R. Bryce, A. S. Batsanov, M. A. Fox, <u>V. Jankus</u>, H. A. Al Attar, and A. P. Monkman, "Luminescent Platinum(II) Complexes Containing Cyclometallated Diaryl Ketimine Ligands: Synthesis, Photophysical and Computational Properties," European Journal of Inorganic Chemistry (13), 1963-1972 (2010).
(contributon: performed photophysical experiments and wrote photophysical part of manuscript)

Y. Zheng, A. S. Batsanov, <u>V. Jankus</u>, M. R. Bryce and A. P. Monkman, "Precision Tuning of Singlet and Triplet Energies of Fluorescent Ambipolar Molecules", (in preparation).
(contributon: performed photophysical experiments and wrote photophysical part of manuscript)

K. T. Kamtekar, K. Dahms, A. Batsanov, <u>V. Jankus</u>, H. L. Vaughan, A. P. Monkman and M. R. Bryce, "Synthesis and properties of fluorene cooligomers and copolymers with incorporated phenothiazine-S,S-dioxide unit", (in preparation)
(contributon: performed photophysical experiments)